NASA TECHNICAL TRANSLATION

NASA TT F-766

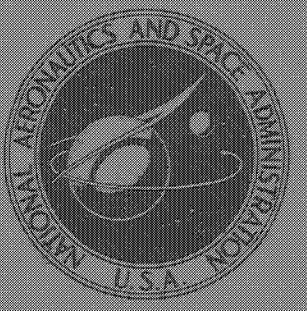

CASE FILE COPY

NASA TT F-766

CURRENT CONCEPTS REGARDING THE MOON

by A. P. Vinogradov et al.

"Nauka" Press, Moscow, 1972

NATIONAL AERONAUTICS AND SPACE ADMINISTRATION • WASHINGTON, D. C. • FEBRUARY 1974

CURRENT CONCEPTS REGARDING THE MOON

by A. P. Vinogradov et al.

"Nauka" Press, Moscow, 1972

NATIONAL AERONAUTICS AND SPACE ADMINISTRATION • WASHINGTON, D. C. • FEBRUARY 1974

1. Report No. NASA TT F-766	2. Government Accession No.	3. Recipient's Catalog No.
4. Title and Subtitle CURRENT CONCEPTS REGARDING THE MOON		5. Report Date February 1974 6. Performing Organization Code
7. Author(s) A.P. Vinogradov et al.		8. Performing Organization Report No. 10. Work Unit No.
9. Performing Organization Name and Address SCITRAN Box 5456 Santa Barbara, CA 93108		11. Contract or Grant No. NASw-2035 13. Type of Report and Period Covered Translation
12. Sponsoring Agency Name and Address National Aeronautics and Space Administration Washington, D.C. 20546		14. Sponsoring Agency Code

15. Supplementary Notes

Translation of: "Sovremennyye Predstavleniya o Lune," Edited by K.P. Florenskiy et al, Moscow, "Nauka" Press, 1972, 1 - 125 pp plus maps

16. Abstract

The current status of scientific concepts regarding the Moon is examined. The goals of the study of the Moon from the Earth are presented, and an attempt is made to generalize the data obtained in recent years by means of space vehicles. The book contains articles giving the results of investigating the lunar soil by means of Luna 16, a geological-morphological analysis of telescopic pictures of the lunar surface, investigations of the Moon's intrinsic radiation, development of the fundamentals of lunar cartography, simulation of lunar soil and processes occurring on the surface of the Moon, as well as the problems involved in drilling on the lunar surface.

17. Key Words (Selected by Author(s))	18. Distribution Statement Unclassified - Unlimited		
19. Security Classif. (of this report) Unclassified	20. Security Classif. (of this page) Unclassified	21. No. of Pages 226	22. Price* $5.75

*For sale by the National Technical Information Service, Springfield, Virginia 22151

PRECEDING PAGE BLANK NOT FILMED

ANNOTATION

This collection is devoted to an examination of the current status of scientific concepts regarding the Moon. The goals of the study of the Moon from the Earth are presented, and an attempt is made to generalize the vast body of data obtained in recent years by means of space vehicles. The collection contains articles on the results of investigating the properties of the lunar soil returned to Earth by the Luna 16 ALP [automatic lunar probe], geological-morphological analysis of large-scale and telescopic pictures of the lunar surface, investigations of the Moon's intrinsic radiation, development of the fundamentals of lunar cartography, simulation of lunar soil and processes occurring on the surface of the Moon, as well as the problems involved in drilling in the lunar surface.

The book is intended for specialists concerned with the study of the Moon and planets, as well as for a broad spectrum of readers who are interested in the problems discussed in this collection.

Editorial board:

K. P. Florenskiy (Editor-in-Chief)
A. A. Gurshteyn (Deputy Editor-in-Chief)
A. T. Bazilevskiy
M. N. Izakov

PRECEDING PAGE BLANK NOT FILMED

FOREWORD

Recent years have seen Soviet science and technology achieve /5* great successes in the conquest of space, especially in the use of spacecraft to study the Moon. It was only six years ago that the Soviet unmanned probe Luna 9 made the first soft landing on the lunar surface, allowing panoramas of the latter to be obtained for the first time. This event was also proof of the possibility of direct studies of the lunar surface by automatic means.

The next conceptually new step on the road to the investigation of the Moon was the successful launching of the Luna 16 probe. As a result of its planned program, this vehicle became the first automatic device to bring samples of lunar soil back to Earth, thus demonstrating the enormous potential of automatic devices in the study of the Universe.

Another tremendous success in the study of our natural satellite by means of unmanned probes in the "Luna" series was the successful transportation tc the lunar surface of the automatic mobile laboratory called the "Lunokhod-1."

The present collection is devoted to the fundamental problems of the study of the Moon and is intended to inform the reader of the current state of the art in various areas of this branch of knowledge.

*The numbers in the margin indicate the pagination of the original foreign text.

The article by A. P. Vinogradov is devoted to a description of the properties of a sample of lunar soil from Mare Fecunditatis, returned to Earth by the Luna 16 automatic probe, as well as a comparison of these data with the results of the U.S. expeditions to the Moon on the Apollo program. The article focuses attention on some of the unsolved problems regarding the origin and evolution of the lunar rocks.

The article by K. P. Florenskiy, A. T. Bazilevskiy, A. A. Gurshteyn, R. B. Zezin, A. A. Pronin, V. P. Polosukhin, Z. V. Popova and I. M. Taborko describes the results of a geomorphological analysis of large-scale photographs of the lunar surface taken by Soviet and U.S. spacecraft. The study of the details and distribution of details on the lunar microrelief will make it possible in future to put together the picture of the evolution of the lunar surface, many parts of which still remain unclear.

The article by V. S. Troitskiy and T. V. Tikhonova presents the results of many years' study of the surface layer of the Moon from the Earth, with respect to its intrinsic radiation. The accumulated data have enabled the authors to construct a model of the structure of the upper layers of the lunar crust.

The article by M. S. Markov, A. L. Sukhanov, V. G. Trifonov, P. V. Florenskiy and L. M. Shkerin is devoted to the results of studying small-scale photographs of the Moon obtained at various terrestrial observatories. The geological-morphological analysis of details on the lunar relief has enabled the authors to classify the rocks in the upper strata of the lunar crust into several stratigraphic formations of different ages and to trace the distribution of these formations over the lunar disk. The present publication continues the series of geological-morphological charts compiled by these authors.

The article by K. N. Florenskiy, A. A. Gurshteyn, V. I. Korablev, /6
L. M. Bugayevskiy and K. B. Shingareva deals with questions of rational classification, scales, and nomenclature of lunar charts.

The article by M. D. Nusinov, V. A. Kochnev, Yu. B. Chernyak, A. V. Kuznetsov, A. I. Kosolapov and O. I. Yakovlev deals with problems of laboratory simulation of processes which occur on the surface of the Moon.

The article by Z. A. Atsagortsyan, G. G. Akopyan, R. R. Sarkisov, I. I. Cherkasov and V. V. Shvarev provides the reader with a description of analogs of lunar soil that can be used to solve a number of problems in pure and applied science.

The article by B. V. Zakhar'yev and V. G. Kardysh describes the solutions which designers have found for drilling in the lunar surface in conjunction with the U.S. Surveyor and Apollo programs for lunar exploration.

Hence, the present collection largely reflects those scientific problems being emphasized at the current stage of lunar exploration, as well as the nonuniformity in the analysis of the individual problems which is characteristic of every rapidly developing field of knowledge.

The individual articles in this collection were written at different times, vary in content, and cannot be considered today to be the last word on lunar structure. However, they do constitute the result of many years of work by the authors and express their points of view, which naturally cannot be considered indisputable in every case. The further study of the Moon, which is proceeding at the present time with amazing speed, may call for significant corrections to be made in the concepts put forth herein.

Nevertheless, the publication of such materials, which serve as the basis for the subsequent development of science, is timely and important.

The editors would like to express their gratitude to their colleagues at the USSR Academy of Sciences, Institute of Space Research, M. I. Shtern and G. A. Burbe, for all of the work they devoted to preparing this collection for publication.

TABLE OF CONTENTS

Foreword v

A. P. Vinogradov

Preliminary Data on the Lunar Soil Collected by the Luna 16 Automatic Probe 1

K. P. Florenskiy, A. T. Bazilevskiy, A. A. Gurshteyn, R. B. Zezin, A. A. Pronin, V. P. Polosukhin, Z. V. Popova and I. M. Taborko

The Problem of the Structure of the Surface of the Lunar Maria 25

V. S. Troitskiy and T. V. Tikhonova

Results of Investigation of the Surface Layer of the Moon on the Basis of Its Intrinsic Radiation 63

M. S. Markov, A. L. Sukhanov, V. G. Trifonov, P. V. Florenskiy, and L. M. Shkerin

Geological Mapping of the Moon 97

K. P. Florenskiy, A. A. Gurshteyn, V. I. Korablev, L. M. Bugayenskiy and K. B. Shingarev

Classification, Scale Series and Nomenclature of Lunar Charts 139

M. D. Nusinov, V. A. Kochev, Yu. B. Chernyak, A. V. Kuznetsov, A. I. Kosolapov and O. I. Yakovlev

Laboratory Simulation of Processes of "Evaporation, Condensation and Sputtering" Taking Place on the Surface of the Moon 155

Z. A. Atsagortsyan, G. G. Akopyan, R. R. Sarkisov, I. I. Cherkasov and V. V. Shvarev

Development of an Analog of Lunar Soil 186

B. V. Zakhar'yev and V. G. Kardysh

U.S. Studies in the Field of Shaft Drilling on the Lunar Surface 192

N74-19476

PRELIMINARY DATA ON THE LUNAR SOIL COLLECTED BY THE LUNA 16 AUTOMATIC PROBE

/7

A. P. Vinogradov

ABSTRACT. The results of preliminary studies of a sample of lunar soil taken by the automatic probe "Luna 16" are given. Information on the granulometric characteristics of the regolith, its optical properties, types of rocks, and mineral composition are described. The chemical composition of macro- and microelements for different parts of the core sample is determined for the lunar basalt. The isotopic composition of inert gases of certain elements is studied. The age was established by the Rb/Sr method as 4.85 — 4.25 billion years.

As we know, the Luna 16 automatic probe collected a sample of lunar soil taken from Mare Fecunditatis, in the northeastern part, at a point with the coordinates 0°41' S and 56°18' E, approximately 100 km west of the crater Webb (Figure 1).

Mare Fecunditatis contains traces of comparatively quiet uplifting, its borders are not marked by an annular ringwall, and its outlines are blurred. The mare is a plain with low (100 — 300 m) branching ridges traversing it. The ray systems of the large craters are not found in this area. The lunar soil from Mare Fecunditatis is characteristic of the new region of the "mare" surface of the Moon. Hence, the three large maria on the near side, arranged along the

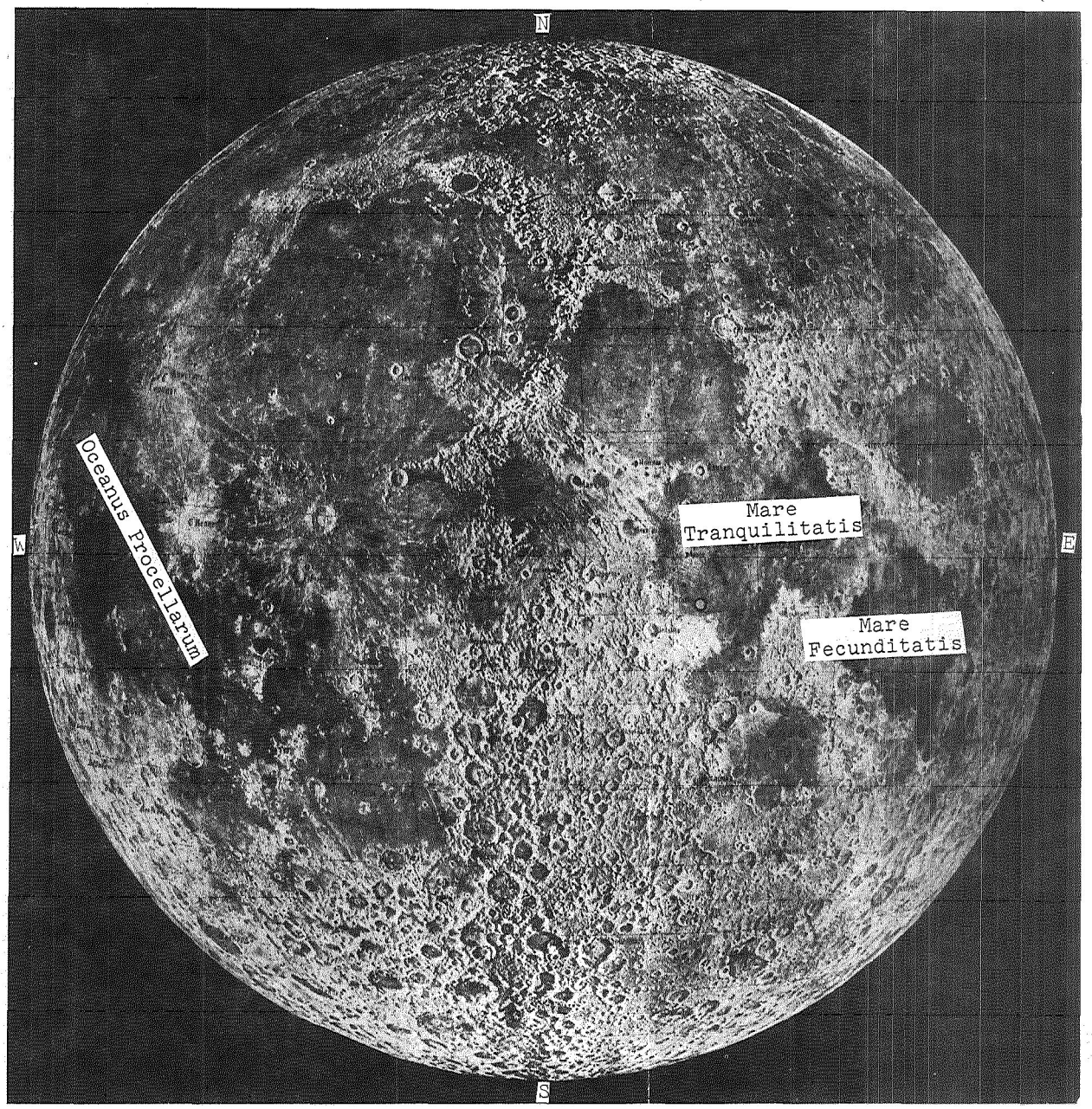

Figure 1. Map of the Moon.

* — Landing site of Luna 16; ○— Apollo 11 landing site; • — Apollo 12 landing site.

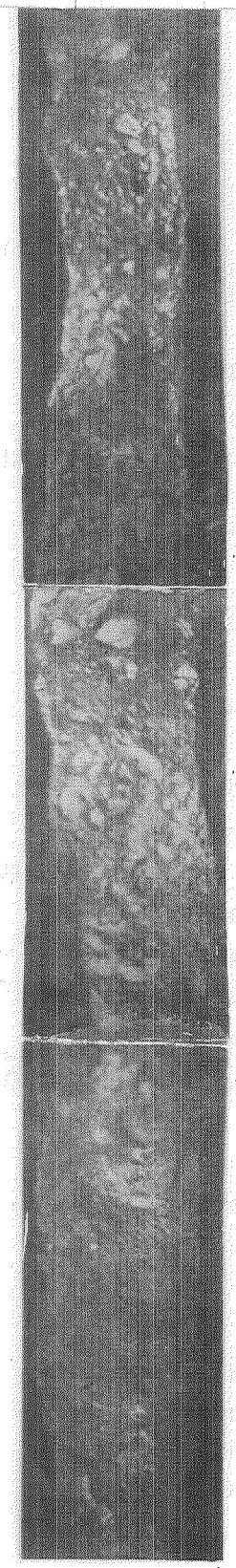

Figure 2. Photograph of lunar soil in pan in receiving chamber. At the bottom is the deeper part of the core, where coarser material can be seen.

lunar equator (Mare Tranquilitatis — Apollo 11 samples; Oceanus Procellarum — Apollo 12 samples; Mare Fecunditatis — Luna 16 samples) give a fairly complete idea of the nature of the surface rocks on the Moon.

The friable surface material of Mare Fecunditatis, the regolith, was collected by means of a drill which penetrated the rock to a depth of 35 cm. Further down, it struck hard rock or individual large fragments of rock. A column of regolith filled the core sampler. In a helium-filled chamber, the column of sandy soil — regolith — was transferred to a collecting pan and showed no visible stratification, appearing to be uniform (Figure 2). Only a small portion of the soil in the core sample, at a depth of 35 cm, was composed of coarse-granular material. The total weight of the regolith collected by Luna 16 was 101 grams. On the whole, the regolith is a multi-granular dark-grey (blackish) powder which is easy to shape or agglutinate into individual friable lumps. The grains are either molten and rounded or angular. The granularity of the regolith increases with depth; an average grain size of 0.1 mm predominates. The numerical distribution of the grains closely follows a power law, which governs the distribution of particles in the case of repeated crushing. The median grain size in the regolith increases from the surface downward from 70 to 120 μm. On this basis,

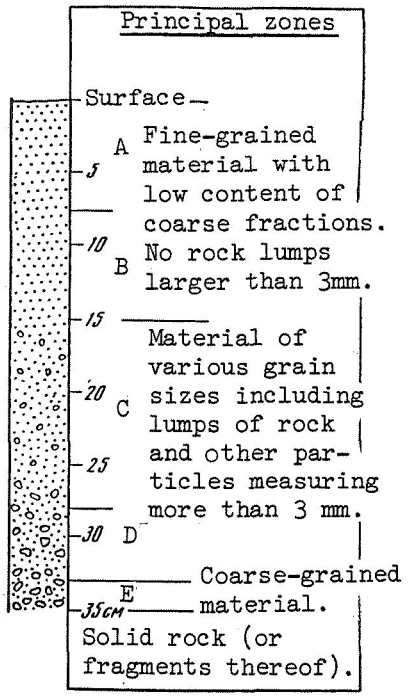

Figure 3. Schematic diagram of lunar soil core sample.

and according to the nature of the regolith core, it could be divided into several zones: A, B, C, D, and E. The regolith from each zone has been studied. Zones A and B are fine-grained material with a low content of the coarse fraction, making up 0 to 15 cm of the length of the core; C and D are composed of different grain sizes larger than 3 mm, and make up 15 to 33 cm of the core; zone E is made up of coarse-grained material and occupies 33 to 35 cm of the length (Figure 3).

Hence, the thickness of the regolith in Mare Fecunditatis at the point where the sample was collected is shallow (about 35 cm) and may possibly reach 0.5 to 1 m or slightly more when approaching the regolith in Oceanus Procellarum, where it can reach approximately 1 to 3 m, while in Mare Tranquilitatis it reaches up to 6 m. We probably still do not know the true average thickness of the regolith.

A study of the physical characteristics has indicated that the regolith has a specific gravity in natural deposits of 1.17 (1.20) g/cm^3.

Its density may be raised to 2.3 g/cm^3 by mechanical compaction. /8 The specific thermal capacity is 0.17 kcal/kg·degree, thermal conductivity is $1.9 \cdot 10^{-3}$ kcal/m·hr·degree, the specific electrical resistance is $3.42 \cdot 10^6$ ohms/meter, etc. This applies to the regolith, not in a natural deposit but with an environmental pressure of 10^{-5} torr and a stress of 160 kgf/m^2 on the regolith.

The optical properties were determined. In the case of Mare Fecunditatis, the average albedo was 0.069; near the landing site of the Luna 16 it was 0.105. A direct determination made on a sample of regolith yielded 0.107. The normal albedo rises somewhat in red light: 0.086 in the ultraviolet range, 0.126 in the near infrared and 0.107 in the visible. The reflection indices clearly show the mirror component, with the angle of maximum light reflection slightly greater than the angle of incidence. This characteristic becomes more pronounced as the wavelength of the light increases and the angle of illumination decreases.

The friable soil of the lunar maria, the regolith, reveals a highly contrasty appearance under the microscope, in comparison with friable soil from Earth. The regolith also is not similar to the ash from terrestrial volcanoes. Two basic combinations of particles can be distinguished: particles of primarily magmatic surface rocks of the basalt type, as we mentioned previously in conjunction with the data from the gamma spectra of the lunar surface, obtained by the Luna 10 unmanned probe in 1966,[1] and particles which have undergone significant transformation on the surface of the Moon. The former are characterized by a remarkable bright appearance which is observed on Earth only in freshly fractured samples of unchanged rocks (they show practically no traces of rolling and are angular in shape). The latter have definite indications of melting: sintered particles of complex shape, vitrified from the surface, a significant quantity of spherical molten formations — like congealed droplets, with a glassy and metallic appearance, similar to the "space spherules" on Earth. These particles indicate that they were formed from liquid and hardened rapidly. The regolith particles are shown in Figure 4 as they appear under the microscope, while in Figure 5 the various particles have been collected into groups: gabbro, basalt, anorthosite, breccia, slag and cinders, glass and clinker, spherules, various particles (cf. also Figure 6). Under the scanning electron microscope, one can see (Figures 7 and 8) how the coarse silicate particles

---

[1] Doklady AN SSSR, Vol. 170, No. 3, 1966, p. 561.

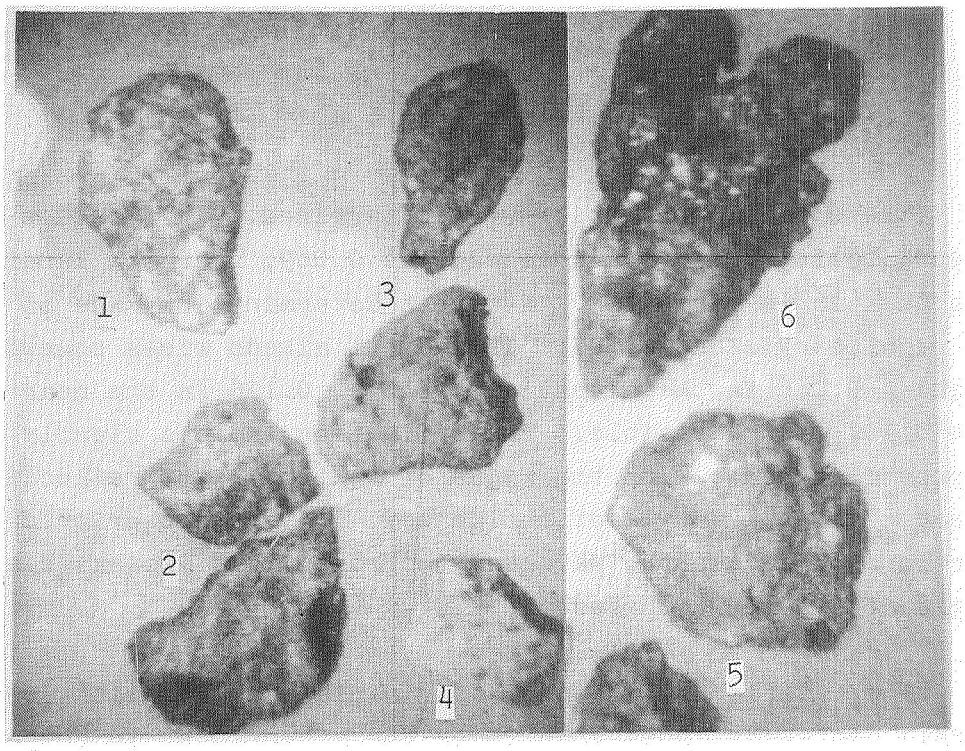

Figure 4. Large pieces of lunar rock.

1 — large-grain basalt (gabbro), leucocratic; 2 — large-grain basalt (gabbro) melanocratic; 3 — basalt, partly porous; 4 — anorthosite; 5 — breccia; 6 — molten slag particle.

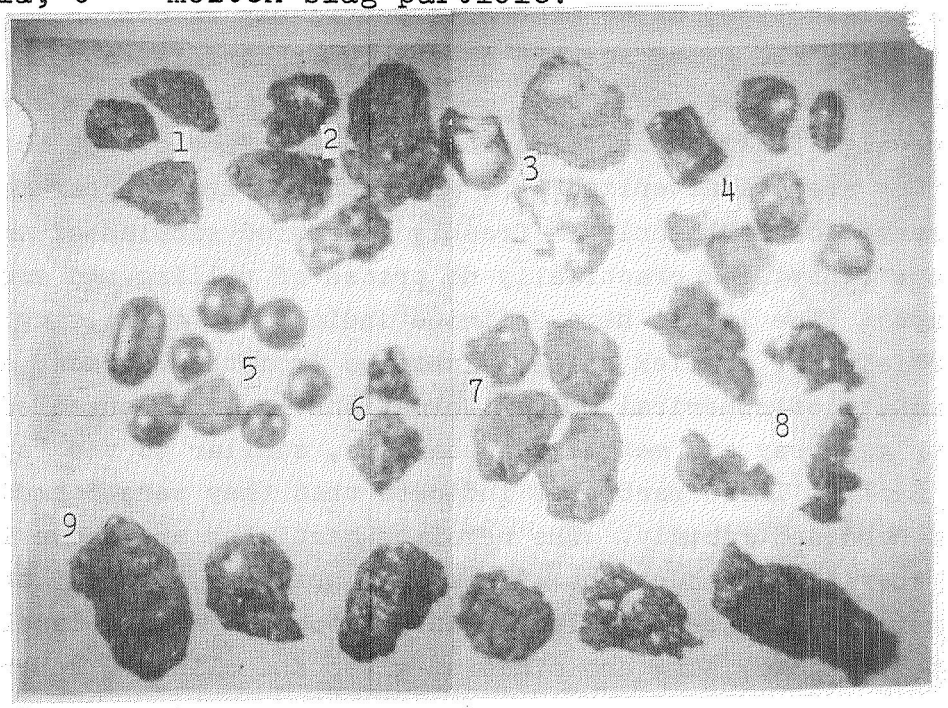

Figure 5. Groups of the most characteristic particles of lunar regolith from the +0.45 mm fraction.

1 — basalt; 2 — coarse-grained basalt (gabbro); 3 — anorthosites; 4 — uniform glasses and grains of minerals; 5 — spherules and spherical formations; 6 — turbid glass; 7 — breccia; 8 — calcined particles (clinker); 9 — slag and molten particles.

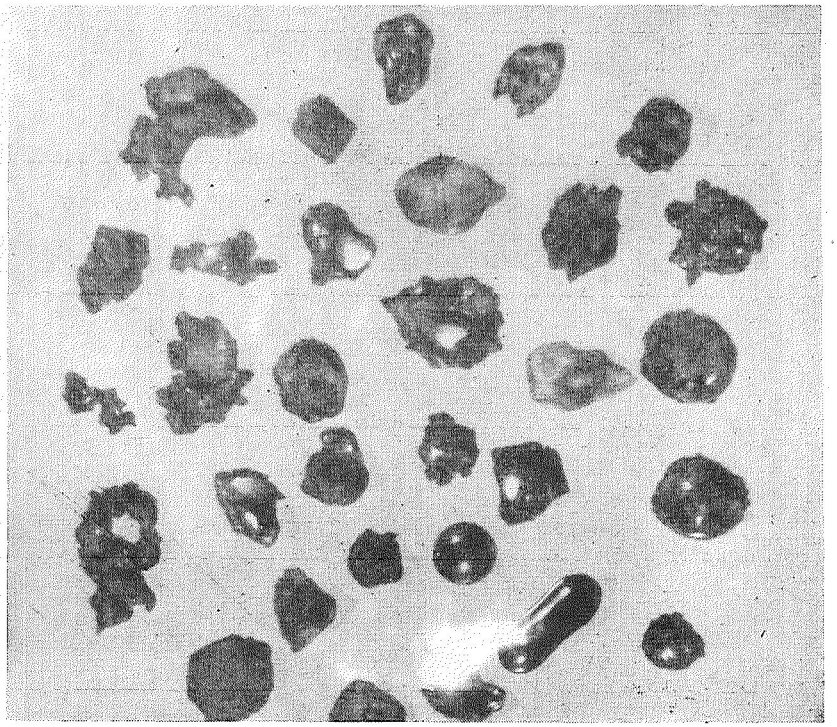

Figure 6. Various types of particles: spherules and spherical formations, glasses, clinkers.

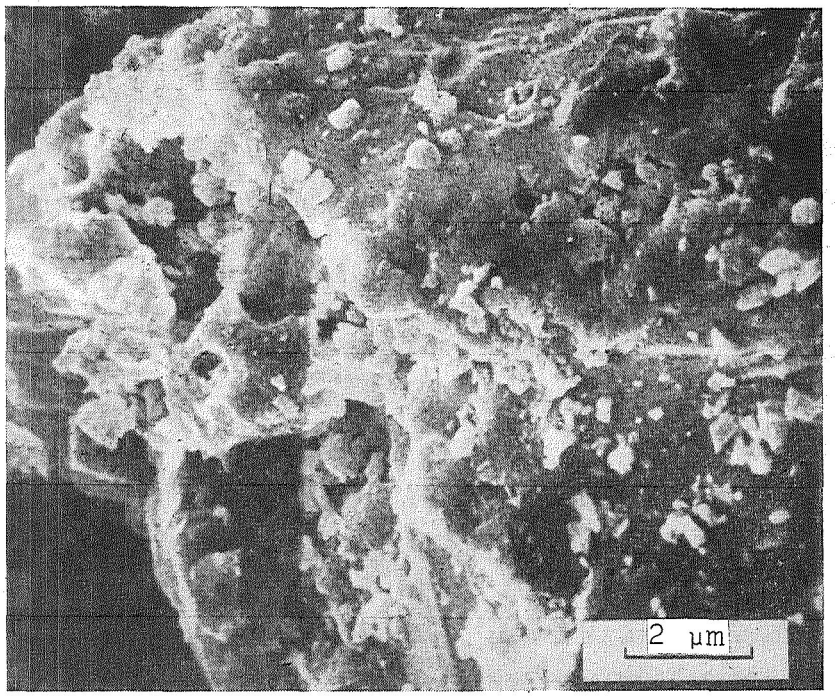

Figure 7. Scanned image of particles of the fine fraction of regolith obtained with the scanning electron microscope using secondary electrons. The large silicate particles are adhered to by the smaller ones.

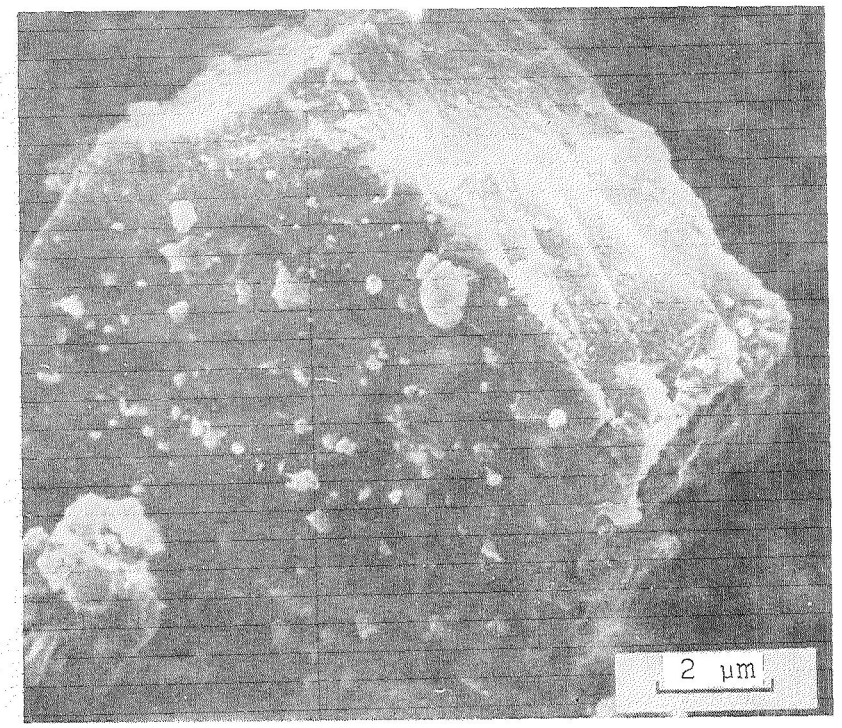

Figure 8. Scanned image of particles of the fine fraction of regolith obtained with the scanning electron microscope using secondary electrons. The large silicate particles with a cross section similar to the hexagonal and traces of protuberances on the surface are sprinkled with very fine material.

adhere to the fine fraction of other particles. The content of different particles in the regolith fraction larger than 0.45 mm is shown in Table 1.

The particles of basalt are of at least two types, characterizing the conditions of solidification of the basalt melt — fine-grained basalt (with glass) and coarse-grained basalt of the gabbroid type (Figure 9). They have an ophitic structure and make up about 1/4 of the entire coarse-grained fraction (larger than 0.45 mm). The principal materials of these rocks are plagioclase, pyroxene, ilmenite, and rarely olivine. Their relative content changes notably in various particles. Thus, we can say that a volcanic process occurred on the Moon with efflux of basalt and evidently formation of the lunar crust, whose thickness is still not known precisely.

TABLE 1

DISTRIBUTION OF PARTICLES OF DIFFERENT ROCKS BY FRACTIONS LARGER THAN 0.45 mm IN ZONES A, B, C, AND D

(PERCENT OF NUMBER OF GRAINS)

Rock	Zones			
	A	B	C	D
Gabbro	13.1	17.5	8.1	15.2
Basalt	7.3	9.0	4.9	7.9
Anorthosite	1.1	3.7	2.5	4.5
Breccia	33.9	41.4	35.5	8.3
Slags and clinkers	40.0	17.5	41.8	53.5
Glass and single grains	2.3	4.0	6.2	6.1
Spherules	1.2	1.3	1.2	1.6
Various particles	1.2	5.7	—	2.6
Total number of particles	838	297	2351	755
Weight of fraction, g	0.230	0.100	0.560	0.260

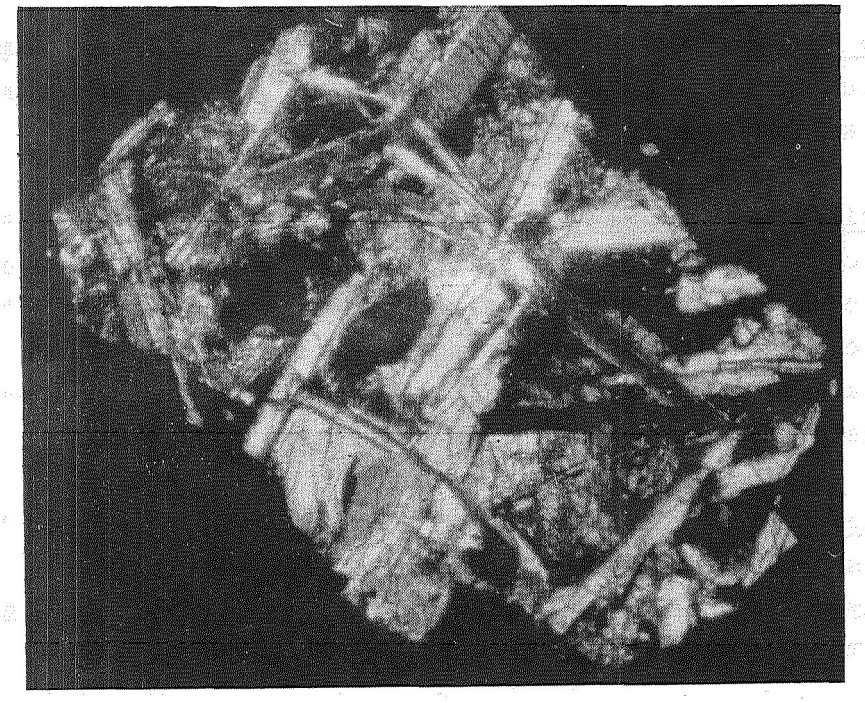

Figure 9. Section of large-grained basalt (gabbro) in polarized light using crossed nicols (enlarged). Idiomorphic grains of plagioclase and some ilmenite (black), xenomorphic pyroxene, a few extrusions of olivine.

In our opinion, this universal process of efflux of readily molten material from the Moon's core (with degassing) proceeded according to a zone melting mechanism. One finds feldspathic rocks (anorthosites), white crystalline grains. Their numbers are insignificant and their origin even on the Earth is not very clear.

Breccia — cemented, lithified rocks, formed as the result of compaction of the finely powdered material of the regolith and containing in various proportions all the components, including the particles of the primary magmatic rocks, ferronickel alloy, etc. In some breccia there has been observed a rolled form of the particles /12
and sometimes a slight compaction, which leads to their easy fracture. Breccia is magnetic; it makes up as much as 40% of the total number of particles.

Slag and cinders are fine calcined particles that form aggregates of very complex irregular branching shape. All of the components of the regolith are included in their composition.

Glass, vitrified and calcined particles make up at least half of all the particles of regolith. Depending on the composition (content of Fe, Ti, etc.), they have colors that range from dark brown to black. One sees both bubble-like slag-type melting and smooth glaze-like vitrification. This is typical lunar melting, which takes place during the instantaneous heating of a completely cold particle.

Solidified drops — spherules and similar formations are found in different shapes — pear-shaped, dumbbell-shaped, etc., and transparent, cloudy-white, greenish, yellowish-turbid and opaque. Some are hollow. Their sheen ranges from glassy to metallic; their numbers increase among the fine fractions. They are formed at temperatures far in excess of the temperature of molten rock, when they spray out in the molten state.

Finally, there are the grains of individual minerals: plagioclase, olivine, anorthite, pyroxene, spinel, ilmenite, iron particles, etc. Table 2 gives some idea of the nature of the content of various minerals in the regolith. It follows from the data in the table that the content of olivine, for example, on the whole is quite significant and approaches its content in the regolith in the Apollo 12 samples, while the olivine content in the Apollo 11 samples is much less. However, the content of ilmenite, for example, is similar to the content in the Apollo 12 samples, while there is much more of it in the Apollo 11 samples than in those from Luna 16 and Apollo 12. Olivine occurs in the regolith only in the form of individual monocrystalline fragments of irregular shape (acute-angled pieces) of different colors, as well as in the composition of gabbro particles. X-rays reveal the lack of lattice deformation and the effects of twinning, i.e., the absence of lattice stress. This is the ordinary alpha modification of olivine; it is characterized by a non-ordered distribution of magnesium and iron atoms in the structure. From the data of micro-X-ray spectral analysis of a section of a silicate particle of this /13
type, it is evident that it has the following composition (wt. %): SiO_2 — 36.0, MgO — 27.5, FeO — 33.8, CaO — 0.38, MnO — 0.29, Cr_2O_3 — 0.15, Al_2O_3 — 0.05, TiO_2 — 0.01, CoO — 0.03, NiO < 0.01, Σ — 98.2. This is a homogeneous crystal of olivine whose iron content is 40 mol. % Fe_2SiO_4 and corresponds to the molecular formula

$$[Mg_{1,11}Fe_{0,79}(Ca, Mn, Cr)_{0,02}]SiO_4.$$

The most widespread mineral in the regolith is anorthite, followed by augite and ilmenite. Anorthite is found in the form of fine-crystalline aggregates in samples of basalt, gabbro, spherules and in fine fractions of regolith. No individual single crystals were found.

Plagioclase is found also in the form of single crystals with triclinic symmetry. The pyroxenes of the augite-pigeonite type are found in pieces of rock where in many cases they play the primary role in basalt and gabbro. X-ray spectral analysis has been used to

TABLE 2

RESULTS OF MEASUREMENTS OF MOSSBAUER SPECTRA OF LUNAR MATERIAL

Material	Fraction of total area of Mossbauer spectrum of iron-containing mineral, %				
	USSR (Luna 16)			USA (Apollo 11)	
	Sample				
	A3-1	A3-3	D8-2	84-14	45-24
Ilmenite	7.7	6.7	9.2	19.7	26.9
Pyroxene	69.0	71.5	65.1	67.6	60.8
Olivine	16.8	16.7	25.5	4.4	6.1
Iron	4.5	5.1	not determined	5.8	2.1
Troilite	≤1	≤1	≤1	≤1	≤2
Magnetite	≤2	≤2	≤2	1.4	2.1

study the distribution of elements in sections of basalt, which has made it possible to identify the minerals (Figure 10).

Ilmenite is found in the bulk sample of regolith, sometimes in combination with augite. Chromium spinel has been seen in the form of single dark crystals. As far as magnetic material is concerned, micro X-ray spectral analysis can be done on Sample 3-4b. Analysis with the surface intact (without preparing a section) reveals the irregular distribution of Fe, Ni, Cr, Ti, Si, Al, Mg, and Ca. Zones can be distinguished with lithogenic elements and zones with increased concentrations of Fe (6%) and Ni (1%) (Figure 11). At some points, an iron content of up to 66% is seen, while the amount of nickel may reach 6%. However, it has not been possible to use the Mossbauer spectroscopic method to detect nickel in magnetic particles. X-ray analysis of iron particles reveals alpha-iron, i.e., kamacite. Tenite could not be found. The volume of iron particles does not reach 1% in the regolith. It is difficult to say anything definite at the present time concerning the origin of these particles. As we shall see later on, the quantity of nickel in the regolith in comparison with its content in monolithic rock (basalt) is higher in the case of the Luna 16 material and also in that from Apollo 11 and 12 by a factor of 5 on the average, while the amount of cobalt increases by a factor of 1.5 at the most. In addition, we see a very low content

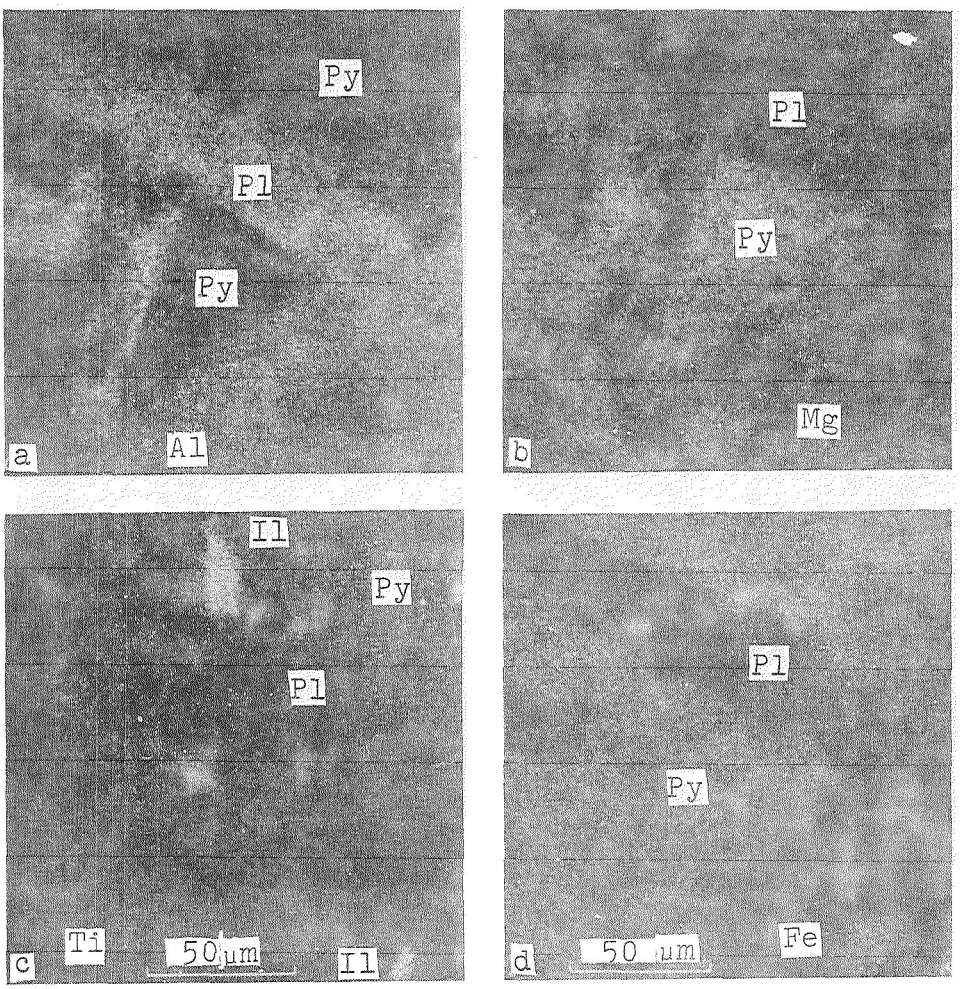

Figure 10. Photograph of portion of section of coarse-grained basalt (gabbro) obtained on X-ray microanalyzer.

a — aluminum distribution pattern; b — magnesium distribution pattern; c — titanium distribution pattern; d — iron distribution pattern. Minerals: Py — pyroxene; Pl — plagioclase; Il — ilmenite.

of platinoids in the regolith, while in the iron meteorites there are hundreds of times more of them than in the rocks. A chemical analysis was performed in parallel with the X-ray spectral analysis (mainly for the basic elements) and the mass-spectral (all elements) and spec- /14 tral as well as activation methods — selectively, for individual elements (Table 3).

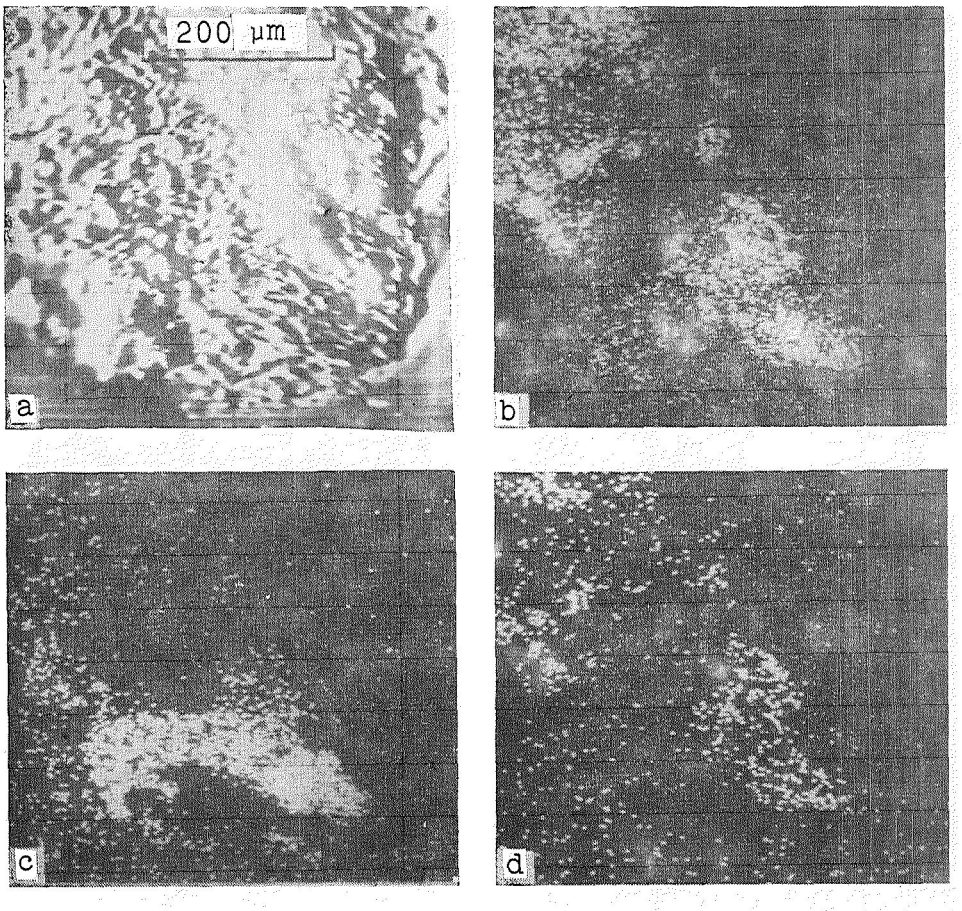

Figure 11. Scanned pictures of magnetic particle recorded on X-ray microanalyzer.

a — image with absorbed electrons; b — iron distribution pattern; c — silicon distribution pattern; d — nickel distribution pattern.

TABLE 3

CONTENT OF MACROELEMENTS IN REGOLITH FRACTION FROM ZONES A, B, C, AND D (X-RAY METHOD), wt., %

Component	Regolith				Basalt	Component	Regolith				Basalt
	A	B	C	D			A	B	C	D	
SiO_2	41.7	41.2	42.5	41.3	43.8	ZrO_2	0.015	—	0.013	—	0.04
Al_2O_3	15.32	15.40	15.45	15.15	13.65	Cr_2O_3	0.31	0.25	0.30	0.26	0.28
FeO	16.80	16.55	16.30	16.90	19.35	MnO	0.21	0.20	0.20	0.22	0.20
CaO	12.20	12.80	12.42	12.55	10.40	Na_2O	0.37	0.36	0.36	0.28	0.33
MgO	8.73	8.82	8.96	8.60	7.05	K_2O	0.10	0.12	0.10	0.10	0.15
TiO_2	3.39	3.46	3.30	3.42	4.90	S	0.19	0.20	0.18	0.25	0.17

As we can see, the variations in the principal composition of /15
the regolith on four levels were insignificant. The differences in content between the regolith and the basalt were much more striking. If we compare the composition of the Luna 16 rocks with the rock samples collected by Apollo 11 and 12, the differences are not so great on the whole, with the exception of the content of Ti, Zr and several other chemical elements that are found in the lunar rocks in small amounts (trace elements) (Table 4). Mention should be made of the high contents of F, S and Cl and other volatile elements which have dissipated away from the Moon. However, vacuoles are found in particles of regolith that may possibly contain common gases; they are being studied.

A comparison of the chemical composition of the regolith and the monolithic rocks of the three maria indicates that the material has the exact same nature everywhere, with variations in the composition of both the regolith and the monolithic rocks. The most marked difference in the composition of the Luna 16 rocks consists in the low Ti content. It is practically the same as in the rocks from Oceanus Procellarum (Apollo 12) but nearly half that in Mare Tranquilitatis. The variations in the content of Mg and Fe are small (Table 5).

The highest Zr content is found in the crystalline rocks from Mare Tranquilitatis, where there is a great deal of Ti, Y and Sc. The content of the majority of macroelements as well as Ni and many microelements in the three maria is practically the same. The Ni content in the regolith from the three maria is strikingly similar. /16 The variations in the composition of the regolith and continental rock of a given mare is of the greatest interest. These variations are repeated in the three maria. For example, the content of Fe, Ti and Zr is always higher in the continental rock than in the regolith. However, the Ni content is always higher in the regolith than in the crystalline rock. Similarities in the Ti content in the crystalline rocks and in the regolith indicate that the regolith was formed on the spot and was not conveyed from a distance (like volcanic ash). The amount of Ca increases in the regolith as does the amount of Al_2O_3.

TABLE 4

CONTENT OF TRACE ELEMENTS IN ROCKS COLLECTED BY LUNA 16 (MASS SPECTRAL DETERMINATIONS), ppm

Element	Regolith				Basalt	Element	Regolith				Basalt
	A	B	C	D			A	B	C	D	
Li*	—	10	—	10	—	Ag*	0.05	0.059	0.02	0.07	0.2
Be*	—	2.8	2	2.7	—	Cd	1	0.75	1	1.3	—
F	265	292	246	277	181	In	0.06	0.025	0.086	0.08	—
B	4.5	3.9	6	4.6	5	Ba	42	259	37	48	206
P	—	254	—	200	511	Sn	1.6	1.4	—	2	4
Sc	27	33	23.3	25	20	Sb	0.4	0.3	0.7	0.35	0.5
CL	66	74	36	72	—	Te	0.2	—	0.15	0.2	—
V	64	73.5	55.3	55	42.5	W	—	4.7	5.3	5.7	9
Co	68	56	44	61	29	Au	—	0.0013	0.003	—	—
Ni	190	137	250	178	147	Tl	—	0.2	—	0.5	—
Cu	36	39.8	35	36	13	Pb	—	6.6	7	6	7.7
Zn	10	20	33	21.5	26	I	—	—	0.26	0.14	—
Rb	3	6.3	5.5	—	—	Y	45	49	50	56	58
Sr	90	156	—	182	445	La	7.3	8	7.4	7.2	7.7
Cs	0.06	0.26	—	0.08	0.75	Ce	21	26	24	23	24.6
Zr	350	334	354	346	—	Pr	4.5	4.7	4.6	4.5	4.8
Hf	1.1	3.6	1.2	1	0.3	Nd	20	28	21	23	25
Mo	7	12	3.6	5	1.2	Sm	5.6	6.8	2.6	6.8	7.1
Ga	11	—	4.9	—	1.2	Er	1.6	1.2	1.3	1.4	1.2
Ge	1.3	1.2	1.2	1.5	2.5	Gd	6.0	4.7	4.6	5.8	4.8
As	0.4	0.36	0.6	0.3	2.9	Tb	0.75	1.0	0.9	0.9	0.9
Se	0.45	0.5	—	0.4	0.7	Dy	5.0	5.3	5.0	5.0	5.2
Br	0.26	0.27	0.24	0.33	1.3	Ho	2.0	2.2	1.9	1.8	2.0
Ru	0.03	0.044	0.01	—	6	Er	5.0	5.0	5.0	4.7	5.0
Rh	—	0.0037	—	—	—	Tm	0.4	0.4	0.4	0.4	0.4
Pd	0.0086	0.012	—	0.01	0.027	Yb	3.4	3.6	3.5	3.5	3.6
						Lu	0.28	0.3	0.3	0.3	0.3

*Spectral determination.

TABLE 5

COMPARISON OF COMPOSITION OF REGOLITH AND CRYSTALLINE ROCKS FROM THREE MARIA

Component	Crystalline rocks			Regolith		
	Area where collected					
	Mare Tranquilitatis, Apollo 11	Oceanus Procellarum, Apollo 12	Mare Fecunditatis, Luna 16	Mare Tranquilitatis, Apollo 11 (average)	Oceanus Procellarum, Apollo 12	Mare Fecunditatis, Luna 16 (average)
	Weight percentages					
SiO_2	41	40	43.8	43	42	41.7
Al_2O_3	12	11.2	13.65	13	14	15.33
TiO_2	10	3.7	4.9	7	3.1	3.39
FeO	19	21.3	19.35	16	17	16.64
MgO	8	11.7	7.05	8	12	8.78
CaO	10	10.7	10.4	12	10	12.49
Na_2O	0.5	0.95	0.38	0.54	0.4	0.34
K_2O	0.12	0.065	0.15	0.12	0.18	0.10
MnO	0.4	0.26	0.20	0.23	0.25	0.21
Cr_2O_3	0.6	0.55	0.28	0.37	0.41	0.28
ZrO_2	0.1	0.023	0.04	0.05	0.09	0.013
NiO	(0.007)	—	0.04	0.03	0.025	—
	ppm					
Rb	2.5	0.64	—	2.2	3.2	5.9
Ba	90	72	206	68	420	114
Sr	110	145	445	90	170	169
Yb	2.5	—	3.5	2.5	—	3.5
Y	250	51	54.0	130	130	58.0
Zr	700	170	300	400	670	347
V	45	88	42.5	42	64	61
Sc	110	50	20	55	47	27
Ni	55	54	147	250	200	190
Co	9	40	29	18	42	53
Cu	5	—	13	—	—	37
Li	15	5.5	—	15	11	10*
Ga	6	—	11	—	—	4.9

*Spectrally, all others mass-spectrally.

Hence, the regolith is enriched with plagioclase and impoverished with respect to pyroxene, olivine, ilmenite (and spinel), i e., the crystalline rocks are more maphic than the regolith. The rare lithophilic elements are usually found in the crystalline rocks of Mare Tranquilitatis: Y, TR, Zr, Cr, and Th and U as well (Table 6).

TABLE 6

CONTENT OF Th AND U, ppm

Element	Regolith			Crystal ro ks		
	Apollo 11	Apollo 12	Luna 16	Apollo 11	Apollo 12	Luna 16
Th	2.24±0.06	6.0±0.6	0.474±0.05*	2.9±0.4	0.88±0.09	1.4±0.1*
U	0.59±0.02	1.5±0.2	0.1±0.01*	0.7±0.1	0.24±0.0035	0.2±0.02*
Th/U	3.8	4.0	4.7	4.0	3.7	5.7

*Determined mass-spectrally

We have already called attention to the low content of platinoids and gold in the regolith. We still do not have a great deal of data in this regard, but the following distribution of platinoids and gold can be seen in the lunar rocks (Table 7).

TABLE 7

DISTRUBUTION OF PLATINOIDS AND GOLD IN LUNAR ROCKS, ppm

Rock	Pt	Pd	Ir	Ru	Rh	Au
Terrestrial basalt	0.02	0.02	—	—	—	0.004
Lunar crystalline rocks collected by Apollo 11	—	0.006*	0.01	—	—	—
Apollo 11	—	0.1**	0.0001	—	—	0.0016**
Apollo 12	—	—	0.0013***	—	—	0.0011***
Luna 16	—	0.027	—	6.3	—	—
Regolith collected by Apollo 11	—	0.04**	—	—	—	0.0021****
Luna 16	—	0.01	—	0.027	0.0037	0.002
Iron meteorites	12.0	3.7	2.8	—	—	1.0

*Baedecker, Wasson — Science, 1970, 167, N 3918.
**Morrison, et al. — Science, 1970, 167, N 3918.
***Laul, et al. — Earth and Planet. Sci. Lett., 1970, 9, N 2.
****Wanke, et al. — Science, 1970, 167, N 3918.

The determination of all the rare earths is not yet complete. The isotopic analysis of Li^7/Li^6 for the regolith is 12.28; K^{39}/K^{41} — 14.00 ± 0.18; Rb^{85}/Rb^{87} for an average sample is 2.57 ± 0.04, i.e., the isotopic composition corresponds to that of these elements on Earth. On the other hand, for example, a disruption of the isotopic composition has been observed for lithium in meteorites.

As we know, shearing products are produced in rocks under the influence of the "solar wind." They have been observed in the regolith — Na^{22}, Al^{26}, etc. For example, Al^{26} yields 173 ± 113 dis- /17
integrations/minute/kilogram. This work is continuing and we hope to have data on both the zone A fraction and the zone D fraction from the deeper part of the regolith core. This would make it possible to explain more.

It is interesting to mention in this connection that the infrared spectrum of the regolith has revealed the presence of a broad unstructured absorption band in the region of the oscillations of the silicate bonds. Calcination of the regolith sample in an argon atmosphere up to 1000° C leads to the appearance in the IR spectrum of a distinctive structure — individual bands associated with the absorption of isolated and combined SiO_4 groups, framework silicates, etc. Consequently, we can assume that there has been an irradiation of the regolith material and the possible changes that occurred as a result of this are removed by calcination.

The "solar wind" acts on the rock, causing its metamictization and the formation of shearing products to a shallow depth, about 3 — 5 cm. Hence, we decided to measure the activity both in the upper layers of the regolith and in its base. The results may explain the history of the accumulation of the regolith.

The regolith contains inert gases of unusual composition; the /18
latter is independent of the depth of the regolith (the regolith sample is from zone D) (Table 8).

TABLE 8*

CONTENT AND ISOTOPIC COMPOSITION OF INERT GASES IN DUST SAMPLES (IN 10^{-8} cm^3)

Isotopes	Mare Fecunditatis sample D-7	Apollo 11		
		Schaffer, Zahringer	Reynolds	Hindenberger
He^4	18000000	11000000- 19000000	29000000	9000000
He^4/He^3	2670	2540	2130	2770
Ne^{20}	340000	313000	530000	125000
Ne^{20}/Ne^{22}	12.80	12,4	12,85	12,6
Ne^{21}/Ne^{22}	0.0352	0,0340	0,0332	0,0332
Ar^{40}	53000	38500	57000	56000
Ar^{40}/Ar^{36}	0.98	1,1	1,126	3,04
Ar^{36}/Ar^{38}	5,26	5,20	5,19	5,08
Kr^{84}	22	21	37	8,5
Xe^{132}	8.5	10	4,6	2,2

*[Translator's Note: Commas represent decimal points.]

The predominant component of the gases is the gases of the "solar wind." Their composition differs sharply from that of terrestrial gases and gases from meteorites. The concentration of the gases is very high, several orders higher than in terrestrial objects and in meteorites. The He and Ne contents are about the same as in several meteorites that are rich in neutral gases. They are usually distinguished by an isotopic composition with Ar — for example, $Ar^{40}/Ar^{36} \sim 1$, and $Ar^{36}/Ar^{38} \sim 5.25$ corresponds to that on Earth. The amount of Ar^{40} is 4 to 5 times greater than the amount which could be formed in the rocks as a result of the decay of K^{40}. The isotopic composition of Xe also differs from that on Earth and is being investigated further. On the basis of the content of inert gases, the substance of Mare Fecunditatis is closer to the regolith of Mare Tranquilitatis. The first determinations of the age of the Moon have been made using the Rb/Sr method and the fine fraction of the regolith, which gave a figure of $(4.85 \cdot 10^9$ to $4.25 \cdot 10^9) \pm 0.75 \cdot 10^9$ years. The average along the isochron is 4.45 and $4.65 \cdot 10^9 \pm 0.5 \cdot 10^9$ years. Hence, the samples from the three maria are very similar in absolute age, i.e., the age of the Moon corresponds to the age of the Earth. The same values are obtained according to Pb^{206}/Pb^{207}. The age according to the K/Ar method is difficult to calculate. The exposure time of the regolith is of particular interest.

Hence, the lunar rocks from the three maria are of a single common type (basalt), and the variations in their composition are a function of the conditions of their melting, while those of the regolith are due to its somewhat different history.

The rocks from Mare Fecunditatis, as we have seen, resemble those /19
from Oceanus Procellarum. However, they resemble the regolith of Mare Tranquilitatis, for example, in their content of neutral gases in the regolith.

Let us formulate some preliminary concepts. It is still premature to make a conclusive statement regarding the nature of the processes on the lunar surface. We shall limit ourselves to the data obtained from the study of the rock samples brought by Luna 16 from Mare Fecunditatis and naturally compare them with the data collected on the flights of the Apollo 11 and 12. The material from all three maria — Mare Tranquilitatis, Oceanus Procellarum and Mare Fecunditatis — is surprisingly similar in its petrological, mineralogical and chemical composition. The vast lunar maria, located along the Moon's equator, are depressions that were flooded with basic lava at some time in the past. Long ago, during the era of intensive volcanic activity, an enormous mass of basalt flowed out onto the lunar surface, accompanied by the dissipation of gases. Depending on the conditions of the eruption, the depth, temperature, etc., the basalt surface rock on the Moon differs in terms of the content of Fe, Ti, Zr, Ba and other elements. The iron content of the magma was not the deciding factor in this endogenic process. It is possible that rocks will be found on the Moon which are derivatives of basalt (anorthosites, rhyolites). We do not know exactly the depth of the basalt crust of the Moon. The absolute age of the surface rocks of the Moon (rather, the age of the Moon) is practically the same as that of the Earth. The lunar maria are covered by a layer of regolith. Its thickness is evidently quite variable, and in Mare Fecunditatis, at the site where the Luna 16 sample was collected, it was a maximum of 0.5 meter. The limits of variation probably amount to several meters. As we have already seen, the regolith is an inhomogeneous

mixture of grains of rock, minerals of various sizes, shapes and colors — both molten and particulate. With depth, the ratios between the various grains change, although no stratification of the material can be seen. This material is the result of powdering of rock under the influence of high temperature, causing the formation not only of molten particles of regolith but of spherules as well. The regolith does not resemble the volcanic ash from terrestrial volcanoes. As we have seen, the composition of the regolith differs slightly from the composition of the lunar crystalline rocks. It contains a reduced amount of maphic elements, and consequently must be more molten than the primary basalt. Before touching on the problems of the formation of the regolith, let us recall the main factors of lunar "erosion." First of all, there is the temperature variation of the lunar surface rocks in the course of billions of years, from lunar day to lunar night — over a temperature range of ± 100° C. Then there is the irradiation of the surface rocks of the Moon by the "solar wind" and the galactic cosmic radiation. Furthermore, there is the vacuum in which the lunar rocks are located; finally, the possible impacts of meteorites are involved as well. Probably the temperature drop of the surface rocks on the Moon has some effect on their hardness, but we are not in any position to measure this at the present time. /20

The "solar wind" and galactic radiation have a much more significant effect. First of all, it would seem from our observations that the entire regolith shows signs of the influence of the "solar wind" to a depth of 35 cm. In a sample from zone D, the regolith contained an enormous amount of solar neutral gases.

Then the infrared spectrum of the regolith indicates that it has been irradiated. We must await the determination of the radioactive products of splitting from the deep layers of the regolith. All of this is a preliminary indication either of the displacement of the regolith at the site, or the fact that the history of its formation is written in its strata. Radiation does not penetrate deeply; it only passes through the first few centimeters of soil. On the basis of the observations and study of the so-called metamiction in minerals

containing radioactive elements, we can conclude that they lose hardness and undergo deformation of their crystal lattices. However, this usually does not lead to a complete disruption of the minerals. We are attempting to detect metamiction in particles of regolith. In addition, radiation begins to have an effect, especially when the mineral is already fractured. Hence, during the crumbling of the material, the "solar wind" does not participate directly in the formation of the regolith (melting) and does not affect the strength of the material. Usually the formation of the lunar maria and consequently the regolith in particular, which fills them, is linked to the action of falling meteorites and their impacts. It is interesting to think of the fall of a swarm of meteorites on the side of the Moon that faces the Earth in the region of the present lunar maria, which are located along the equator. Why did they fall in swarms only on the visible side of the Moon, the most convex part that faces the Earth? This is difficult to explain. The most reliable proof of the "work" of meteorites would be their observation on the lunar surface. However, meteorites and micrometeorites strike the Moon at cosmic velocities. Experiments and calculations show that 1 gram of meteorite substance under these conditions would be capable of excavating an amount of lunar rock that is 2 — 3 orders larger, pulverizing it, etc. The rock particles would strike with enormous velocities (over a broad spectrum). Some could escape from the Moon, breaking free of its gravity, and reach the Earth (for example, eucrites). We must always keep in mind this situation with the balance of matter on the Moon, when trying to find an explanation for the formation of the regolith. However, some portion, admittedly very small, of the meteorite substance will remain on the lunar surface. Earlier, we presented preliminary data on finding meteoritic material in the regolith. It will undoubtedly be found. But this is far from being a sufficient explanation of the formation of all the regolith on the Moon.

The most striking fact about the endogenic process of the eruption of basalt on the Moon is the instantaneous contact with the vacuum of space. The lunar magma reaches the crust and breaks through. The liquid magma and its gases burst out into a vacuum. There must

be a spraying of the liquid magma and a simultaneous loss of its gas and other volatile components. It would be desirable to find on this "endogenic track" the explanation for the origin of the regolith by conducting appropriate experiments. This is especially true, because the main question regarding the nature of the balance of the lunar material is critical to an understanding of geochemical processes on Earth, especially during the first billion years of its evolution.

N74-19477

THE PROBLEM OF THE STRUCTURE OF THE SURFACE OF THE LUNAR MARIA

/21

K. P. Florenskiy, A. T. Bazilevskiy, A. A. Gurshteyn, R. B. Zezin, A. A. Pronin, V. P. Polosukhin, Z. V. Popova and I. M. Taborko

ABSTRACT. The paper describes the results of geological and morphological interpretation of large-scale photographs of the surface of lunar maria. A morphological classification is proposed for small craters. It is shown that the classification of a crater in a given morphological category, reflecting the degree of its morphological maturity, is determined by the age of the given crater. A check on the nature of distribution of small craters, as done on the basis of the "nearest neighbor" method, showed that the distribution is governed by a near-random law. It is found that variations of the probability density function for the craters conform to a normal distribution law. An empirical relation is found for the coefficient of variation as a function of crater diameter and the dimensions of the area on which the counts are made. The rockfalls near craters of various morphological classes are described.

Nowadays there is no question of the geological complexity of the Moon and the multiplicity of the stages of formation of its surface. It has been established that the plains of the lunar maria were created primarily by enormous lava flows of the basalt type [1 — 4]. There is obviously no doubt of the multiplicity of the stages of these flows, although the difference in the ages of the maria requires further study.

Experience from terrestrial geology indicates that the melting of basaltoid material from primary material is accompanied by crystal-

lization differentiation and proceeds according to the principles of zone melting [5 — 8]. From this it follows that the Moon is not homogeneous within the maria and has at least a two-layered structure, while the basalt crust overlies a mantle material with a different composition [9]. One external manifestation of the two-layered nature of the Moon in the plains of the lunar maria is the so-called mascons, i.e., local concentrations of mass which produce inhomogeneities in the gravitational field of the Moon [10]. Although their nature is still not interpreted unambiguously [10 — 12], the most logical theory holds that they are linked to irregularities in the crust-mantle interface.

The nature of the lunar continents is likewise not uniformly interpreted. One viewpoint [13] holds that the lunar continents are the product of further differentiation of the original substance, and the rocks composing them are more acid. This interpretation is based on an analogy with the Earth and derives from isostatic concepts which require at least a three-layered planetary structure of the continental regions, which is not very likely. Another group of researchers holds the directly opposite view and considers the lunar continents as the least reworked part of the Moon, essentially not having undergone the stage of planetary differentiation [9]. Evidently the relative structural antiquity of the continents with respect to the maria is not a source of dispute. There is a theory that a significant portion of the continents constitutes subsequent complication of the tectonic history of the surface of the most ancient of the maria [14] of another generation. It is also beyond doubt that the surface of the Moon shows everywhere the traces of meteoritic activity.

Hence, the old dispute (still unresolved today) between the proponents of the volcanic and meteoritic hypotheses has largely lost its central significance and revolves not so much around the planetary structure of the Moon as around the mechanism that caused the unleashing of internal stresses and the structure of individual details of the Moon's surface relief. At the present time, the most important task we face is the establishment of concrete relationships between the exogenic and endogenic processes in various stages of the Moon's existence.

A very important contribution to the knowledge we have regarding the history of the Moon is the data on the absolute and radiational age of rocks in Mare Tranquilitatis, Oceanus Procellarum and Mare Fecunditatis, obtained in the study of the samples collected by the Apollo 11 and 12 expeditions and the Luna 16 automatic probe. /22

It has been established that the rock samples from these areas, which belong to one of the geologically young formations, have an absolute age of 3 to 4.5 billion years and the time of their existence on the surface (radiational age) has been set at tens and hundreds of millions of years. By means of these findings, the geological history of the Moon has essentially been shifted to the initial periods of the formation of the solar system, which sharply reduces the probable significance of later processes. At the same time, the study of the Moon is acquiring particular significance for the geology of the Earth, leading to the development of a theory of the initial stages of the Earth's history which, in contrast to the situation on the Moon, have been concealed by subsequent processes mainly having the nature of the cycle of matter.

Concepts regarding the early phases of differentiation of the planets, occurring during the time of their growth by accretion, and regarding the general negative balance of material of the Moon in the modern stage [15] have acquired particular importance for an understanding of the history of the Moon. Consequently, processes of exposure of ancient rocks may predominate in the course of the development of the Moon, rather than their burial by more recent exogenic formations. The young formations may be destroyed first, and their role may remain undetermined.

The enormous amount of new factual material that has been collected as the result of space research in recent years is still undergoing analysis for the most part. Attempts at a broad generalization of the material are still contradictory in nature, most likely indicating a certain degree of prematurity and the necessity for a more careful study of them.

The present work contains some results of an analysis of the photographic materials obtained with the aid of spacecraft in the course of American as well as Soviet investigation. The objects selected for study were the geologically most uniform areas of the lunar maria, the idea being to obtain data approximating the average characteristics of the maria surfaces for the purpose of developing general concepts regarding their nature, required for a subsequent study of specific features of the structure of individual regions. These areas each covered an expanse of several hundred square kilometers. The first is located in Oceanus Procellarum, 110 — 120 km southeast of the crater Reinhold; the second is also in Oceanus Procellarum, 125 km south-southwest of the crater Encke; the third is in Sinus Medii, and the fourth in Mare Tranquilitatis, 120 km east of the crater Sabine. In the course of performing several aspects of this work, data were also collected on other regions of the equatorial zone and on isolated regions in Mare Imbrium.

Craters

Among the subtelescopic elements of the relief of the lunar surface, the dominant role is played by craters of various sizes. In this paper, it is mainly the craters with diameters of 10 to 600 m that are studied. In the following, we shall discuss the results of a study of the morphology of the craters, the nature of their distribution on the surface, the number of craters of a given size per unit area of surface, and the nature of the variations in this parameter.

Crater Morphology

As a result of the study of the pictures taken of the lunar surface by the Luna 12 and Lunar Orbiter spacecraft, a morphological classification of the small craters has been devised [16]. It classifies the craters on the basis of two characteristics. The /23
morphological types are determined on the basis of the geometric shape. Morphological classes are organized within each type on the basis of their prominence in the relief. Pictures of craters

belonging to different morphological types and classes are shown in Figure 1, while Figure 2 shows typical profiles through these craters.

The following are the results of observing the details of sub-telescopic objects which are primarily relief-forming forms in areas of this type. These forms are represented by the craters for the macro- and mesorelief, and by craters and stones for the microrelief.

Among the craters of the size investigated, one can distinguish at least four morphological types that differ markedly in shape: cup-shaped, or spherical (ω), conical (γ), flat-bottomed (α), and craters with a double wall, or concentric (φ).

The cup-shaped ω-craters, whose form may be approximated by a spherical segment, predominate among the craters, usually comprising no less than 80 to 95% of the total. Hence, the general statistical features established without mention of the type of crater largely refer to them in particular. They are usually interpreted as craters of impact-explosive origin and are found over the entire investigated range of craters.

The conical γ-craters make up approximately 3 to 10% and are found primarily among smaller craters that are several meters in diameter (up to 50 m). They have the greatest relative depth with respect to craters of other types, and the ratio of the diameter to the depth D/H reaches 3.5. Usually they lack a clearly defined ring-wall. It is assumed that these craters may have either an impact-explosive or sink origin.

The flat-bottomed α-craters are scattered among the larger craters with diameter of hundreds of meters. Their total number usually varies between 5 and 15%.

Craters with a double ringwall, or the concentric φ-variety, are the rarest type and number less than 3 to 5%. In some individual cases, it appears that the doubling of the ringwall is associated with landslide phenomena.

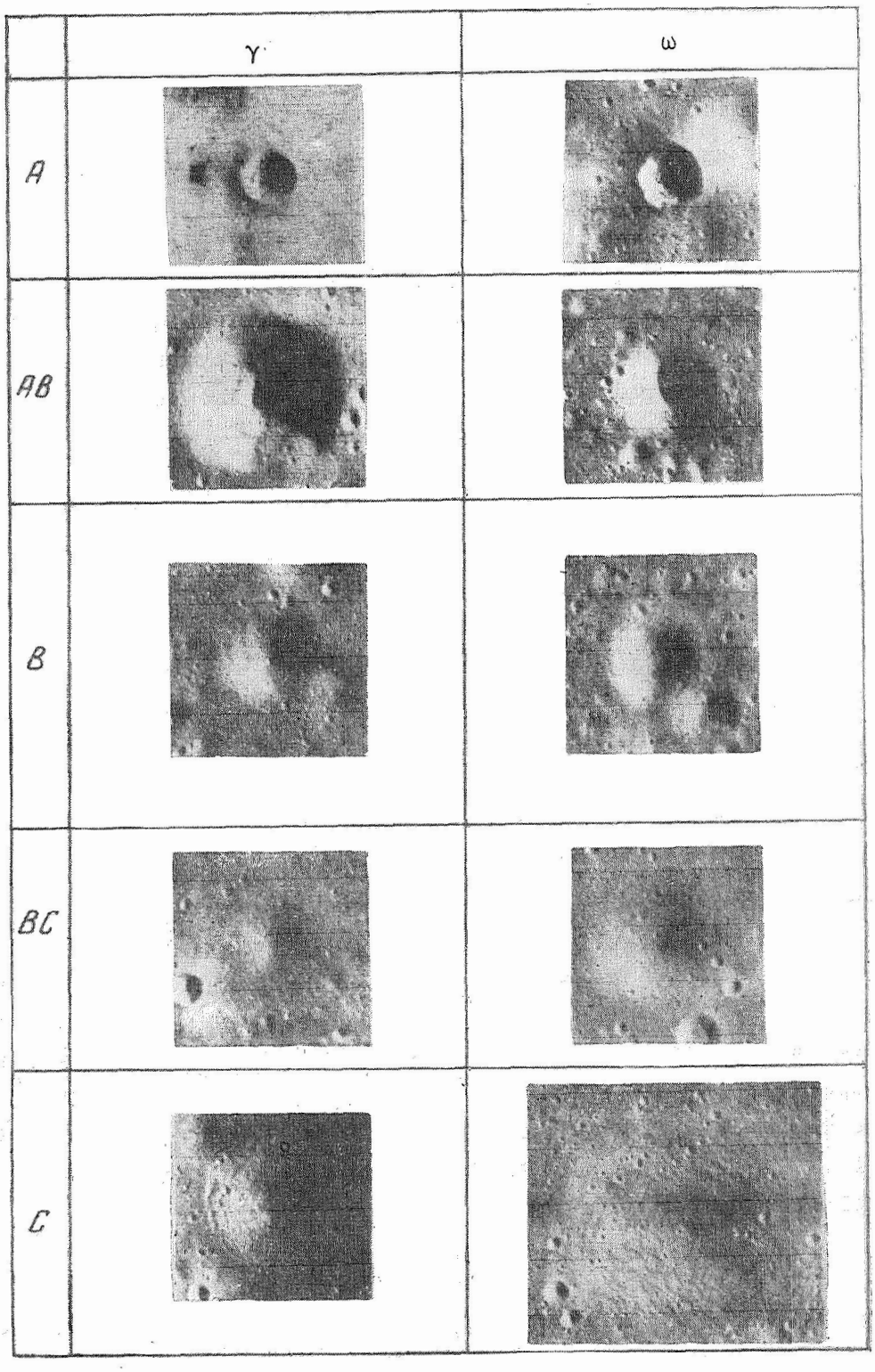

Figure 1. Photographs of typical craters of different groups, classified on a five-point scale.

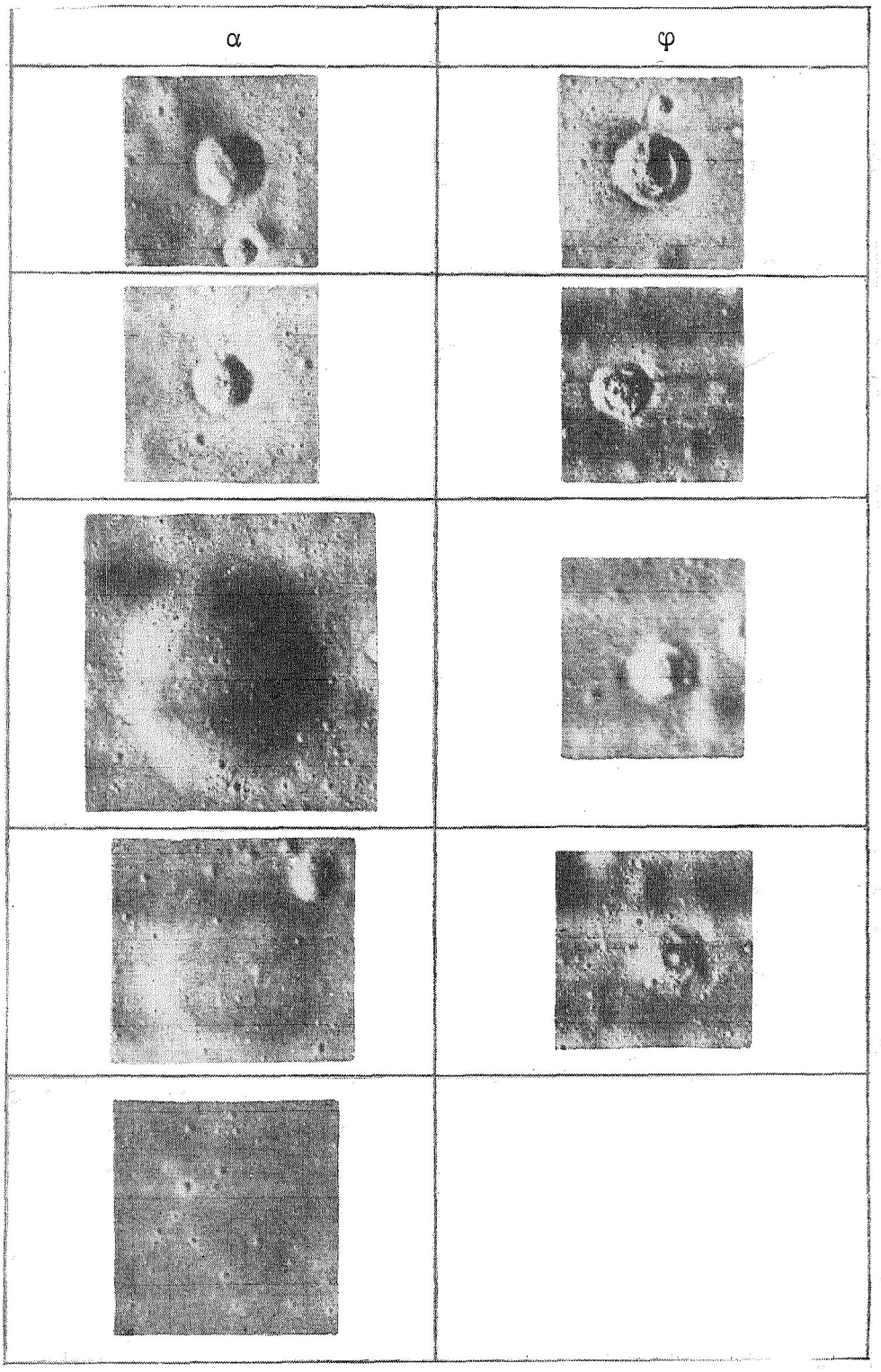

Figure 1 (Continued).

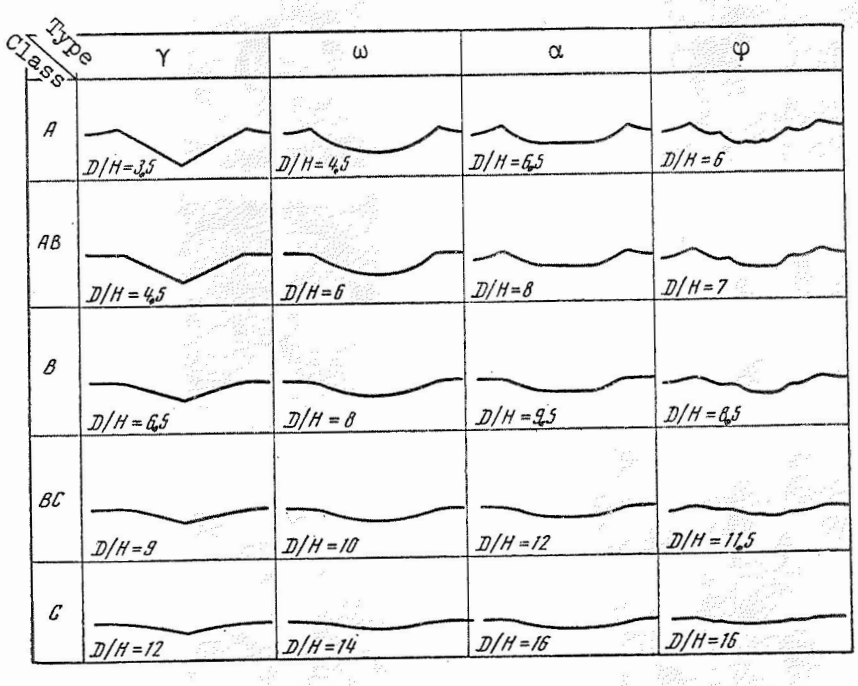

Figure 2. Typical profiles of craters in different groups on a five-point scale.

In general, a clearly defined ringwall is found in comparatively few craters. The frequency of craters with ringwalls varies markedly for different parts of the surface and makes up 5 to 25% of the total number of craters.

Craters of all types may vary considerably with respect to the clarity of definition of their outlines and depth. As a matter of fact, they form a continuous series: from the most clearly defined forms to complete blurring and merger with the general irregularities in the surface relief. A detailed morphological investigation breaks this series down into five complete classes: three basic ones A, B and C, and two intermediate ones — AB and BC. The intermediate classes can be defined advantageously only in a special study of photographs with a sufficiently low position of the Sun.

Dividing the craters into classes has been performed visually with consideration of the nature of the transition in phototones at the boundary between the illuminated and dark areas in pictures taken with the Sun at various elevations above the Horizon, varying from 7 to 30 degrees.

The depth and diameter of the craters were determined from the Lunar Orbiter pictures on a scale of approximately 1:10,000 with the Sun at an elevation of 13 degrees, using the example of 60 specially selected typical craters with diameters from 14 to 410 meters (Table 1). Using the five-class division of craters, the characteristic intervals have the appearance shown in Table 2. Using selected prototypes, specific craters were compared and assigned to the corresponding classes. The divergence in the treatment of the shapes of the craters /26 and their assignment to various classes on the basis of various identifying features in the photographs of different quality did not exceed ±15% of the number of craters of any given class. In the case of craters with ringwalls, the depth H was calculated from the lip to the floor of the crater, i.e., the height of the ringwall was not computed from the calculated depth of the crater.

TABLE 1

CHARACTERISTIC D/H INTERVALS FOR VARIOUS MORPHOLOGICAL CLASSES OF CUP-SHAPED CRATERS

A craters		B craters		C craters		A craters		B craters		C craters	
D, m	D/H	D, m	D/H	D, m	D/H	D, m	D/H	D, m	D/H	D, m	D/H
14	6.0	26	9.0	20	17	65	6.5	118	7.5	83	21
18	6.0	28	9.5	25	20	65	6.0	130	7.5	128	11
20	7.0	28	10.0	27	18	100	6.0	145	8.0	160	9
23	3.5	32	8.5	38	13	110	6.0	160	8.0	164	11
25	6.0	38	7.0	42	16	350	5.0	160	8.0	200	12
27	6.5	42	8.5	50	25	365	6.5	170	7.0	311	13
30	5.5	50	7.0	52	14	410	6.0	175	9.0	—	—
35	7.0	50	8.0	54	13	—	—	180	9.0	—	—
38	4.5	60	6.0	58	19	—	—	185	7.0	—	—
40	7.0	66	8.5	64	10.5	—	—	200	8.0	—	—
46	6.5	70	9.0	80	13	—	—	230	6.0	—	—
61	5.5	75	7.5	83	14	Assumed average value	6		8		16

TABLE 2*

D/H RATIO FOR VARIOUS TYPES AND CLASSES OF CRATERS ON A FIVE-POINT SCALE

Class	Type									
	Cup-shaped		Conical		Flat-bottomed		Concentric		Average	
	Max. D/H	Av. D/H	Max. D/H	Av. D/H	Max. D/H	Av. D/H	Max. D/H	Av. D/H	Max. typ. D/H	Av. D/H
A	4—6	4,5	3—4	3,5	5,5—7	6,5	5—7	6	3—7	5
AB	5—7	6	4—5	4,5	6,0—10	8	6,5—8	7	4—8	6,5
B	6,5—9	8	4,5—7	6,5	6,5—12	9,5	7—10	8,5	6—10	8
BC	8—12	10	6,5—11	9	10—14	12	9—14	11,5	6,5—12	10
C	>11	14	>10	12	>12	16		16	>11	More than 14

*[Translator's Note: Commas represent decimal points.]

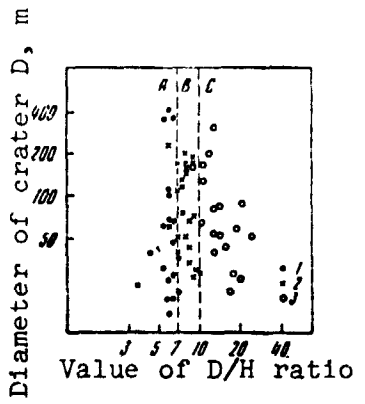

Figure 3. Value of D/H ratio versus diameter for various morphological classes of craters.

1 — A craters; 2 — B craters; 3 — C craters.

The most representative measurements were those for craters with diameters from 20 to 200 meters, whose results are considered typical. It was found that, within the sizes investigated, the variation in the diameter of a crater did not have a significant effect on the D/H value (Figure 3). Division of the craters into morphological classes was based on the following criteria (see Table 2). /27

Class A is composed of those craters which usually have external walls with prominent relief and a clearly marked ridge. Characteristic examples of craters of this class are shown in Figure 1. In the absence of walls, Class A craters are characterized by a sharply outlined lip on the inner slope. The majority of the Class A craters are characterized by accumulations and splashes of stones which are concentrated both inside the crater and around it. Among the craters of similar diameter, the Class A

craters are characterized by the least depth and consequently the lowest D/H ratio, which is approximately 5 on the average (cf. Figures 2 and 3).

Class B craters are marked by less clear shapes: the lips of the ringwalls and the inner slopes of the craters are smoothed off, the ringwalls themselves are not very pronounced (cf. Figures 1 and 2). The numbers of stones inside and outside the craters are markedly less than in the Class A craters. The D/H value is approximately 8.

Class C is composed of craters with blurred, hard to define outlines (cf. Figures 1 and 2). The ringwalls (if they indeed exist) are so difficult to make out that it is not considered possible to define their outlines exactly. Stones are rarely found in craters of this class or around them, and only in small numbers. The D/H ratio is 16 on the average. The assignment of craters to Class C is largely dependent on the image quality of the picture of the surface and the altitude of the Sun above the horizon.

The relative distribution of craters of various classes may vary from one region to another and with a change in crater size. Estimation of this parameter calls for massive crater interpretation with /28 the parallel task of performing several interpretations on pictures of the surface which have uniform contrast. The results of this work will be presented in an article to follow; here we shall present only the preliminary estimates. Using a five-point crater classification system, the most typical values for the frequency of occurrence of morphological classes are shown in Table 3. With a three-class system, the values shown in Table 4 were obtained.

Hence, in studying the distribution of the craters by classes, it is still necessary to limit ourselves to the following conclusions:

1. A common feature is the marked predominance of Class B and C craters over Class A over the entire crater diameter range from 60 to 440 meters.

TABLE 3

NUMBERS OF CRATERS OF DIFFERENT CLASSES IN THE 60 — 440 METER SIZE RANGE ON THE FIVE-POINT SCALE (IN %)

Class	Maria region	
	Typical variations of values	Rough distribution
A	0.8 — 2.6	1.5
AB	0.8 — 3.3	2
B	14 — 17	16.5
BC	20 — 30	26
C	50 — 61	54

TABLE 4

NUMBERS OF CRATERS IN THE 60 — 440 METER SIZE RANGE DIVIDED INTO THREE CLASSES IN SELECTED AREAS (IN %)

Class	Maria region	Sinus Medii
A	3	4
B	15	17
C	82	79

2. The ratio of craters of different classes changes in various regions. This is evidently governed by the regional conditions of crater formation.

The nature of the interrelationships of the craters with different morphological classes indicates that the prominence (class) of a crater is determined primarily by its degree of preservation. Hence, Class A are the youngest craters with fresh forms, Class B are mature craters with incipient destruction of the initial formations, and Class C are the oldest craters with forms that are smooth and considerably broken down.

To support this hypothesis, the mutual locations and cross sections of craters were compared for different classes in one of the regions of Oceanus Procellarum [17]. A total of 235 mutual cross sections of craters were studied with a clear relationship between the sections. Then they were grouped according to the different ratios of the diameter of the "intersecting" craters to the diameter of the intersected craters. It was found that with respect to all parameters the ratio /29 of the number of intersections to intersected craters was distributed over the classes of the five-point system. The intersectivity of the craters of different classes (ratio of the number of intersections to intersected craters in each class) is shown below.

Class	A	AB	B	BC	C
Intersecting/intersected	19	2	1.2	1.1	0.56

It is evident from the above that the Class A craters are 19 times more frequently superimposed on craters of the other classes than they are intersected by them, while the Class C craters are intersected almost twice as frequently by other classes of craters than they intersect the others. At all diameter ratios the younger craters intersect the mature ones in 111 cases (47%), intersection of craters of one class was observed in 77 cases (33%), and the mature ones intersect the younger forms in 47 cases (20%), which is usually observed with a significantly smaller diameter of the superimposed craters.

Taking into account the sizes of the intersecting craters, their relationships can be seen quite clearly from Table 5.

TABLE 5

MUTUAL INTERSECTION OF CUP-SHAPED CRATERS OF VARIOUS CLASSES AS A FUNCTION OF THE RATIO OF THEIR DIAMETERS

Nature of intersection	Ratio of diameter of intersecting crater to diameter of intersected crater		
	0.1 — 0.5	0.5 — 1.1	1.1 and more
New ones intersect older ones	31	70	82
Intersection of craters of the same class	38	26	18
Old craters intersect newer ones	31	4	0
	100%	100%	100%

It follows from the results obtained that:

1) Various morphological classes of craters of a given size actually reflect, on the average, the relative age of the craters.

2) Destruction of small-size craters proceeds much more rapidly than the destruction of large craters. Therefore, specific relative age scales apply to craters of different size intervals.

3) In investigating the ratios of the morphological classes of craters of different sizes, it is possible to estimate the rate of destruction of the craters and to compile a scale of their relative ages.

Nature of Crater Distribution over the Surface

In order to answer a number of scientific and practical questions, it is important to establish the distribution of the craters on the surface of the lunar maria [18 — 20]. The question of whether they are distributed in a random pattern or are combined to form groups and chains may be answered objectively using the method of the "nearest neighbor" which is employed in biological and geological studies [21, 22]. In accordance with this method, we measured the distance from the center of each crater to the center of the neighboring crater nearest to it. The sum of these distances Σr, divided by the number of investigated craters N, constitutes the actual average distance to the nearest neighboring crater r_A. If the distribution of the craters /30 in the investigated area is random, i.e., the probability of encountering a crater at any given point in the investigated area A is equal to the probability of encountering it at any other point in the same area, the average distance to the nearest neighbor will be equal to $r_E = \sqrt{A/4N}$. The measure of the randomness of distribution may be expressed as follows: $R = r_A/r_E$. Then in the ideally random distribution R = 1, with a tendency toward local groupings, chains $0 < R < 1$, and with a tendency toward ordered uniform distribution, $1 < R < 2$.

The study of the crater distribution was conducted in the four regions mentioned earlier. For each region we selected photographs of two typical areas 0.8 x 0.8 km, on a scale of 1:10,000, where two measurements were carried out. All craters with diameters above 10 m were measured regardless of their morphological characteristics. The overwhelming majority of the measurements were performed on craters from 10 to 50 m in diameter. Larger craters are found more rarely. The maximum crater diameter reached 100 meters.

TABLE 6*

NATURE OF CRATER DISTRIBUTION.

Region	Section	A, м	N	Σr, м	r_A, м	r_E, м	R
Oceanus Procellarum, region 1	1	640000	253	6124	24,2	25,2	0,963
	2	640000	233	5395	23,3	26,2	0,893
	1+2	1280000	486	11519	23,7	25,6	0,927
Oceanus Procellarum, region 2	1	640000	179	5415	30,2	29,9	1,010
	2	640000	227	5777	25,4	25,6	0,990
	1+2	1280000	406	11192	27,6	28,1	0,983
Sinus Medii, region 3	1	640000	333	7621	23,0	22,0	1,045
	2	640000	421	8738	21,0	19,5	1,078
	1+2	1280000	754	16359	21,7	20,6	1,059
Mare Tranquilitatis, region 4	1	640000	165	4752	28,9	36,0	0,803
	2	640000	123	3996	32,4	35,5	0,913
	1+2	1280000	288	8748	30,4	33,4	0,910

*[Translator's Note: Commas represent decimal points.]

The results of the studies are presented in Table 6. The data presented for individual sections of each region and the data averaged over regions indicate that the distribution of small craters is close to random. Since the results change slightly from region to region, it can evidently be concluded that the random distribution of small craters on the surface is sufficiently characteristic of the lunar maria in general. This conclusion applies basically to craters with diameters from 10 to 50 meters. The characteristics of the distribution of the larger craters have not been firmly established and require additional research.

Crater Distribution Density

The number of craters per unit area of the surface, or their distribution density, was determined in all four regions of the detailed investigation. In each of the regions, a count was made of the individual sections uniformly distributed over the region. These sections are hereafter referred to as sampling foci. The number of foci in each of the regions was 13 to 26. The counts of individual sampling foci were averaged for each region to give the average esti- /31
mate of the density in the region. The averaging was carried out by calculating the arithmetic mean from the values of the individual sampling foci. The correctness of this procedure is discussed in the next section of this paper, devoted to determining the variations in the density of crater distribution. The distribution of the sampling foci over the areas of the regions and the variability in the crater density within each region are illustrated in Figures 4, 5, and 6, which show fragments of charts of isodenses (equal density distributions) compiled for a region in Sinus Medii. The points correspond to the centers of the sampling foci, and the numbers around them are the values of the crater density in a given sampling focus.

Computations were carried out using pictures on a scale of 1:10,000. In each sampling focus, successive counts were made of the number of craters with diameters of 10, 30, 50, 70, 90, 100, 200, and 300 meters. The area of the sampling focus for craters with diameters over 10 meters was 1.44 km^2; over 30 m, 1.96 km^2; over 50 meters, 3.24 km^2; over 70 m and over 90 m, 5.76 km^2. Craters of larger diameter (200 — 400 m) were counted over the entire area of the investigated regions. The results of the calculations were normalized for an area of 10^6 km^2 and plotted on a graph. The ordinate corresponds to the integral (cumulative) distribution density of craters, whose diameter exceeds D, while the abscissa is used to plot the assumed boundary values of D.

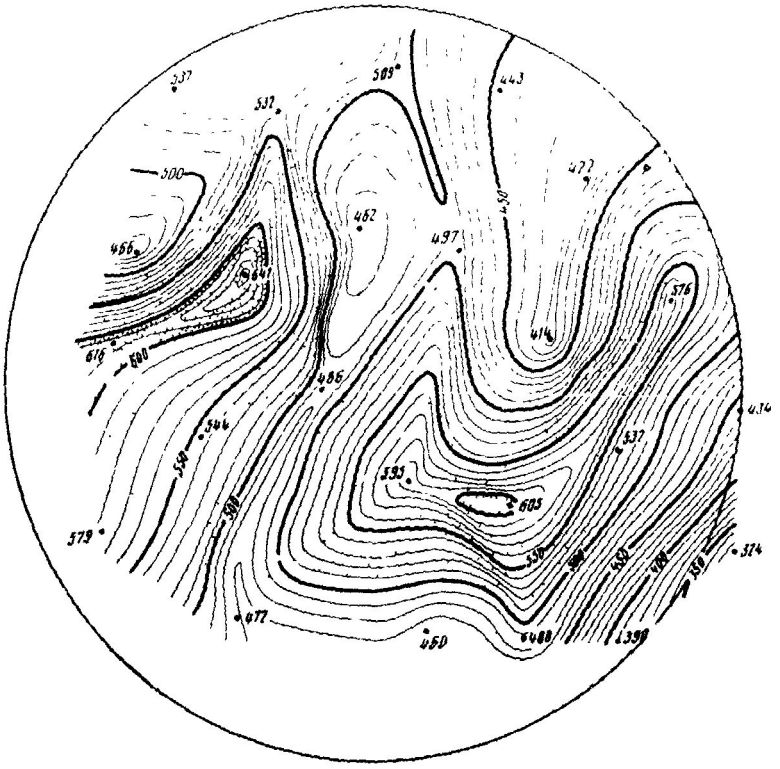

Figure 4. Chart of isodenses for craters with diameters greater than 10 m for an area with 15 km radius in Sinus Medii. Standard area: 1 km^2.

The numbers indicate the densities of craters in sampling sites with an area of 1.44 km^2, relative to the centers of these sites.

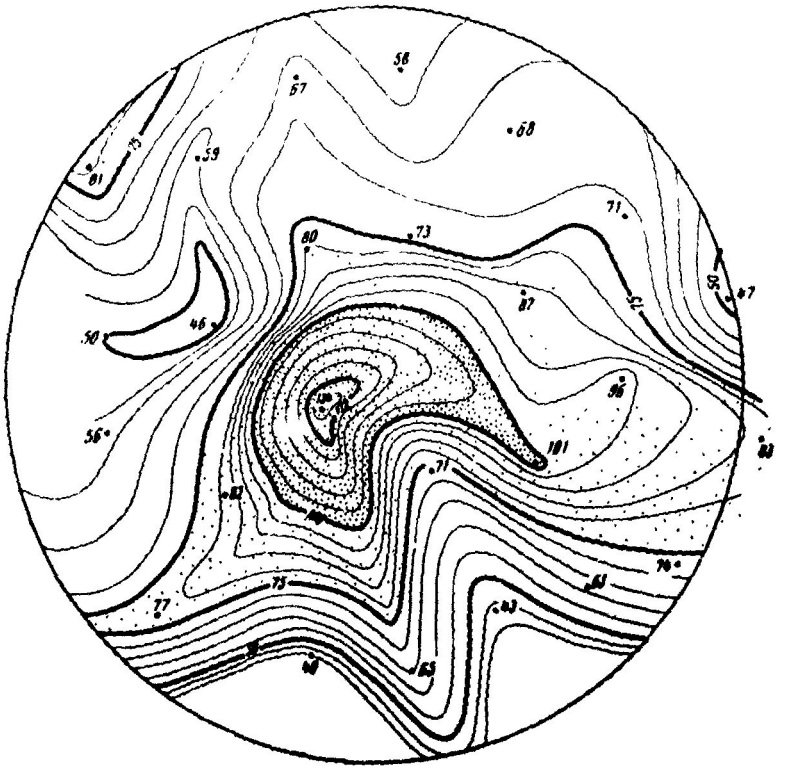

Figure 5. Chart of isodenses for craters with larger than 30 m diameter in an area with 15 km radius in Sinus Medii. Standard area: 1 km^2.

The numbers indicate the densities of craters in sampling sites with an area of 1.96 km^2 relative to the center of these sites.

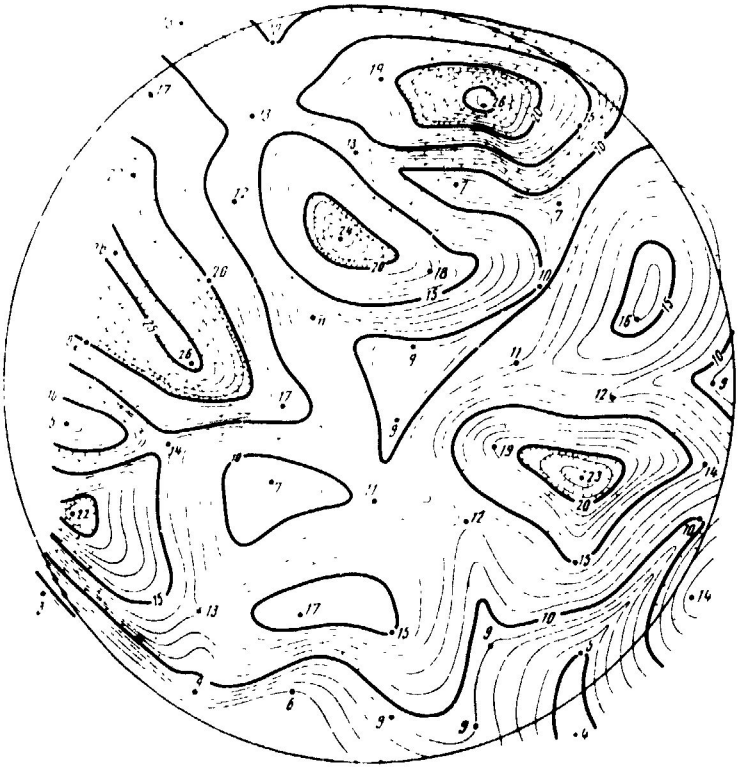

Figure 6. Chart of isodenses for craters with larger than 200 m diameter in an area with 15 km radius in Sinus Medii. Standard area: 1 km^2.

The numbers indicate the densities of craters in sampling sites with an area of 20 km^2, relative to the centers of these sites.

The present paper contains determinations of the dependence of the crater distribution density on crater size for Region 1 in Oceanus Procellarum and Region 3 in Sinus Medii (Figures 7 and 8). An analysis of the data obtained and the results of determining these same parameters for the regions containing the landing sites of the Surveyor spacecraft [23] indicate that the population of small craters in the lunar maria breaks down into two parts. In the case of craters of a size less than a certain critical size D_{crit}, the average distribution density in various regions is close to the estimate obtained from the Ranger photographs [24]:

$$N = 10^{19,8} \cdot D^{-3}, \qquad (1)$$

where N is the integral number of craters whose diameter exceeds D (in meters) in an area of 10^6 km^2.

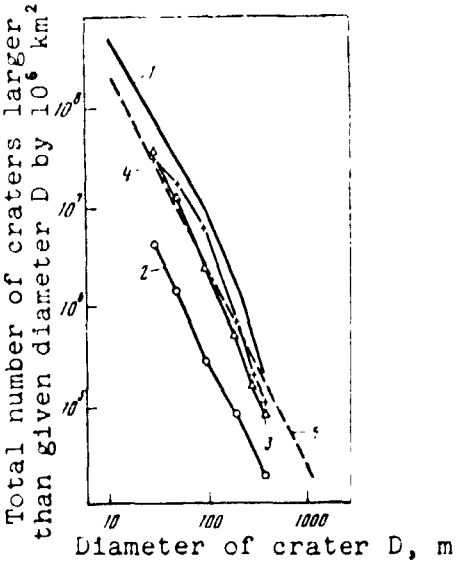

Figure 7. Size distribution of craters of various classes in the region of Oceanus Procellarum.

1 — A + B + C craters; 2 — A craters; 3 — B craters; 4 — C craters; 5 — average crater distribution according to data from Ranger spacecraft.

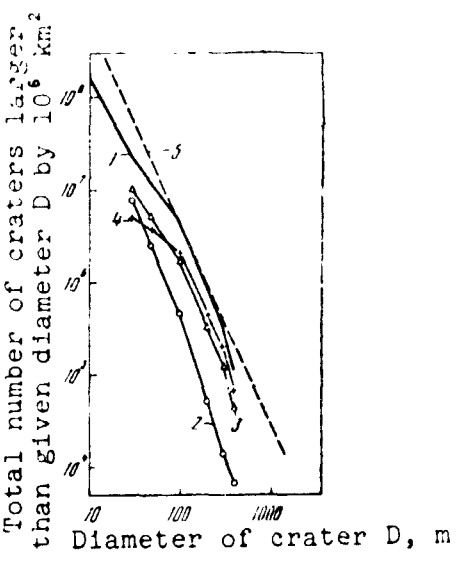

Figure 8. Size distribution of craters of various classes in the region of Sinus Medii. The designations are the same as in Figure 7.

The value of D_{crit} for different regions of maria type varies from several tens to a few hundred meters.

In the case of craters whose diameter is greater than D_{crit}, the function N(D) is also nearly a power function, but the exponent here is almost -3:

$$N = cD^{-3}. \tag{2}$$

The constant c changes markedly from one region to another, and its value is evidently correlated with the age of the surface in the region under study. The function N(D) changes gradually in the range of values close to D_{crit}.

Variations in Crater Distribution Density

It is evident from the fragments of the chart of isodenses for Sinus Medii (see Figures 4, 5, and 6) that within the investigated region the distribution density for craters of all sizes varies significantly. An analogous pattern is seen for other regions as well. The study of these variations is of interest for the solution of a number of practical and theoretical problems and especially for a correct estimate of the average crater distribution density in a region.

In order to obtain information on this question, a special project was carried out. Computations of the crater distribution density in the sampling foci in the regions of Oceanus Procellarum, Sinus Medii, and Mare Tranquilitatis (Regions 2, 3, and 4) were used to clarify the variations in density and to determine the relationship of the degree of variability to the crater size and the size of an individual section (i.e., sampling focus). The area of the sampling foci in this portion of the work varied in different series of experiments from 0.04 to 21 km^2. The foci of any size from a given series of tests were never overlapped by foci from another series of tests. We computed the integral density of the craters whose diameters exceeded D. The limiting values of D adopted were 10, 30, 50, 70, and 90 meters. /34

The data obtained were used to determine the law governing the distribution of the density values. By means of a probability template, it was established that the observed empirical density distribution of craters with diameters greater than some D in sampling foci of a given size shows a sufficiently good agreement with the law of normal or Gaussian distribution. Correspondence of the distribution of the crater density values to the normal distribution is shown in Figure 9.

Agreement with the law of normal distribution requires that the estimate of the density be performed by calculating the arithmetic mean from the density values in the sampling foci N. The measure of the density variation in this case is the scatter S^2 or standard deviation S

$$S = \frac{\sum_{i=1}^{i=n} (N_i - \bar{N})^2}{n-1}, \qquad (3)$$

where n is the number of tests, in this case the number of sampling foci in the test series.

To compare data on craters of different diameters as a measure of the density variation, it is convenient to use the coefficient of variation v:

$$v = \frac{S}{\bar{N}}. \qquad (4)$$

In analyzing the data obtained, it was established that the coefficient of variation of the density of the craters v is a function of the limiting value of the crater diameter D and the area of the sampling focus A_{sample}. With the sampling foci equal, the coefficient of variation increases with the value of D. With equal values of D, the coefficient of variation increases inversely with the size of the sampling focus. This relationship is shown graphically in Figure 10, which shows the results of calculations for Region 2. A similar relationship is observed in other regions as well. /35

The regular nature of the arrangement of the curves in graphs of this kind tends to indicate the possibility of combining this family of curves. An argument in favor of this might be the parameter that simultaneously takes into account the size of the sampling focus A_{sample} and the limiting crater diameter D. Such a parameter is the ratio of the area of a crater with the limiting diameter $A_{crater} = \pi D^2/4$ to the area of the sampling focus A_{sample}, i.e., A_{crater}/A_{sample}. The data thus expressed for three regions are plotted on the graph shown in Figure 11.

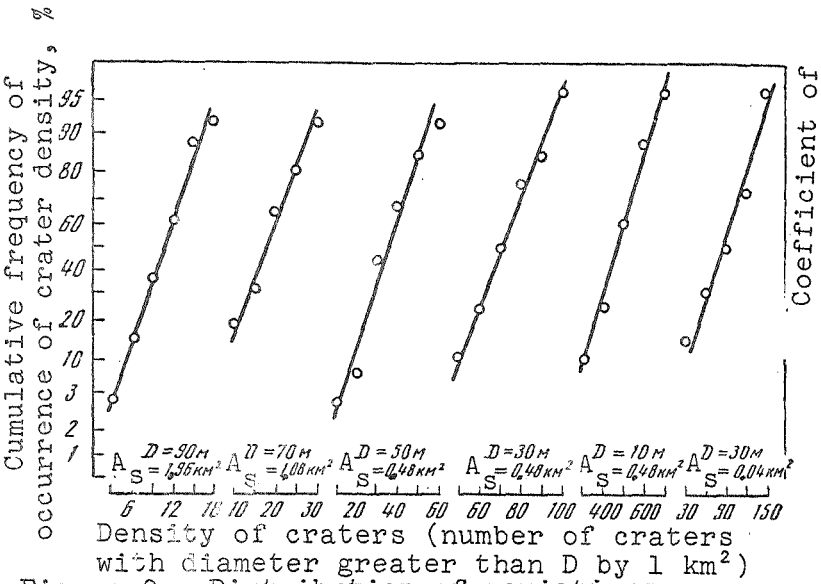

Figure 9. Distribution of variations of crater density in the region of Sinus Medii.

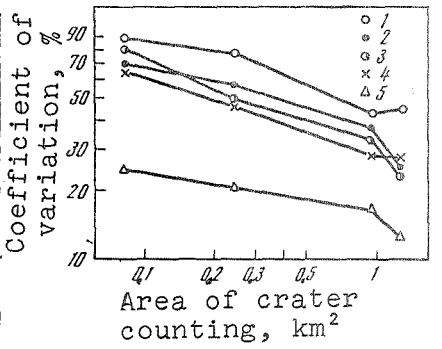

Figure 10. Coefficient of variation of crater density as a function of the measured area in the region of Oceanus Procellarum. Craters larger than: 1 — 90 m; 2 — 70 m; 3 — 50 m; 4 — 30 m; 5 — 10 m.

As we can see from the graph, there is a definite relationship between the coefficient of variation and the ratio A_{crater}/A_{sample}:

$$A_{crater}/A_{sample} = f(v).$$

The relationship between the logarithms of these parameters is nearly linear. In the case of the regions representing Oceanus Procellarum and Sinus Medii, this relationship may be approximated by the general equation /36

$$\lg v = 1/3 \lg \frac{A_{crater}}{A_{sample}} + 2.46 \qquad (5)$$

or in the form of an exponential function:

$$v \approx 300 \sqrt[3]{A_{crater}/A_{sample}} \qquad (6)$$

In the case of the investigated part of Mare Tranquilitatis, this relationship may be approximated by the equation

$$\lg v = 1/3 \lg \frac{A_{crater}}{A_{sample}} + 270 \qquad (7)$$

or

$$v \approx 500\sqrt[3]{A_{crater}/A_{sample}} \qquad (8)$$

Hence, for the three investigated regions of the lunar maria there is a relationship between the coefficient of the variation of the crater density v and the ratio of the area of a crater of limiting diameter to the area of the sampling focus A_{crater}/A_{sample} which can be expressed in a general form:

$$v = k\sqrt[3]{\frac{A_{crater}}{A_{sample}}} \qquad (9)$$

where k is a constant.

Inasmuch as the number of craters per unit area of the surface is a function of the diameter ($N = cD^2$), for the investigated range of diameters (D = 10 to 90 m) it can be shown that the ratio A_{crater}/A_{sample} is inversely proportional to the number of craters N with diameter greater than D in the area of the sampling focus

$$A_{crater}/A_{sample} = c'/N \qquad (10)$$

where c' is a constant.

Then Expression (7) can be written

$$v = \frac{c''}{\sqrt[3]{N}}, \qquad (11)$$

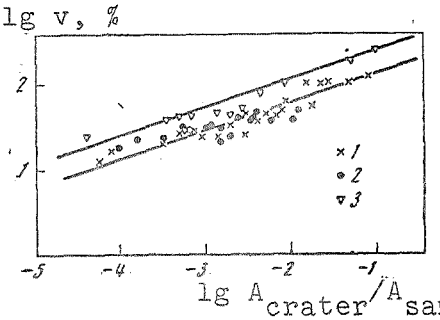

Figure 11. Relationship between coefficient of variation of crater density v with ratio of the area of the crater of limiting diameter A_{crater} and area of sampling focus A_{sample}.

1 — region of Oceanus Procellarum; 2 — region of Sinus Medii; 3 — region of Mare Tranquilitatis.

where c'' is a constant, i.e., the coefficient of variation is inversely proportional to the cube root of the number of craters in the area of the sampling focus.

The empirical relationships presented above are apparently a reflection of the formation of the small craters on the surface of the lunar maria.

Stones /37

While observations from space have primarily confirmed and enriched our knowledge only about the craters that have been known for a long time on the basis of terrestrial observations, the discovery of stones on the lunar surface has revealed a new phenomenon, whose possibility was assumed speculatively.

The panoramas of the Luna 9 automatic lunar probe [2] revealed stones of the lunar surface. The panoramas from the Luna 13 revealed their irregular distribution on the surface [3] aside from the connection with small craters. The Surveyors provided examples of individual stony craters and the large-scale pictures taken by the Lunar Orbiters made it possible to establish this relationship.

Without taking into account the individual stones which typify certain parts of the lunar surface, frequently its positive forms, for example certain ridges and hills, we can assume that approximately 90% of all the stones are associated with craters and crater ejecta, and that only about 10% are stones what have no visible link with crater ejecta.

As far as crater ejecta are concerned, the surfaces of the lunar maria are covered with stones ranging in size from several centimeters to several meters in diameter. Larger stones measuring tens of meters are rarely found.

The number of stones n_s per unit area is described by the empirical formula:

$$n_s = cd^{\gamma}, \tag{12}$$

where c and γ are constants, and d is the diameter of the stones.

A rough approximation of the average number of stones per unit area in the lunar maria may be estimated according to our data by the approximate formula:

$$n_s = 10^3 \cdot d^{-2,5}, \tag{13}$$

where n_s is the number of stones whose diameter exceeds d by 1 km^2 of the maria surface; d is the diameter of the stones expressed in meters.

The derived formula may be used for calculating the number of stones with diameters from 10 to 20 cm up to 5 to 10 meters.

The literature contains references to a somewhat different distribution of the number of stones as a function of their diameter than we have assumed. This may be related either to the different physical and mechanical properties of the rocks located in the various regions, or to the formation and destruction of the stones.

Thus, in the case of the various landing sites of the Surveyor spacecraft, we have the following parameters for the formula showing the dependence of the number of particles on their diameter in millimeters in a size interval from 1 mm to 0.5 — 2 meters for an area of 100 m^2 (Table 7).

It follows from the above that the results of the stone counts must be viewed as preliminary, showing only the order of magnitude.

Within the craters the number of stones is 4 to 6 times greater than is indicated by the above formula. In approximately 5% of the cases, this difference reaches two orders, and in approximately 50% of the cases, it does not exceed half an order, i.e., the craters are essentially inhomogeneous in terms of the degree of stoniness, especially if their different morphological classes are taken into account.

Stony walls are observed in approximately 10% of the craters 10 to 500 m in diameter. The width of the zone of increased stoniness on the average is close to half the diameter of the crater as determined from its rim, but in individual cases it may reach 2 — 3 and /38
more crater diameters; we observed this in approximately 1% of the craters. The number of stones within these zones is 3 to 6 times higher than average, and can sometimes increase up to two orders.

In the intercrater space, the average number of stones per unit area is approximately one order smaller than the value obtained by the above formula (average estimate). As we have already mentioned here, there are individual stony deposits of areal or linear type, frequently associated with positive forms of relief and occupying comparatively small areas of surface. The location of individual stones in the intercrater space (outside the zone of obvious ejecta from a crater) is nearly random, while the average density of distribution of stones of a size greater than 2 m is about 0.010 ± 0.005 per 100 m^2.

The processes of crater formation are accompanied by the ejection of stones which are located within the craters themselves and the annular zones of increased density of stones around the craters. The outer limits of these annular zones are determined here arbitrarily as the so-called limiting density, which is assumed equal to the density of the stones per unit area in the landing area of the Surveyor III spacecraft ($1.6 \cdot 10^{-2}$ per 100 m^2 for stones with a diameter

TABLE 7

PARAMETERS OF EMPIRICAL FORMULAS OF DEPENDENCE OF STONE DISTRIBUTION DENSITY ON THEIR DIAMETER

Experiment	Location	Parameters of empirical formulas	
		c	γ
Surveyor I	Oceanus Procellarum	$5 \cdot 10^5$	-2.1
Surveyor III	Oceanus Procellarum	$3.3 \cdot 10^6$	-2.5
Surveyor V	Mare Tranquilitatis	$1.2 \cdot 10^6$	-2.6
Surveyor VI	Sinus Medii	$1.9 \cdot 10^6$	-2.5
Surveyor VII	Vicinity of crater Tycho	$7.9 \cdot 10^5$	-1.8

greater than 2 m). The inner limit of the annular zone is the rim of the crater. The density of stones per unit area in the intercrater space, outside the annular zones, will be referred to from now on as the intercrater density. Judging by the height of the stones, somewhat flattened forms predominate among them, apparently due to the partial burial of the stones in the lunar soil. On the average, we can assume that the ratio of the height of the stone to its diameter is nearly 0.7. Stones are found comparatively rarely which give the impression of being fragments, in which this ratio rises to 1.2 to 1.3 and which are sometimes described with the term "obelisks."

In the investigated regions, the stones are divided into two morphological groups — the stones proper and the "hillocks" or "hummocks." The stones have an isometric or angular form in the plan. Their appearance in flat photographs is characterized by a clear distribution of light and shadow. The hillocks are the smoothed forms of the microrelief which are characterized in pictures by gradual transitions from light to dark. In the plan they are usually rounded or isometric. The slopes on the sides of the hillocks usually do not exceed 8 to 10°. Stones measuring more than 2 m are clearly recognizable in photographs. The identification of the hillocks is largely subjective. The impression is gained that the hillocks are one of the stages of surface breakup of stones.

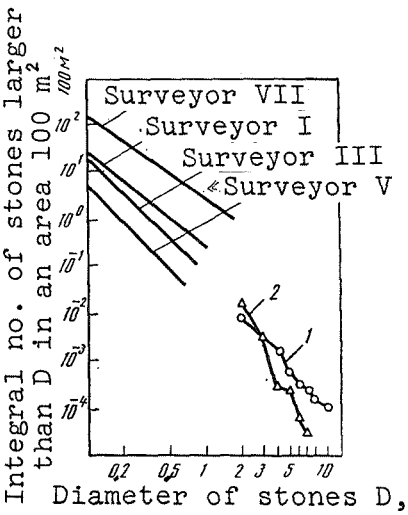

Figure 12. Integral distribution of stones in two regions.
1 — region of Sinus Medii;
2 — region of Oceanus Procellarum.

To determine the distribution density of stones in the investigated area, we selected 10 sheets of large-scale pictures of the Orbiter II that /39 cover the area uniformly. In each picture, we counted the number of stones in a specific band (usually the fourth from the top) and estimated their diameters. An individual band corresponds to approximately 0.8 km^2 of the terrain. Hence, the total size of the area in which the estimates were made in each region was approximately 8 km^2. The calculated number of stones was normalized for an area of 100 m^2.

The results of the counts are shown in Table 8 and illustrated in Figure 12.

TABLE 8

INTEGRAL DENSITIES OF STONES $n \cdot 10^{-3}$ WITH DIAMETERS GREATER THAN d IN TWO INVESTIGATED REGIONS

Diameter of stones, m	No. of stones whose diameter is greater than d in an area 100 m^2 ($n \cdot 10^{-3}$)		Diameter of stones, m	No. of stones whose diameter is greater than d in an area 100 m^2 ($n \cdot 10^{-3}$)	
	Region of Oceanus Procellarum	Region of Sinus Medii		Region of Oceanus Procellarum	Region of Sinus Medii
2	10.0	8.3	6	0.06	0.33
3	3.1	3.2	7	0.03	0.25
4	0.3	1.3	8	—	0.16
5	0.25	0.6	10	—	0.1

It follows from these data that in the region of Oceanus Procellarum the distrubution density of stones up to 3 m in diameter is slightly higher than in the region of Sinus Medii and lower for larger ones. On the whole, however, the regions of Oceanus Procellarum

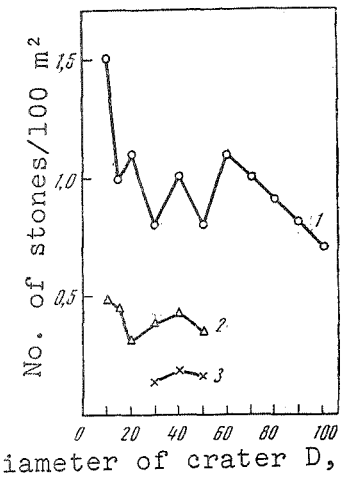

Figure 13. Densities of stones in inner zones of craters as a function of crater diameter (region of Oceanus Procellarum, area of counting 8 km², norming area 100 m²).

1 — A craters; 2 — B craters; 3 — C craters.

and Sinus Medii are similar in terms of the number of stones 2 — 10 m in diameter, and are comparable with the landing site of the Surveyor III spacecraft.

The distribution density of the fragmental material, depending on the class of the crater and the distance to its rim (for craters 10 — 100 m in diameter) was studied in detail in the region of Oceanus Procellarum. The stones were counted in a section of the surface in the shape of a discontinuous band about 0.2 km wide and with a total area of 8 km². A total of approximately 1000 stones were counted.

The stone densities are given in Table 9 and Figure 13. Norming was carried out for 100 m² of area of the inner zone of the crater and two concentric annular zones around it, determined from the rim of the crater, each with a width equal to the crater radius. The calculation of the density was performed on an arbitrarily selected stony crater whose size corresponds to the beginning of the selected ranges of diameters. A glance at Table 9 will reveal the following:

1. The density of distribution of scree is maximal in the inner parts of the craters and on their walls near the rim. It drops off sharply with distance from the crater.

2. The distribution density of the stones in craters 10 to 100 m in diameter of all classes is independent of the diameter and changes slightly as the latter increases.

TABLE 9

DENSITITES OF STONES LARGER THAN 2 m IN OUTER ZONES OF EJECTA FROM CRATERS OF VARIOUS CLASSES AND DIAMETERS. REGION OF OCEANUS PROCELLARUM (NORMALIZED FOR 100 m^2)

Diameters of craters, m	A craters			B craters		C craters
	N_{cr}	N_R	N_{2R}	N_{cr}	N_R	N_{cr}
10	1.54	0.017	0.001	0.51	0.006	—
15	1.02	0.021	0.001	0.45	0.006	0.19
20	0.99	0.033	0.002	0.32	0.006	0.11
30	0.81	0.061	0.001	0.34	0.011	0.11
40	1.03	0.101	0.003	0.40	0.006	0.16
50	1.22	0.106	0.002	0.36	0.007	0.14
60	1.12	0.087	0.001	—	—	—
70	0.94	0.071	0.003	—	—	—
80	0.89	0.080	0.002	—	—	—
90	0.79	0.088	0.002	—	—	—
100	0.74	0.087	0.003	—	—	—

3. In a general form, the ratios of the densities of stones in various zones of A craters are expressed in the form $N_{crater} > N_R > N_{lim} \geq N_{2R}$, where N_{crater}, N_R, N_{lim} and N_{2R} are the stone densities for the inner zone of the crater, the first annular zone with a width equal to the crater radius, the limiting density, and the density in the second annular zone, respectively.

4. For Class B craters the ratios are as follows: /40

$$N_{crater} > N_R \geq N_{lim};$$

5. Class C craters have the following ratios:

$$N_R \approx N_{lim}.$$

The density distribution of the stones with some variations remains constant by zones in all three classes of craters, so that regardless of their sizes the ratio between the densities of the stones in the craters of all classes in the range of diameters from 10 to 100 m may be expressed by the rough average densities (Table 10).

TABLE 10

RATIO BETWEEN ROUGH AVERAGE DENSITIES OF STONES LARGER THAN 2 m IN A, B, AND C CRATERS WITH DIAMETERS OF 10 — 100 m IN CRATER ZONES (NORMALIZED FOR 100 m^2)

Class of crater	Inner zone of crater	First external zone of crater	Second external zone of crater
A	1.0	0.07	0.002
B	0.4	0.007	—
C	0.14	—	—

The study of the stony deposits around the most clearly pronounced Class A craters was performed using the example of two craters in Oceanus Procellarum. The diameter of one crater was 540 m, while that /41 of the other was 170 m. The surface around the craters was divided into a series of concentric annular zones (the width of each ring was 1/4 the diameter of the crater), which in turn were divided by radii originating in the center of the crater into 8 to 16 sectors. (From here on, the zones are identified by Roman numerals in the text.) Within the limits of each sector, using a binocular loupe, the stones were counted and their sizes determined. The data for each sector were normalized for 100 m^2 and represented in the form of cumulative frequencies of incidence. Then, after relating the data obtained to the centers of the sectors, diagrams were drawn in which isolines were used to show the variations in distribution density of stones around the craters. In addition, the distribution density of the stones was calculated for each annular zone and a parameter was determined for each of these zones that represented the geometric mean of the diameters of the ten largest stones in the zone. Below we have listed the results for each of the investigated craters and analyzed them.

Crater No. 1. In plan, the crater is very nearly a circle 540 m in diameter. Around it is an annular zone saturated with stones whose size in some instances reaches 15 to 16 m. The total number of stones counted was 9719. Variations in the density for stones with diameters larger than 2 m are shown graphically in Figure 14. In order to take into account the possible influence of illumination on the results of the calculations, an arrow indicates the direction of the incidence of the Sun's rays at the time the picture was taken.

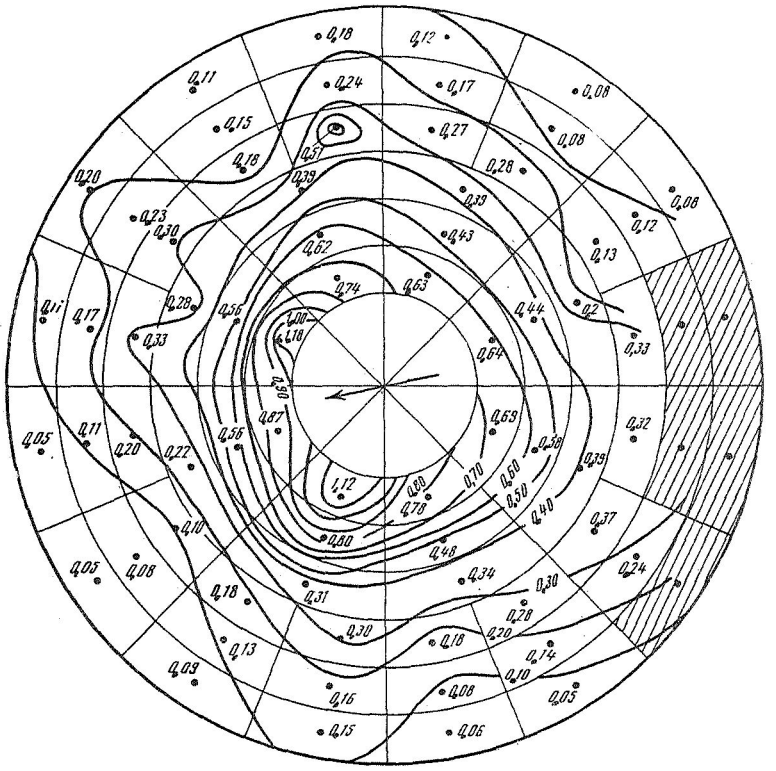

Figure 14. Distribution density of stones with diameters greater than 2 m near Crater No. 1.

Numbers — number of stones normalized for 100 m^2. The concentric lines are drawn through 0.25 of the crater diameter.

The number of stones per unit area is maximum around the crater and drops off gradually with increasing distance from it. Thus, for stones with a diameter greater than 2 m, the average density varies by zones as follows: Zone I (closest to the crater) — 0.823; Zone II — 0.558; Zone III — 0.342; Zone IV — 0.266; Zone V — 0.130; Zone VI — 0.084. The density of distribution of stones changes significantly within each zone as well. For example, in Zone I these changes vary from 0.63 to 1.12, with an average density of 0.823. Then the density variations within the limits of each zone obey a certain rule: the density is maximum in the western part of the majority of zones. In the eastern part of each zone, they have a minimum or a secondary maximum, while the minimal density in this case is observed in the northern or southern parts of the zones.

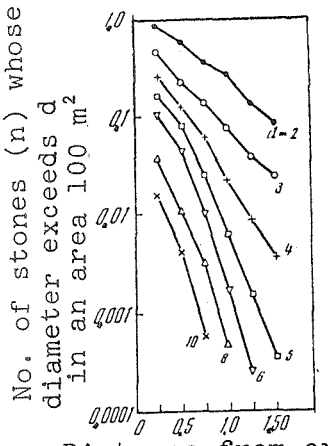

Figure 15. Dependence of distribution density of stones of a given diameter upon the distance from the crater.

Hence, the axial symmetry in the distribution of stones around the crater is distorted, and approximates a bilateral arrangement. For Crater No. 1, the axis of this bilateral symmetry is close to the direction of incidence of the Sun's rays at the time the picture was taken. The latter circumstance is very important, inasmuch as it may indicate that the distortion of the axial symmetry of distribution of the stones does not reflect the true distribution, but is explained by the illumination conditions at the time the picture was taken. This fact must be emphasized inasmuch as the conditions of illumination during photography may distort the real distribution of stones on the lunar surface.

The change in the number of stones with distance from the crater is shown in Figure 15. The abscissa shows the distance from the crater to the outer limit of each zone, while the ordinate has been used to plot the logarithm of the density of distribution of stones in a given zone (for stones of a given diameter). The lines which reflect the relationship between these two values are nearly straight, and consequently, this relationship is reliably approximated by an exponential law. From an analysis of Figure 15, it also follows that, with increasing distance from the crater, the number of stones per unit area decreases inversely with the size of the stones. Thus, at a distance from the crater equal to one of its diameters (from Zone I to Zone V), the number of stones per unit area for stones larger than 2 m drops by a factor of 6; for stones larger than 3 m, by 11; for stones larger than 4 m by a factor of 30, and for stones larger than 5 m, by a factor of 100.

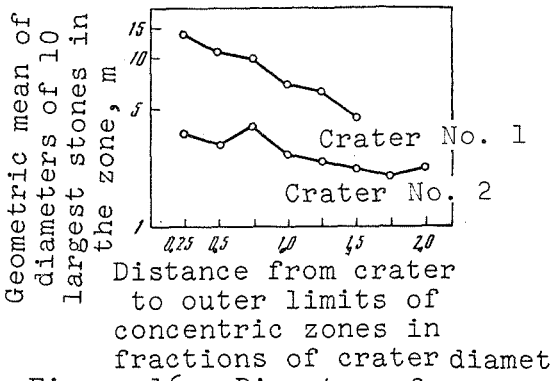

Figure 16. Diameter of largest stones in the zone versus distance from crater.

Around the investigated crater, /42 stones with a diameter of more than 15 m are found only in Zone I (closest to the rim of the wall). Stones with diameters greater than 10 m are found in Zones I, II, and III. Stones with diameters larger than 8 m are found up to Zone V, inclusive. Finally, in Zone VI, the maximum diameter of the stones reaches only 5 m. The decrease in stone size with distance from the crater is also illustrated by means of a parameter which represents the geometric mean of the diameters of the ten largest stones in each zone. The magnitude of this parameter changes as follows: Zone I — 14.0; Zone II — 11.0; Zone III — 10.1; Zone IV — 6.8; Zone V — 5.4; Zone VI — 4.3 m. The variations in this parameter as a function of the distance from the crater are shown in Figure 16. It follows from an analysis that this dependence is also close to an exponential one.

Crater No. 2. Its shape in the plan approximates a circle 170 m in diameter. Around the crater there is an annular deposit of stones within whose limits individual stones reach 5 m in diameter. Even a preliminary (without quantitative calculations) study of this deposit reveals that the zone with the maximum distribution density of stones is not in direct contact with the edge of the crater, but is a short distance from it. The total number of stones counted was 713. The variations in the density of distribution of stones with diameters greater than 2 m are shown in Figure 17. The arrow shows the direc- /43 tion of incidence of the Sun's rays at the time the picture was taken.

The results of the calculations confirm the preliminary finding that in the deposits around crater No. 2 the maximum distribution density of stones is observed not in the immediate vicinity of the crater, but at some distance from it (in Zone III). The number of stones with diameters greater than 2 m, normalized for an area of 100 m^2,

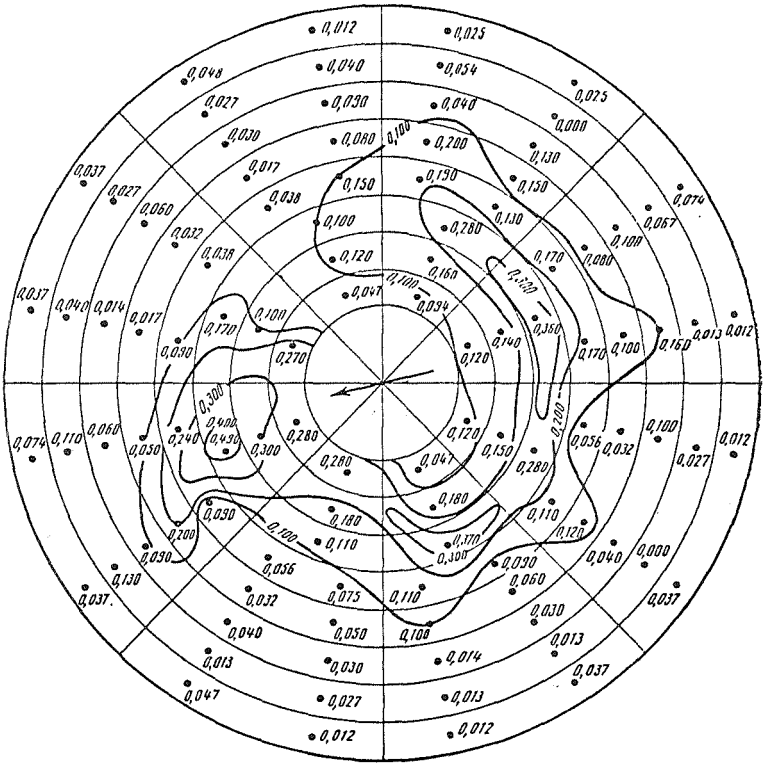

Figure 17.* Distribution density of stones with diameters greater than 2 m around crater No. 2.

Numbers — numbers of stones normalized for 100 m^2. The concentric lines were drawn through 0.25 of the crater diameter.

* Translator's Note: Commas represent decimal points.

is distributed over annular zones as follows: Zone I — 0.170; Zone II — 0.160; Zone III — 0.270; Zone IV — 0.114; Zone V — 0.077; Zone VI — 0.062; Zone VII — 0.038; Zone VIII — 0.034.

The stone distribution density in different parts of a given zone may change several times. Thus, in Zone I with an average distribution density of stones with diameter of 2 m equal to 0.170, their density in individual sectors varies from 0.047 to 0.280. In Zone III, with an average density of 0.270 it varies from 0.1 to 0.49. These variations in density in the described deposits are also very regular within the zones. A territory with increased distribution density of stones has in the plan a clear horseshoe form (the crater itself is

inside the horseshoe, but it is open at the northwest), which is clearly evident from Figure 17. As in Crater No. 1, the deposit is characterized by disruption of axial and development of bilateral symmetry. In this case the axis of bilateral symmetry forms an angle of approximately 45 degrees with the direction of the Sun's rays at the time the picture was taken.

The change in stone distribution density with distance from the crater is shown in Figure 16, where one can see a slight increase in density from Zone I to Zone III and a clear decrease with a transition to the outer zones. The variations in Zones III and VIII is similar to that around Crater No. I: the density decreases with distance from the crater according to an exponential law, so that the density of larger stones drops off more rapidly. At a distance equal to one crater diameter, from Zone III to Zone VIII the distribution density of stones with a size of more than 2 m drops by a factor of 7 and /44
that of stones larger than 3 m — by a factor of 47. Some deviations from an exponential law (stones larger than 3 m in Zone VIII) clearly bear a random nature. The variations in distribution density from Zone I to Zone III are completely different and, judging by the results of a preliminary (without counting) study of some other relatively large Type A craters, they can be viewed as anomalous.

Around the investigated crater, stones with diameters larger than 5 m were found only in Zones I and III. Stones with diameters greater than 4 m were found in Zones I, V and VIII. Stones larger than 3 and 2 m are found in all investigated zones. The parameter that constitutes the geometric mean of the diameters of the ten largest stones in each zone changes as follows: Zone I — 3.6; Zone II — 3.2; Zone III — 4.2; Zone IV — 2.7; Zone V — 2.5; Zone VI — 2.2; Zone VII — 2.1; Zone VIII — 2.3 m.

References

1. Khabakov, A. V. The Principal Problems in the History of the Development of the Lunar Surface. Zap. vses. geogr. Ob-va, nov. ser., Vol. 6, Leningrad, 1949.

2. Pervyye panoramy lunnoy poverkhnosti (First Panoramas of the Lunar Surface), Part I. Moscow, "Nauka" Press, 1966.

3. Pervyye panoramy lunnoy poverkhnosti (First Panoramas of the Lunar Surface), Part II. Moscow, "Nauka" Press, 1969.

4. Spurr, J. E. Geology Applied to Selenology. Part II, The Features of the Moon. Lancaster, Sci. Press, 1945.

5. Vinogradov, A. P. The Origin of the Material of the Earth's Crust. Geokhimiya, No. 1, 1961. /45

6. Vinogradov, A. P. The Origin of the Mantles of the Earth. Izv. AN SSSR, Ser. geol., No. 11, 1962.

7. Magnitskiy, V. A. Zone Melting as a Mechanism for the Formation of the Earth's Crust. Izv. AN SSSR, Ser. geol., No. 11, 1964.

8. Yaroshevskiy, A. A. Some Geological Aspects of Zone Melting. In the book: Problemy geokhimii (Problems of Geochemistry). Moscow, "Nauka" Press, 1965.

9. Vinogradov, A. P., et al. Measurements of the Gamma Radiation of the Lunar Surface by the Luna 10 Space Probe. Geokhimiya, No. 8, 1966.

10. Muller, P. M. and W. L. Sjogren. Mascons: Lunar Mass Concentrations. Science, Vol. 161, No. 3842, 1968.

11. Gilvarry, G. G. Mensuration and Isostasy of Lunar Mascons and Maria. Nature, No. 5203, 1969, p. 223.

12. Markov, M. S. and A. L. Sukhanov. Mascons in the History of the Lunar Maria, Priroda, No. 3, 1971.

13. von Buelow, K. Geological Detection of Weight Distribution on the Visible Side of the Moon. Geologie, Vol. 18, No. 7, 1969.

14. Problemy geologii Luny (Problems of Lunar Geology). Trudy GIN, No. 204. Moscow, "Nauka" Press, 1969.

15. Florenskiy, K. P. The Initial Stage of Differentiation of the Earth. Geokhimiya, No. 8, 1965.

16. Florenskiy, K. P. and I. M. Taborko. Some Findings from Morphometry of Areas of the Moon, Taken by the Luna 12 Probe. Paper delivered at the Symposium on Physics of the Moon and Planets (abstracts). Kiev, 1968.

17. Florenskiy, K. P., A. T. Bazilevskiy and N. N. Grebennik. Morphological Maturity of Small Lunar Craters as a Function of their Age and Size. Kosmicheskiye issledovaniya, Vol. IX, No. 3, 1971.

18. Stanyukovich, K. P. and V. A. Bronshten. The Role of External Space Factors in the Evolution of the Moon. In the book: Luna (The Moon). "Fizmatigiz" Press, 1960.

19. Tyurk, G. T. Relationship between Number and Size of Annular Forms on the Moon. Byull. nablyud. obshch. lyub. astron., No. 9, Moscow, 1927.

20. Vinogradov, A. P., Yu. A. Surkov, K. P. Florenskiy, et al. Lunar Surface Explorations with Soviet Automatic Probes "Luna 9" to "Luna 13." Report, XI Session COSPAR, 1968.

21. Miller, R. and J. Kan. Statistical Analysis in the Geological Sciences. Moscow, "Mir" Press, 1965. Translated from English.

22. Clark, P. I. and F. C. Evans. Distance to Nearest Neighbor as a Measure of Spatial Relationship in Populations. Ecology, Vol. 35, 1954.

23. Surveyor Project Final Report. Part II. Science Results. Pasadena, 1968.

24. Quaide, W. L. and V. R. Oberbeck. Geology of the Apollo Landing Sites. Earth Sci. Revs., Vol. 5, No. 4, 1969.

N74-19478

RESULTS OF INVESTIGATION OF THE SURFACE LAYER OF THE MOON ON THE BASIS OF ITS INTRINSIC RADIATION

V. S. Troitskiy and T. V. Tikhonova

ABSTRACT. The intrinsic thermal radiation of the Moon is an indicator of the temperature regime of the lunar surface, its physical conditions and structure, as indicated by data from Luna 9 and 13, as well as Surveyor I — VII.

The first measurements of the intrinsic radiation of the Moon were made at a wavelength of $\lambda = 1.25$ cm in 1946 [1]. Since then, a large body of experimental data on the study of the intrinsic radiation of the Moon over a broad range of wavelengths from the submillimeter (0.7 mm) to meter (150 cm) has been acquired. The majority of these measurements were made at the Gorkiy Scientific Research Radiophysical Institute (NIRFI). If we add to this the studies of the intrinsic radiation of the Moon in the infrared and the radar studies of the Moon performed mainly abroad, we see that the data gained to date allow us to draw certain conclusions regarding the properties and structure of the outer crust of the Moon, to put together a rather complete, internally non-contradictory picture of the physical conditions on the Moon. Some generalization of the results obtained up to 1965 is given in [2 — 4] and up to 1967 in [5].

The purpose of the present survey is to approach the goals set by the work that has been done and to provide a description of the current model of the structure of the upper crust of the Moon by using all available experimental and theoretical results and the methods developed for their interpretation.

The Thermal Regime of the Surface

The radiation of the Moon is thermal, and its principal characteristics are determined by the heating of its surface by the radiation of the Sun. Since the Moon lacks an atmosphere, the thermal regime of its surface and distribution of temperature in the depths are determined by the customary equation of thermal conductivity with appropriate limiting and initial conditions:

$$\frac{\partial}{\partial y}\left[k(y,\ T)\frac{\partial T}{\partial y}\right]=\rho(y)\,c(y,\ T)\frac{\partial T}{\partial t}. \tag{1}$$

In the case of a periodic thermal regime (lunation) the boundary conditions have the form:

$$\left(k\frac{\partial T}{\partial y}\right)_{y=0}=\sigma(1-R_1)[T(0,\ t)]^4+q-\begin{cases}S_0(1-R_2)\cos\psi\cos(\Omega t-\varphi) & \text{with } |\Omega t-\varphi|\leqslant\frac{\pi}{2}\\ 0 & \text{with } \frac{\pi}{2}<(\Omega t-\varphi)<\frac{3\pi}{2}.\end{cases} \tag{2}$$

In a non-periodic regime (eclipse) the boundary conditions have the form:

$$\left(k\frac{\partial T}{\partial y}\right)_{y=0}=\sigma(1-R_1)[T(0,\ t)]^4+q-S_0(1-R_2)\cos\psi\cos\varphi f(t). \tag{3}$$

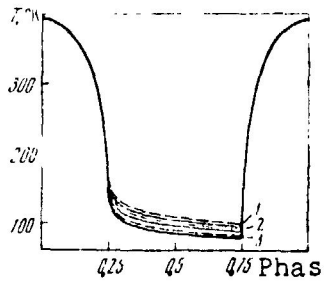

Figure 1. Change in surface temperature at the center of the lunar disk as a function of the phase for various values of the parameter γ. 1 — γ = 600; 2 — γ = 800; 3 — γ = 1000; solid curves — without consideration of the temperature dependence of thermal conductivity. Dashed curves — with consideration of this dependence.

Here $k(y, T) = k_0 + k_r$ is the total thermal conductivity, equal to the sum of the molecular k_0 and radiational conductivity k_r; $\rho(y)$ is the density; $c(y, T)$ is the thermal capacity; R_c and R_i are the light and infrared surface albedos, respectively; S_0 is the solar constant, $f(t)$ is a function of the change in flux during an eclipse; φ and ψ are the longitude and latitude, respectively, of the element of the surface whose thermal state is under study; Ω is the frequency of lunation. The initial conditions in calculation of the lunation mode are arbitrary, inasmuch as a steady-state forced periodic solution is being sought. In the case of an eclipse, the initial conditions are determined by the temperature distribution before the start of the eclipse. Since eclipses occur only at full moon, this temperature distribution is obtained as the solution of the equation of thermal conductivity for the lunation mode at time $t = 0$. To calculate the thermal state of the surface, it is necessary to use some model of the structure of the upper layer. As a first approximation, a homogeneous model was assumed, in which the properties do not change with depth. In this case the surface temperature at a given flux and albedo depends on only one parameter $\gamma = (k\rho c)^{-1/2}$. Figure 1 shows the relationship of the surface temperature at the center of the lunar disk to the lunation phase (solid curves), obtained in [6] by solving equations (1) and (2) on a computer for various values of the parameter γ.

However, as we shall show later on, it is advantageous in calculating the radiation of the Moon to obtain an analytical expression for the distribution of temperature with depth. Since insolation has a periodic nature, the most convenient form of giving the surface temperature is a function expressed as a Fourier series. Therefore, the results of calculating the surface temperature will have the form [7]:

$$T(\varphi, \psi, t) = T_0(\psi) + \sum_{n=1}^{\infty} (-1)^{\alpha_n} T_n(\psi) \cos(n\Omega t - n\varphi - \varphi_n), \tag{4}$$

where φ_n is the phase shift for the n^{th} harmonic of the change in surface temperature with respect to the phase of the incident flux. As was shown in [6], the first five harmonics $T_n(\psi)$ are approximated well by the expressions

$$T_0(\psi) = T_0(0)\cos^{0.25}\psi, \qquad T_3(\psi) = T_3(0)\cos^{0.46}\psi,$$
$$T_1(\psi) = T_1(0)\cos^{0.33}\psi, \qquad T_4(\psi) = T_4(0)\cos^{0.3}\psi,$$
$$T_2(\psi) = T_2(0)\cos^{0.27}\psi,$$

and the sign of these harmonics is determined by the exponent $\alpha = \frac{(n-1)(n-2)}{2}$.

However, the solution of the equation of thermal conductivity (1) for boundary condition (4) leads to the following expressions for distribution of temperature with depth at a given point on the lunar surface with coordinates (φ, ψ):

$$T(y, \varphi, \psi, t) = T_0(\psi) + \sum_{n=1}^{\infty} (-1)^{\alpha_n} T_n(\psi) e^{-y\sqrt{\frac{n\Omega\rho c}{2k}}} \times \cos\left(n\Omega t - n\varphi - \varphi_n - y\sqrt{\frac{n\Omega\rho c}{2k}}\right). \tag{5}$$

/48

The temperature at any depth is composed of a constant component and a variable one, formed by the sum of the harmonics with a period which is a multiple of the lunation period ($\tau = 2\pi/\Omega = 29.5$ Earth days). Each of the harmonics is damped with increasing depth, so that at a depth of $l_T = \sqrt{2k/n\Omega\rho c}$ the amplitude of the temperature

oscillations decreases by a factor e in comparison with the value at the surface. This value has received the name depth of penetration of the temperature wave. It characterizes the depth of the surface layer heated by the Sun in the course of a lunar day. At some depth, three to four times greater than l_T, there are practically no temperature variations.

In the second approximation, a homogeneous model was assumed with thermal conductivity and thermal capacity that are functions of temperature [8 — 10]. Calculation of the thermal state conducted in [9] showed that consideration of these relationships causes insignificant changes in the surface temperature. In Figure 1, the dashed curves show the relationship of the surface temperature at the center of the lunar disk to the phase of the Moon when the temperature dependence of thermal conductivity is considered. Calculations show that the consideration of this relationship indicates that the constant component increases by 2.5 to 3 K, while the amplitude of the first harmonic of the surface temperature drops by the same value. Consideration of the temperature dependence of thermal conductivity leads to changes of the same order.

Therefore, the calculation of these influences on the surface temperature does not produce significant changes falling outside the general precision of the analysis and experiment. However, as we shall show later on, the influence of the temperature relationship is significant in the determination of the constant component in the depth of the layer and must be taken into account.

Theory of Lunar Radiation

The intrinsic radiation of a medium is described by the equation of transfer of radiant energy. For a dense substance (such as the surface layer of the Moon) this equation is simplified, since it is possible to use the principle of local thermodynamic equilibrium. Further, it is also simplified by the fact that it is usually possible

to consider a plane problem, since the thickness of the layer responsible for the radiation is much less than the radius of the planet. With consideration of all the above, the equation of radiation transfer at frequency ν will have the form:

$$\cos\vartheta \frac{d}{d\tau}\left(\frac{I_\nu}{n^2}\right) = -\frac{I_\nu}{n^2} + \frac{B_\nu}{n^2}. \qquad (6)$$

In (6) B_ν will have the form

$$B_\nu = \tilde{\lambda} \int I_\nu f(r) \frac{d\omega}{4\pi} + (1-\tilde{\lambda}) n^2 B_{\nu_0}. \qquad (7)$$

In relationships (6) and (7) $\tau = \int_0^l \alpha_\nu dy$ is the optical thickness; α_ν is the damping factor, n is the index of refraction of waves in the medium; f(r) is the scattering indicatrix; ϑ is the angle between vertical and the direction of the radiation, r is the angle between the direction of radiation incident on an element of volume, and the direction of the radiation scattered by this volume; $\tilde{\lambda}$ is the coefficient characterizing the fraction of scattered power in the total amount absorbed; B_{ν_0} is the radiation function of the medium. In this case (since it is possible to use the principle of local thermodynamic equilibrium), this is Planck's function for the radiation flux of the medium into a vacuum. /49

The combination of Equations (1) — (3), (6), (7) completely determines the intrinsic radiation of the Moon. Consequently, on the basis of the different characteristics of radiation it is possible (at least in theory) to determine all the parameters of a substance that enter into these equations. Knowing them makes it possible to draw conclusions regarding the nature of a substance and its microstructure.

The general method of investigating the properties of an object is a comparison of observed phenomena with theory. In particular, the determination of the parameters of the surface layer of the Moon amounts to finding the parameters of the above equations which satisfy the solution I_ν obtained experimentally, i.e., amounts to the solution of the reverse problem. However, its solution involves great difficulties. Therefore, it is usual to seek the direct solution for a family of parameter values which are then found by comparing calculation with experiments. This is possible in practice when the solution is determined by only one parameter. We have, however, about ten unknown parameters (k, c, ρ, ε, α, q, etc.) and the majority in the general case are functions of depth, but sometimes functions of temperature as well. Hence the method of analysis must consist in selecting from the radiation characteristics those which are determined essentially by one parameter. Other parameters either have no influence whatever upon them, or have an effect that is so weak that it may be disregarded in the first approximation. To explain a specific phenomenon or group of phenomena, an appropriate particular model is constructed. The set of particular models which explains all of the available experimental data makes it possible to construct a general model that satisfies all the data in the optimum fashion. It is this approach that the authors have taken.

If the medium is sufficiently homogeneous with depth in terms of its thermal and electrical properties, the solution of the transfer equation will be

$$I_\nu = (1-R)\int_0^\infty E_\nu e^{-\tau\sec\Phi}\sec\Phi\, d\tau, \qquad (8)$$

where R is the coefficient of reflection of the radiation from the interface. If the interface is sufficiently smooth, the Fresnel formulas will be valid for R. If it is very rough, R must be assumed to be the albedo of the surface. However, if the medium is quite inhomogeneous (for a given wavelength), Expression (8) will be more complex, since the value of R in this case will depend upon the depth

τ and will be determined by the Raccati differential equation [11]. Therefore, the coefficient of radiation transmission through the surface (1 - R) must be placed beneath the integral sign. The function B_ν in (8) is an unknown function which is determined as the solution of (7). The entire theory of the Moon's radiation until now has been based on the assumption that for radio waves $\tilde{\lambda} = 0$. Obviously this is valid with sufficient accuracy for waves longer than a millimeter. Scattering in the lunar substance may be significant for waves shorter than millimeter waves. Thus, if $\tilde{\lambda} = 0$, $B_\nu = n^2 B_{\nu_0}$ is a known function and the solution for the radio range, i.e., at $h\nu \ll kT$, is simplified considerably [7]:

$$T_e(0, t, \varphi, \psi) = [1 - R(\varphi, \psi)] \int_0^\infty T(y, \varphi, \psi, t) \times \sec \vartheta' \cdot e^{-\kappa y \sec \vartheta'} dy, \qquad (9)$$

where T_e is the effective radiation temperature of an element of the surface with coordinates φ and ψ; κ is the true absorption of radiation by the Moon, ϑ' is the angle at which the radiation strikes the interface from below; T(y, φ, ψ, t) is the actual temperature of the lunar substance at depth y at time t, obtained above in the form (5) as the solution of the equation of thermal conductivity (1) with boundary condition (4). After substituting this distribution of temperature with depth in (9) we obtain the following expression for the effective temperature of an element of the surface [7]: /50

$$T_e(\varphi, \psi, t) = [1 - R(\varphi, \psi)] \left\{ T_0(\psi) + \sum_{n=1}^{\infty} (-1)^n \frac{T_n(\psi)}{\sqrt{1 + 2\xi_n \cos \vartheta' + 2\xi_n^2 \cos^2 \vartheta'}} \times \right.$$
$$\left. \times \cos [n\Omega t - n\varphi - \varphi_n - \xi_n(\varphi, \psi)] \right\}, \qquad (10)$$

where $\delta_n = \frac{\sqrt{\frac{n\Omega\rho c}{2\kappa}}}{n}$ is the ratio of the depth of penetration of an electromagnetic wave $l_e = 1/\kappa$ to the depth of penetration of the n^{th} harmonic of the thermal wave l_{T_n}; $\xi_n = \text{arc tan} \frac{\xi_n \cos \vartheta'}{1 + \xi_n \cos \vartheta'}$ is the phase shift for the n^{th} harmonic of the effective temperature relative to the phase of the surface temperature.

In experimental studies of the Moon, the width of the polar pattern of the receiving antenna is usually greater than the angular dimensions of the Moon, i.e., integral radio emission is received. Therefore, for a valid interpretation of the measurement results, it is necessary to compare them with an exact solution of the integral radiation of the Moon. This was done in [12] on the assumption of uniformity of the properties of the upper crust of the lunar surface.

The average effective temperature over the disk according to [7] is:

$$T_e = \frac{1}{\pi} \int_{-\pi/2}^{+\pi/2} \int_{-\pi/2}^{+\pi/2} [1 - R(\varphi, \psi)] T_e(\varphi, \psi, t) \cos^2 \psi \cos \varphi d\varphi d\psi. \tag{11}$$

Since the principal contribution to the radiation comes from the central parts of the disk, it is advantageous to express this radio temperature, averaged over the disk, by the radiation of the center of the disk, introducing the appropriate conversion coefficients. As a result, for the effective temperature of integral radio emission, we will have the expression:

$$T_e = (1 - R_\perp) \beta_0 T_e(0) + (1 - R_\perp) \sum_{n=1}^{\infty} (-1)^n \frac{T_e(0) \beta_n}{\sqrt{1 + 2\delta_n + 2\delta_n^2}} \times \cos(n\Omega t - \varphi_n - \xi_n + \Delta\xi_n), \tag{12}$$

where β_0 and β_n are the corresponding averaging coefficients; $\Delta\xi_n$ is an additional phase shift that occurs during averaging. Calculation of these values was performed on a computer for a wide range of changes in ε and δ [12]. Thus, β_0 changes from 0.96 to 0.91 when ε changes from 1 to 6. The coefficients β_1 and β_2 with $\delta_1 > 10$ remain practically constant with changing δ_1. The maximum value of $\Delta\xi_1$ with changing ε within wide limits does not exceed -5°. The higher harmonics of the effective temperature averaged over the disk are considerably attenuated in comparison with the corresponding harmonics of the effective temperature at the center of the disk. This means

that the variation of the radio temperature averaged over the disk is described well by the first harmonic alone, which is confirmed by the results of measurements of the integral radiation of the Moon on different wavelengths, i.e.,

$$T_e = T_{e_0} + T_{e_1} \cos(\Omega t - \xi_1). \tag{13}$$

The theory of radiation of the Moon during an eclipse is given in [13]. Initially, to determine the temperature distribution with depth as in the case of the periodic regime, a thermal problem is solved, as formulated in (1) and (3). The function f(t) in Equation (3) is given as follows: in the interval from t_1 (the beginning of the penumbral phase of the eclipse) to t_2 (the start of the umbral phase) it decreases nearly linearly to zero, remains equal to zero until t_3 (end of umbral phase). It then increases nearly linearly once again to the original level at t_4 (end of penumbral phase). Exact and approximate expressions for the effective radio temperature of the center of the disk are given in [13] for each of the four time intervals listed above. For a comparison with experiment, it is interesting to know the maximum drop in the radio temperature ΔT_{e_m} which obviously is reached at t_3, the end of the umbral phase of the eclipse. This value, according to [13], is /51

$$\Delta T_{e_m} = -(1-R)\frac{4}{3\sqrt{\pi}} \varkappa a \left[a_1 (t_3 - t_1)^{3/2} + (a_2 - a_1)(t_3 - t_2)^{3/2}\right] + \\ + (1-R)\frac{\varkappa^2 a^2}{2}\left[a_1 (t_3 - t_1)^2 + (a_2 - a_1)(t_3 - t_2)^2\right]. \tag{14}$$

where

$$a = \sqrt{\frac{\varkappa}{\pi c}}; \quad a_1 = \frac{T_2 - T_1}{t_2 - t_1}; \quad a_2 = \frac{T_3 - T_2}{t_3 - t_2},$$

T_1, T_2, T_3 are the surface temperatures at times t_1, t_2, and t_3, respectively.

As we can see from (14) the effect of the change in radio temperature is determined by the value $\kappa a = 2\pi \frac{b\sqrt{\varepsilon}}{c\lambda}$, i.e., by the same relationship between the electrical and thermal parameters of the material as in the periodic regime, where $\delta = \frac{l_e}{l_T} = \sqrt{\frac{\omega}{2}} \frac{c\sqrt{\lambda}}{2\pi b\sqrt{\varepsilon}}$, where $b = \frac{\operatorname{tg}\Delta}{\rho}$ is the specific tangent of the loss angle.

Experimental Results of Lunar Investigation

As we can see from (13) the intrinsic radiation of the Moon is advantageously characterized by the spectra of three values: (1) the spectrum of the constant component; (2) the spectrum of the amplitude of the first harmonic; (3) the spectrum of the delay in radio waves with respect to the optical phase.

The spectrum of the constant component of the integral radiation, obtained by using the method of exact measurement by means of an "artificial Moon" [14 — 16] is shown in Figure 2. The spectrum of the amplitude of the first harmonic, characterized by the relationship $M(\lambda) = \frac{T_{a_1}(\lambda)}{T_{a_0}(\lambda)}$, is shown in Figure 3. At waves longer than 15 to 20 cm, the variations in radiation intensity practically vanish [1, 14 — 47].

Figure 4 shows the spectrum of the phase lag of the first harmonic /52 $\xi_1(\lambda)$ [1, 14 — 47].

Important information on the properties of the material of the upper crust was included in the data on changes in radiation intensity during lunar eclipses [13, 48 — 56]. These data are presented in Figure 5, where the value $\bar{M}_e = T_{e_m}/\Delta T_e$, equal to the reciprocal of the maximum relative drop in intensity, characteristic of the end of the umbral phase of eclipse of the center of the lunar disk, is plotted on the ordinate. As we can see from this figure, the change in intensity during the eclipse is practically nonexistent at waves longer than 1.5 cm.

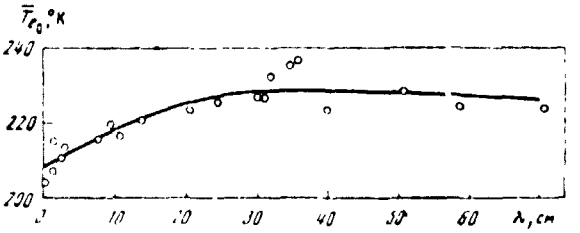

Figure 2. Experimental spectrum of constant component of integral radio emission.

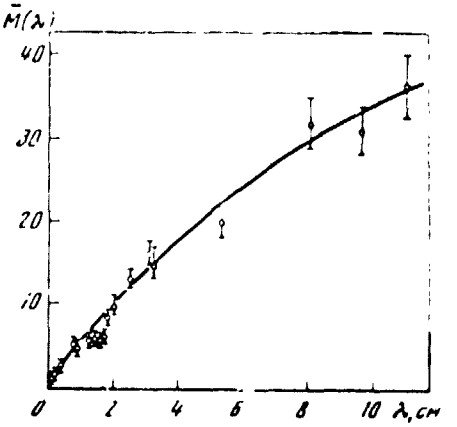

Figure 3. Experimental spectrum $\bar{M}(\lambda) = \bar{T}_{e_0}(\lambda)/\bar{T}_{e_1}(\lambda)$.

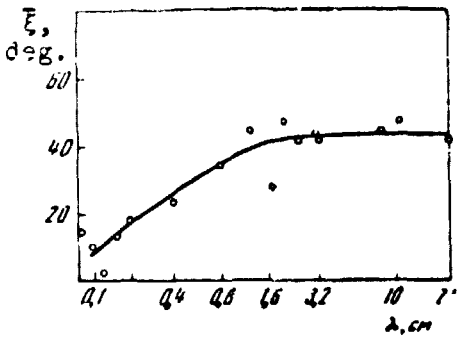

Figure 4. Experimental spectrum of phase lag of first harmonic.

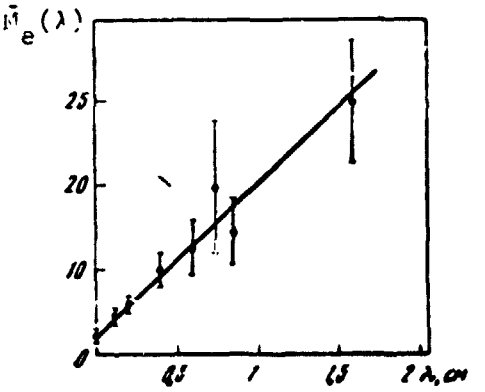

Figure 5. Experimental spectrum $\bar{M}_e = \bar{T}_{e_m}/\Delta\bar{T}_e$.

A highly significant characteristic of the surface layer of the Moon is the spectrum of the reflection coefficient. Here, in addition to the radioastronomical measurements of the coefficient of reflection (for example, on the basis of the polarization of the radiation [57 — 63]), it is necessary to use the radar data obtained over a wider spectrum [64 — 70]. In the following, we shall use values that we have reduced considerably for the coefficients of radar reflection. As a matter of fact, the radar experiment yields a value $gR_\perp$, where $R_\perp$ is the reflection coefficient for perpendicular incidence, while g is a factor that takes into account the roughness, whose estimation usually involves a number of assumptions [65].

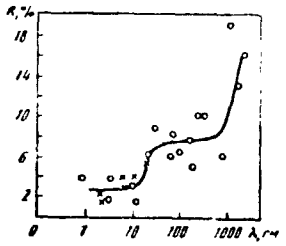

Figure 6. Experimental spectrum of reflection coefficient.

Moreover, the experiments on models in the optical range [71] have shown that for roughnesses that are characteristic for the Moon, g = 1.6 at centimeter waves, and g = 1.06 at decimeter waves. In Figure 6 the points indicate the values of the coefficient of radar reflection, reduced in accordance with the indicated values of g. The crosses represent the data obtained primarily from measurements of the polarization of the radiation. /53

An important role in the determination of the average chemical composition of the material composing the outer crust of the Moon is played by laboratory tests of the dielectric constant ε and the specific loss tangent $\tan \Delta/\varepsilon$ of certain terrestrial rocks, conducted over a broad range of wavelengths. The measurements of these values showed that they depend quite strongly on the chemical composition, and may therefore serve to determine the latter.

The entire body of data presented above leads to unambiguous results regarding the temperature state of the surface as well as the properties and structure of the material of the surface layer and its chemical composition.

Structure and Properties of the Material of the Upper Crust of the Moon

The upper crust of the Moon can be described most completely by a four-layer model. True, the actual density must vary from one layer to the next quite smoothly, so that such a division into layers has been introduced somewhat conditionally to simplify the situation. The properties of these layers are shown in Table 1.

TABLE 1

MODEL OF PHYSICAL PROPERTIES OF LUNAR ROCKS

Layer	Depth of layer d, cm	Density ρ, g·cm	Porosity $\mathcal{P}$, %	Thermal conductivity k(300), 10^{-6} kcal/ $cm^{-1}\cdot sec^{-1}\cdot deg^{-1}$	Thermal capacity c (300), $cal\cdot g^{-1}\cdot deg^{-1}$	Thermal inertia, γ, (300) $cal^{-1}\cdot cm^{2}\cdot sec^{1/2}\cdot deg^{-1}$	Penetration depth of thermal wave l_T, cm	Heat flux density q, $10^{-6} cal\cdot cm^{-2}\cdot sec^{-1}$	Dielectric constant, ε	Specific tangent of loss angle tan $\Delta/\rho\cdot 10^{-3}$	Penetration depth of electro-magnetic wave l_ν, cm
Porous surface	0-4	0.7±0.2	80	7±3	0.19	1000	7.5	0.7-0.8	2±0.2	9±3	(15-17)λ
Porous layer	4-400	$1\pm^{0.2}_{0.1}$	60	9±3	0.19	800	7.5	0.7-0.8	2.5±0.2	8±2	(15-17)λ
Transi-tional layer	400-600	1.5-2	30	10^3	0.19				3.5		
Rocks	Greater than 600	2.5-3	0-10	$5\cdot 10^3$	0.19				5-6		

Now let us examine the methods of interpreting the experimental data on intrinsic radiation and reflection of radio waves to obtain data on the properties and structure of the material of the upper crust of the Moon, as shown in this table. We shall not be going into great detail regarding the calculations performed in these works, but shall merely limit ourselves to a description of the physical analysis.

The possibility of observing sharp inhomogeneities in the surface layer by comparing the data at various wavelengths is connected, on the one hand, with a changing thermal state and, on the other, with the fact that the data at various wavelengths correspond to measurement of temperature at various depths. In fact, the spectrum of the amplitude of the first harmonic of the radio temperature of the Moon (see Figure 3) indicates that, as the wavelength increases, the variations in radiation intensity decrease. The amplitude of the variations is maximum at infrared wavelengths. This can only be explained as follows. At infrared wavelengths, the radiation comes from the surface itself, and consequently the value of the temperature as well is obtained for the surface. At longer wavelengths, it is a layer of finite thickness that is radiating, and this thickness increases with the wavelength, i.e., a change in the wavelength of the radiation received involves a sounding of the layer with depth. Any sharp changes in the properties of the upper crust with depth lead to a change in the temperature distribution and consequently may be observed in the radiation. By virtue of the fact that in the upper layer with a thickness (3 - 4) l_T considerable temperature gradients arise due to the solar flux, the study of this layer is the most appropriate. (For example, the spectra of the amplitude of the first harmonic and phase lag give information only on this layer, with a thickness on the order of several tens of centimeters). /54

However, as will be shown below, due to the significant heat flux from the Moon's core and the low thermal conductivity of the material composing the outer layer, it is possible to study the surface layer down to considerable depths.

An analysis of the spectrum of the amplitude of the first harmonic of the radio temperature (see Figure 3) has shown that it satisfies well the homogeneous model of the surface layer, and does not correspond in any way to the highly inhomogeneous model that assumes the existence of a dust layer several millimeters thick, covering the dense rocks [72, 73]. The roughly homogeneous distribution of thermal properties of the material with depth is also indicated by the spectrum of the phase lag of the first harmonic $\xi_1(\lambda)$ (see Figure 4). The limiting phase lag with an increase of λ is equal to 45°. It is precisely this value that is obtained in the theory of the homogeneous model [7]. Any significant inhomogeneity, especially of a dust layer, leads to an abrupt increase in the limiting lag [74]. Hence, the homogeneous model of the uppermost layer shows a quite good agreement with the spectrum of intrinsic radiation.

Thermal Parameter γ

As was shown above, in calculating the thermal state of the surface in the first approximation, a homogeneous model was assumed, in which the properties are independent of depth. In the second approximation, a homogeneous model was used with thermal conductivity and thermal capacity dependent upon temperature.

From measurements we know quite precisely that the midnight temperature of the Moon's surface T_m = 100° K, the noon temperature T_n = 395° K, the ratio of the constant component to the amplitude of the first harmonic of the integral radiation at λ = 0 (i.e., in the infrared range T_0/T_1 = 1.3 (see Figure 3), and the relative temperature drop during an eclipse (in the same range) $\Delta T_e/T_{e_m}$ = 0.52 (see Figure 5). A comparison of these values with the results of a theoretical calculation of the thermal state of the surface in the approximation of a homogeneous model, with consideration of the temperature relationship of the thermal conductivity and thermal capacity [8], will yield the following values of the parameter γ: /55

$$\gamma_1\ (300^\circ\ K) = 1000\ cal^{-1} \cdot cm^2 \cdot sec^{1/2} \cdot deg^{-1};$$

$$\gamma_2\ (300^\circ\ K) = 800\ cal^{-1} \cdot cm^2 \cdot sec^{1/2} \cdot deg^{-1}$$

for eclipse and lunation, respectively.

The eclipse values of γ refer to the uppermost layer, while the lunation values refer to a layer ten times thicker. In fact, the process of the eclipse lasts 4 to 5 hours. During this period, only the uppermost layer, on the order of 1 to 2 cm, manages to cool off. In 29.5 days (lunar days) the deeper layers are involved in the process of temperature change. The ratio of the depths is proportional to the root of the ratio of the time of the processes, i.e., it equals 10. The similarity of the values of γ for eclipse and lunation processes also speaks in favor of the approximate homogeneity of the properties with depth.

Parameter $\delta = l_e/l_T$

The effective thickness of the radiant layer is characterized by the depth of penetration of an electrical wave $l_e = 1/\kappa_\nu$. Obviously, the greater the depth of the radiant layer l_e in comparison with the depth of penetration of the thermal wave l_T, the smaller will be the amplitude of the oscillations in intensity. Consequently, the spectrum $\bar{M}(\lambda)$ characterizes the value of the relationship $\delta = l_e/l_T$. A comparison of the experimental spectrum $\bar{M}(\lambda)$ with the corresponding theoretical relationship $\bar{M}_t(\lambda)$ which as we can see from (12) has the form

$$\bar{M}_t(\lambda) = \frac{T_0(0)}{T_1(0)} \frac{\beta_0}{\beta_1} \sqrt{1 + 2\beta_1 + 2\beta_1^2},$$

leads to the value $\delta \cong 2.3\lambda$. The spectrum obtained for the value $l_e = 2.3 l_T \lambda$, as in the case of the model of the first approximation ($l_e = 2 l_T \lambda$) indicates the dielectric nature of the substance of the upper crust of the Moon. It is most likely that rocks which are analogous to terrestrial ones (i.e., silicates) might constitute such

a dielectric. The value of thermal capacity for all silicates (with an accuracy of up to 10%) at T = 300° K is equal to c (300° K) = 0.19 cal/g/degree.

Density ρ of Material of Surface Layer of the Moon

Data are available that indicate a slight inhomogeneity in the properties of the material with depth in the upper layer on the order of several centimeters. This does not contradict the statement made earlier that the spectra of the amplitude and phase of the lag correspond to a homogeneous model. As a matter of fact, the spectra are not very sensitive to slight inhomogeneities. Weak inhomogeneity, involving a slight and continuous change in the properties of matter with depth (by a factor of 1.2 - 1.3 in density) is shown by calculations to have little effect on the nature of these spectra. spectra. In this case their changes lie within the limits of measurement accuracy, i.e., they assume the existence of some inhomogeneity.

To observe this inhomogeneity, one must find those radiation /56
parameters which are sensitive to it and which can be measured. Such parameters are the reflection coefficient of radio waves, the polarization of radiation and data on "eclipse" and night temperature of the surface. An increase in the coefficient of reflection in the range λ =(15 - 30) cm (see Figure 6) may indicate either a real frequency dependence of the dielectric constant of the substance or the existence of inhomogeneity of dielectric properties with depth. The first assumption is invalid, since a sharp increase in ε with wavelength according to the Kramers-Kronig theorem would necessarily lead to an increase in the losses in this range of wavelengths that would have made itself evident in the spectrum M(λ). This has not yet been observed.

Evidently it is the second case that occurs. In fact, if the upper layer is less dense, it has a lower dielectric constant. The waves incident on the surface, whose length is much less than the thickness of this layer, will be reflected from the upper interface

of the medium with a vacuum. For waves whose length is much greater than the thickness of this layer, it is practically nonexistent and these waves are reflected from a lower, denser layer. Hence, the coefficient of reflection for such a medium will change in a certain interval of frequencies from the value of the reflection coefficient for the surface to its value for the substrate. Calculation of the coefficient of reflection for an exponential change in density with depth is

$$\rho(y) = \rho_2 - (\rho_2 - \rho_1)\exp(-y/y_0),$$

where $\rho_1 = \rho(0)$, $\rho_2 = \rho(\infty)$ showed that the wavelength λ near which there is a change in the coefficient of reflection is linked to the characteristic dimension of the layer y_0 by the relationship [75]:

$$2\pi y_0 = \lambda_1.$$

From experiment (see Figure 6) $\lambda_1 \approx 30$ cm; consequently $y_0 \approx 1.5$ cm. The total thickness of the inhomogeneous layer $d_1 \approx 3$ to 4 cm. The following data satisfy the observed spectrum $R(\lambda)$:

$$\rho_1 = (0.6 - 0.7)\text{g}\cdot\text{cm}^{-3}, \quad \rho_2/\rho_1 = 1.5, \quad y_0 = 1.5 \text{ cm}.$$

The same degree of inhomogeneity is indicated by measurements of γ on the basis of the surface temperature during eclipse and lunation. The difference between γ_1 and γ_2 also indicates a slight increase in density with depth.

The study of the properties of the deeper layers of the Moon has become possible in conjunction with the fact that accurate measurements using the method of the "artificial Moon" have made it possible to detect an increase in the constant component of the integral radio emission with the wavelength, which is equivalent to observing a temperature increase with depth (see Figure 2). For an interpretation of this phenomenon, a calculation was made for the constant component of the radio emission of a surface layer of the Moon that was homogeneous to great depth, in the presence of a heat flux from the core. However, subsequent measurements have shown that the radio emission

temperature ceases to increase at waves longer than 25 to 30 cm, clearly indicating a significant compaction of material in the depths, corresponding to the depth of penetration of these waves. The authors discuss the theory of the constant component of integral radio emission of the Moon in the presence of heat flux from the core for a two-layer medium. The following relationship $\bar{T}_e(\lambda)$ was obtained for $\lambda \geq 3$ m:

$$\bar{T}_e(\lambda) = \bar{T}_e(300) + (1 - R_\perp) A_1 \lambda \cdot 2{,}2 \sqrt{\frac{2}{\pi}} \pi q [1 - A_2 \exp(-\varkappa d_2)], \qquad (15)$$

where q is the density of heat flux from the core; $A_1 = 0.82$ and $A_2 = 0.9$ are the coefficients that appear with averaging over the lunar disk; d_2 is the thickness of the porous layer, within whose limits the properties of the substance remain constant. Figure 7 shows the theoretical curves plotted according to (15); in addition, we have plotted the experimental points taken from Figure 2. We can see from Figure 7 that a good agreement of the theoretical and experimental results is obtained when the thickness of the porous layer $d_2 = 400 \pm 100$) cm (whose density $\rho_2 = 1$ g/cm^{-3}) and heat flux density is

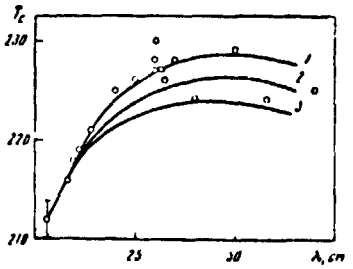

Figure 7. Theoretical dependence of effective radio temperature averaged over the disk on the wavelength for a thickness of the porous layer d_2.

1 — 300; 2 — 400; 3 — 500 cm. The circles represent the experimental results.

$$q = (0.72 \pm 0.08) 10^{-6} \text{ cal} \cdot \text{cm}^{-2} \cdot \text{sec}^{-1}.$$

/57

Significant compaction of the material at a depth on the order of several meters is indicated by the spectrum of the reflection coefficient of radio waves. The increase in the reflection coefficient at $\lambda > 10$ m [65] clearly indicates that the reflection of these waves occurs from denser rock. Solving the Riccati equation on a computer provided the spectra of the reflection coefficient for a complex model of the surface layer of the Moon, plotted according to radioastronomical measurements. Figure 8 shows the qualitative dependence

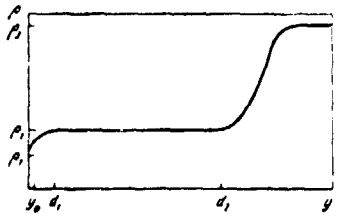

Figure 8. Qualitative nature of change in density with depth.

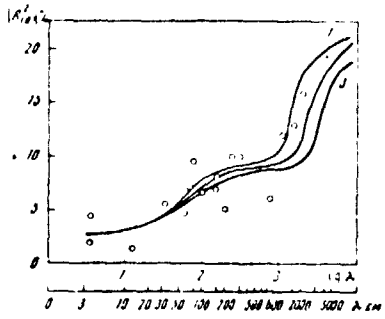

Figure 9. Theoretical dependence of reflection coefficient on wavelength for various values of parameters.

$\rho_1 = 0.7$ g·cm^{-3}; $\rho_2 = 1$ g·cm^{-3}; $\rho_3 = 2.5$ g·cm^{-3} d_2; 1 — 150; 2 — 250; 3 — 350 cm.

The circles indicate experimental results.

of density on depth for which the calculation of $R(\lambda)$ has been performed. In the calculations we used the frequency dependence of the dielectric constant. As has been shown by laboratory studies of losses in various terrestrial dielectric rocks over a broad range of wavelengths, the dielectric constant changes with wavelength. In the range 0.03 m $\leq \lambda \leq$ 200 m this relationship is approximated quite well in the form

$$\sqrt{\varepsilon(x, \lambda)} = 1 + \xi(\lambda)\rho(y), \tag{16}$$

where $\xi(\lambda) = 0.5 + 0.05 \log \lambda/3$. Figure 9 shows the calculated spectra of the reflection coefficient with the following parameter values: $y_0 = 1.5$ cm; $\rho_1 = 0.7$ g·cm^{-3}; $\rho_2 = 1$ g·cm^{-3}; $\rho_3 = 2.5$ g·cm^{-3}; $d_2 = 150, 250, 350$ cm. In addition, we have plotted the experimental points taken from Figure 6 for comparison. It is evident that the model of the surface layer in question for the indicated values ρ_1, ρ_2, ρ_3 describes quite well the observed spectrum of the reflection coefficient. For the thickness of the porous layer, we obtain a value $d_2 = 250 \pm 100$ cm. From radioastronomical measurements, we have a value of $d_2 = 400 \pm 100$ cm. Evidently the latter is more reliable. In fact, the information on the value of d_2 in the spectrum of the reflection coefficient is based mainly on three measurements at $\lambda > 10$ m, and the accuracy of even these measurements is low. In

/58

order to obtain d_2 reliably from the spectrum $R(\lambda)$, it is clearly necessary to obtain additional radar data at $\lambda > 10$ m.

Thermal Conductivity k and Depth of Penetration of Thermal Wave l_T

Using the values obtained above for γ_1 (300), γ_2 (300), ρ_1, ρ_2 and c (300), we see that the thermal conductivity of the substance of the porous surface k_1 (300) = $(7 \pm 3)\cdot 10^{-6}$ cal·cm^{-1}·sec^{-1}·deg^{-1} and the thermal conductivity of the porous layer $k_2 = (9 \pm 5)\cdot 10^{-6}$ cal·cm^{-1}·sec^{-1}·deg^{-1}. The values given here for thermal conductivity k_1 and k_2 correspond to the temperature T = 300 K. As we know, the thermal conductivity of porous bodies a priori must depend on the temperature because of the radiational transfer of heat through the pores. In the "lunar" interval of temperatures, the radiant transfer is accomplished through radiation at infrared waves, whose length corresponds to the Planck maximum $\lambda = 0.38/T \simeq (10 - 30)$ μm. For a porous body in which the effective pore size is equal to l_{po}, and the substance itself is impermeable to infrared rays, the value of the radiation thermal conductivity k_p is

$$k_{pn} = \frac{R_n}{2-R_n} 4\sigma l_{po} T^3. \qquad (17)$$

Here σ is the Stefan-Boltzmann constant. It can be shown that for lunar temperatures the radiation thermal conductivity is much less than the molecular, if the pores are no larger than a tenth of a millimeter.

If the material is itself permeable to infrared waves, $k_p = (16/3)\sigma\varepsilon_n l_\nu T^3$, where l_ν is the Rosseland average depth of penetration of infrared radiation into the substance and ε_n is the dielectric constant of the substance for infrared waves. Calculations show that in the equation $l_\nu = a\lambda$ (which follows from the radiation measurements and the theory of non-resonance absorption of waves in a substance) $l_\nu = 0.365\ a/T$. Then [10]:

$$k_p = 2e_n a z T^2. \qquad (18)$$

Repeated attempts have been made to observe the influence of radiation transfer on the radio emission of the Moon. A theoretical analysis of this effect [8] led to the conclusion that the phase dependence of the intrinsic radiation both in the infrared and radio ranges is not sensitive to radiation transfer. The experimental data agree with a wide variety of models with thermal properties that do and do not depend upon temperature. To estimate the amount of radiation transfer, it is necessary to find phenomena which are determined to a sufficiently high degree by the temperature dependence of thermal conductivity. As has been explained, there is such a phenomenon.

It has been shown that the presence of a weak temperature dependence of thermal conductivity leads to a qualitatively new effect [76], consisting of an increase of the constant component with depth in a layer on the order of l_T. This effect was then calculated quantitatively according to Equations (6) and (7) with different laws of the temperature dependence [8, 9]. It was found that the increase in temperature ΔT_{max} depends upon γ and the value k_p/k_0. It was shown in [9] that the constant component of the true temperature increases with depth according to the law $T_0(y) = T_0 + \Delta T_{max}[1 - \exp(-2y/l_T)]$. This leads to an increase of the constant component of the radio temperature with increasing wavelength. However, the increase must cease /59 at waves that proceed from depths greater than (2 to 4) l_T. The calculation shows that the constant component of the brightness temperature of the radio emission depends upon the wavelength according to the relationship

$$T_{e_0} \simeq T_0 + \Delta T_{max} \frac{4,6\lambda}{1+4,6\lambda}.$$

From the above, it is clear that even at wavelengths of ~2 to 3 cm the constant component reaches its maximum value of $T_{e_0} = T_0 + \Delta T_{max}$.

Hence, by measuring the surface temperature (in the infrared range) and in the depths (at waves with $\lambda \simeq (2 - 3)$ cm) one can determine the temperature rise ΔT_{max} and determine k_p/k_0. Such a determination has become possible owing to the exact measurements of radio temperature by the method of the "artificial Moon." It was shown in [10] that the difference that exists in the constant components on the basis of infrared and radio measurements at 10 — 15° is explained by this effect. By comparison with theory, it was found that — if the substance of the Moon were impermeable to infrared waves and had $\gamma_2 \approx 800$ cal^{-1}·cm^2·sec$^{1/2}$·degree — the relative amount of radiation transfer through the pores at T = 300° K would be equal to $k_{p_{po}}$ (300)/k_0 = 0.25. In a permeable substance k_p (300)/k_0 = 0.4. In all of these calculations homogeneous models were used, inasmuch as inhomogeneity of the substances does not lead to the indicated increase in the constant component with depth, but affects the value ΔT_{max}.

Electromagnetic Properties of the Substance: Depth of Penetration of the Electrical Wave l_e, Dielectric Constant ε, and Specific Loss Tangent tan δ/ρ

It was shown earlier that $l_e/l_T = 2.3\lambda$, $l_T \approx 7.5$ cm; then $l_e = 17\lambda$.

The dielectric constant of any substance at radio wave frequencies depends on the porosity or density ρ. As a result of laboratory investigations of silicate rocks, the following relationship was established between ε and ρ [7]:

$$\sqrt{\varepsilon} = a\rho + 1 \qquad (19)$$

with the coefficient a slightly dependent upon frequency. When λ changes in the range $0.03 \text{ m} \leq \lambda \leq 200$ m, this value changes from 0.55 to 0.7. Therefore, a measurement of ε serves simultaneously as a new independent measurement of density.

To determine the dielectric constant ε of the substance of the upper crust of the Moon, several methods have been proposed: determination of ε on the basis of the polarization of the intrinsic radiation [59], on the basis of the distribution of the brightness temperature over the disk [57], on the basis of the determination of the phase delay of the radio emission from portions of the disk located at various longitudes along the equator of the Moon, by comparison with the phase of heating of the corresponding parts of the surface [60], and on the basis of direct radar measurement of reflection [65 — 69]. All of these methods are based on the fact that the lunar surface is quite smooth, since the Fresnel law is valid for the coefficient of reflection.

The polarization method of determining ε was used in [61 — 63, 70]. These measurements give a value $\varepsilon_1 = 2$ for the dielectric constant of the porous surface, and for the dielectric constant of the porous layer, $\varepsilon_2 = 2.5$. From the value of ε obtained according to (19), for the densities ρ_1 and ρ_2 we obtain the values $\rho_1 = 0.75$ g·cm^{-3} and $\rho_2 = 1$ g·cm^{-3} which coincide with the parameters obtained above from the spectra of the reflection coefficient and the constant component of radio emission.

Comparison of the spectrum of change in intensity during a lunar eclipse with the theory of this eclipse makes it possible to determine the specific loss tangent $b_1 = \tan \Delta/\rho_1$ for the first centimeter of the layer (see above). This value is found to be /60

$$b_1 = (9 \pm 3) \cdot 10^{-2}.$$

From the lunation measurements above it was found that $l_\theta/l_T = 2.3$, i.e., $\frac{\gamma_2}{\sqrt{\varepsilon_2 b_2}} = 12.6 \cdot 10^3$. Taking into account the indicated values for c, γ_2, ε_2, for b_2, we obtain the value $b_2 = (8 \pm 2) \cdot 10^{-3}$.

Chemical Composition of the Lunar Substance

The method of estimating the chemical composition of the lunar substance from radioastronomical measurements is based on the assumption that the solid substance of the Moon is a composition of silicate rocks as on Earth. Measurement of the loss tangent tan Δ and the dielectric constant ε of various terrestrial rocks has shown that these values are greatly dependent upon the chemical composition, and can therefore serve in determining the latter. However, as we know, the parameters tan Δ and ε depend not only on the chemical composition, but on the density of the rock as well. Hence, in [78] it was noted that it is necessary for purposes of comparison to use several functions of tan Δ and ε which are independent of the density of the material, i.e., would be invariants of the density. Theoretical and extensive experimental studies of igneous rocks indicated that with sufficient accuracy the values $\tan\Delta/\rho = b$, $(\sqrt{\varepsilon} - 1)/\rho = a$ [77] are independent of the density ρ over a broad range of its variation, and depend only on the chemical composition of the rock and partly on the type of crystalline structure, in other words, the history of the rock's formation (intrusive, effusive). The values b and a increase by factors of 10 to 20 and 2, respectively, with a shift from acid to basic rock. The dependence of a and b upon the chemical composition was found to be most conveniently represented in a form analogous to the variational diagram of Harker [79]. On the abscissa, the value of a or b is laid out for a given rock, while on the ordinate we plot the values of the content of basic oxides in the rock. As a result, a diagram was obtained for several intrusive rocks (Figure 10); in constructing the diagram, data on the chemical composition of the rock were introduced primarily from the typical analyses given in the literature for each type of rock. The connection between the parameters a and b and the chemical composition has to do with the fact that in the rocks the variations of composition are not arbitrary. There are no silicate rocks with arbitrary contents of various oxides: a decrease, for example, in the SiO_2 content upon transition from one rock to another on the average leads to certain changes in the content of one or more oxides. This actually means that, for example, the average percentile content of SiO_2 in the rock determines the content of remaining oxides.

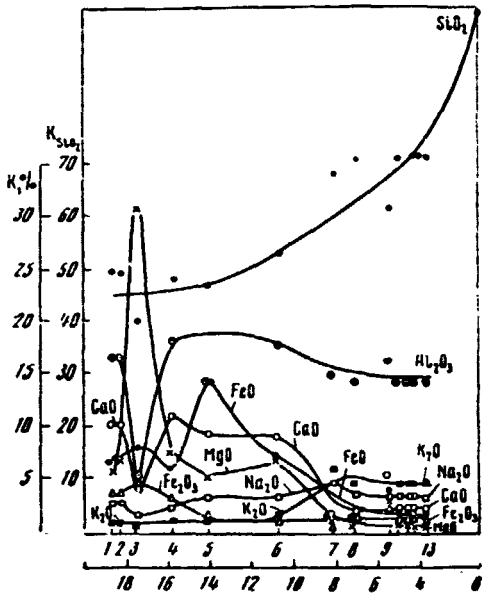

Figure 10. Variational diagram of losses of igneous intrusive rocks.

1 — gabbro-diabase No. 1; 2 — gabbro-diabase No. 2; 3 — peridotite; 4 — gabbro No. 1; 5 — gabbro diabase No. 3; 6 — gabbro No. 2; 7 — granite-aplite; 8 — granite No. 1; 9 — quartz diorite; 10 — granite No. 2; 11 — granite No. 3; 12 — medium-grained granite; 13 — granite No. 4.

The existence of a regular connection between the concentration of each oxide with the values of b and a may be explained mathematically as follows. The losses, for example, in a given rock may be represented as $b = dD + eE + fF$, where d, e, f are the percentile contents of oxides D, E, and F. If there is a change in d upon transition from one rock to another, i.e., the percentage of oxide D, there is at least a change in the percentage of one or more of the oxides, i.e., e(d), f(d), etc., which finally gives a certain relationship $b = b(d)$. For the lunar substance, the radioastronomical methods at centimeter waves for b gave a value $b \cong (8 \pm 2)\cdot10^{-3}$. For a frequency f = 100 mHz, we can expect $b = 9\cdot10^{-3}$. Using the graph in Figure 10, we can readily see that /61 the upper crust of the Moon has the following average chemical composition (in percent): SiO_2 — 57 ± 3, Al_2O_3 — 16 ± 1, Fe_2O_3 — 1 ± 0.2, FeO — 5 ± 1, CaO — 5.5 ± 2.5, MgO — 3.5 ± 2, Na_2O — 4 ± 0.5, K_2O — 3 ± 1. Table 2 presents a comparison of the results of a chemical analysis obtained by this method with the results of an analysis by the Surveyors (the content is given as the percentile content of atoms).

From the data in Table 2 one can see the good agreement of the data. On comparing the data for Ca, one must keep in mind that the figures obtained by the Surveyors include the concentration of K as well.

TABLE 2

RESULTS OF CHEMICAL ANALYSES

Element	Surveyor V	Surveyor VI	Surveyor VII	Radio-astronomical methods
O	58 ± 5	57 ± 5	58 ± 5	62 ± 4
Si	18.5 ± 3	22 ± 4	18 ± 4	20 ± 1
Al	6.5 ± 2	6.5 ± 2	9 ± 3	7 ± 0.5
Mg	3 ± 3	3 ± 3	4 ± 3	2 ± 1
Fe	13 ± 3	5 ± 2	2 ± 1	2 ± 0.5
Ca		6 ± 2	6 ± 1	2 ± 1
K	—	—	—	1.5 ± 0.5
Na	<2	<2	<3	1.5 ± 0.2

Microstructure of the Substance of the Upper Crust of the Moon

It was shown earlier that the amount of radiation transfer of radiation through the pores $k_{p_{po}}/k_0 = 0.25$; with a permeable substance it is $k_p/k_0 = 0.4$.

Assuming $k = k_p + k_0 = (9 \pm 3)\cdot10^{-6}$ cal·cm^{-1}·sec^{-1}·ged $^{-1}$, we find that $k_{p_{po}} = (1.5 \text{ to } 2.5)\cdot10^{-6}$ cal/cm^{-1}·sec^{-1}·deg^{-1} and $k_p = (2.0 \text{ to } 3.5)\cdot10^{-6}$ cal·cm^{-1}·sec^{-1}·deg^{-1}.

According to the $k_{p_{po}}$ obtained from (17), we see that the effective pore size is (170 to 350) μm. Inasmuch as the porosity of the substance is nearly 50%, the pore sizes must be approximately equal to the size of the particles. If we consider the substance to be permeable to infrared waves, then according to (18) and the value of k_p, we find that a = (6 - 12) and consequently for infrared waves $l_e = (6 - 12)\lambda$. For waves longer than 1000 μm, as we saw, $l_e = 17\lambda$. It seems to us most likely that the substance is permeable to infrared waves. Then, in order for the heat transfer through the

/62

pores to be insignificant, the pores (and consequently the particles of material) must be much smaller than the mean free path of an infrared quantum, equal to l_e (60 - 120) μm. Evidently these can be particles ranging in size from tens to several tens of micrometers.

Homogeneity of the Properties over the Surface

The data obtained earlier with the exception of the data on γ are averaged over the entire hemisphere of the Moon. Therefore, it is natural for the question to arise: to what extent do they correspond to local values? According to studies at infrared wavelengths, the thermal properties over the disk (with the exception of the floors of the craters with rays) change very little, by no more than 20 — 25% [80]. These changes fall practically within the limits of measurement accuracy. A high degree of uniformity has also been observed over the disk with respect to the radiation characteristics, such as $M(\lambda)$ and ξ_1, with averaging over areas from tens to hundreds of kilometers [42 — 46, 80]. In this connection, one can speak of the existence of radiometric homogeneity, analogous to the familiar photometric homogeneity [81], associated with the homogeneity of the characteristics of the reflected light. The radiometric homogeneity indicates homogeneity of the electrical properties of the upper crust of the lunar surface in a layer at least 10 cm thick. In particular, it seems that the substance on the surface of the maria and continents is practically identical [80]. Finally, the hypothesis that the upper layers of rock in the continents are granite and those in the maria are of basalt does not correspond with the radiation characteristics.

The high degree of homogeneity in the properties of the upper crust along the horizontal is supported by the fact that the characteristics obtained constitute real properties of the substance at each site. The high degree of homogeneity of the properties is supported by the results obtained by the Luna 9, Luna 13, and Surveyor I — VII probes.

□□□

The foregoing discussion shows that the investigation of the intrinsic thermal radiation of the Moon makes it possible to obtain rather complete data on the temperature state of the lunar surface, its physical conditions, and the structure of the material. The objectivity of the data obtained is supported by the results of the automatic probes Luna 9, Luna 13 and Surveyor I — VII. This allows us to state with certainty that the methods devised for analysis and interpretation of the data may be used successfully for the investigation of certain other planets — Mars, for example — where the physical conditions are similar to those on the Moon.

References

1. Dicke, R. H. and R. Beringer. Astrophys. J., Vol. 103, 1946, p. 735.
2. Krotikov, V. D. and V. S. Troitskiy. UFN, Vol. 81, 1963, p. 588.
3. Troitskiy, V. S. J. Res. NBS, Vol. 69D, No. 12, 1965, p. 1585.
4. Weaver, Horalld. Solar Systm. Radio Astron., Athens Ionosph. Inst. Nat. Observ., 1965,p. 295.
5. Troitskiy, V. S. Izv. VUZov, Radiofizika, Vol. 10, No. 9 — 10, 1967, p. 1206. /63
6. Krotikov, V. D. and O. B. Shchuko. Astron. Zh., Vol. 40, No. 2, 1963, p. 297.
7. Troitskiy, V. S. Astron. zh., Vol. 31, 1954, p. 51.
8. Linsky, I. L. Icarus, Vol. 5, No. 6, 1966, p. 606.
9. Troitskiy, V. S., A. B. Burov and T. N. Aleshina. Icarus, Vol. 8, 1968, pp. 423-433.
10. Troitskiy, V. S. Nature, Vol. 213, 1967, p. 688.
10a. Troitskiy, V. S. Izv. VUZov, Radiofizika, Vol. 10, No. 8, 1967, p. 1051.
11. Brekhovskikh, A. M. Volny v sloistykh sredakh (Waves in Laminar Media). USSR Academy of Sciences Press, 1957.
12. Krotikov, V. D. Izv. VUZov, Radiofizika, Vol. 6, No. 5, 1963, p. 889.

13. Troitskiy, V. S. Astron. zh., Vol. 42, No. 6, 1965, p.1296.

14. Krotikov, V. D., V. A. Porfir'yev and V. S. Troitskiy. Izv. VUZov, Radiofizika, Vol. 4, No. 6, 1961, p. 1005.

15. Bondar', L. N., M. R. Zelinskaya, V. A. Porfir'yev and K. M. Strezhneva. Izv. VUZov, Radiofizika, Vol. 5, No. 4, 1962, p. 802.

16. Semenov, B. N., S. A. Kamenskaya, V. S. Troitskiy and V. M. Plechkov. Izv. VUZov, Radiofizika, Vol. 5, No. 5, 1962, p. 882.

17. Krotikov, V. D. Izv. VUZov, Radiofizika, Vol. 5, No. 3, 1962, p. 604.

18. Tseytlin, N. M. Izv. VUZov, Radiofizika, Vol. 6, No. 6, 1963, p. 1265.

19. Krotikov, V. D. and V. A. Porfir'yev. Izv. VUZov, Radiofizika, Vol. 6, No. 2, 1963, p. 242.

20. Krotikov, V. D. Izv. VUZov, Radiofizika, Vol. 6, No. 6, 1963, p. 1087.

21. Dmitriyenko, D. A., S. A. Kamenskaya and V. L. Rakhlin. Izv. VUZov, Radiofizika, Vol. 7, No. 3, 1964, p. 555.

22. Zakharov, A. V., V. D. Krotikov, V. S. Troitskiy and N. M. Tseytlin. Izv. VUZov, Radiofizika, Vol. 7, No. 3, 1964, p. 553.

23. Krotikov, V. D., V. S. Troitskiy, and N. M. Tseytlin. Astron. Zh., Vol. 41, No. 5, 1964, p. 951.

24. Alekseyev, V. A., V. D. Krotikov, Yu. G. Matveyev, N. G. Mikhaylova, V. A. Porfir'yev, V. P. Ryazanov, A. I. Sergeyeva, K. M. Strezhneva, V. S. Troitskiy and S. A. Shmulevich. Izv. VUZov, Radiofizika, Vol. 9, No. 5, 1966, p. 1030.

25. Plechkov, V. M. Astron. zh., Vol. 44, No. 1, 1967, p. 154.

26. Alekseyev, V. A., L. N. Bondar', S. A. Kamenskaya, V. D. Krotikov, Yu. G. Matveyev, K. M. Strezhneva and V. S. Troitskiy. Astron. zh., Vol. 44, No. 3, 1967, p. 593.

27. Piddington, J. H. and H. C. Minnet. Austral. J. Sci. Res., Vol. 2A, 1949, p. 643.

28. Hagen, J. P. NRL Report, No. 3504, 1949.

29. Piddington, J. H. and H. C. Minnet. Austral. J. Sci. Res., Vol. 4A, 1951, p. 459.

30. Troitskiy, V. S. and M. R. Zelinskaya. Astron. zh., Vol. 32, No. 6, 1955, p. 550.

31. Solomonovich, A. Ye. Astron. zh., Vol. 35, No. 1, 1958, p. 129.

32. Zelinskaya, M. R., V. S. Troitskiy and L. I. Fedoseyev. Astron. zh., Vol. 36, No. 4, 1959, p. 643.

33. Zelinskaya, M. R., V. S. Troitskiy and L. I. Fedoseyev. Izv. VUZov, Radiofizika, Vol. 2, No. 3, 1959, p. 506.

34. Kislyakov, A. G. Izv. VUZov, Radiofizika, Vol. 4, No. 3, 1961, p. 433.

35. Strezhneva, K. M. and V. S. Troitskiy. Izv. VUZov, Vol. 4, No. 4, 1961, p. 600.

36. Medd, W. J. and N. W. Broten. Planet. Space Sci., Vol. 5, 1961, p. 307.

37. Kislyakov, A. G. Astron. zh., Vol. 38, No. 3, 1961, p. 561.

38. Kislyakov, A. G. The Moon. Sympos., No. 14. IAU, N. Y., London Acad. Press, 1962.

39. Naumov, A. I. Izv. VUZov, Radiofizika, Vol. 6, No. 4, 1963, p. 847.

40. Fedoseyev, L. I. Izv. VUZov, Radiofizika, Vol. 6, No. 4, 1963, p. 655.

41. Razin, V. A. and V. T. Fedorov. Izv. VUZov, Radiofizika, Vol. 6, No. 5, 1963, p. 1052.

42. Kashchenko, V. N., A. D. Kuz'min, and A Ye. Solomonovich. Izv. VUZov, Radiofizika, Vol. 4, No. 4, 1961, p. 596.

43. Solomonovich, A. Ye. and V. N. Kashchenko. Izv. VUZov, Radiofizika, Vol. 4, No. 4, 1961,p. 591.

44. Solomonovich, A. Ye. and V. Ya. Losovskiy. Astron. zh., Vol. 39, No. 6, 1962, p. 1074.

45. Solomonovich, A. Ye. Astron. zh., Vol. 39, No. 1, 1962, p. 79.

46. Kislyakov, A. G. and A. Ye. Solomonovich. Izv. VUZov, Radiofizika, Vol. 6, No. 3, 1963, p. 431.

47. Solomonovich, A. Ye. Proc. Roy. Soc., Vol. 296, 1967, p. 354.

48. Pettit, E. and S. B. Nicolson. Astrophys. J., Vol. 71, 1930, p. 102.

49. Pettit, E. Astrophys. J., Vol. 91, 1940, p. 408.

50. Gibson, I. E. Astrophys. J., Vol. 133, 1961, p. 1072.

51. Sinton, W. M. Astrophys. J., Vol. 123, No. 2, 1956, p. 325.

52. Shorthill, R. W., H. C. Borough and J. M. Canley. Publ. Astron. Soc. Pacif., Vol. 72, No. 429, 1960, p. 481.

53. Castalli, J. P., C. P. Terioli and J. Aarons. Astron. J., Vol. 65, No. 9, 1960, p. 485.

54. Saary, J. M. and R. W. Shorthill. Boeing Sci. Res. Lab, July 1962.

55. Kamenskaya, S. A., A. G. Kislyakov, V. D. Krotikov, V. M. Plechkov, A. I. Naumov, V. N. Nikonov, V. A. Porfir'yev, K. M. Strezhneva, V. S. Troitskiy, L. I. Fedoseyev, L. V. Lubyako and E. P. Sorokina. Izv. VUZov, Radiofizika, Vol. 8, No. 2, 1965, p. 219.

56. Plechkov, V. M. Astron. zh., Vol. 43, No. 1, 1966, p. 172. /64

57. Krotikov, V. D. and V. S. Troitskiy. Astron. zh., Vol. 39, No. 6, 1962, p. 1089.

58. Alekseyev, V. A., T. N. Aleshina, V. D. Krotikov and V. S. Troitskiy. Astron. zh., Vol. 44, No. 5, 1967, pp. 1070-1075.

59. Troitskiy, V. S. and N. M. Tseytlin. Izv. VOZov, Radiofizika, Vol. 3, No. 6, 1960, p. 1127.

60. Troitskiy, V. S. Astron. zh., Vol. 38, No. 5, 1961, p. 1001.

61. Soboleva, N. S. Astron. zh., Vol. 39, 1962, p. 1124.

62. Heiles, G. E. and F. D. Drake. Icarus, Vol. 2, 1963, p. 281.

63. Baars, J. W., P. G. Mezger, N. Savin and H. Wendker. Astron. J., Vol. 70, 1965, p. 132.

64. Evans. J. V. Physics and Astronomy of the Moon. N. Y., London Acad. Press., 1962, p. 429.

65. Evans, J. V. J. Res. N. B. S., Vol. 69D, No. 12, 1965, p. 1637.

66. Giraund, A. J. Res. N. B. S., Vol. 69D, No. 12, 1965, p. 1677.

67. Davis, J. R., D. C. Rohlfs, G. A. Skaggs and J. W. Joss. J. Res. N. B. S., Vol. 69D, No. 12, 1965, p. 1659.

68. Evans, J. V. and T. Hagfors. J. Geophys. Res., Vol. 71, No. 20, 1966, p. 4871.

69. Hagfors, T. Simpozium po fizike Luny i planet (Symposium on the Physics of the Moon and Planets). Kiev, 1968.

70. Davies, R. D. and F. F. Gardner. Austral. J. Sci. Res., Vol. 19, No. 16, 1966, p. 823.

71. Bogdanov, A. A., I. Ya. Brusin, M. S. Kagorlitskiy and T. V. Tikhonova. Izv. VUZov, Radiofizika, Vol. 11, No. 6, 1968, p. 801.

72. Troitskiy, V. S. Izvestiya komiteta po fizike planet, No. 3, 1961, p. 16.

73. Troitskiy, V. S. Astron. zh., Vol. 39, No. 1, 1962, p. 73.

74. Piddington, J. H. and H. C. Minnet. Austral. J. Sci. Res., Vol. A2, 1949, p. 643.

75. Matveyev, Yu. G., G. L. Such[illegible] and V. S. Troitskiy. Astron. zh., Vol. 42, No. 4, 1965, p. 810.

76. Krotikov, V. D. and V. S. Troitskiy. Astron. zh., Vol. 40, No. 6, 1963, p. 1076.

77. Krotikov, V. D. Izv. VUZov, Radiofizika, Vol. 5, No. 6, 1962, p. 1057.

78. Troitskiy, V. S. Novoye o Lune. Doklady i soobshcheniya na mezhdunarodnom simpoziume po issledovaniyu Luny (New Information on the Moon. Papers and Reports Delivered at an International Symposium on the Investigation of the Moon). Moscow-Leningrad, USSR Academy of Sciences Press, 1962.

79. Betekhtin, A. G. Kurs mineralogii (Course in Mineralogy). Moscow, State Scientific and Technical Press, 1956.

80. Troitskiy, V. S. Astron. zh., Vol. 59, No. 4, 1964, p. 724.

81. Barabashov, N. P., V. A. Yezerskaya, V. I. Yezerskiy and T. I. Ishutina. Izvestiya komiteta po fizike planet, No. 1, 1959, p. 67.

N74-19179

GEOLOGICAL MAPPING OF THE MOON

/65

M. S. Markov, A. L. Sukhanov, V. G. Trifonov,
P. V. Florenskiy and L. M. Shkerin

ABSTRACT. Compilation and labelling of geological and morphological charts on a scale of 1:1,000,000 are discussed with emphasis on the regions of Maria Tranquilitatis, Crisium, Fecunditatis, Humorum and Nukium as well as certain prominent craters.

Until recently, the geological approach to the study of the Moon consisted in a detailed description and interpretation of genetic features of the individual structures on its surface. There was practically no systematic areal geological mapping. The fundamentals of such mapping were devised by J. E. Spurr [1] and A. V. Khabakov [2, 3]. Lack of space prevents us from going into detail concerning the results of these efforts. We do consider it necessary to mention, however, that the authors defined the principal age generations of lunar structures, traced their propagation, interrelationships and sequence, and also devised hypotheses explaining the origin of the various forms. The lack of large-scale photographs did not allow the authors of these papers to carry out sequential areal mapping of the lunar disk. The maps and diagrams which they prepared usually showed only the most prominant positive and negative structures of various ages, between which the gaps remained unfilled.

Consequently, two interrelated trends have developed in selenological mapping. One consists in mapping all of the linear structures which can be recognized and systematizing them, for the purpose of clarifying the nature of the forces which formed these structures. This is a structural rather than a purely geological approach. The other method consists in areal mapping, in which principal attention is devoted to areas of propagation of various types of relief and the age of rocks, i.e., stratigraphy. This approach is more "geological"; the maps which are compiled do not lack structural and morphological elements. The use of this method became possible following the appearance of atlasses of large-scale photographs [4] and topographic charts on a scale of 1:1,000,000 [5]. Geological-morphological charts on this basis were compiled simultaneously in the USSR and USA. To a certain degree, they serve the purposes of geological mapping of the Moon without the aid of spacecraft; therefore, special attention has been devoted to them. In particular, we wanted to evaluate the degree of reliability of such charts and to show several of the methodological difficulties that arise in their compilation.(1)

□ □ □

In the course of the geological interpretation of photographs of the Moon, conducted at the Geological Institute of the USSR Academy of Sciences, a method was devised for compiling and labelling the geological and morphological charts on a scale of 1:1,000,000 [6, 7] and charts were compiled for several regions of the Moon (Figure 1). In the following, the fundamentals of mapping will be expanded and discussed in detail. /66

(1) The quality of the photographs and cartographic materials is not discussed here, although it plays an important role. The resolution in the pictures is frequently inadequate for the one-to-one million scale of mapping and the topographic charts sometimes contain traces of subjective perception of details of the relief by the compilers.

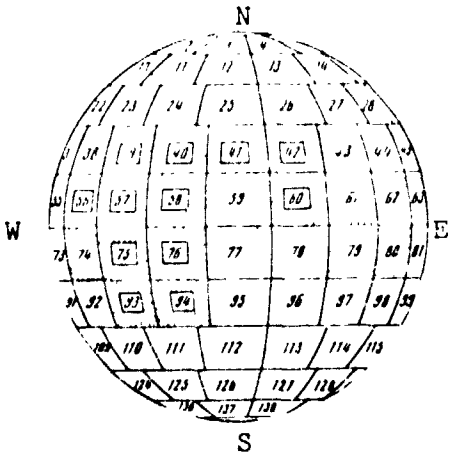

Figure 1. Locations of areas on a scale of 1:1,000,000 on the visible side of the Moon. The thickly dotted areas are the sheets that are in the present article. The sparsely dotted areas show the sheets compiled by the authors in their previously published paper [28]. The ones with squares were used in American geological charts.

The stratigraphic diagram was worked out by previous investigators to a significant degree. The scope and the stratigraphic position of the crater complexes correspond to the diagrams of A. V. Khabakov [2, 3], V. V. Kozlov and A. V. Artemov [8], U. M. Shoemaker and J. Hackman [9]. The most significant difference consists in the more detailed classification of the continental formations and extensive definition of the rocks in the continental intercrateral complexes: Median, Altaic, and Nebular, similar to the distribution, occurrence and structure of the surface with the Procellarian complex of lunar maria, but subject to a more detailed analysis. In addition to showing the outcroppings of rock complexes of different ages, the charts show faults of various ages and morphologies, structural elements of large craters, mare walls and domes.

The definition of the complexes of various ages (see the table below) is based on the following criteria.

1. The superposition of crater ejecta on the surrounding surface, especially the superposition of individual craters on others; a different degree of destruction and deformation of the craters.

2. Covering of separate areas of mantle-like complexes of less dislocated rocks with "ingressive" contact, especially "flooding" of craters with the formation of crater-semicircles and partial covering of individual systems of faults.

FOLDOUT FRAME

COMPARISON OF STRATIGRAPHIC SYSTEMS OF VAR

Proposed system: Complexes		A. V. Khabakov [3]	E. M. Shoemaker [14]				
Crater	Extracrateral	Periods					
Copernican Cr	Newest mare M	Modern	Copernican period			CEv Schroter's Valley formation [21]	Ch — Head tion
Eratosthenian Er	Procellarian Pr_2	Copernican	Eratosthenian period				
	Pr_1	Oceanic	Imprian period	Archimedean series	Procellarian group		
Archimedean Ar	Median Md	Ptolemaic					
Ptolemaic Pt					Material of post-Apennine craters	IpIg — Gassendi [24, 25]	
Hipparchic Hp	Altaic Al	Altaic		Apennine series			
Pre-Hipparchic pHp	Nebularian Nb	Hipparchic			Ejecta in Mare Imbrium formation	pIv — Vitello f [24, 25]	
Antique Ant		Antique	Pre-Imbrian non-differentiated			pIc — craters, buried pIv [24,	

FOLDOUT FRAME

2

RIOUS AUTHORS

Crater material

— Cobra
i forma-
ı [21]

Cge — Reiner Gamma formation [19]

Cc — Copernican crater material

Ec — Eratosthenian crater material

Id — Diophantus formation [21]

i group

Ic — pre-Procellarian craters [15 — 18, 21]

Ic — pre-Procellarian craters [19]

formation

If — Fra Mauro formation [15 — 17, 20, 21, 23]

Ih — Havelius formation, impact-explosive forms of Orientale [19]

partly
25]

pIc — pre-Imbrian craters [20]

IpIc — pre-Imbrian and Imbrian craters [19]

Cca — Cavalerius formation [19
Ccd — Dark crater formation [1

Em1–4 — Marius group [19]

EIs — Sulpicia Galla formation [16, 26]

Ipm1–4 — pre-Procellarian grou complexes on the basis of albed
Ipd — mare domes.

Iab — Apennine steppe formatio [18]
Ifh — slightly hilly continent surface [18]
Ica — Kelly formation [22]

IpIu — pre-Imbrian non-differentiated [19]

FOLDOUT FRAME

2

Supplements to system of E. M. Shoemaker and R. J. Hackman [9], developed in the course of charting individual regions [15 — 26]

Extracrater material

ıs formation [19]
ɔer formation [15]

EIs — Sulpicia Galla formation [16, 26]

Etd — part of Take formation [16]

Etl — part of Take formation [16]

Emd — dark material from region of Littrow Rill [16]

EIh — Harl formation

rocellarian group. Material of mare plains. Divided in areas into four
e basis of albedo.
es.

IpIdd, I?d — domes [20, 25

?

Iab — Apennine steppe formation [18]
Ifh — slightly hilly continental surface [18]
Ica — Kelly formation [22]

Ip₁₋₃ — material of continental plains with different density of covering craters [20]

IpIp — material of continental plains [16]

IpIp — material of continental plains [24,25]

IpId — br [25]

If — Fra Mauro formation. Ejecta in impact-explosive formation of depression of Mare Imbrium [16, 18, 20, 26]

pIv — Vitello formation. formation of Mare Humorum [

pIu — pre-Imbrian non-differentiated [16]

pIrh — substrate of Mare H

4

maker and R. J. Hackman [9],
individual regions [15 — 26]

ter material

material from region ill [16]		EIh — Harbinger formation [21]	EId — Doppelmayer formation [24]
areas into four	IpIdd, I?d — dark continental domes [20, 25]		
rial al	IpIp — material of continental plains [24.25]	IpId — bright continental domes [25]	
]	pIv — Vitello formation. Ejecta in impact-explosion formation of Mare Humorum [24, 25]		
d	pIrh — substrate of Mare Humorum [24, 25]		

3. Differences in the brightness of rocks, their interrelationships with rays.

The outcroppings of each extracrateral complex in a given region correspond to a flat surface which in the case of young complexes usually is located below the adjacent, older extracrateral formations. The older the crater complex, as a rule, the brighter its surface, and the larger the hills, faults and craters in it. (1) Tracing the flat surfaces with characteristic features makes it possible to map the extracrateral complexes in areas where the age relationships of the complexes are not clear. In particular, V.G. Trifonov [10] used the /67 tracing method to establish that the oldest rocks in the cordilleras are on their crests. This indicates that the cordilleras (and the maria along with them) were formed in several stages.

The boundaries of extracrateral complexes are only visible where their periods of formation are divided by certain events, which left traces on their surface. Thus, the depcsit of complex M was preceded by the formation of ray systems. The Nebularian and Altaic complexes to the east of Hipparchus were separated by a period in which faults were produced. In the regions of relatively quiet stratification of rocks, for example, to the east of Mavrolich, it is difficult to distinguish complexes differentiated in time. If several gradually changing maria complexes emerge on the surface within one region, their boundaries are frequently indistinct, "diffused", and then we would seem to observe a gradual shift in the complexes. These changes provide a basis for assuming that the formation of extracrateral rocks was continuous, reoccuring first on one, then on other sections of the lunar surface.

---

(1) In the case of greatly dislocated ancient surfaces, one can see that a number of only relatively large craters have developed, while the number of craterlets has become stable or even decreases. This probably takes place due to the more rapid breakup of the craterlets on the slopes of the hills and ridges, and the attainment of a saturation density at which the number of newly forming craterlets is equal to the number of craterlets that vanish through being covered and broken up.

The "diffused nature" of the boundaries may sometimes be explained differently. In the region of the Sinus Aestuum, the relief is slightly worn down and has an anomalously dark color. The impression is created that the relief of this section is mixed with ancient structures, but covered with a thin layer of dark young rocks, i.e., the age of the surface (mantle of rocks) is younger than the age of well developed forms of relief. If this is the case, the "diffused" boundaries may be explained by the dispersed expansion of a young complex on an old one (1).

It is valid to divide crater complexes by the degree of preservation and overlapping. It is apparent that craters of the Ptolemaeus-Valter chain are younger than Hipparchus, and Theophilus is younger than Cyrillus. The younger of two similar craters may be readily determined if one is covered by any complex of rocks having an areal distribution, and the swell of another is superimposed on this complex. If one of two craters in a single, broken zone is intersected by faults, and the other is slightly touched by them, the first is naturally older.

Such a distinction is very arbitrary. A crater located in a zone of radial and concentric systems of faults around a maria may differ in terms of its disrupted character from single-aged craters in slightly dislocated areas. The age of the latter is only apparent in a certain decrease in the depth and "deliquescence" of the swell. The overlapping of two craters does not indicate that they were formed far apart in time. It may happen that in a zone of dislocations one crater is superimposed on an adjacent one, but their degree of preservation is the same. On the other hand, sometimes craters close together in one complex differ greatly in their degree of preservation. The Ptolemaic d'Arrest and Pallas are like this. If d'Arrest is a typical Ptolemaic formation, then Pallas holds a middle position between Ptolemaic and Hipparchic cirques in terms of its morphological features.

---

(1) Not only lava covers, but also pyroclastic formations capable of "pulverising" the relief may be included in maria complexes.

There are well developed circular crater chains and individual craters on the swells of many large cirques, and frequently they have a more recent appearance than does the main portion of the crater. Evidently the development of the latter continued in subsequent periods of crater formation. Finally, there are crater chains, in which one part is Hipparchic and its continuation is Ptolemaic, or one part is Archimedian and another is Eratosthenian and Copernican in separate sections. The possibility is not excluded that such chains are of equal age, while the different appearance of the craters has to do with their various sizes. In general, however, it is more natural to assume that the process of crater formation did not consist of distinctive periods, but /68
was continuous. It is possible to speak of a concentration of craters of similar age in specific zones; however, when we look at the entire range of transitions from ancient forms to more recent ones, it becomes impossible to state that there were epochs of a general intensification of the crater-formation process.

Hence, we lack the ability to specify reliably periods of primarily crater- and maria formation in the history of the Moon. The covering of the crater complexes of similar age by mare formations (and vice versa) merely indicates that one of the two processes at the time ceased at a given point. However, on the scale of the Moon as a whole, they took place more or less simultaneously. Therefore, the stratigraphic column of lunar rocks presented herein consists of two continuous series with a rough approximation of the members of each series of similar age.

Inasmuch as the basis of this mapping method consists of

delimiting the rock complexes on the basis of the characteristics of the relief and to a lesser degree on the brightness, each complex can be distinguished only at those points where these characteristics are clearly pronounced. Naturally, it is far from universally possible to carry out this process successfully everywhere.

The crater ridges shown in the maps are outlined by fields of crater ejecta with a specific radially-scattered or fragmental relief. Remote ejecta have almost no intrinsic relief, and can be observed only when they are bright against the subjacent rock, usually rock in the maria. On the continents, however, even the close-in ejecta of the young craters, masked by the contrast of the subjacent relief, cannot always be made out. The pre-Eratosthenian craters are even more difficult to make out, inasmuch as they are frequently destroyed by faults.

Likewise, small fields of rock of the Altaic complex are lost here and there in the system of ancient furrows and ridges, and do not stand out against the depressions of the nebular surface. The shallow fields of the Altaic complex are sometimes masked by partial outcroppings of ancient substrate. The problem is complicated still further by the fact that, in addition to the outcroppings of substrate, the mare surface may occasionally display positive forms that are synchronous with it and may even be later: structures of formation or compression, volcanic ridges and domes, etc. In some cases, they may reach significant dimensions.

Hence, in addition to the ringwalls, in the opinion of A. L. Sukhanov [11], it is sometimes possible to distinguish a specific group of positive relief forms which are probably of volcanic or extrusive origin. These are conical, isolated peaks and ridges, intersected by the walls of craters or combined with them, as well as the sharp bilateral ridges running along the mare walls and certain faults. On the tops of these formations, one can often find one or more craterlets. The material of such forms is shown partially

on the chart in the composition of the crater complexes. Unfortunately, they may be distinguished and mapped primarily in those instances when they are superimposed on other elements of the relief and have nothing to do with the ejecta of a large crater. Superposition provides a lower age boundary for these formations, but the upper limit has not been determined inasmuch as these forms, in addition to being difficult to make out, completely merge with the older formations when they are covered or mixed with their ejecta.

The charts which are displayed usually do not show the fine outcroppings of extracrateral complexes and portions of the discontinuous propagation of the crater ejecta, and the extensive outcroppings of rock complexes are shown only in their characteristic structural expression. This distinguishes our maps from the purely geological ones, and makes it possible to view them as structural-geological maps.

The representation of faults on the maps described also has its specific characteristics. /69 In those instances when the fault system consists of parallel furrows and ridges, the lines of the cracks run along the bottom of the furrows, so that we felt that the most important process was that of the subsidence and development of the furrows along the displacement. Many parallel ridges are not distinguished by signs of faults, inasmuch as they are the edges of crater chains, which very frequently are developed along a given line. Finally, the faults were found only in places where it was possible to localize exactly the emergence of the plane of the displacement in the locale (for a given scale). Therefore, the charts do not contain any large faults like the scarp to the south of the Ariadeus Rill; in the chart, it is broken up into a group of small dislocations. In addition, there are no faults along the polygonal walls although they are undoubtedly associated with a multitude of cracks.

The study of the charted faults revealed several interesting characteristics. Thus, the coastal cordilleras are broken up by a network of interconnected faults which form a rhomboid structure and

extend for a considerable distance. With increasing distance from a mare, the cracks associated with it become less pronounced; some of the ancient faults are covered beneath Altaic formations, and the younger ones intersect them. This supports the view of the duration of the development of maria depressions and the faults associated with them, frequently combined into systems that are radial and concentric with respect to the mare depressions. In addition, an analysis of the explosive tectonics of the near-equatorial belt reveals predominance of certain trends in the faults: northwest, and meridional and northeast which are subordinate to the northwest direction. The extensive belt of particularly frequent faults extends along the mare depressions to the southeast of Mare Imbrium. The influence of the belt, in particular, takes the form of a reinforcement of the northwestern direction among the faults of the radial systems of Mare Imbrium and Mare Nectaris. In the center of the belt, along many of the faults, it is possible to make out a dextral shift of the relief forms.

□ □ □

The principles of mapping set forth above expand on the ideas of A. V. Khabakov [2, 3] and differ from the mapping principles of the contemporary American school of selenologists. J. E. Spurr [1] proposed the dominant role of endogenic processes in the formation of the lunar relief and rocks. However, many of his concepts have not been adopted by other American selenologists; they have followed a different path, working out a theory and practical basis for the impact-meteoritic origin of the basic forms of the lunar relief. Such a methodological approach, based on the principles of catastrophism, does not alter the principles of geological mapping of crater forms, but has a significant influence on the classification by ages and the interpretation of the structural characteristics of the intercrateral space. A concept has been developed which holds that the circular depressions of the lunar maria arose as the result of the impacts of large cosmic bodies and were filled nearly simultaneously by the dark, primarily volcanic material of the Procellarian group.

The principal shortcoming of this approach is the fact that it ignores details of structure and features of the relief of different portions of the intercrateral areas of the lunar continents. All of these areas around the large maria have been found to be covered to a considerable extent by ejecta in the formation of the mare depressions. In the first stratigraphic diagrams that were devised for charts on a scale of 1:1,000,000 [9, 12, 13, 14], the ejecta were shown for the depression of Mare Imbrium, later referred to as the Fra Mauro formation, and a number of other stratigraphic classifications. These and later systems [15 — 26] are shown in the table. Later, similar ejecta were shown for the depressions of Mare Humorum — the Vitello formation [24, 25] and Mare Orientale — the Hevelius formation [19]. The age relationships of these formations /70
are hypothetical: the Vitello formation is considered to be more ancient than the Fra Mauro formation, and the Hevelius formation is youngest.

In addition, a detailed mapping of the continental areas and the appearance of photographs taken from spacecraft has shown that the fields of catastrophic ejecta of different ages and the crater formations covering them do not lack diversity and complexity in the forms of continental relief. This forces the compilers of the maps to diverge from the initial hypothesis and to show (on the one hand) craters and blocks of the older substrate and, on the other hand, the formations of the continental plains. The latter covered the fields of catastrophic ejecta, but are probably older than the Procellarian group, inasmuch as they are broken up by a multitude of small craters [18, 24, 25]. The majority of investigators recognize the volcanic origin of the plain formations, but R. J. Hackman [18], and M. G. Carr [16] mention their similarity to the Procellarian group. Although the formations of the continental plains of different authors are not correlated with each other, we can suggest that on the whole they are equivalent to the Altaic and to some degree the median complexes of our system.

The stratigraphic concepts regarding the younger extracrateral formations have also undergone evolution (see the table). The Procellarian group is divided on the basis of brightness into four complexes. One might think that the relatively dark and possibly young members of this series are of Eratosthenian age. The group of Eratosthenian formations of the "mare" type includes the Marius group, the Sulpicius Gallus formation, and the relatively bright portion of the Tacquet formation. The darkest mare formations are apparently younger still: the Cavalerius formation, a portion of the Tacquet formation, and the rocks in the vicinity of the Littrow trenches. The Cavalerius formation covers the rays of the Copernican craters. Finally, the formations of the "mare" type form a continuous series corresponding to the lower and upper Procellarian subcomplexes and the M complex of our diagram. Hence, the systems of stratigraphy of the lunar deposits of the American authors confirm our own with respect to the definition of the pre-Procellarian rocks, but frequently go beyond it with respect to the classification of the younger formations.

An important shortcoming of the American work is the lack of correlation between the stratigraphic diagrams of the charts of the various authors. Objections can also be raised vis à vis the pictures of the faults in these charts and profiles. The faults are usually shown in the form of separate rectilinear segments, although in fact they frequently curve, combine, and split up. The concentric faults of the inner slopes of the craters are shown in the profiles as rapidly flattening out and converging beneath the bottom of the crater, they are interpreted as the traces of enormous settlings of the slope of an impact crater. We feel that in a homogeneous crust composed of igneous rock, settlings of such a scale are not very probable, and therefore we treat faults as results of subsidence above a magmatic focus. The steep inner slopes are indicated by a special symbol, implying that ejecta here may provide some idea regarding the rocks underlying the crater; the American charts show sloping deposits at such places.

In general, many elements of the American stratigraphic charts and diagrams are similar to ours. This indicates the objectivity of the geological interpretation. For the entire Moon, one can reliably establish four groups of complexes: (a) from ancient to Altai, (b) from Altai to the rocks of the young maria; (c) maria; (d) post-maria. In a number of regions, however, one can reliably perform a much more detailed classification. Although the reliability of the charts described is clearly less than that of terrestrial geological charts compiled only on the basis of aerial photographs, they still make it possible to make out the most general patterns of the structure of the lunar surface.

The geological mapping of the Moon is entering a new stage, involving the utilization of photographs obtained by spacecraft. /71
They are on a scale 10 — 100 times larger than those obtained with telescopes. The method of geological interpretation used for the compilation of charts with a scale of 1:1,000,000, when working with these photographs, can be used only in the most general fashion. Pictures with this interpretation and labelling have only been analyzed to a small extent thus far. At this point, we would like to mention only a few of the problems that are associated with large-scale interpretation.

The details in the pictures make it possible to observe in these pictures structures that are obviously volcanic: cones, domes, stratified outcroppings. Sometimes it is evident that these forms are superimposed on the surrounding terrain. It is possible that many of the outcroppings in the maria which formerly were related to outcroppings of a pre-maria relief, are in fact post-mare volcanoes. In the event such volcanoes are close to each other, a relief may be formed which is similar to the relief of ancient complexes, i.e., some areas which are interpreted as outcroppings of ancient complexes may turn out to be young. The walls of some of the annular structures, including the crater phantoms, reveal signs of extrusive origin at high resolution, i.e., they may be younger than the mare surrounding them. If this is confirmed, the presence of crater phantoms may not

be considered a reliable sign of flooding of the locale, and the problem of flooding can be solved only if a number of characteristics are present. The same applies to some of the positive linear details of the relief which may turn out to be new formations and not flooded remains.

The examination of this type of structure in the walls of the large craters may lead to a deviation from the images of these walls in the form of complex fill formations: they will break down into individual coverings, flows, lava lakes and volcanoes [27].

We can also not exclude the fact that the morphological volcanic formations were formed by various types of volcanism, and a detailed analysis may show the simultaneous formation of highly different forms.

The enormous number of craterlets which show up on large-scale pictures theoretically makes it possible to compare the age of relatively small generalized areas (if we assume constancy and uniformity of distribution of the meteor flux). To do this, however, it is necessary to evaluate the speed and completeness of "erosion" of the craterlets on a flat surface and on a slope beforehand and to work out the criteria for distinguishing endogenic craterlets from the impact variety — primary and secondary.

Finally, one must keep in mind that, as the scale of mapping increases, we will shift to a detailed study of those structures which in many instances do not have analogs on Earth. Hence, the genetic interpretation of these forms must be carried out with great care.

The article includes 11 sheets of geological-morphological charts. These pages and brief explanatory notes were compiled by the following: M. S. Markov (sheet 93), A. L. Sukhanov (79, 80), V. G. Trifonov (61, 62), P. V. Florenskiy (39, 56, 57), and L. M. Shkerin (74, 75, 94). Eight sheets of the central portion of the visible side were compiled and published earlier [28].

Region of Mare Tranquillitatis and Mare Crisium
(LAC-61, 62) (Figures 2, 3)

The geological-morphological charts (see the end of the book) cover the eastern part of Mare Tranquillitatis, the southern half of Mare Crisium, the northern half of Mare Fecunditatis and the continental region between them. Here, all of the complexes of rock shown in the proposed labelling system can be seen. The upper limit of the Procellarian formations can be seen as well.

In Mare Tranquillitatis, one can see areas where all of the distinctive craters are Copernican, while the Eratosthenian craters are probably covered with mare material. As a rule, such material is darker than the remaining Procellarian surface. It evidently belongs to the upper portion of the Procellarian complex, approximately the same age as the Eratosthenian rock complex. Consequently, the Procellarian complex has a longer formation time than was formerly believed and is probably continued directly by the stratigraphic mare M complex. The portions of the Procellarian complex of different ages extend into Mare Tranquillitatis in the form of a mosaic; their contact points are not clear. /72

One of the most important structural elements of the region is the isometric depression of Mare Crisium. It is bordered on the south by an extensive continental massif, within whose limits the hypsometric elevations are highly variable, but on the whole increase in the direction of Mare Crisium. Therefore, regardless of the unevenness of the coastline, it may be considered that the mare is bounded on the south by a coastal cordillera. Behind it is a discontinuous peripheral belt of depressions which surrounds Mare Crisium on all sides. The belts include a region of Median mare formations near the walled plain Condorcet, Mare Undarum and Mare Spumans, the region of the outcroppings of the Altai mare rocks to the south of Apollonius, the nothern part of Mare Fecunditatis. In the region of the walled plain Taruntius, the peripheral band breaks up into two branches, one of which extends (with interruptions) to the north

of Proclus, while the other covers a portion of Mare Tranquilitatis (to the northeast of the Cauchy trench) and the Mare gulf between Lyell and Maraldi D. In the territory in question, the first branch of the depression is made up of Altai rocks, while the second is basically Procellarian. /73

Mare Tranquilitatis has an irregular outline, and apparently is not an independent circular depression. It is located at the junction of the peripheral belts of depressions around Mare Crisium, Mare Serenitatis and around Mare Nectaris in its outlines of Altaic time.

The explosive disruptions are indicated by furrows and scarps which rarely have the form of grabens or narrow valleys. The crater chains are probably related to these faults. A small number of the faults are located on the continental region which surrounds Mare Crisium on the south. Therefore, to the southeast and also in the continental region there are fewer faults, and we can assume that the degree of disruption increases with proximity to Mare Crisium and that its formation stimulated the formation of the faults. In addition, it is evident on the charts that have been compiled that the faults are not located in a ring or radially with respect to the mare depression [29, 30], but frequently contact it at acute angles and are grouped in several characteristic directions. In the general rose diagram of all the faults and crater chains of a region (Figure 4) there are maxima: a northwestern one and a less significant one which is meridional and northeastern. The latter, as may be seen from individual rose diagrams of the older faults in different parts of the region (see Figure 4) link two maxima: the submeridional (10°) and the northeastern. All three maxima extend from one area to the other, although their extent changes somewhat. There is a constant predominance of pre-Archimedian and pre-Procellarian faults with a northwesterly direction.

Rarely, there are dextral displacements of ancient structural forms along the nothwestern faults. The amplitudes of the displacements do not exceed one or two kilometers. Pre-Archimedian crater

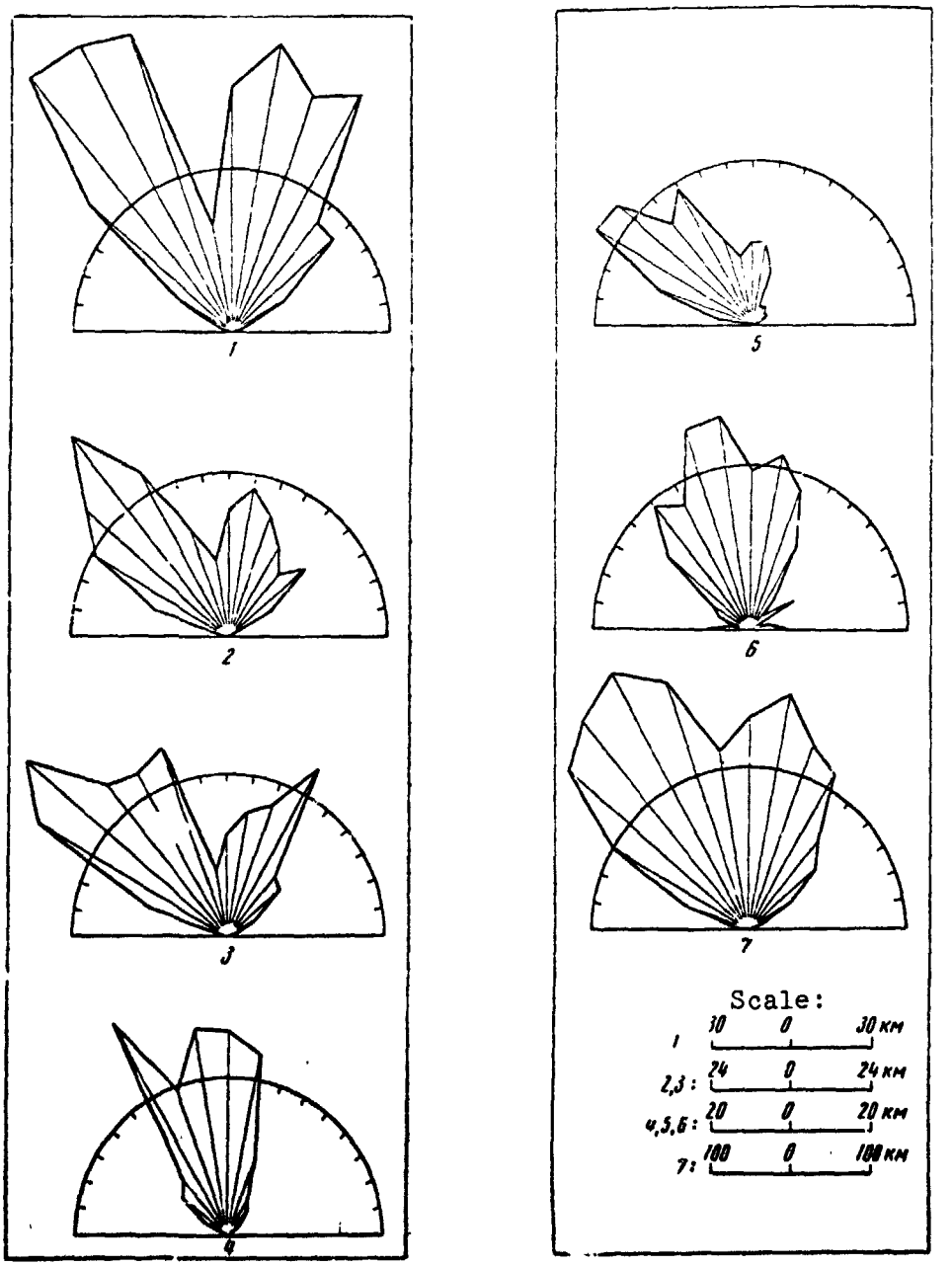

Figure 4. Rose diagrams of faults and crater chains in the territory of sheets LAC-61 and 62. Compiled by V. G. Trifonov.

1 — pre-Archimedean faults in the territory of sheet LAC-61; 2 — pre-Archimedean faults in the western half of sheet LAC-62; 3 — pre-Archimedean faults in the eastern half of sheet LAC-62; 4 — pre-Archimedean crater chains; 5 — post-Median faults; 6 — post-Median crater chains; 7 — all faults and crater chains in the region. Grouping intervals — 10°; total extent of faults or crater chains in one direction is given in the scale shown. The extent of the assumed faults is reduced by a factor of 2 with respect to the definite faults.

chains, which probably are of endogenic origin and arose under conditions of transverse stress, as a rule, extend submeridionally (see Figure 4). The combination of the northwesterly dextral displacements and the submeridional structures of stress suggest that they were formed in a single field of horizontal stresses with submeridional direction of relative compression. These data on the orientation and the dynamics of the formation of disruptive disturbances in the region coincide with the data obtained by V. G. Trifonov [10] for the southeastern outlines of Mare Imbrium and the Haemus Mountains. /74

Among the course of the post-Median faults, there is a clear maximum at 300 — 310° [Figure 4 (3, 5)], while a significant portion of the more ancient northwesterly faults extend in the directions of 310 — 330°. The extent of younger crater chains [Figure 4 (3, 6)] is more diverse than that of the older ones, with the bare maximum being displaced somewhat (340 — 350°) with respect to the older chains with regard to the change in the predominant directions of the faults. It is probable that these changes in the extensions of the faults and crater chains relative to the older directions reflect a change in the orientation of the horizontal tectonic directions: a relative compression becomes north-northwesterly. The same changes were noted by V. G. Trifonov [10] in more westerly regions (the Aridaeus rill, Huygens and other young disturbances).

The morphology of the large craters may be shown to best advantage by using the example of the walled crater Taruntius (Figure 5), whose wall measures approximately 60 kilometers in diameter. The central peak has an irregular shape. On its slopes and the adjacent portions of the floor are small radially deployed crater chains. The crater floor is finely furrowed. Immediately to the south of the central peak there are flat and relatively dark fields of rock outcroppings which probably are of the same age as the M complex. In the external part of the floor, the surface becomes more furrowed. The largest hills, perhaps, are similar to the central peak although they are larger in their dimensions. There are many small craters

Figure 5. Structural-geological map of the Taruntius cirque region, determined by V. G. Trifonov in a photograph from the lunar satellite Orbiter 1. This was borrowed from the work of B. M. Middlehurst [40].

The authenticated post-Median faults and fractures are shown by the heavy solid lines. The heavy dashed lines designate assumed faults and the boundaries of the ridges of the outer slopes of Taruntius. Pre-Archimedian faults are shown by dashed lines, and the ridges of the crater walls — by circles. The remaining notation is the same as in Figure 2.

and crater chains. Arcuate disruptive furrows combine to form a complex concentric system. The circular-polygonal crater wall has a width of 6 — 10 km. In contrast to the floor and the external surroundings, small craters are rare here. The wall is monolithic and disturbed only by a few concentrically located short chains of craters and relatively large individual craters. The altitude of the inner slope of the wall exceeds 2,000 m, and the outer slope measures hundreds of meters.

The zone of the external slope surrounding the wall consists of a number of ridges, located radially or tangent to the crater wall and falling off toward the periphery. There are many small craters on the surface, especially on the flat peripheral areas with a mesh-like structure. The crater formations "shine through," and positive forms of pre-crater relief appear on the surface in places. The zone of crater rays in telescope pictures shows a number of radial, relatively bright discontinuous bands which gradually disappear with increasing distance from the walled plain. In a picture taken by the Lunar Orbiter 1 (see Figure 5), these bands show up as a group of small craters and crater chains in the ejecta around them. Although the majority of the chains are arranged radially with respect to Taruntius, there are some chains which extend tangentially and even perpendicular to this direction. Some of the chains, especially those that are tangent, are arranged in rows relative to one another. The majority of the large forms of the relief of the zone of crater rays arose prior to the development of Taruntius. The relatively large Eratosthenian craters are younger. The mare walls to the south of Taruntius form a fan that extends radially from this walled plain; it is probable that the walls arose during its formation.

The zones of the outer slope of the walled plain and the crater rays are intersected by young faults, which usually do not cut through the crater wall. Two basic trends for the young faults can be identified: northwesterly and submeriodionally with respect to the former; the latter coincides with the directions of the older faults. It is /75

obvious that the young faults were formed in the zone of the formation of the walled plain, but the more ancient structure of the region influenced their position.

It follows from the above that the walled plain Taruntius was created by a single multiphasal process which took different forms in various zones. Most likely, this process was governed by endogenic /76
factors. The floor of the crater resembles a large volcanic-tectonic depression with concentric caving and individual projecting volcanoes (central peak). The surface of the floor represents a field of block lava, with the central portion possibly being younger than the peripheral one. The specific monolithicity of the crater wall makes it possible to assume that it is of extrusive-subvolcanic origin. It may have arisen along the largest annular system of faults, and in its final form was formed later than the zone of the outer slope. To some extent, the elements of the outer slope have the appearance of formations that slipped or slid from the crater wall. Some of the radial trenches and mare walls to the south of Taruntius may perhaps be structures like subvolcanoes or dikes. The numerous crater chains indicate a distinctive volcanic activity in the peripheral zones of the walled plain. Judging by the brightness of the rays, the principal portion of Taruntius may be considered post-Eratosthenian. However, the formation of the walled plain continued still later, as indicated by the presence of rocks of the M complex on the floor and Copernican craters on the wall and outer slope. In the Hipparchan crater to the south of Proclus A and in the two pre-Hipparchan craters to the west of Heisher, large meridional ridges have been observed which intersect the crater wall and extend from it to the north. A narrow meridional ridge of the same type runs to the south from the Eratosthenian crater Condorcet G. Without dwelling on the details of the structure and arrangement of the small craters, we will merely note that the greatest density of the post-Ptolemaic craters with diameters above 5 km is found in the continental massif which surrounds Mare Crisium.

The sequence of geological events in the region can be seen on the published geological-morphological charts. The most important significance is attached to the signs of prolonged formation of Mare Crisium and the belts of mare depressions around it. The formation of the depression of Mare Crisium stimulated the development of fault systems; consequently, judging by the duration of this development, we can get some ideas of the duration of the mare formation process. The faults in the coastal zone began to be formed before the Altaic stage. Afterward, but prior to the Procellarian stage, secondary displacements took place along some of the faults and new disturbances were created parallel to the old ones. The latest phenomena of the process are indicated by the development of post-Procellarian faults (the rills Cauchy I, II and Apollonius I) along the perpheral belt of the depressions. Judging by the degree of settling of Mare Crisium and the peripheral belt of depressions, they were filled with Altaic, Median and Procellarian formations.

Region of Mare Fecunditatis and Its Vicinity (LAC-79, 80)

(Figures 6, 7 — see the charts at the end of the book)

In a tectonic sense, the region projects into the zone of the southeastern closure of the belt of the maria on the visible side.(1) The axis of this belt clearly passes through, running northwest-southeast through Mare Fecunditatis, and is also oriented parallel to the southwestern coast of the mare. To one side of this zone is Mare Nectaris with its concentric slopes. The young Procellarian depression of Mare Nectaris is displaced relative to the center of the external depression to the north, in the direction of the mare belt, and is combined with a north-northwesterly strait. Hence, a belt of Procellarian formations so to speak "branches off" here from the basic chain of mare depressions, oriented at an acute angle to the axis of the belt. /77

(1) Further on, to the southeast on the limb there is one raised region, Mare Australe. While indistinct, it may be assumed to be a continuation of the maria belt.

In the construction of the continental peninsula, dividing these /77
branches, one can see characteristics which are determined, on the one hand, by the influence of the concentric structure of Mare Nectaris and, on the other, by the northwesterly dislocation along the belt of the maria. The influence of Mare Nectaris is apparent by virtue of the fact that, while the ancient relief is comparatively smooth to the north, in the south the terrain is slightly upthrust and more markedly differentiated. This arcuate upthrust, called the Pyrenees, is a portion of the concentric system which surrounds Mare Nectaris. Between the Pyrenees and the ancient relief on the north, there is a narrow "rear Pyrenees trough" filled with deposits of pre-Procellarian age, primarily Median. The trough evidently belongs to the same concentric system; similar "rear depressions" are characteristic of maria with cordilleras. From this it follows that the formation of Mare Nectaris began at least with the Altaic-Median stage and continued into Procellarian time, when the central fault was filled. Hence, this mare cannot have developed as the result of the explosion of an asteroid; it is also impossible to think of this structure as a "dry" depression in which only the most depressed central portion was filled.

The northwestern belt of faults in this region is created through the predominance of linear structures with an azimuth of 310 — 320°, which is located precisely on the continuation of the faults in the Haemus Mountains and the walls in Mare Tranquilitatis. The system of northwesterly dislocations intersects the continental peninsula, but is intersected by the mare. However, several faults in this same direction intersect the mare surface in the form of yawning rills. This indicates a renewal of the activity of the northwesterly system in postmare time. The faults of this system are indicated by furrows, rills, and chains of craterlets, as well as individual ridges and sections of walls of polygonal craters (the two latter forms in many instances are not shown on the map as faults, inasmuch as it is not clear where the projection of the plane of the fault should be shown). Unilateral slopes are encountered comparatively rarely.

The characteristic feature of this system is the presence of features of horizontal displacement. Thus, in the above-mentioned curvature of a rill, the extensions form an echelon picture which is characteristic of systems with displaced directions. One can see more clearly the shift with respect to Capella and Goclenius. Along the fault that intersects Capella, the southeastern ridge of the crater is somewhat depressed (dextral shift) [2]. However, it is difficult to determine its amplitude, inasmuch as the intersection of the ridge with the fault is occupied by an 8 km crater. In any case, the amplitude does not exceed 10 km. 100 km to the southeast along the same fault Gaudibert is distorted. It is interesting that this fault, which deforms the young crater Capella, is covered in some areas by Altai rocks, indicating its regeneration.(1) Goclenius does not show a single shift plane but it does have traces of a general dextral distortion. If we consider that the initial crater was round, the amplitude of the displacement must amount to 15 to 20 km. Obviously, the deformation of the crater is associated with northwesterly faults which then were covered by the mare; however, after flooding of the mare and wall of the crater, new rills with the same direction appeared.

Thus, the system of northwestern dislocations developed for a long period of time, evidently following the course of a dextral shift in the same fashion as the extension of this system in the Haemus Mountains. The total amplitude of the displacement may reach 30 km.

The northeastern and submeridional structures of the peninsula /78 are less clearly evident. They extend out from the intersection with northwestern faults and are clearly older than they. At least some are related to the formation of Mare Nectaris; they are not oriented strictly radially, but rather at a tangent to the inner depression of the mare. The vertical displacements along it are greater than along the northwesterly fault.

---

(1) If the Capella deformation arose in the pre-Altaic period, then this crater received its "fresh" appearance during subsequent "rejuvenation." This is confirmed by the location of the central hill, which apparently intersects a fault.

The annular shapes of the peninsula are broken up by faults to such an extent that it is only conditionally possible to distinguish the Hipparchic ones from the older ones. The similar level of filling of these mutually intersecting shapes led to the fact that only confused fragments of the subannular walls project above the average level of the ancient mare material.

More preserved craters cover the Altaic formations (or are synchronous with them). Such walled plains, which are located near the mare, are covered by mare material along the outer perimeter and inside, but the mare rocks are located several hundreds of meters lower within. Only Gutenberg is filled to the level of the surrounding mare, although the wall is not broken at any point and drops down only toward the northeast. Either the filling of Gutenberg took place from the same focus from which the mare was filled, or the bare rocks penetrated there through the aperture in the wall as a consequence of plugging by volcanic accumulations.

These large filled walled plains (Gutenberg, Goclenius, Columbus, et al.) form a certain crater community: they have a similar appearance, the same degree of distortion, and they are grouped in a single zone — along the periphery of the Altai depression around Mare Nectaris. They are similar to the group of craters composed of Theophilus, Cyrillus and Catharina which is located in the same peripheral zone and are also clearly evident among surrounding craters.

On the whole, the craters on the described charts are characterized by certain anomalous characteristics, for example, a richness of central peaks. Out of 50 craters with a diameter larger than 30 km, 20 have central peaks. Among the mass of lesser craters, only 6 have central peaks. At the same time, however, the ray systems are noted primarily in the small craters 10 — 15 km in diameter and in Langrenus.

The 140 km walled plain Langrenus, located on the closure of the mare belt, is a nothern branch of the submeridional chain of similar craters (Furnerius — Petavius — Vendelinus). The walled plain is slightly polygonal, inasmuch as the ridge of the wall is similar to

a hexagon; the northwestern and northeastern boundaries are closely linked with the trend of the structures on the adjacent territory. The ridges and furrows in these directions extend for a distance of 200 km from the ridge of the wall. The furrows are sometimes located on the craterlets and become slopes within the limits of the wall. Many of these furrows are elements which are not radial to the Langrenus system, but to the regional "lattice" system [31]. They are directed at a tangent to the wall, intersecting its ridge and coming in contact with the inner slopes, forming characteristic "flow structures," which are typical of nothern and southern sectors of craters [1, 2]. In these sectors, Langrenus shows dome-shaped hills, located in a checkerboard arrangement, possibly of volcanic origin.

The inner slope of the wall is terraced, so that depressions can usually be seen in the rear areas, i.e., the terraces may not be interpreted as simple landslides. The chains of craterlets and depressions also extend along the outer slope of the wall, along the ridge. On the floor of the crater one can see shallow domes and structures resembling mare walls. All of the above — the relationship of the structure of the wall to the tectonics of the locale, the chain of craterlets and depressions, peaks on a flat floor — indicate the volcanic nature of the walled plain.

On the mare plains of the region, one can comparatively frequently notice walls and crater phantoms. The walls may be divided roughly into two systems: a few northwestern ones, parallel to the basic system of faults, and randomly branching walls which approximately trace the contours of the mare depressions. In the internal structure of the walls, one can see linear elements of other courses, for example in Mare Nectaris — north-northeasterly, parallel to certain ridges of the adjacent continent. Sometimes one can see a transition from "ridged" walls to a single-sided slope. One can see intersections of one wall with another or intersections of individual "corrugations" within a wall. Some of the walls are closely related to crater phantoms (Daguerre, Goclenius U]. /79

All of this makes it highly unlikely that the supposition is valid concerning the folded structure of the walls. It is more likely that they arose due to magmatic activity along the faults. This kind of magmatic activity is the simplest explanation for the isolated ridges of the continent (the wall in Censorinus X; the elongated hill in Censorinus N; the ridge that intersects Bohnenberger; the hill with two craterlets that intersects the rill 20 km northwest of Gutenberg).

All of the above applies to the territory which is approximately 60 — 65° E. To the east of Langrenus, the faults on the continent are less markedly evident, while the crater rings appear broken and flooded. However, it is difficult to state how they really look, inasmuch as the distortions of the pictures of the border zone of the disk are too large. Here one cannot get any help even from a study of the "corrected" photographs which were obtained by projecting the images on a white globe. Therefore, in the boundary zone, geological mapping by means of telescopic photographs is being changed into a very dubious task.

Region of Mare Humorum (LAC-93)

(Figure 8 — see the chart at the end of the book)

The central portion of the region in question is occupied by the depression of Mare Humorum, surrounded by elevations on almost all sides. It is only in the northwestern part that several straits link it with Oceanus Procellarum and Mare Cognitum.

Here one can see all of the stratigraphic complexes, with the exception of the Median. However, their limited distribution along the eastern and southeastern edges of the sheet in the vicinity of the crater Agatharchides, Rabbi Levi and Dunthorne is not excluded, as well as in certain portions on the west of the region.

The principal structural element in the region i. he rounded depression known as Mare Humorum. In the southwester corner, its roundness is disrupted by the fact that the unflooded walls of the craters Doppelmayer and Pueseux penetrate into it. It is not clear whether this is associated with a decrease in the thickness of the rocks of the Procellarian complex or with the anomalous height of the above-mentioned craters. In the east, the elevation of Cape Kelvin protrudes within the depression, directly in contact with the formations of the older complex, composing the elevation. This is the reason why the rocks composing it are combined with formations of the older complex. However, we cannot exclude the possibility that the cape consists of a younger positive relief formation, associated with the formation of a volcano of the central type. The distribution of such formations on the lunar surface is becoming more and more apparent as the geological interpretation of large-scale photographs proceeds [11, 32].

On the west and east, Mare Humorum is bounded by distinct systems of ejecta slopes, which show up clearly even in small-scale photographs. While in the southeast these faults are located along the boundary of the depression and are of similar elevation, in the west the degree of displacement is evidently much less, inasmuch as the deposits of the Procellarian complex extend further to the west, occurring in the form of a shallow covering even on the continent. It is interesting that deposits of Altai and recent mare complexes /80 are located there, and extend even farther west. Hence, the regions of bending in the Altai, Procellarian and recent time did not coincide completely.

Within the depression of Mare Humorum one can clearly see systems of mare walls, domes and young crater structures. Attempts have been made [33, 34] to view the mare walls as folded structures of surface layers of the lunar crust. It is mentioned in this context that the spatial position of certain groups of walls is reminiscent of the paragenesis of structures associated with shifts ("horse's tail"). Indeed, the propagation of these structures in Mare Humorum is

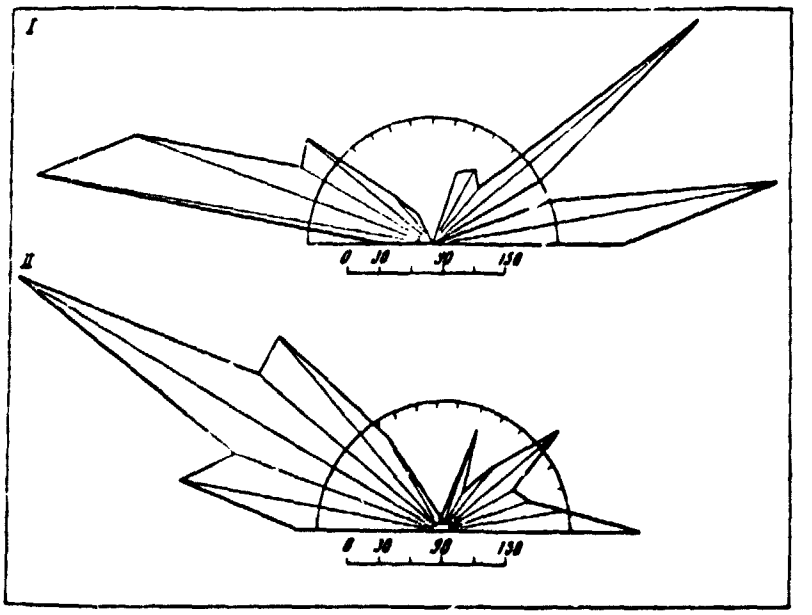

Figure 9. Rose diagram of the course of maria swells (I) and fractures (II) in the region of Mare Imbrium (according to data of J. W. Salisbury, et al. [35]).

In the rose diagram, elements with a length of 0 — 30 km correspond to one scale division; 30 — 60 km corresponds to two scale divisions, etc.

associated with the existence of slopes which are buried beneath the deposits of the Procellarian complex and are parallel to the modern boundaries of the depression. J. W. Salisbury, V. G. Smalley and L. B. Ronga [35] made an attempt to explain the predominance of extension of mare walls in Mare Humorum. Their data have been transferred by us to a rose diagram (Figure 9, I). However, they must be treated with care, inasmuch as these authors felt that the walls consist of individual rectilinear portions at various angles to one another. In many instances, however, it is clear that the mare walls bend smoothly along their length.

The elevations that surround the depression of Mare Humorum are typical cordilleras. The parts that are located close to the depression are the most elevated ones, and are composed of formations of the ancient complex. The cordillera in the southeastern part of the

region constitutes a narrow elevation bounding the depression of Mare Humorum and the small depression of Palus Epidemiarum. The elevation is assymetric; its northwestern edge is the highest part, broken up by a series of longitudinal faults and slopes. To the north, toward the region of the crater Agatharchides, the elevation is les prominent.

On the western side of Mare Humorum, the cordillera is traced /81
from the crater Doppelmayer to the crater Mersenius D and thence to Gassendi, forming an arc which is convex in the western direction. The highest part of it on the southwest is located on the very edge of the depression and runs somewhat away from it in the interval between the craters Mersenius D and Gassendi. To the southwest, west and northwest, the cordillera drops off more gradually, replaced by continental structures of the western edge of the visible side of the Moon.

Among the broken, discontinuous features of the region, one can clearly see a system of arcuate faults which ring the depression of Mare Humorum. They are faults, definite slopes, sometimes crossing over into the yawning trenches (faults to the southwest of the crater Gassendi). These faults evidently have been developing for a long time. In individual cases, they are covered by deposits of the Procellarian complex (to the east of Mare Humorum); in others they intersect (in the west). One can clearly see the system of northwesterly faults which is probably more ancient than the ejecta which surround the depression of Mare Humorum. This system is clearly shown in the rose diagram compiled according to the table of Salisbury, Smalley and Ronga [35] (Figure 9, II). In this region, craters of various ages have developed, with the Hipparchic definitely in the majority, deformed to different degrees in various parts of the region. Thus, Agatharchides and Hippalus are very markedly broken up, in contrast to the relatively slightly deformed Gassendi, Mersenius and Dopplemayer.

An important factor as far as understanding the nature of the geological structure of the Moon is concerned is the prolonged formation of the depression of Mare Humorum. From an analysis of the chart, it unavoidably follows that the formations of the Procellarian complex show a tendency to follow a more ancient negative structure formed by Altaic formations. The latter, however, extended much further to the west, and consequently the contours of the "Altaic" depression of Mare Humorum were significantly larger. Its contraction in Procellarian time evidently was associated with the development of young slopes along the western edge of the depression. It is interesting that the deposits of the recent mare complex are again tending toward the western edge of the depression, indicating continuing development of a system of bordering ejecta.

In the course of further detailed studies, it will be necessary to direct our attention toward the different dislocation of the Hipparchic craters and in this conjunction the possibility of their more detailed differentiation on the basis of age.

The Region of Mare Nubium (LAC-94)

(Figure 10 — see the chart at the end of the book)

The region in question takes in a portion of Mare Nubium, portions of Oceanus Procellarum and Palus Epidemiarum. The flat Procellarian surface predominates, rising slightly toward the northwest. Above this flat area there rise craters and mare ridges, the remains of ancient rocks. The extracrateral formations of the Nebular and Altaic complexes take up comparatively small areas that bound Mare Nubium on the west and south.

The majority of craters that have developed on the Procellarian surface are of Eratosthenian age. The largest is Bullialdus with a diameter of 60 km. Without dwelling on all aspects of the structure, we would like merely to mention the presence of a complex structured central elevation complicated by a trench, the multiple terracing of the inner slopes of the wall, the limitation of elongated depressions to the trench, consisting of merged craterlets, the presence of a

broad external ejecta field, the correspondence of the basic parameters of the crater to the curves of R. Baldwin [36]. One is struck by the abundance around Bullialdus of young faults running northwesterly and northeasterly. Some of the faults are cut by crater formations, while /82 some disturb the latter. It is especially interesting to note the graben that runs from Bullialdus toward the southern limits of the walled plain Lubiniezky E. Around the wall of Bullialdus, one can see the highest density of craters, up to 6 km in diameter, probably due to the abundance of secondary crater formations. To the south of Bullialdus, there are three craters ranging in diameter from 22 — 25 km. The northern one is of the same age as Bullialdus, while the other two cover its ejecta. All have complexly structured floors, while one also has an inner wall which is separate from the northern slope and terminates in a central elevation with a craterlet at the apex.

It is worth mentioning the young craters with double walls — Marth and Hesoid A. The inner wall is less massive and much lower than the outer one.

The pre-Procellarian craters and walled plains, partially filled with mare material, are more numerous. Six walled plains have diameters greater than 45 km. Usually, the Procellarian surface inside and outside the craters is at the same level. An exception to this is the Ptolomaic crater Campanus in which the Procellarian surface of the floor is 900 meters below the surrounding terrain.

The Hipparchic walled plain Pitatus (wall diameter = 90 km) is located on the southern boundary of Mare Nubium. The walls of this plain are very low, and there are no grabens. The entire eastern part of the wall is a merged chain of annular depressions. They are also found in other parts of the wall. Along the edges of the "flooded floor" there is an annular system of young faults. One of them extends into the center and is continued by the mare wall. At the end of the radial fault is the central peak of Pitatus with an altitude of 480 meters. The relative age of the fault and the peak has not been determined reliably, but it has been shown conditionally to be a formation of Hipparchic age.

The distinctive chain of annular structures extends from Wolf to Opelt, located radially toward Mare Imbrium. Opelt and three annular structures that are further to the south were formed by a system of arcuate walls. The western walls are higher than the eastern ones. They consist partly of ordinary mare walls and partly of sharply projecting bright ridges with altitudes up to 600 meters. The eastern arcs do not differ in any way from ordinary mare walls, and do not appear to be related to faults, inasmuch as the northwestern and northeastern faults (slopes and chains of craterlets), which have developed on the Procellarian surface, change insignificantly at certain places into the arcuate walls of the Opelt system.

In its structure, Wolf is not similar to most craters. Within its irregular outlines, one cannot make out any traces of two or more overlapping craters, which could make such a shape. The entire isometric inner part was hollowed out as a single unit, more similar to terrestrial volcano-tectonic depressions than the other round craters. The similarity is made even more striking by the nearly complete absence in Wolf of a crater wall. On the boundary of this depression, there are two small hills (about 6 km in diameter at the base, 500 and 700 meters high) with craterlets on the peaks; plumes of bright material extend from them toward the mare. We cannot exclude the possibility that these hills are young volcanoes with lava flowing out from them.

In the western part of the region, one can see enormous furrows, most of which extend roughly parallel to the edge of Mare Humorum. The furrows intersect the rocks of the Procellarian complex, but they are covered by Eratosthenian craters. However, one can see three ridges which intersect the furrows Campanus I and Hesoid I. It is possible that these ridges were formed by young extrusions.

The Region of Craters Grimaldi and Letronne (LAC-74, 75) /83

(Figures 11, 12 — see the maps at the end of the book)

The majority (approximately 55%) of this region is a typical mare surface. In the area between the craters Hermann, Flamsteed G and Sirsalis E the absolute heights are approximately the same, although undulation of the terrain is apparent. To the east of this area, there is a uniform rise in the terrain, while to the south of it one can see a slight general slope from Oceanus Procellarum toward the continent.

Within the limits of Oceanus Procellarum, the most interesting formations are the mare walls and the crater phantoms. One can clearly make out the system of walls that extend from the crater Lubiniezky E (outside the limits of the sheet) through the crater Erigonius, up to the northern edge of the annular structure Letronne. These walls are located parallel to the shift in the northwesterly direction in the region of the Riphaeus Mountains [28], and possibly their formation is associated with movements according to this shift.

In addition, one can clearly make out the systems of walls that randomly bend and have a looping appearance (to the east of the crater Wichmann, to the north of the crater Sirsalis E), whose origin evidently is different. A special category of structures evidently must be created for the crater phantoms (Flamsteed G, Flamsteed P, Sirsalis K and many others). On all of the enclosed charts they are shown (in accordance with the previously existing viewpoint) as eroded and flooded remains of former large annular structures. However, these rings may be post-mare neoformations. The age of the crater phantoms requires further study.

The thickness of the deposits of Procellarian complex in this region of Oceanus Procellarum is not great, as indicated by the numerous unfilled projections of the base. Calculations that are based on the degree of coverage of craters by mare rocks give a thickness of the Procellarian complex which is no more than 1200 meters.

The continental part of the region is structured relatively simply. It consists of flat areas composed of rocks of Altai complex and of individual upthrust blocks in which more ancient and more severely broken up (by faults) formations can be seen. The greatest number of such blocks is located in the western part of the region. Some of them have been interpreted as remains of ancient crater structures. Let us examine the structure of some of them.

The annular structure Grimaldi is located on the edge of the disk of the Moon, and therefore telescopic pictures show considerable distortion with respect to longitude. Nevertheless, it has been definitely established that this structure has an annular shape when seen in the plan; its central part is filled with dark complex rock on the surface of which one can see mare walls, domes and faults. The annular wall is only slightly evident, and its outer limits are traced only conditionally. The wall has an enormous number of crater-like shapes of the most diverse size and preservation (on the chart we have shown only the most significant craters). In terms of retention of the relief forms, it may be classified with structures of Hipparchic age. It is interesting that its floor shows many features of the structures of the mare depressions on the Moon.

Damoiseau has two annular walls which fall away in the north. The outer wall can be seen less clearly. Its northwestern part is particularly difficult to see, where the surface even rises from the outer wall toward the inner one. The southeastern part of the outer wall is nearly merged with the continent, so that its inner slopes can be clearly seen. The area which is outlined by the inner annular wall is not flat. Most of it is on the same level as the surface of Oceanus Procellarum, while above it the remains of ancient rocks rise to an altitude of 300 meters. The inner annular wall is constructed /84 asymmetrically. Its northwestern part has an elevation of 200 — 400 meters above the outer one, and 700 — 1000 meters above the inner surfaces. The southeastern part of the inner wall is significantly lower. It does not form a complete ring, being broken at the north, while in the southern part it makes a direct connection with the outer

one. The boundary between the inner and outer walls is provided here on a highly conditional basis. The features of Damoiseau described above indicate the duration and multiple stages of development.

The destructive changes in the region are associated primarily with the continental areas. The most interesting feature is the system of yawning rills of post-Altaic age, the largest of which is the Sirsalis furrow.

For further studies in this region, it is suggested that it would be advisable to explain the nature of the crater phantoms, the double crater Damoiseau and the annular structure Grimaldi with typical mare features of the floor structure. Clarification of their nature would make it possible to proceed to a solution of the question of the origin of the large annular structures on the Moon.

The Region of the Craters Aristarchus, Vacalerius and Kepler (LAC-39, 56, 57) (Figures 13, 14, 15 — see the maps at the end of the book)

In this region there is a predominant distribution of deposits of "mare" Procellarian complex. In a structural respect, the entire region constitutes a portion of the concentric zones of extensive peripheral settlings [29], which contact the southwest of Mare Imbrium, determining the extent of the principle structure elements (walls, faults, etc.). The inner central depression of Mare Imbrium is located to the east [10, 14, 37].

The ring of the outer zone of Mare Imbrium is bounded for a considerable distance by a cordillera, but on the territory of the described maps it is broken off, filled with mare rocks, and Mare Imbrium is connected with Oceanus Procellarum by a broad strait. The edge of the depression beneath the Procellarian rocks is traced by two systems of walls, whose imbricate arrangement makes it possible to assume the existence of shifting stresses in their formation. One system extends from the western terminus of the Carpathians to the

north-northwest. It consists of the post-mare craters Euler, Diophantus and Delisle. The second system of walls runs from the eastern terminus of the Carpathians toward the northeast, and can be traced to Aristarchus and further north to the peak Rumker. It is precisely to this system that a number of features of the recent mare complex (M) belong, whose deposits even cover the rays of Copernicus and Aristarchus.

The next, more peripheral system of walls is traced from the southeast to the Eratosthenian craters Reiner, Marius, and further to Aristarchus. The walls which are usually linearly elongated in the region of Marius and Reiner form random curves, and frequently are changed into discontinuous rings — nearly closed or only indicated by individual dome-like elevations. The initial completely logical supposition that these represent filled pre-Procellarian craters turned out to be erroneous when pictures were examined taken by the Orbiter spacecraft [38]. They clearly show that the surface of these elevations is in no way different from the structure of the ordinary linear walls whose extension they are. It is probable that the origin of these rounded structures is controlled by annular faults. If this is true, we can assume that a number of other annular structures, especially the crater phantoms which are considered to be filled ancient pre-mare walled plains, are elevations which are composed of rocks that are of /85 the same age as the Procellarian formations or are younger and are extrusive or intrusive along the annular faults [39].

The next system of walls extends through the region which is covered by the chart LAC-56, to the northwest. It contains, in addition to a number of craterlets, the crater Galileo. In the southwestern corner of this territory is the edge of a continent which borders Oceanus Procellarum. Oceanus Procellarum is not bounded by a cordillera at any point; everywhere, the zone of contact of the Procellarian rocks with more ancient ones is gradual. Their boundary is sinuous and uneven, clearly indicating a very flat structure and filling of the continental deposits by Procellarian maria. The above, as well as the structural relationship of Oceanus Procellarum and Mare Imbrium, make it possible to view Oceanus Procellarum as a portion of the band

of peripheral mare depressions that surround the clearly pronounced ring of Mare Imbrium on almost all sides. This is particularly clearly evident in the case of the extension of Oceanus Procellarum to the north, to Sinus Roris and Mare Frigorum.

The "mare" rocks in this territory are definitely of different ages. On the charts, one can see outcroppings of rock only from the newest mare complex M (they are located to the east of Kepler and to the west of Reiner, where they are associated with a zone of abrupt brightening of the rocks). In addition, the Procellarian rocks proper are quite clearly divided into gwo groups: the younger ones are dark, and the older ones are bright. This brightness is evidently due in part to the fact that they are covered by ancient rays, probably of Eratosthenian age, and partly may be viewed as a result of a lightening of the rocks due to the effect of exogenic factors. Both Procellarian subcomplexes of rocks are covered by systems of rays from the Copernican craters. The principal systems of rays charted in this region extend from the east (the rays of Copernicus) and also extend from the craters Kepler and Aristarchus. On the west the rays extend from the crater Olbers. They all form a complex interwoven network; in many instances, it is clear that individual rays cover others. In addition to the above-mentioned principal centers of the rays, numerous small craters and craterlets have been charted which are surrounded by a halo of bright surface.

Outcroppings of pre-Procellarian (Nebular and Altaic) rocks and the ancient crater complexes associated with them are associated with the vicinity of craters Kepler and Aristarchus. In the vicinity of Kepler, there are Nebular complexes of rock and Hipparchic craters. We cannot exclude the fact that there are more ancient crater formations here but it is difficult to make them out in this area. These deposits are intersected by faults, basically northeasterly and to a lesser degree submeridional and northwesterly.

The region of the crater Aristarchus is one of the most interesting parts of the visible side of the Moon due to the numerous occurrences of activity which have been observed in the last 300 years [40]. More than half of the phenomena that have been recorded on the surface of the Moon, i.e., several hundred, have to do with the region of Aristarchus, with the first observation dating from 1550. These include "bright spots," "lunar volcanoes," abrupt changes in color, worsening of visibility and other nonstationary phenomena.

To the north and beyond the limits of the region to the northwest and west of the crater Aristarchus, the rocks of the Altai complex are intersected by the graben-like Schroter's Valley, 170 km long and 10 — 20 km wide. The fact that it has curves in it indicates the extension of very widespread faults in the region. Both sides are steep slopes, while on the bottom, filled with rocks of the M complex, there are numerous small craterlets.

The entire system of wider, but equally extensive yawning cracks can be traced to the northeast of Aristarchus, with outcroppings of the M complex associated with it here and there.

Thus, it has been established that the region of Oceanus Procellarum has a complex structure, which is structurally related to Mare Imbrium and is a part of the system of its peripheral depressions. The system of walls emphasizes its concentric structure. The young Copernican and Eratosthenian craters are therefore related to these structural lines. /86

References

1. Spurr, J. E. Geology Applied to Selenology. Lancaster, Sci. Press, 1944, 1945.

2. Khabakov, A. V. The Principal Problems of the History of the Development of the Surface of the Moon. Zap. vses. geogr. ob-va, Nov. Seriya, No. 6, Leningrad, 1949.

3. Khabakov, A. V. Characteristic Features of the Lunar Relief. Principal Problems of the Genesis and Sequence of the Development of Lunar Formations. In the book: Luna (The Moon). "Fizmatgiz" Press, 1960.

4. Kuiper, G. P. Photographic Lunar Atlas. Chicago, 1960.

5. Lunar Charts. Scale 1:1,000,000. Serie's code LAC. Publ. by Aeronaut. Chart and Inform. Center, U. S. Air Force, 1960 — 1964.

6. Sukhanov, A. L. and V. G. Trifonov. Geological-Morphological Mapping of the Moon (Method and Results of Investigations), Astron. vestnik, No. 4, 1967.

7. Sukhanov, A. L., V. G. Trifonov and P. V. Florenskiy. Geological-Morphological Mapping of the Moon and Characteristics of the Structure of the Lunar Surface. Geotektonika, No. 5, 1967.

8. Kozlov, V. V. and A. V. Artemov. Principles and Methods of Photoselenological Mapping. In the collection: V. soveshchaniye po problemam planetologii (5th Congress on Problems of Planetology). Leningrad, mimeo. Geographical Society of the USSR, 1965.

9. Shoemaker, E. M. and R. J. Hackman. Stratigraphic Basis for a Lunar Time Scale. The Moon. Sympos. No. 14, IAU. New York, London, Acad. Press, 1962.

10. Trifonov, V. G. Explanatory Guide to the Geological-Morphological Charts of the Region of the Apennine and Haemus Mountains. In the book: Problemy geologii Luny (Problems of Lunar Geology). Trudy GIN, No. 204, Moscow, "Nauka" Press, 1969.

11. Sukhanov, A. L. Volcanic Ridges on the Moon. In the book: Problemy geologii Luny (Problems of Lunar Geology). Trudy GIN, No. 204, Moscow, "Nauka" Press, 1969.

12. Hackman, R. J. Geologic Map and Sections of the Kepler Region of the Moon. (LAC-57). U. S. Geol. Survey, Washington, 1962.

13. Marshall, C. H. Geologic Map and Sections of the Letronne Region of the Moon. (LAC-75). U. S. Geol. Survey, Washington, 1963.

14. Shoemaker, E. M. The Geology of the Moon. Scient. Amer., Vol. 211, No. 6, 1964.

15. Carr, M. H. Geologic Map and Section of the Timocharis Region of the Moon. (LAC-40). U. S. Geol. Survey, Washington, 1965.

16. Carr, M. H. Geologic Map of the Mare Serenitatis Region of the Moon (LAC-42). U. S. Geol. Survey, Washington, 1966.

17. Eggleton, R. E. Geologic Map of the Riphaeus Mountains Region of the Moon (LAC-76). U. S. Geol. Survey, Washington, 1965.

18. Hackman, R. J. Geologic Map of the Montes Apenninus Region of the Moon (LAC-41). U. S. Geol. Survey, Washington, 1966.

19. McCauley, J. F. Geologic Map of the Hevelius Region of the Moon (LAC-56). U. S. Geol. Survey, Washington, 1967.

20. Shoemaker, E. M., et al. Progress in the Analysis of the Fine Structure and Geology of the Lunar Surface from Ranger VIII and IX. NASA Technical Report No. 32-800. Part II. Pasadena, 1966.

21. Moore, H. J. Geologic Map of the Aristarchus Region of the Moon (LAC-39). U. S. Geol. Survey, Washington, 1965.

22. Morris, E. C. and D. E. Wilhelms. Preliminary Geologic Map of the Julius Caesar Quadrangle (LAC-60). U. S. Geol. Survey, Washington, 1965.

23. Rowan, L. C. Orbiter Observation of the Lunar Surface. The Physics of the Moon. Sympos. Amer. Astronaut. Soc. California, 1966.

24. Titley, S. R. Geologic Map of the Mare Humorum Region of the Moon (LAC-93). U. S. Geol. Survey, Washington, 1967.

25. Trask, N. J. and S. R. Titley. Geologic Map of the Pitatus Region of the Moon (LAC-94). U. S. Geol. Survey, Washington, 1966.

26. Schmitt, H. H., N. J. Trask and E. M. Shoemaker. Geologic Map of the Copernicus Quadrangle (LAC-58). U. S. Geol. Survey, Washington, 1967.

27. Strom, R. G. and G. Fielder. Multiphase Development of the Lunar Crater Tycho. Nature, Vol. 219, No. 5129, 1968.

28. Problemy geologii luny (Problems of Lunar Geology). Trudy GIN, No. 204, Moscow, "Nauka" Press, 1969.

29. Hartman, W. K. and G. P. Kuiper. Concentric Structures Surrounding Lunar Basins. Comm. LPL, Univ. Arizona, Vol. 1, 1962.

30. Hartman, W. K. Radial Structures Surrounding Lunar Basins. Comm. /87
LPL. Univ. Arizona, Vol. 2, 1963.

31. Fielder, G. Structure of the Moon's Surface. Pergamon Press, Oxford; London, New York, Paris, 1961.

32. Novikov, V. V. Stratovolcanoes in the Mesorelief of the Moon. Astron. zh., Vol. 45, No. 5, 1968.

33. Voronov, P. S. The Vectorial Direction of the Tangential Stresses in the Lithosphere of the Moon. In the book: Tezisy VI soveshchaniya po problemam planetologii (Abstracts of the 6th Contress on Problems of Planetology), Leningrad, mimeo, Geographical Society of the USSR, 1968.

34. Sulidi-Kondrat'yev, Ye. D. and V. V. Kozlov. The Folded Deformations on the Moon. In the book: Tezisy VI soveshchaniya po problemam planetologii (Abstracts of the 6th Congress on Problems of Planetology), Leningrad, mimeo, Geographical Society of the USSR, 1968.

35. Salisbury, J. W., V. G. Smalley and L. B. Ronga. Origin in Linear Elements of Mare Humorum. Nature, Vol. 206, No. 4982, 1965.

36. Baldwin, R. B. The Face of the Moon. Univ. Chicago Press, 1949.

37. Florenskiy, P. V. Explanatory Description of the Geological-Morphological Charts of the Region of the Craters Copernicus and Timocharis. In the book: Problemy geologii Luny (Problems of Lunar Geology), Trudy GIN, No. 204, "Nauka" Press, 1969.

38. McCauley, G. F. Geologic Results from the Lunar Precursory Probes. AIAA Journal, Vol. 6, No. 10, 1968.

39. Filder, G. Volcanic Rings on the Moon. Nature, Vol. 213, No. 5074, 1967.

40. Middlehurst, B. M., J. M. Burley, P. Moore and B. L. Welther. Chronological Catalogue of Reported Lunar Events. NASA TR-R-277. Washington, 1968.

N74-19479

CLASSIFICATION, SCALE SERIES AND NOMENCLATURE OF LUNAR CHARTS /88

K. P. Florenskiy, A. A. Gurshteyn, V. I. Korablev,
L. M. Bugayevskiy and K. B. Shingarev

ABSTRACT. Lunar charts are classified with an eye toward solution of special problems of lunar catography. The initial state of mapping the Moon will require charts with scales of 1:5,000,000; 1:1,000,000; 1:250,000; 1:50,000; and 1:10,000.

The further development of work on the investigation of the Moon, required for an understanding of its nature and the solution of problems of comparative planetology, calls for an ever-expanding application of methods of the natural sciences — geological, geophysical, geochemical and geodesic — for the investigation of its surface and internal structure. The development of these investigations by space stations as well as the development of the actual methods of experimentation in space necessitates the mapping of the Moon on various scales and with various degrees of generalization.

However, the traditional principles of mapping the Earth cannot be used without certain corrections, necessitated by the unusual nature of the lunar surface and the methods of its investigation. Thus, for example, in the course of preparing charts of the Earth's surface, one of the important steps is the interpretation of the data from special aerial photographs on a given scale. Interpretation consists of identifiying objects whose nature and properties are

considered important and well-known on the basis of many years of experience on the part of mankind. The objects are represented with conditional scales and extra-scale symbols not always necessitated by the nature of the photographic images, but based on a close similarity of cartography to the nature of the objects. The system of conditional symbols, as a rule, is based on the practical significance of various categories of interpreted objects. In other words, the mapping of the Earth, with the exception of special cases, does not follow strictly scientific goals. Each map has a concrete purpose, which determines its content, the system of conditional symbols, the written data, border data, and coloring formulation, etc.

The compilation of the charts of the lunar surface at the present, on the other hand, serves scientific purposes above all else. Thus, for example, the interpretation of the details of the lunar surface consists in determining their morphological and genetic characteristics, with the process of interpretation becoming a process of scientific analysis of the surface characteristics. The establishment of categories subject to interpretation takes place during the actual process of the investigation of the Moon and may not be determined in advance. Requirements for photography are therefore not limited in part to the interest of cartography. They can dictate the necessity for carrying out additional work — for example, perspective pictures, which are important for understanding the geological objects which are studied by analogy with terrestrial formations.

The monotonic nature of the lunar landscape requires the development of specific methods for its representation. One such method which is very handy from a practical standpoint is the mapping of the Moon by putting together photoplates and photocharts of its surface. However, photocharts and photoplates are not appropriate in all instances, since the external appearance of the lunar surface changes imperceptibly with a change in the altitude of the Sun.

By comparison with terrestrial conditions, the original materials used for compiling the charts and their processing methods change. For example, in the near future the principal resource for the mapping /89 of the Moon will be photographs taken from space. In this regard, the absence of an atmosphere and the monotonic appearance of the lunar surface will make it possible to use, in addition to the familiar stereophotogrammetric methods, other methods as well. One of the possible methods that we can mention in particular is the determination of the relative altitudes of lunar objects in a picture by the photometric method, which has a certain degree of analogy with determining the depths of the seas.

Thorough mapping of the Moon requires the development of fundamental reference networks on its surface as well as the development of theoretical bases of lunar cartography: determination of the optimum scales for the solution of different kinds of scientific problems, the selection of appropriate projections and the nomenclature of numbering, working out the types of charts, methods of determining their details, the adoption of a single system of conditional symbols of various morphological and genetic forms. However, in the lunar cartographic work which has been carried out thus far, there has been a feeling that the absence of a single generally accepted concept was sorely missed. As a rule, the scales and projections for lunar charts are selected quite arbitrarily, and there is no uniform system of nomenclature for the numbering, there are no uniform procedures regarding the type and classification of lunar charts, there is a lack of coordination even in the arbitrary designations and the terminology of the categories of the relief.

In conjunction with this, it makes sense to make a number of preliminary remarks in connection with the classification of lunar charts.

According to the classification that is used for the Earth, geographical charts are divided on the basis of their content into general-geographic and special-purpose, with the prominent role being played by the general-geographic charts which include charts which are synoptic,

synoptic-topographic and topographic. They are intended to show primarily the topography of the Earth's surface and are distinguished by a wide range of scales. As far as the Moon is concerned, led by the necessity for complex investigations, one can conclude that the specific importance of the special-purpose charts by comparison with the Earth is considerably higher.

As a matter of fact, in the complex study of the surface of the Moon, it is possible to distinguish a number of principal parallel trends in the work. Thus, the geological-morphological trend takes up a number of questions that have to do with determining the age of the lunar formations, their structure, form and composition, genesis and evolution, i.e., it covers a broad range of problems involving lunar tectonics, stratigraphy, morphology, and petrography. The principal distinguishing feature of the second trend — the study of the areal physical properties of the lunar surface — is the fact that the studies in this direction may be carried out and are being carried out by terrestrial means. On the basis of observations from Earth, generalized charts of the physical properties of the surface have been compiled, to wit: there are thermal anomalies, regions have been defined with various polarization properties, signs of lunar activity have been detected, and finally the division of the Moon into regions has been carried out on the basis of colorimetric and photometric features. The final goal of these investigations in particular is the definition of regions which are promising for further detailed study. The geophysical trend presupposes gravimetric recordings using methods of active and passive seismics, electrometric prospecting, study of tidal deformations. In working out practical problems, it is characteristic to use the spacecraft landing conditions and the characteristics of their stay on the surface, as well as the possibility of using natural resources. The results of the investigations in practically all of the areas that have been mentioned require representation on the special-purpose maps. The preliminary classification /90 of the charts which is proposed as a basis for evaluation takes into account these areas of investigation and is shown in Figure 1.*

*The cells that have been left empty indicate that the classification will be completed in the future.

The diverse results of the investigation of special-purpose maps that are presented facilitate the comparison and generalization of information, obtained by various methods and from different sources. In turn, the use of such diverse data leads us to a solution of the principal planetological problems that have to do with the origin and evolution of the Moon.

For purposes of retaining continuity and convenience of work, it is desirable when establishing a scale series and working out the corresponding nomenclature for numbering charts of the lunar surface — to retain to the greatest degree possible those basic principles of terrestrial cartography which have become traditional and are very convenient, having been worked out as the result of a great deal of practical experience.

As we know, under terrestrial conditions the following scales of charts have been used widely: 1:5,000,000; 1:1,000,000; 1:500,000; 1:250,000;* 1:100,000; 1:50,000; 1:25,000; 1:10,000. This scale series should ideally be retained even for cartography of the surfaces of the Moon and other planets.**

In view of the fact that the lunar relief is characterized by a striking monotony and the predominant number of lunar charts will be of the special-Purpose type, generalizing information about certain properties of the surface, it is desirable in the first stage of the investigation to cut down on the number of working scales. An analysis of the characteristics of the details of lunar charts makes it possible to state that in the first stage of the investigation of the Moon it would be sufficient to limit ourselves to a certain scale series with reduction of each subsequent scale by a factor of 4 — 5.

Let us examine the scale series which is obtained by reducing the terrestrial scale series. Such a series would contain the following scales: 1:5,000,000; 1:1,000,000; 1:250,000; 1:50,000; 1:10,000.

---

*Scales of 1:200,000 and 1:300,000 are used in the USSR.

**Map scales larger than 1:10,000 will not be covered in this paper.

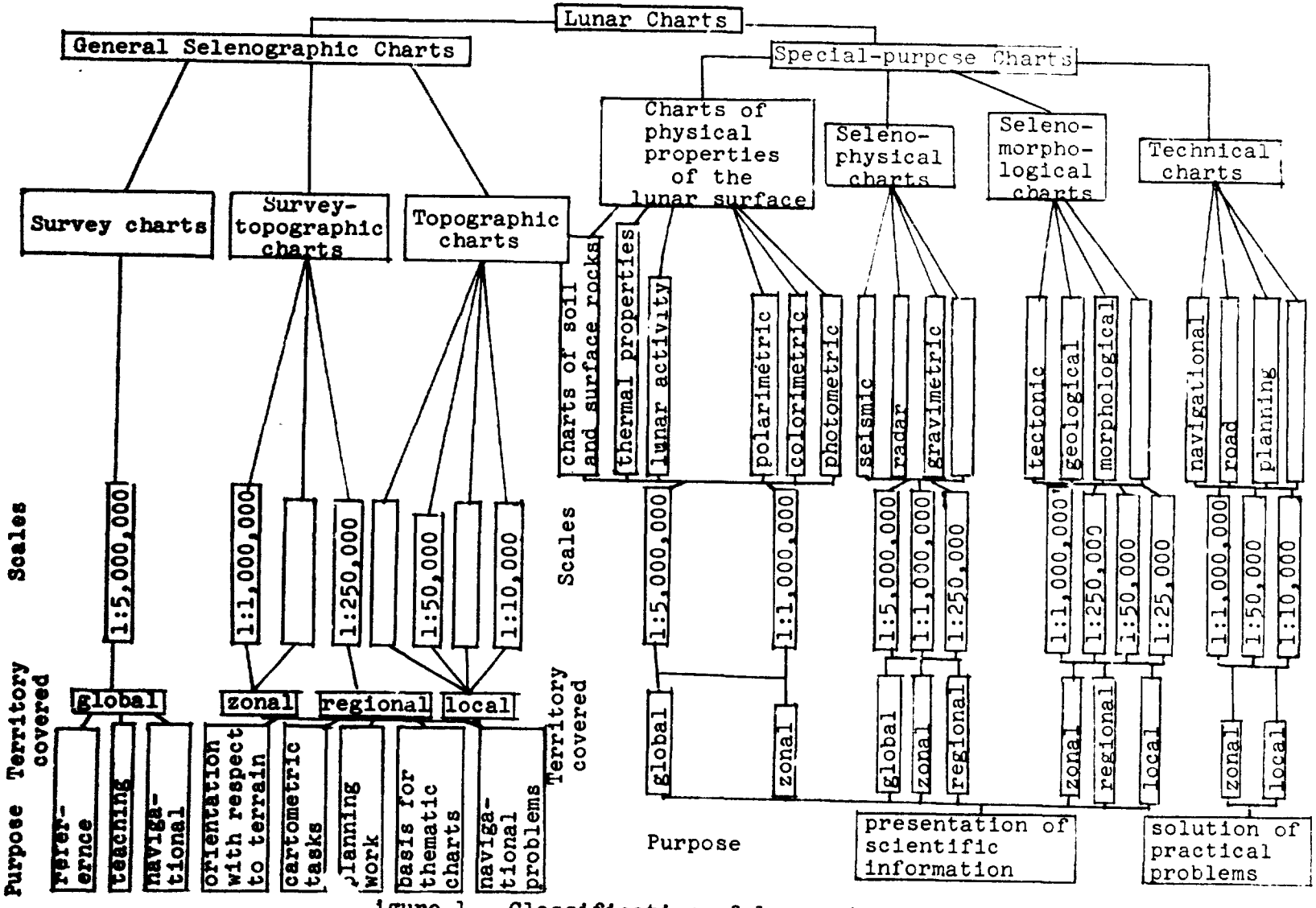

igure 1. Classification of lunar charts.

The original working scale, in our opinion, must remain the scale of 1:1,000,000. This scale is the largest of those which can be retained, although in individual regions they are provided by materials from terrestrial observations. Thus, they serve as the linking member between the large-scale charts on which details are shown that cannot be seen from Earth, and the small-scale survey charts which, in the case of the visible hemisphere, may be compiled on the basis of materials from terrestrial observations. It should be kept in mind in this regard that ideally (with ideal atmospheric conditions in high-mountain observatories and the presence of corresponding astronomical instruments) details on the order of 0.5 — 1 km can be resolved in terrestrial photographs.

A number of lunar charts have already been compiled on this scale. Thus, for example, a chart on the scale of 1:1,000,000 was compiled in the United States for almost the entire visible hemisphere. To ensure this work, the Pic-du Midi (France) observatory carried out systematic photography of the Moon and made motion pictures of the lunar surface near the terminator. As a result, the best pictures of the Moon in terms of quality were obtained. The collection of pictures consists of approximately 100,000 photographs. At the same time, a chart on the scale of 1:1,000,000 was compiled in the USSR for the equatorial zone.

The scale of 1:1,000,000 is convenient in terrestrial geology and may play a similar role in selenology, especially since for future comparative planetological investigations it will be advantageous to have sets of thematic charts of the planets and their satellites, compiled on identical or at least slightly different scales. The /92
topographic charts on this scale may be used for navigational purposes, as well as in carrying out map-measuring work. From the standpoint of the complex investigation of the Moon, charts on a scale of 1:1,000,000 are convenient both from the standpoint of the geological-morphological and geophysical interpretation, but also for reflecting the physical characteristics of the lunar surface. Finally, this scale is traditionally the original one for establishing the terrestrial

nomenclature of the numbering system. On the basis of territorial coverage, charts on a scale of 1:1,000,000 may be zonal — circumpolar, equatorial, etc. — or global — reflecting the surface of the hemisphere or of the Moon as a whole.

The scale of 1:5,000,000 is suggested as the basic small scale. In addition, it is very convenient for extensive charts which are used in demonstration, teaching, and finally for reference purposes. This scale has been used repeatedly in lunar cartography. Thus, the scale of 1:5,000,000 was used for the charts for the far side of the Moon that were compiled in the USSR and USA, giving the first complete map of the Moon. Finally, the charts on this scale make it possible to make out the global features of the geological structure of the Moon — planetary tectonics, the distribution of tectonic-magmatic formations on the surface of the Moon, and the stages in the formation of the surface. They reflect either the Moon as a whole or the individual hemispheres.

In contrast to the charts on a scale of 1:1,000,000 and 1:5,000,000, charts on still larger scales have had only limited use thus far. At the present time, there is a very small number of sheets of large-scale maps which were compiled on the basis of materials from individual photographs taken from space. The necessity of compiling large-scale charts in the future (when appropriate original data is obtained) is unquestioned at the present time.

In the first stage of the work, it is proposed to limit selection to an average scale of 1;250,000, inasmuch as this scale is very convenient from the standpoint of lunar cartography. The dimensions of its trapezoid in terms of degrees can be expressed in whole numbers — 4 x 5°. A sheet with a scale of 1:1,000,000 contains 16 sheets on a scale of 1:250,000. This satisfies the condition for multiplicity of scales. At the same time, however, the length of the sides of the trapezoid of the scale in kilometers in the landscape is 120 x 150 km, which agrees with the requirements of special-purpose charting. Thus, for example, a similar area satisfies a regional geological mapping.

In addition, the sheet of the lunar map is on a larger scale — 1:100,000 — and makes up a polygon with sides measuring 40 x 60 km, which in an areal sense leads to a loss of the regional nature of the investigation and in turn prevents the solution of a number of tectonic, stratigraphic and other problems, thus leading among other things to a significant increase in the volume of work involved in the geological-morphological interpretation. In terrestrial geology, the compilation of charts on a scale of 1:100,000 was due primarily to convenience in carrying out the field work. In the case of work on the planets and on the Moon, the volume of work on the surface itself will necessarily remain minimal and the need for a larger working scale to cover significant territories will itself disappear. The compilation of charts on a smaller scale than 1:250,000 — for example, 1:500,000 — would lead to an unjustifiable increase in the area covered and amounts to cartographic generalization.

Large scales of 1:50,000 and 1:10,000 are necessary primarily for solving the practical problems of further development of space study as well as for investigating areas in geologically interesting regions and studying individual forms of relief. The geological-morphological interpretation on a scale of 1:50,000 thus involves determination of zones of contacts, tectonic disturbances, the structure of intrusions, lava flows, individual elements of craters, etc.; on a scale of 1:10,000, the thickness of the friable layer, stoniness, crater density per unit area, age and genetic characteristics. In terms of territorial coverage, maps on this scale will have a local nature. /93

In determining the scale series for compilation of charts at the first stage of the investigations, we proceed on the assumption that in future there will be cartographic, photographic and other necessary materials that will make it possible to plot charts on these scales that will be valid both in accuracy and completeness of content.

Terrestrial charts on medium and large scales in the overwhelming majority of cases contain a number of sheets; for each of the scales there is a corresponding series of sheets whose limits coincide with the meridians and parallels. In conjunction with the number of sheets in such charts, a nomenclature numbering system has been devised for them. Nomenclature numbering is intended to represent the system for division of the terrestrial ellipsoid into a series of trapezoids of various dimensions in latitude and longitude, depending on the scale of the chart. The basis of the mapping of the Earth is a sheet on a scale of 1:1,000,000. The symbols on the sheet are international.

On the basis of the dimensions of the lunar sphere, for the edges of a uniform trapezoid on the million chart of the Moon, it is advantageous to establish (as was done previously in the case of LAC USA charts and the charts of the equatorial belt issued in the USSR) lengths of 16° latitude and 20° longitude. Dimensions of the edges in centimeters on the scale of the chart in the equatorial zone amounted to 49 x 61 cm or in km at the site — 490 x 610 km. The sheets which are contained in the 16-degree latitudinal zone form a series (belt). Each series has its own specific Latin letter from A to E, beginning at the equator, and running toward both poles, up to the parallels with latitudes of ±80°. The sheets in 20° meridional zones form a column. The columns are given Arabic numerals. It is obvious that there will be a total of 18 columns of 20° each on the surface of the Moon. Counting the columns is performed from 1 to 18 moving eastward, beginning with the column which intersects the zero meridian. The proposed numbering of the million chart is shown in Figure 2, a and b. There are a total of 138 sheets on this scale for the surface of the Moon (not counting the polar caps).

The polar caps, including the territories that are located from parallels ±80° to the poles, are shown on a scale of 1:1,000,000, one on each sheet, measuring 61 x 61 cm.

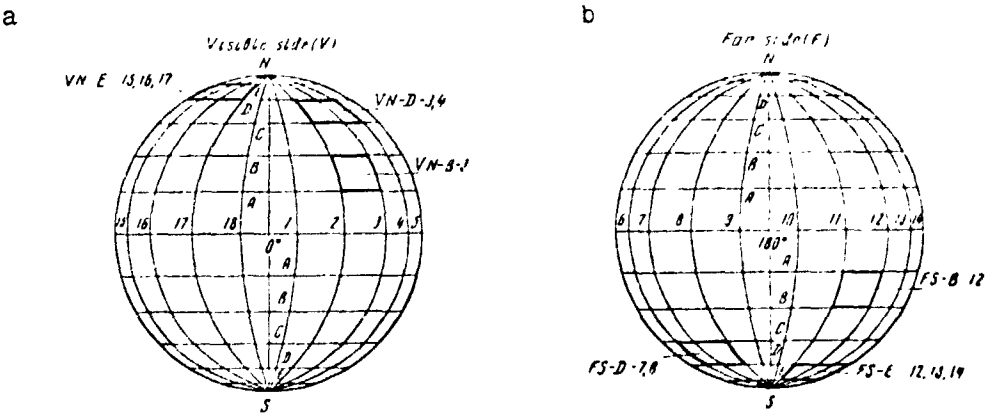

Figure 2. Numbering of the lunar hemispheres.

a — numbering of the visible side on chart sheets on a scale of 1:1,000,000 (example of the nomenclature of the sheets of the northern hemisphere); b — numbering of the far side on map sheets on a scale of 1:1,000,000 (example of nomenclature of sheets of southern hemisphere).

In conjunction with a noticeable increase in the degree of similarity of the meridians of the sheet for belt D (between parallels 48 and 64°) it is advantageous to double the longitude, and in the case of the sheets for belt E (between parallels 64 and 80°) to triple it.

In carrying out such deciphering operations, in which the zero meridian is located in the middle of the first column, the equatorial zone up to the ±40° parallel is covered by a number of sheets on both the visible and far sides of the Moon.

The nomenclature of each sheet of the million chart consists of letters which represent series and numbers of columns.* In addition, a letter is placed in front of it which indicates whether the sheets belong to the visible or far hemisphere: V (visible) for the visible hemisphere and F (far) for the far side. This letter is followed by

*In addition to the nomenclature, the chart sheets of all scales also advantageously show, as is done on the charts for the Earth, the proper name of the sheet derived from the most important object.

the preliminary designations for north — N or south — S, which show the direction away from the equator. As a result, the nomenclature of the million sheet runs like this: FN-A-8 or VS-B-1.

The nomenclature of the sheets that have been cut into two or three parts will have the following appearance: FN-D-7, 8 and FN-E-6, 7, 8. /94

By analogy with Earth, the sheet of the million chart serves as the basis for further graphing on different trapezoids as a function of scale. In contrast to the nomenclature on medium and large-scale Earth charts, for the designations on sheets of lunar charts of all scales, it is advantageous to use the Latin alphabet, inasmuch as it is desirable to have a single nomenclature in the international sphere for all scales. This would facilitate both scientific and space cooperation. In addition to the letters of the Latin alphabet, Arabic numerals will be used in the future for the nomenclature. Corresponding to the reduction in the scale series, the numbering nomenclature of the lunar charts must take into account the theoretical possibility of a second mapping scale for the Moon, creating a scale series which is as complete as that for terrestrial cartography.

The million sheet of the chart is divided into four sheets on a scale of 1:500,000 (Figure 3a) which are marked by capital letters in the Latin alphabet — ABCD. The nomenclature of sheet 1:500,000 includes the nomenclature of the million sheet with addition of a corresponding letter, for example, FN-B-1-D. The sheet measures 8° latitude, 10° longitude, and the dimensions of the frame in the scale of the chart are 49 x 61 cm, 245 x 305 km for the terrain.

The sheet of the chart on the scale of 1:500,000 is divided into four sheets with a scale of 1:250,000, which are designated by small letters of the Latin alphabet — abcd (Figure 3b). The nomenclature of the sheet of the chart on a scale of 1:250,000 is as follows for example: FN-B-7-A-c.

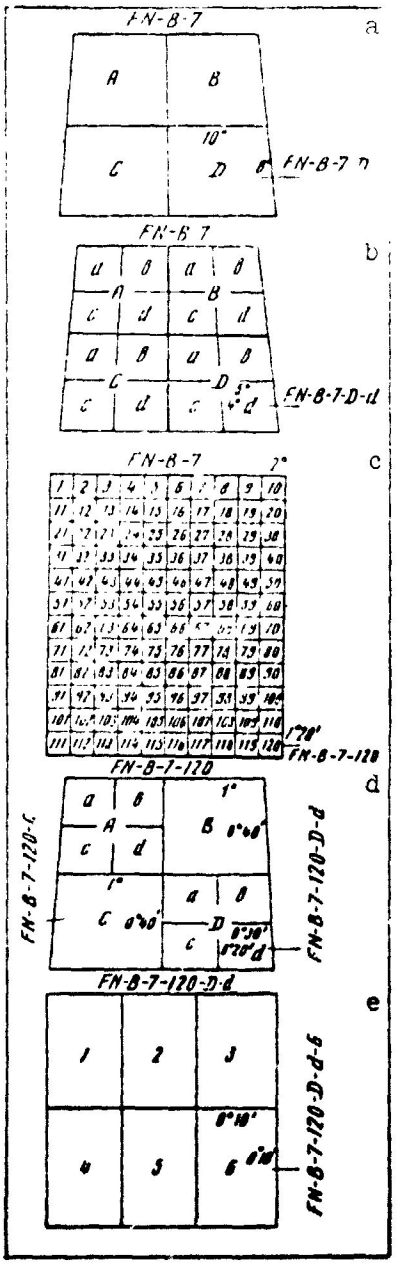

Figure 3. Example of numbering of sheets of charts on various scales and examples of nomenclature of certain sheets.

a — scale of 1:1,000,000 on map sheets with scale of 1:500,000; b — scale of 1:1,000,000 on chart sheets on scale of 1:250,000; c — scale of 1:1,000,000 on chart sheets on scale of 1:100,000; d — scale of 1:100,000 on chart sheets of scales of 1:50,000 and 1:25,000; e — scale of 1:25,000 on chart sheets on scale of 1:10,000.

Each sheet on a scale of 1:250,000 extends 5° in longitude, 5° in latitude, while the dimensions of the frame on the scale of the chart measure 49 x 61 cm, and in terms of the terrain this is 122.5 x 152.5 km.

The million sheet is divided into 120 sheets with a scale of 1:100,000 (Figure 3c). The sheets are listed by Arabic numerals 1, 2, ..., 120. The nomenclature of the sheet on a scale of 1:100,000 includes the nomenclature of the million sheet with addition of a number of the 100,000 sheet, for example, FN-B-7-120. Each sheet on the scale of 1:100,000 extends 2° in longitude, 1°20' in latitude. The dimensions of the frames on the scale of the chart are 40 x 60 cm, and 40 x 60 km for the terrain. The sheet of the chart on a scale of 1:100,000 serves as the basis for numbering on a trapezoid with larger dimensions. /95

The trapezoids with a scale of 1:50,000 are divided like the 100,000 sheet into four parts (Figure 3d). Thus, on the million sheet there are

480 sheets on this scale. They are designated by capital letters in the Latin alphabet — A, B, C, D which, when the complete nomenclature is written, are inscribed after the nomenclature of the 100,000 sheet, for example FN-B-7-120-D. The dimensions of the trapezoid are 1° in longitude, 0°40' latitude; the dimensions of the trapezoids on the scale of the chart are 40 x 61 cm, and 20 x 30.5 km for the terrain.

In dividing the trapezoid with a scale of 1:50,000 into four parts, the result is four trapezoids with a scale of 1:25,000 (Figure 3d). These trapezoids are designated by small letters of the Latin alphabet, which are used in the nomenclature of the 50,000 sheet, for example FN-B-7-120-D-d. On the million sheet there are 1,920 trapezoids on this scale. The dimensions of each trapezoid are as follows: 0°20' latitude, 0°30' longitude. Dimensions of the frame in the scale of the chart are 40 x 60 cm; for the terrain — 10.0 x 15.5 km.

In the above-described numbering, within the limits of each trapezoid with a scale of 1:25,000 there are 6 trapezoids with a scale of 1:10,000 (Figure 3d). They are represented by Arabic numerals — 1, 2, 3, 4, 5, 6. The million sheet contains 11,520 sheets on this scale. The nomenclature of a sheet with a scale of 1:10,000 is obtained from the nomenclature of the 25,000 sheet by the addition of appropriate figures, for example FN-B-7-120-D-d-6. The dimensions of the trapezoids in degrees are 0°10' in latitude, and 0°10' in longitude; the dimensions of the outline of the trapezoid in the scale of the chart are 50 x 50 cm.

The proposed nomenclatural interpretation, in addition to the pictures, is illustrated by tables. It follows from the data in the tables that with a selected interpretation for four scales out of seven, the sheets of maps near the equator are similar to squares. On the whole, however, the sizes vary from 40 to 60 cm. These dimensions /96 show a good agreement with the usually technologically possible production conditions. In addition, it is convenient to work with sheets of such a size. The dimensions of the frames in degrees for the average scales are expressed by a whole number of degrees, for large scales by rounding off to 10^{th}s of a minute, which also makes it more convenient to operate with them.

Scale	Frame sizes		Frame sizes on map scale, cm		Frame sizes for terrain, km		No. of sheets in previous scale	No. of sheets on scale of 1:1,000,000	Example of nomenclature
	lat.	long.	lat.	long.	lat.	long.			
1:1,000,000	16°00'	20°00'	49	61	490.0	610.0	1	1	FN-B-7
1:500,000	8°00'	10°00'	49	61	245.0	305.0	4	4	FN-B-7-A
1:250,000	4°00'	5°00'	49	61	122.5	152.5	4	16	FN-B-7-D-a
1:100,000	1°20'	2°00'	40	61	40.0	61.0	120*	120	FN-B-7-120
1:50,000	0°40'	1°00'	40	61	20.0	30.5	4	480	FN-B-7-120-A
1:25,000	0°20'	0°30'	40	61	10.0	15.2	4	1920	FN-B-7-120-A-d
1:10,000	0°10'	0°10'	50	50	5.0	5.0	6	11520	FN-B-7-120-A-d-4

*120 sheets on 1:1,000,000 scale.

Conclusions

1. At the present time, the need has arisen to work out a general concept which will make it possible to solve problems of a mathematical nature, as well as the establishment and formulation of lunar charts. In this paper, an attempt is made to classify lunar charts and to propose a solution for individual problems involving lunar cartography.

2. An analysis of the characteristics of the load on the lunar charts makes it possible to state that, in the first stage of investigations of the Moon, it will be sufficient to limit ourselves to a short scale series, with reduction of each successive scale by a factor of 4 — 5, including specifically the following scales: 1:5,000,000; 1:1,000,000; 1:250,000; 1:50,000; 1:10,000.

3. It is suggested that the dimensions of individual sheets on the scales mentioned above and their nomenclature be used in conformance with data in the tables.

N74-19479

LABORATORY SIMULATION OF PROCESSES OF "EVAPORATION, CONDENSATION, AND SPUTTERING" TAKING PLACE ON THE SURFACE OF THE MOON

/97

M. D. Nusinov, V. A. Kochnev, Yu. B. Chernyak, A. V. Kuznetsov, A. I. Kosolapov and O. I. Yakovlev

ABSTRACT. Study of evaporation, condensation and sputtering on the Moon can provide information on the same processes on other planets, and reveal details of the formation of the lunar regolith. Simulation methods include vacuum evaporation, laser evaporation, and bubbling gas through melts.

The surface layers of the Moon are in contact with the space surrounding the Moon, characterized by a number of specific conditions. These conditions include:

1. Ultrahigh vacuum (concentration of neutral particles $n \approx 10^{-5} - 10^{7}$ cm^{-3}, $p \sim 10^{-10} - 10^{-16}$ torr with possible components of Ar, Kr, Xe, etc.) [1, 2];

2. Fluxes of meteor substance ($m \approx 10^{-10} - 10^{-10}$ g; $v = 10 - 72$ km/sec) [3, 4];

3. Fluxes of charted particles (primarily protons) — "solar wind" ($j \approx 10^{8} - 10^{9}$ particles/cm^2·sec, $v \sim 300 - 800$ km/sec) [2];

4. Electromagnetic radiation from the Sun [2].

Volcanic processes and radioactive decay of material [1] are also possible. In addition to those above, it is necessary to keep in mind the reduced gravitational field (in comparison with terrestrial conditions) and the practical absence of a magnetic field. Such conditions lead to the occurrence of a number of processes which have an effect on the structure and composition of the surface layers of the regolith of the Moon. Here we shall consider only the processes of evaporation (sublimation) of particles of surface material, its secondary condensation (desublimation), the sputtering of material in the liquid phase and the loss of material from the surface of the planet.

Evaporation of material from the liquid phase or the solid (sublimation) takes place as a result of thermal heating of material in the course of volcanic processes [5], as well as collisions with the surface of the planet by fast meteor particles. These processes take place either in a quasi-stationary fashion or they have the nature of a rapid "pulsed" evaporation that leads to the ejection of material in the form of a cloud of ionized and dissociated gas as well as liquid and solid particles. The pulverization of the material on the surface of the Moon takes place primarily as the result of bombardment by particles of the "solar wind" and radioactive decay. Inasmuch as the pulverization, evaporation and sputtering take place under conditions of an ultra-high vacuum and reduced gravitational field, only those particles which have a velocity which is lower than the escape velocity (in the case of the Moon, $v_{es} \approx 2.4$ km/sec [1, 6]) can remain within the limits of the lunar atmosphere and, moving along ballistic trajectories, return to the surface. The gas particles that return to the surface will remain on it (condense, desublimate, penetrate) either on first impact or after several secondary collisions and "jumps" along ballistic trajectories. The path traveled by particles during drift in the atmosphere, determined by masses, initial velocities and escape angles of the particles reaches 10^2 - 10^3 km, and the drift duration is approximately 10^0 sec [1, 7]. These processes may lead to the formation of a surface layer of dust with unusual properties which differ from the properties of the initial substance.

Inasmuch as the processes enumerated above (all or at least a part of them) are taking place constantly, they cause a transformation of the surface material and are responsible for the condition of the surface layers and their specific physical (especially optical) characteristics, composition and structure. /98

For many years, the studies of the surface layers of the Moon had been carried out primarily by astronomers. These studies have been supplemented by experiments in laboratory simulation. They have led to the advancement of a number of hypotheses and theories concerning the state and properties of the surface layers of the Moon: this includes the "dust" hypothesis of Gold [3, 4, 8], the "meteor-slag" hypothesis of Sytinskiy-Sharonov [3, 4, 8], the hypothesis of a negative balance and differentiation of material of Florenskiy [9, 10] and a number of other hypotheses.

A survey of the results of the investigations is given, for example, in the monograph by R. Keydl [8], et al.

As a result of astronomical measurements, it has been established in particular that there are unusual photometric properties of the lunar surface which differ from the properties of normal diffusion-scattering surfaces. These properties are characterized by a reduced mirror reflection and pronounced back scattering. Hapke and von Horn [8] [sic] mention that the powerful back scattering may be due to small spherical or angular transparent particles with corresponding indices of refraction. They are apparently wrong, however, in suggesting that such structures on the Moon cannot exist as a consequence of micrometeoritic bombardment. As will be shown later on, it is precisely this bombardment that serves as one of the possible reasons for the formation of such particles. Hapke and von Horn agree with Fesenkov that the surface of the Moon consists of material that has a complex structure. In order for the required back scattering to arise, the characteristic size of the particles must be much larger than the wavelength of visible light.

The bombardment of the surface by protons of the "solar wind," as was demonstrated by experiments in laboratory simulation, causes a darkening of the irradiated substance [3, 4, 8, 11]. The influence of radiation on a number of powdered substances was investigated. It was found that the albedo and other reflective properties of powdered basalt with particle diameter ~2 - 10 μm are most similar to the corresponding characteristics of the lunar surface.

In irradiation, a role is played by the chemical effect of hydrogen, and the surfaces of iron and copper oxide following irradiation were found to contain metallic FeCu. In addition, the surfaces that had been subjected to bombardment were covered with very small needles and sharp, almost opaque substances which possibly may make a contribution to the unusual photometric characteristics of the surface. Gibbs [12] developed a theory according to which the lunar substance, evaporating and precipitating again as the result of meteoritic impact, must exist on the surface of the Moon in the form of acicular single crystals (so-called "whiskers"). He suggests, on the basis of laboratory experiments on condensation of vapors of many substances into the solid phase, that such "whiskers" may be the primary form of solid material in the Solar System. According to MacCrea [13], the author of the theory of the formation of the planets of the Earth group, on the basis of its chemical nature such a substance is silicate and the Moon and Mars must consist primarily of silicate materials.

The interaction of meteorites with the lunar surface was investigated experimentally and theoretically. Golt, et al. [3, 4, 8] performed a great many studies on laboratory simulation of processes of high-velocity impact of meteorites on different materials, including silicates. As a result of these studies, he concluded that in the /99
case of high-velocity impacts on silicates there is only a fragmentation of the latter and not melting. Keydl [8] notes that, inasmuch as the ratio of the surface to the volume in these experiments and for the impacts on the Moon is considerably different, these results are not completely reliable, although they have generated several ideas. It may also be suggested that the collision velocities of

particles with a target in such experiments were not so high as on the Moon. In addition, such a finding also contradicts the basic concept of analytical consideration of the collision process of a meteorite with the surface of a planet lacking an atmosphere (the Moon) developed in the work of Zel'dovich and Rayzer [14, 15] and Stanyukovich [16].

Florenskiy, et al [10], studying the finely dispersed cosmic substance in terrestrial deposits (primarily in the region of the Tungus Depression) found and investigated in detail a great many magnetic and silicate spherules and sheets.

They suggested two mechamisms for the formation of cosmic spherules:

a) melting of a body, sputtering and hardening of droplets;

b) partial or complete evaporation of a body and subsequent condensation of the substance from a supersaturated vapor.

The authors of [10] feel that in the evaporation of bodies from space and subsequent condensation of the material one must expect profound differentiation. It is natural that under the conditions of an extremely rarified lunar atmosphere this process will take on even greater importance.

Newton, et al. [17] as well as Vonnegut, et al. [18] and Gutkin, et al. [19] studied the processes of "evaporation-condensation" of basalt in a vacuum, assuming similar processes in the formation of the surface layers of the Moon. In their papers they also point out the possibility of differentiation of the material in the processes of "evaporation-condensation." Thus, in [17, 19] mention is made of the enrichment of a film of condensate by alkaline metals in the recondensation of basalt; in [17] mention is made of the possible formation of a powdered layer due to the erosion of the basic material in the course of interaction with recondensing alkali metals. The authors of [18] state that a film of a condensate contains K, Ca and Fe. In a film of condensate, crystals with dimensions of approximately 10^2 to 10^3 Å were found.

Investigation of substances artificially produced by rapid decompression of melts, modelling lunar material, were carried out by Dobar [3, 4, 8] and Filder, et al. [20].

Very recently, the timeliness of studies aimed at clarification of various mechanisms of processes taking place on the lunar surface has increased sharply in the light of investigations of the surface layers of the Moon carried out by Soviet and American automatic probes in the Luna and Surveyor programs, as well as by expeditions to the Moon performed by the crews of the Apollo spacecraft [21, 22, 23].

The results of studies of samples of lunar material brought back to Earth by the crew of the Apollo 11 [24] indicate that the substance is a silicate material (SiO_2 ~ 40 - 45%) of a basalt type of volcanic origin. This substance differs mineralogically and chemically from typical terrestrial rock and, in the opinion of Academician A. P. Vinogradov, resembles feldspathic achondrites. It contains traces of metamorphism from impacts, and in particular has on its surface a great many vitrified pits which may have been produced by impacts of small particles. A small (dust) fraction contains an appreciable amount of vitreous spherules and particles (in a number of cases, up to ~ 50%).

The elementary composition of the material is similar to that of terrestrial volcanic rocks and meteorites, but in comparison with the latter, it is enriched with refractory oxides (TiO_2, etc.) and oxides of iron, and is impoverished with respect to alkaline and other highly volatile elements. /100

In terms of its physical and mechanical characteristics, the lunar soil at the site where the Apollo 11 landed is a fine-grained, granular, and readily compacted substance, similar in its properties to wet sand. According to the data from investigations of the material that was brought back by the Apollo 12 crew, this material from the surface of the Moon at the landing site in Oceanus Procellarum is different in composition from that obtained previously (less TiO_2 content, etc.).

The substances collected by the Apollo 12 and the Luna 16 are similar in chemical composition [23].

The results of lunar material investigations indicate that the substance in the surface layers of the Moon is constantly in a state of transformation under the influence of external and internal factors. Interest in this connection is directed at a study of mechanisms of its transformation, including the processes of "evaporation-condensation" as well as the sputtering of material in various phenomena involving the formation of dust, formation of glassy particles, etc., playing an important role.

At the same time, however, the specificity of the morphological forms of the particles of the regolith (bodies of rotation) is unquestionably linked to the dynamic processes that accompany both a meteoritic impact and the various endogenic processes. The simulation of such processes, especially sputtering, is discussed below. These studies make it possible to determine the composition, size distribution, angles and velocities of escaping particles, which determine the structure of the substance on the surface of the Moon and the instantaneous composition of the atmosphere especially in the light of the hypothesis of Mirtov [25]. The data from these investigations may be utilized in establishing from lunar satellites the sites of possible volcanic phenomena.

On the basis of the results of investigations, it may be possible to determine the possible existence on the lunar surface of certain highly volatile substances, etc.

Now let us look in greater detail at the features of stationary and momentum processes of the "evaporation-condensation and sputtering" type as well as some methods of their laboratory simulation.

I. Simulation of Stationary Processes of "Evaporation-Condensation"

The possibility of the evaporation and subsequent condensation of vapors in lunar endogenic (volcanic) activity is mentioned in [6, 18]. These processes may have a complex nature.

In conjunction with the problem of thin films, a study has been carried out involving the processes of evaporation and condensation of oxides of Si, Fe, Al and other inorganic compounds. The results of mass spectrometric studies of the gas phase during the evaporation of oxides SiO_2 and Al_2O_3 [26, 27] indicate their dissociation. Thus, Al_2O_3 evaporates in the form of Al, O, AlO and Al_2. The molecule $(Al_2O_3)_n$ is not found in the vapors. When SiO_2 evaporates, there is also a dissociation of the oxide [26]. Rocks of the basalt type, as well as tuff, granite, and others, obviously will evaporate in the form of individual component parts (molecules, atoms). There may be selective evaporation and fractionation of individual simple compounds and elements as a function of their volatility. Subsequent divisive condensation on a surface may lead to enrichment of condensate with individual elements and a change in the stoichiometric ratios, and may cause the appearance of new compounds and structures in the form of a condensate. For example, it is possible for the reduction of metals [17] to take place in this fashion, as well as impoverishment /101 of a condensate of non-condensing components (for example, oxygen) or development of other modifications of the same substance. Thus, evaporation-condensation of Al_2O_3 independently of the modifications of the evaporating material leads to the formation of various condensate modifications as a function of the substrate temperature: amorphous disperse film, γ-modification, or alpha modifications (corundum) [28].

SiO_2 frequently recondenses in a vacuum with formation of the monoxide SiO [29]. Some sublimates of rocks of the basalt type are enriched with alkaline metals with recondensation in a vacuum [17]. In these same processes the water of crystallization which is chemically bound in the crystal structures of certain minerals, type n

(H_2O), may change to the unbound state and accumulate in places on the surface that have the lowest temperature ("temperature traps") in multiple processes of the "evaporation-condensation" type [7] [in the case of water ice, $p_s = 2.93 \times 10^{-10}$ torr at $T_s = -140°$ C (133° K) and $p_s = 7.4 \times 10^{-15}$ torr at $T_s = -150°$ C (123° K)] [30]. Evidently final condensation may take place at places on the surface with temperatures below -140° C (133° K) since the maximum pressure in the atmosphere of the Moon on the side which is visible from Earth clearly does not exceed a value of $p_{max} \sim 10^{-10}$ torr [1].

Evaporation and especially sublimation under conditions of an ultra-high vacuum from surfaces which are cleaned, during bombardment by corpuscular particles and ultraviolet, of a film of adsorbed gas and impurities, may take place more intensively than under ordinary conditions.

In the case of ionized particles, the condensation mechanism may be complicated by the presence of local charges on the surface of a planet, formed presumably by photoionization.

In summing up the above, we can conclude that for the study of possible stationary processes of "evaporation-condensation" which take place on the surface of the Moon, it is necessary to obtain the following experimental data:

1. The velocity of the evaporating (or sublimating) particles of lunar material;

2. The mass composition of vapor and the degree of its dissociation for different temperatures of the source;

3. The condensation coefficient of basalt vapors;

4. The chemical composition, structure, and the modification of the condensate and the residual glasses as a function of the temperature of the source and the substrate;

5. The thermal-physical and physical-mechanical characteristics of the condensate;

6. The sorption capacity of the condensate.

Simulation of the processes of evaporation and condensation assumes the presence of a vacuum in an experimental situation. The pressure is determined as follows:

a. freedom of the medium from collisions ($l \gg d$);
b. high degree of purity of the condensate film ($\tau_m \leq 10^{-3}\ \tau_{m\Sigma}$);
c. low restitution factor ($\Sigma \leq 10^{-2} - 10^{-3}$) [2, 31, 32].

A number of experiments for which the multiplicity of collisions with a target may be disregarded (for example, investigation of the structure and phase composition of a condensate as a function of the temperature of the substrate, the mass vapor composition) may be conducted with a pressure of approximately 10^{-6} torr. The requirement for condensate purity is fulfilled in this case due to the significant increase in the rate of formation of a single layer of condensate, as compared with a single layer of impurities ($\tau_{evap} \ll \tau_{imp}$).

Thus, the rate of condensation of SiO_2 may reach $10^5 - 10^6$ single layers per second at an evaporation temperature $T_{evap} \sim 2300°$ K; the rate of formation of a single layer of adsorbed particles of residual gases and vapors is 1 - 10 (at a wall temperature of approximately 100° K*). Consequently, at a background pressure of 1×10^{-6} torr the surface purity may be 10^3. These conditions may be satisfied in typical evaporating systems which are intended for the production of thin films, and which have been modernized (introduction of screens, cooling by liquid nitrogen, etc.). /102

*Estimates were performed with the aid of Langmuir's equations [2, 33].

In order to keep a basalt melt in a non-oxidized condition $p_{O_2} \leq 10^{-13}$ torr. The measurement of the surface properties requires a much more complete evacuation of those particles of vapor which have not condensed in the first collision and consequently the maintenance of superlow pressures in the vacuum chamber of the apparatus. Similar requirements are needed for investigating the surface forces of condensate films. For such investigations, it is necessary to have experimental apparatus with walls that have good powers of absorption, i.e., which utilize a combination of cryosorbic (nitrogen) and cryogenic methods of evacuation. Thus, to preserve the surface of the condensate in a non-polluted condition for 24 hours, it is necessary to keep the background pressure of the gas at $\leq 10^{-11}$ torr.

To investigate the process of recondensation, it is possible to use ordinary methods of evaporation in stationary conditions (thermal evaporation in a "boat," electron-beam evaporation). The method determines the rate of the process and the purity of the condensate which is obtained. Evaporation of substances like silicates and refractory oxides from heated crucibles and "boats" may lead in a number of instances to the simultaneous evaporation of the material of the evaporating device itself in the form of oxides and other volatile compounds due to contact reactions of the molten material with the walls of the evaporator. This may be avoided by using the method of electron-beam evaporation from the water-cooled crucible (the so-called method of "autocrucible" evaporation) [34].

To measure the mass composition of the vapor and the residual gas a mass spectrometer of the "Chronotron" type, or a radio frequency type known as the "Omegatron", is used, etc. Measurements by means of the "Chronotron" mass spectrometer, whose sensor is located near the substrate and is covered by deposits of the substance itself from the evaporator, make it possible to determine the reflux of non-condensed substance from the substrate, its mass composition and selectivity of condensation.

Condensed films may be investigated both by direct (for example, chemical analysis) and indirect (on the basis of the change in optical characteristics, electrical conductivity of the film) methods. In order to obtain correct results, the measurement of the structure and the properties of the substances obtained are best accomplished in a vacuum, immediately after deposition of the films, since the evaporation of the films in the air may lead to their oxidation, additional absorption of moisture, etc. When these conditions are not observed, it is necessary to employ special measures for the sake of precaution.

In the apparatus described below (see Section III), preliminary experiments were performed in the evaporation of a basalt melt in a vacuum (10^{-6} torr) at a melt temperature t = 1200 - 1800° C. The investigation of the composition of the condensate and the residual glass showed that there is intensive differentiation of the raw material.

The differentiation of basalt was studied as the result of evaporation of the melt in a vacuum (~ 10^{-6} torr) at temperatures t = 1200 - 1800° C. We studied the change in the chemical composition of a high-titanium basalt as a function of temperature and the holding time of the melt. As the final products to be analyzed we used the residual glasses and condensates, as well as the vitreous spherules which are formed by bubbling gaseous helium through the melt. The substance that was collected was analyzed by means of immersion, spectrophotometric, spectral, chemical and diffractometric methods. /103 In the following we shall present some of the preliminary results of these experiments.

The measurement data on the refraction indices of the residual glasses indicate a change in the chemical composition of the basalt melt at various temperature levels. The index of refraction of the residual glass changes from n = 1.653 at T 1230° C (melting point of basalt) to n = 1.676 (maximum value) at T = 1600° C. Further heating to T = 1750° C leads to a decrease in the index of refraction of glass to n = 1.663. The non-linear nature of the change in the properties

of the glass as a function of the temperature indicates that there is a stepwise evaporation of the component parts of the basalt melt. While the rising branch of the curve indicates a loss of the most readily volatile components (for example, alkalis) and the enrichment of the melt with the components which increase the optical density of the residual glass, the descending branch most likely indicates a loss in the melt of such components such as Fe, Mg, Ti and others, resulting in a drop in the optical density of the glass. A chemical analysis of the residual glass and the condensate indicates the presence in the condensate of K, Na, Si, Fe which evaporate from the melt at 1250 - 1500° C. Above 1500° C, there is subsequent evaporation of Mg, Ca, Al and Ti.

With respect to the dependence of the refractive index of the glass on the holding time of the melt, the results obtained allow us to conclude on a preliminary basis that the chemical composition of the melt actually does not change with a change in the melt holding time at a uniform temperature of 30 - 100 minutes. In all probability, with a holding time of the melt up to 30 minutes. the chemical composition is balanced throughout the entire volume of the melt and the glass is formed in accordance with the heating temperature.

In the course of the experiments, there also came to light a geochemical differentiation of the material with respect to the microelements. Spectral analysis of the condensate indicates enrichment of the volatile fraction Ni, Co, Cu, Mo and some other elements.

The preliminary results presented above indicate that the geochemical individuality of the regolith may be due to processes of evaporation and condensation of Ni, Co, Cu, Mo, P, Ga and certain other elements in the basalt flows on the Moon.

II. Simulation of Pulsed Processes

Pulsed processes take place when meteorites strike the surface of the Moon and also during volcanic phenomena. Let us look at these in turn.

When a meteorite strikes the surface of a planet, the result is an area of highly compressed material with specific energy $v^2/8 \sim 1.15 \cdot 10^{11} - 6 \cdot 10^{12}$ erg/g ($v = 10^6 - 7 \cdot 10^6$ cm/sec). The development of the process with time is determined by two processes:

1. The propagation of the disturbed region within the substance in the form of a shock wave; the density of the energy decreases, inasmuch as the initial energy is distributed over an increasingly large volume which is occupied by the shock wave.

2. Following the shock wave, the compressed material is traversed by a rarefaction wave, in which the processes of melting, evaporation and sputtering in which we are interested take place. Inasmuch as the rarefaction wave travels through a region which in turn expands and cools, following cessation of evaporation, there will be ejection of droplets of molten as well as solid lunar material. We shall now discuss the processes that take place in the rarefaction wave.

In the simplest form, the problem of simulating such processes /104
is as follows: Is it possible by means of a focused laser pulse or another method to create conditions which would exist in the region of a shock and, if it is possible, what must the parameters of the impulse be?

Before moving on to a direct solution of these problems, let us dwell on some of the physical processes that take place in a solid under these conditions. The processes of super high velocity impacts have already been discussed in the work of Yu. P. Rayzer [15], K. P. Stanyukovich [16], Ya. B. Zel'dovich and Yu. P. Rayzer [14]. Phenomena which occur during the interaction of pulsed laser radiation with the surface of a solid body have been investigated in numerous papers by various authors, of which we could mention [35].

In the case of an impact, the energy of a meteorite is distributed very rapidly (in a time on the order of $\delta/D \sim 10^{-11} - 10^{-12}$ sec, where $\delta \sim 10^{-5} - 10^{-6}$ cm is the width of the shock wave front and D — 10^6 cm/sec — is its speed), with various degrees of freedom, with a density $\varepsilon = \varepsilon_x(\rho) + \varepsilon_t + \varepsilon_{T.e.}$, consisting of the following: the elastic portion $\varepsilon_x(\rho)$, the phonon portion or the thermal energy of the shock ε_t and the energy of thermal excitation of the electrons $\varepsilon_{T.e.}$ [14]. The relationship between ε_x, ε_t, $\varepsilon_{T.e.}$ is determined according to the shock adiabat and shows a tendency toward predominence of the last two terms with an increase in the shock velocity. Thus, in the case of a shock, there is a simultaneous compression and heating of the solid up to the equilibrium state, which lies on the shock adiabat of the "target" material.

In a laser "shock" compression does not take place generally. The elastic degree of freedom, associated with the term $\varepsilon_x(\rho)$ in the equation of state is not excited. Absorption of visible light in the "skin" layer leads to heating of the electrons ($\varepsilon_{T.e.}$) and then, due to electron-phonon interaction, a phonon temperature is established which makes the contribution ε_t to the specific energy.

For the lasers in which we are interested with a pulse duration τ, the relaxation time is significantly greater than $\tau_{el\text{-}phon}$: $\tau \gg \tau_{el\text{-}phon}$ [36].

Thus, the difference in the states of the excited region without consideration of the parameters connected with the spatial distribution consists in the absence of compression in the simulation of a meteor shock by pulsed laser radiation.

In imitating high-frequency shock, it is necessary to express the values of the determining thermodynamic parameters which exist at a certain moment in time (not necessarily immediately after the end of the shock). It is simplest to determine the value of the shock

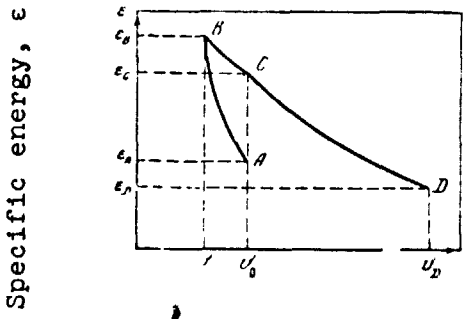

Figure 1. Specific energy ε versus specific volume v during compression of material and its relaxation before and after a meteoritic impact.

parameter which does not change in the unloaded substance during the entire period following the shock. Inasmuch as the unloading of a solid which has been compressed by a shock wave and the divergence are processes that are isentropic, this value is the entropy which averaged over the spatial distribution in the excited region. The value of the second density parameter $\rho = \rho_0$ need not be chosen in the light of the above.

To make this more precise, let us examine Figure 1, which gives a schematic representation of the unloading adiabat BCD in which the substance travels from the state of a highly-heated compressed solid body (point B on the diagram, which also lies on the shock adiabat AB) in a cooling gas (Section CD). The laser "shock," as we have mentioned, does not lead to a significant change in density $\rho = \rho_0$, or $v = v_0$ ($v = \rho^{-1}$), so that the state at point C must be reproduced. At the same time, however, entropy S at point C will be equal to the entropy on the entire curve BCD, particularly /105

$$S_C = S_B \qquad (1)$$

Entropy and density, as we know, completely determine the state of a quasi-equilibrium system, including its specific energy.

It follows from (1) that entropy may be determined on the basis of the initial state prior to unloading on a shock adiabat AB and for the specific energy at a point C may be written

$$\varepsilon_0 = \varepsilon(S_B, v_0), \qquad (2)$$

where $\varepsilon(S, v)$ is the specific internal energy which as we know completely determines the thermodynamic state of the system in the variables S, v.

For realization of the above-mentioned program, let us examine the simplest two-term (ε_x and ε_t) equation of state which is the Mie-Grüneisen equation of a solid (nonmetal). In variables T and v it has the form

$$\varepsilon(T, v) = \varepsilon(v) + c_v T, \qquad (3) \qquad p = -\frac{d\varepsilon_x}{dv} + \frac{\Gamma c_v}{v} \cdot T. \qquad (4)$$

Here $\Gamma(v)$ is the Grüneisen coefficient, and c_v is the thermal capacity. It may be shown that with an arbitrary dependence of Γ upon v with $v = v_0$, the expression for ε_C will not explicitly depend upon Γ. From (2), (3) and (4) and known thermodynamic identities, we can find the following:

$$\varepsilon_C = \varepsilon(S_C, v_0) = c_v T \exp\left\{\frac{S_C - S_0}{c_v}\right\} + \varepsilon_x(v_0), \qquad (5)$$

where the subscript 0 represents the parameters prior to the collision. The entropy $S_C = S_B$ may be found from equations for the iiitial state upon collision, formulated,by Stanyukovich [37]. The results of calculating the values of ε_C corresponding to the impact of meteorites on a target of the same material (SiO_2) at various shock velocities are shown in the table.*

CALCULATED PARAMETERS OF METEORITE IMPACT OF SiO_2 ON A TARGET OF SiO_2**

v (10^{-5}), cm/sec	10	20	30	40	60	70	80
$\varepsilon_B = \frac{v^2}{8}$ (10^{-11}), erg/g	1.25	5	11.25	20	45	61	80
T_B (10^{-3}), °K	7.15	49.3	122	226	524	715	942
ε_C (10^{-11}), erg/g	0.191	1.07	2.53	4.66	10.6	14.5	18.9
T_C (10^{-3}), °K	2.26	12.7	30.2	55.6	127	172	226

*The authors thank V. V. Orlov for performing the numerical calculations.

**Zero isotherms were used in the calculations for the ionic crystal [38].

It follows from the data in the table that the simulated specific energy ε_C is considerably (5 - 6 times) less than the initial energy ε_B. This considerably facilitates the possibility of simulation.

We will consider that the energy E_0 of a laser is emitted in a hemispherical volume $2/3\ \pi R^3$, and we shall determine what the radius R of the focal spot must be and the duration of the pulse τ in simulating the impact of a particle with a velocity v_0, which must be reconstructed in the volume in question, then /1

$$E_0 = \varepsilon_C \cdot \frac{2}{3}\pi R^3 \rho, \tag{6}$$

where $\rho \sim 3\ g \cdot cm^{-3}$ is the density of the target material. From this, we can find the radius of the focal spot:

$$R = \sqrt[3]{\frac{3E_0}{m\varepsilon_C \rho}}. \tag{7}$$

The limit of the duration of the pulse τ with respect to (6) and (7) will be

$$\tau < \frac{R}{C_0} = \sqrt[3]{\frac{3E_0}{2\pi\varepsilon_C \rho c_0}}. \tag{8}$$

Now let us examine a specific laser with a momentum energy of 100 joules = 10^9 ergs. For simulating collision at a velocity which is approximately 40 km/sec, for example, we will find according to the table the required value of $\varepsilon_C \approx 4 \times 10^{11}$ erg/g. Using (7) we find R = 0.75 mm and $\tau < 1.5 \times 10^{-7}$ sec with $C_0 = 5 \times 10^5\ cm \cdot sec^{-1}$. Thus, the diameter of the focal spot will be 1.5 mm.

It is clear that, when we are modelling particles with higher velocities, the radius of the spot must decrease, using (7) for the estimate. Note that when we use a laser with energy $E_0 < 100$ joules the size must decrease in proportion to $\sqrt[3]{E_0}$, i.e., the dependence upon E_0 is slight.

Thus, using a modern laser with a pulse energy of 10 to 100 joules and a duration of 10 - 100 nsec, we can simulate the processes of evaporation and condensation as well as sputtering* in the course of the flight of material from a meteorite crater. The characteristic scale of the process will then be on the order of 1 mm.

To estimate the possibility of an electron-beam method of pulse heating, we shall use the technical data of a pulsed electronic welder [34]. In the pulsed mode of operation for a number of modern installations for pulsed welding using an electron beam, an energy density of $W = 1 \times 10^8$ W $\cdot$ cm^{-2} is reached [39]. With a pulse duration of 1×10^{-6} seconds, with the same values of h and ρ and the electron energy in the gun ~ 50 keV, the specific volume energy will be equal to 5×10^{11} erg/g, i.e., it will be at the limit which is necessary for the simulation of pulsed evaporation. A further increase in the energy density is limited — for the same potential voltage of 50 keV — by the value of the space charge in the electron gun, and the increase in the energy of the electrons will lead to an increase in the absorption depth and consequently the mass of the heated substance.

For observation of pulsed evaporation, it is necessary that the time of development and the dimensions of the cloud at the beginning of inertial collision-free flight of the vapor particles be in accordance with the experimental possibilities of the apparatus.

Evaluation of rough dimensions of an evaporating cloud of vapor at the termination of collisions and the start of inertial flight may be carried out on the basis of the condition that mean free path l and the dimensions of the cloud are the same, L: $l = L$. For a longer flight, $l > L$. If $\sigma \sim 10^{-16}$ cm^2 is the gas-kinetic section and N(t) is the number of particles per cubic centimeter, then $l = 1/\sigma N(t)$. However, $N(t) = N_0[L_0/L(t)]^3$. Now from the equation $l(t) = L(t)$ we can easily obtain /107

*In studying sputtering it is permissible to raise the pulse length to approximately 10^{-5} to 10^{-4} seconds.

$$L = \sqrt{\sigma N_0 L_0^3} = \sqrt{\sigma n_0},$$

where $n_0 = N_0 L_0^3$ is the total number of evaporated molecules.

Taking the fact into account that 1 mm^3 of substance has been evaporated with a molecular weight of approximately 30, we find that $n_0 \sim 10^{19}$ cm^{-3} and L ~ 30 cm. The flight becomes completely collision-free at the moment $t = L/C_0 \sim 6 \times 10^{-4}$ sec ($C_0 \sim 5 \cdot 10^5$ $cm \cdot sec^{-1}$).

Hence, for carrying out the above studies we can use vacuum equipment of ordinary dimensions, but the mass-spectrometric studies may be carried out by means of a pulsed mass-spectrometer, whose time constant is equal to 1 microsecond.

The vacuum requirements for the studies of "pulsed" evaporation must not differ from the requirements which are set forth in Section II, i.e., at pressures on the order of approximately 10^{-6} torr (with respect to the background gases) $l \gg l_{b.g.}$, while the gas separation in the "pulsed" process is limited by the small amount of evaporated substance (~ 10^{-5} g in 10^{-6} sec), i.e., approximately 10 gm/sec when converted to the stationary process (in comparison to 1 gm/sec for the stationary process). Consequently, the rates of evacuation, taking into account a reserve, may be kept at the former level in the apparatus.

Let us consider other methods of simulating pulsed processes taking place in exogenic and endogenic phenomena.

The article by Mills [40] presented a hypothesis concerning the possibility of formation of vitreous droplets and threads in the passage of gases through the surface layers of the regolith, which occurred in a certain period of evolution of the Moon at high temperatures. These temperatures were close to the melting point. In [41], which is devoted to an investigation of the vitreous particles in the regolith of the Moon, the presence of a great many rotational forms is confirmed (spherules, small flasks, dumbbells). However, it is

assumed by analogy with the hypothesis of T. Gold that the probable reason for their formation may have been a solar flare of unusual intensity. In addition, vigorous boiling may accompany the formation of rocks when a meteorite strikes.

We carried out a preliminary experimental test of the possibility of obtaining certain morphological forms of the fine fraction (dust) of lunar regolith in the laboratory simulation of phenomena similar to those which were discussed earlier [42].

The experiments were performed on a simulated VUP-1M apparatus. Modernization of the apparatus consisted primarily in replacing the glass hood of the apparatus with a metal multipurpose chamber and improving the evacuation system. The chamber was made in the form of a cylinder of stainless steel, equipped with a great many flanges, inlets and hatches. The entire internal surface of the chamber, with the exception of the surface of the upper lid, was shielded with a coating of copper, cooled to the temperature of liquid nitrogen (~ 100° K). These surfaces were used for adsorption of the heat radiated by the boat containing molten rock, heated in it to high temperatures on the order of t ≈ 1200 - 1800° C. Within the exhaust apparatus, a thermal power of up to 0.5 - 1 kW was liberated. The surfaces therefore are a nitrogen condensation pump intended for removing a number of condensing vapors and gases (rate of exhaust of the vapors of H_2O, CO_2 ~ 10^4 l/sec).

For "greaseless" exhaustion, there is also an electro-discharge magnetic pump of the NORD-100 type and an ERA-100 assembly, connected in parallel on a single pipe. Some of the seals are made of metal and others made of rubber of the "viton" type, making it possible to heat the apparatus to t ~ 200° C. The apparatus is fitted with "Omegatron" and "Chronotron" mass spectrometers.

The investigated material is heated in a tungsten boat to t = 1200 - 1800° C by passing through the boat an electric current of up to 100 A from a filament transformer. To ensure passage of the gas, a series of holes 1 mm in diameter were drilled in the bottom of the /108

boat. Another verions of the boat was made in the form of a cone of tungsten wire. A stainless steel tube (1 mm in diameter) runs from the needle valve to the boat inside the chamber. At the point where the tube and boat join, there is an adapter in the form of a quartz tube that serves simultaneously as an insulator. A tank of compressed gas located outside is connected to the needle valve through a reducing valve. The experimental procedure is as follows: The boat is charged with powdered mineral or rock. The chamber is brought to a high vacuum ($\sim 10^{-6} - 10^{-7}$ torr). Then an electric current (I = 30 - 70 a; U = 3 - 6 V) is passed through the boat containing the substance under study. The boat and material are heated to a temperature of t = 1200 - 1800° C. The material melts and boils. The temperature of the boiling material is monitored by an OPIR-17 optical pyrometer through an optical peephole. Then the external pump is shut off and gas is passed through the boat containing the molten substance by means of the needle valve. The pressure in the chamber then rises rapidly to $\sim 10^{-2}$ torr. An estimate of the time scale of the process with the aid of motion pictures revealed that it equals $\sim 10^{-2}$ seconds. The molten material sprays out of the boat and strikes screen targets located some distance above and below the boat (~10 cm) and settles on them. In addition, there is intensive evaporation of the boiling material whose vapor condenses on the same target. The investigated substances included: monominerals (diopsides) and composite rocks (tuff, basalt). Gaseous helium was used for bubbling.

As a result of the experiments which were conducted, and which we consider preliminary, various morphological forms were obtained, which are often found in the fine (dust) fraction of the lunar regolith [41] (Figure]). They include vitreous spherules of various sizes (from micrometers to millimeters) and colors (from transparent green to brown with a metallic sheen), little flasks and dumbbells. /109

Among the particles obtained, some were found which provide hints as to the dynamics of the formation of spherical particles from little flasks and dumbbells by fission of the latter. Also found are crystalline threads, individual crystals of various colors (white, orange)

Figure 2. Vitreous particles obtained in bubbling through molten basalt in a vacuum.

as well as conglomerates of crystals. Practically no calcined and slagged particles were seen, how ver. It is possible that they were formed as the result of processes that differ from those in the studies.

The studies revealed that the characteristic dimensions of the particles depend upon the thickness of the layer of the melt, the viscosity of the latter and other parameters. When a tuff melt is bubbled, as the most viscous of the investigated materials, spherules are not formed. It was possible, however, to blow out of the boat, and save, a vitreous powder of the "flashlight" type.

The purpose of subsequent studies will be to investigate the principal characteristics of this process and also devise criteria for simulating it as applied to lunar conditions.

Figure 3. Vitreous particles obtained under the influence of a laser pulse on basalt powder in a vacuum.

The following conclusions were drawn from the preliminary experimental investigation of the effect of pulsed laser radiation [42] as well as bubbling through melts in vacuum, of rocks (basalt, diopside):

1) Vitreous spherical particles are formed during meteoritic impact through the sputtering of liquid particles and their subsequent solidification (Figure 3);

2) The condensation mechanism does not yield a significant number of spherules in particles $r \geq 1$ μm in size;

3) Micrometeorites cause a sharp distribution peak in particle sizes of $0.1 \leq r \leq 1$ μm;

4) Meteoritic impacts as well as certain endogenic processes involved in sputtering result in particles measuring 100 – 500 μm.

Let us note in closing that the problems of this branch of experimental studies are basically analogous to the problems discussed in Section I.

III. Pulverization of the Surface Layers of the Moon by Ions of the "Solar Wind" /110

Bombardment of the lunar surface by protons of the solar wind (up to 85%) with energies of ~1.0 - 0.5 MeV and fluxes of $f \sim 10^8 - 10^9$ particles/cm^2/sec, as well as helium ions (~ 15%) during a period of a "quiet" Sun may cause the occurrence of the following elementary physical and physical-mechanical processes on the surface [43, 44].

1) The pulverization of the surface layers in the form of atomic and molecular particles, leading to the transport of these particles over the surface of the planet and their conveyance beyond the limits of the lunar atmosphere;

2) Cleaning of surface material of adsorbed and oxide films and maintenance of the surface in an automatically pure state;

3) Creation of point radiational defects in the crystal lattice of the substance;

4) "Sintering" together of the particles of the lunar surface;

5) Penetration of hydrogen ions into the surface ("hydrogeneration");

6) Reduction of metals;

7) Selective etching.

In recent years a broad study has been conducted of the processes of cathode melting, especially in metals. The experimental data that have been gathered cannot always be used for interpreting the processes involved in the melting of materials like rocks. However, their

analysis makes it possible to make some preliminary statements regarding possible processes and their results. Thus, we know that the interaction of oxygen ions with the surface of Si leads to oxidation of the latter, and the bombardment of the surface of SiO_2 (quartz) and Al_2O_3 (sapphire) by Ar^+ ions leads to partial reduction of the metals.

It must be taken into account that the melting coefficient of metals by hydrogen ions is of the least significance in comparison with all of the particles that have been studied (~ 10^{-1} to 10^{-2}) [1, 45].

The use of these data by Weiner to estimate the pulverization of the surface layers of the Moon [45, 46] has made it possible to obtain the following results: the surface layers of the Moon can be pulverized at a rate of 30 - 130 atomic layers per year, and the depth of erosion can reach ~ 1 meter in 10^9 years of the Moon's existence (as compared with data published in [24]). The difference in the mechanisms of interaction of ions with metals, on the one hand, and substances such as chemical compounds, on the other, has been studied in a number of papers [26]. It is suggested that atoms of different masses are pulverized differently from the crystal lattice of solids. However, the exact values of the pulverization rate, coefficient of pulverization, distribution of particles by velocities and escape angles can be obtained only as the result of experimental laboratory investigations of the interaction of protons with similar substances.

The bombardment of the lunar surface by hydrogen ions for ~ 10^9 years can cause penetration of hydrogen to a significant depth in view of the intensive mixing of the surface layer (lunar volcanic activity, meteoritic bombardment, [illegible]on).

With such mixing, the penetration of hydrogen can occur without saturation, so that the coefficient of penetration will have a value that is close to the initial flux in the "solar wind," i.e., ~ 10^{24} particles/cm^2 in $1 \cdot 10^9$ years (on the order of 1 g/cm^2).

Hence, the laboratory simulation of the interaction of the "solar wind" with the lunar surface will make it possible to obtain the following data:

a) coefficient of cathode sputtering of analogous rocks;

b) proton penetration coefficient; /111

c) properties, structure and composition of the primary material after bombardment of the surface;

d) rate and angular distribution of sputtered particles;

e) structure and composition of the powder film, and its electrical conductivity.

Laboratory simulation of ion sputtering may be performed in devices for investigating cathode sputtering with ions that have corresponding energy. The vacuum conditions that are ordinarily used in such experiments are determined by the requirement to maintain the purity of the surface with respect to adsorbed molecules of the carrier gas in the vacuum device at a given level ($p \leq 10^{-7}$ torr). Then the rate of formation of a single layer of contaminants must be several orders of magnitude less than the rate of its sputtering by an ion beam. In addition, in this case it is necessary to use so-called greaseless evacuation, inasmuch as there is a danger of cracking the oil vapor at the target and forming an organic residue with heavy masses under the influence of high-energy protons [47].

Conclusions

1. Possible volcanic activity on the Moon, as well as meteoritic and proton bombardment of the surface of the Moon, can lead to processes of stationary and pulsed evaporation, sputtering and pulverization of the lunar surface, transport of substance over the surface, its recondensation with the formation of condensate material with properties different from those of the original material, and its escape beyond the limits of the lunar atmosphere.

2. The processes of condensation, evaporation and sputtering of material have a significance that goes beyond the borders of the Moon alone, and may be common for several other planets in the Earth group (Mars, for example), and also play an important role in the formation of the planets of the Solar System.

3. The simulation of these processes can open up possible mechanisms of formation of surface layers of the lunar regolith (in particular, the mechanisms of pulverization and the formation of spherical vitreous particles), reveal the structure and properties of the surface layers, as well as stability and possible existence on the surface of certain volatile substances, estimate the possible contribution of these processes to the balance of surface material, and clarify the processes that occur in the lunar atmosphere.

4. Investigation of the interesting processes can be accomplished by laboratory simulation.

Simulation of the effects produced by processes of evaporation (sublimation) of the lunar substance with subsequent recondensation and sputtering can be accomplished in laboratory vacuum equipment or by means of thermal sputtering in a stationary mode, or in a pulsed mode by laser evaporation or sputtering by an electron beam, or again by bubbling gas through the melt.

Pulverization by ions of the "solar wind" can be simulated in devices similar to the mechanisms intended for study of cathode sputtering.

References

1. Groves, G. V. Anticipated Vacuum Conditions of the Moon.

2. Voslov, L. V., M. D. Musinov, et al. Modelirovaniye teplovykh reshimov kosmicheskogo apparata i okruzhayushchey yego sredy (Simulation of the Thermal Regimes of a Spacecraft and the Medium Surrounding It). Moscow, "Mashinostroyeniye" Press, 1971.

3. Cherkasov, I. I., et al. Pervyye itogi opredeleniya fiziko-mekhanicheskikh svoystv gruntov Luny (First results of Determining the Physical-Mechanical Properties of Lunar Soil). "Stroyizdat" Press, 1970.

4. Gurshteyn, A. A. The Surface Layer of the Moon. Priroda, No. 6, 1967, p. 3. /112

5. Kuiper, G. P. Volcanic Sublimates of Earth and Moon. Comm. LPL, Univ. Arizona, Vol. 3, 1965, pp. 33-60.

6. Whipple, F. Zemlya, Luna i planety (The Earth, Moon and Planets). Moscow, "Nauka" Press, 1967.

7. Watson, K. K., Bruce C. Murray and Harrison Brown. The Behavior of Volatiles on the Lunar Surface. J. Geophys. Res., Vol. 66, No. 9, 1961.

8. Keydl, R. Tverdyye chastitsy v atmosfere i v kosmose (Solid Particles in the Atmosphere and Space). "Mir" Press, 1969.

9. Florenskiy, K. P. Paper delivered at the 23rd International Geological Congress. Geokhimiya i kosmologiya, 1968.

10. Florenskiy, K. P., A. V. Ivanov, O. A. Kirova and N. I. Zaslavskaya. Phase Composition of Finely Dispersed Extraterrestrial Material from the Area of the Tungus Catastrophe. Geokhimiya, No. 10, 1968, p. 34.

11. Hapke, B. Effects of a Simulated Solar Wind on the Photometric Properties of Rocks and Powders. Ann. N. Y. Acad. Sci., Vol. 123, No. 2, 1965, pp. 711-721.

12. Hibbs, A. R. A Hypothesis that the Surface of the Moon is Covered with Needle Crystals. Icarus, Vol. 2, 1963, pp. 181-186.

13. McCrea, W. H. Nature, Vol. 223, 1969.

14. Zel'dovich, Ya. B. and Yu. P. Rayzer. Fizika udarnykh voln i vysokotemperaturnykh gidrodinamicheskikh yavleniy (Physics of Shock Waves and High-Temperature Hydrodynamic Phenomena). "Nauka" Press, 1966.

15. Rayzer, Yu. P. Zhetf, Vol. 37, No. 6(12), 1959.

16. Stanyukovich, K. P. Elements of the Theory of Impact of Solids with Large Cosmic Velocities. Iskusstvennyye sputniki Zemli (Artificial Earth Satellites). USSR Academy of Sciences Press, No. 4, 1960, p. 86.

17. Naughton, I. I., I. L. Barnes,and D. A. Hammond. Rock Degradation by Alkali Metals: A Possible Lunar Erosion Mechanism. Science, Vol. 149, No. 3684, 1965, p. 631.

18. Vonneguth, B. R. K. McConnel, Jr. and R. V. Allen. Evaporation of Lava and Its Condensation from the Vapor Phase in Terrestrial and Lunar Volcanism. Nature, Vol. 20, No. 5022, 1966, pp. 445-448.

19. Gutkin, A. M., Ts. M. Raytburd, M. V. Slonimskaya, N. G. Sushkin and I. A. Fomina. Characteristics of Formation of Lava Coverings on the Moon. In the book: Problemy geologii Luny (Problems of Lunar Geology). Trudy GIN, No. 204, "Nauka" Press, 1969, pp. 165-187.

20. Fielder, G., I. E. Guest, Z. Wilson,and P. S. Rogers. New Data of Simulated Lunar Material. Planet. Space Sci., Vol. 15, 1967, pp. 1653-1666.

21. Surkov, Yu. A., A. P. Vinogradov, et al. Geokhimiya, No. 8, 1966, pp. 891-899.

22. Jaffe, L. D. Results of Recent Manned and Unmanned Lunar Explorations. Paper to be presented to COSPAR, Leningrad, 1970.

23. Vinogradov, A. P. Preliminary Data on Lunar Soil Retreived by the Luna 16 Automatic Station. Geokhimiya, No. 3, 1971.

24. Preliminary Examination of Lunar Samples from Apollo 11. Science, Vol. 165, No. 3899, 1969; Vol. 167, No. 3923, 1970.

25. Mirtov, B. A. Substance of the Lunar Surface in the Lunar Atmosphere. Geomagnetizm i aeronomiya, Vol. 9, No. 1, 1969.

26. Martynenko, Yu. V. Fizika tverdogo tela, Vol. 6, No. 3529, 1964; Vol. 8, No. 2109, 1966.

27. Brewez, B. L. and A. W. Searcy. J. Amer. Chem. Soc., Vol. 73, 1951, p. 5303.

28. Karklit, A. and I. Yudina. Zhurnal prikladnoy khimii, No. 3, 1966, p. 537.

29. Reichelt, W. and P. Müller. Vacuum technik, No. 8, 1962.

30. Malkov, M. P., I. B. Danilov, A. G. Zel'dovich and A. B. Fradkov. Spravochnik po fiziko-tekhnicheskim osnovam glubokogo okhlazhdeniya (Handbook on the Physical and Technical Fundamentals of Deep Cooling). Moscow-Leningrad, "Gosenergoizdat" Press, 1963.

31. Simulation of Space Conditions in Tests of Unmanned Aircraft (A Survey), Voprosy raketnoy tekhniki, No. 10, 1966, p. 11.

32. Oiti, M. The Current State of the Art of Superhigh Vacuum and Study of Surface Phenomena in the USA. From the journal Oyo butsuri, Vol. 33, No.8, 1964, translated from Japanese. VINITI, No. 51, p. 199.

33. Deshman, S. Nauchnyye osnovy vakuumnoy tekhniki (Scientific Fundamentals of Vacuum Technology). "Mir" Press, 1964.

34. Vinogradov, M. I. PTE, No. 4, 1960, p. 3.

35. Anisimov, S. I., et al. Effect of Powerful Light Fluxes on Metals. Zhtf, Vol. 34, No. 7, 1966.

36. Payns, D. Elementarnyye vozbuzhdeniya v tverdykh telakh (Elementary Excitations in Solids). "Mir" Press, 1967.

37. Stanyukovich, K. P. Neustanovivshiyesya dvizheniya sploshnoy sredy (Unsteady Movements of a Continuous Medium). GITTL, 1954.

38. Zharkov, V. and V. Kalinin. Uravneniya sostoyaniya tverdykh tel pri vysokikh davleniyakh i temperaturakh (Solid State Equations at High Pressures and Temperatures). Moscow, 1968.

39. Ionno-elektronnaya tekhnologiya (Iono-Electronic Technology). Collection of articles. Moscow, "Mir" Press, 1969.

40. Mills, A. Nature, Vol. 224, No. 5222, 1969.

41. Muller, G. and G. Hinch. Nature, Vol. 228, No. 5268, 1970, pp. 254-258.

42. Nusinov, M. D., K. P. Florenskiy, et al. Doklady AN SSSR, Vol. 202, No. 4, 1972.

43. Kaminskiy, M. Atomnyye i ionnyye stolknoveniya na poverkhnosti metalla (Atomic and Ionic Collisions on the Surface of Metals). "Mir" Press, 1967.

44. Dins, J. and J. Vinnard. Effects of Radiation in Solids. "IL" Press, 1960.

45. Pleshivtsev, N. V. Katodnoye raspyleniye (Cathode Sputtering). "Atomizdat" Press, 1968.

46. Wenner, G. K. Sputtering Effects on the Lunar Surface. In the book: The Lunar Surface Layers. Materials and Characteristics. New York, London, Acad. Press, 1964.

47. Akigshin, A. I. Ionnaya bombardirovka v vakuume (Ion Bombardment in a Vacuum). "Gosenergoizdat," 1964.

N 74-19480

DEVELOPMENT OF AN ANALOG OF LUNAR SOIL

/113

Z. A. Atsagortsyan, G. G. Akopyan, R. R. Sarkisov,
I. I. Cherkasov, V. V. Shvarev

ABSTRACT. Volcanic tuff from the Artik deposit in Armenia is especially suited for experiments in simulating lunar soil, with the aid of compaction by vibration.

Preparation for the conquest of the Moon by man calls for the performance of a broad variety of experimental tasks for which it is necessary to have an analog of the lunar soil. This analog must correspond to current concepts of the nature of the properties of the lunar soil, and must simultaneously be quite simple and accessible, inasmuch as the scales of the experimental tasks may be very large, all the way to testing moving craft under conditions in so-called "lunodromes," simulating the lunar landscape.

According to data from measurements by the Luna 13 automatic lunar probe [1], the surface layer of lunar soil is a dark grey or brownish-grey granular material with a specific gravity on the order of 0.8 g/cm^3, composed of dense grains and granules of porous mineral substance of a basic chemical composition, adhering slightly together at points of contact. The grain size varies from 0.02 - 20 mm. The hardness of this layer is characterized by a deep penetration of the calibrating penetrometer in a range from 15 to 50 mm with a load maintenance time of 5 seconds.

Judging from the results of the experiments conducted by the Surveyor craft, the specific gravity of lunar soil in the top few centimeters is 1.1 - 1.5 g/cm^3; the material is of the consistency of fine sand. The first samples of lunar soil returned to Earth by the Apollo 11 craft had specific gravities of 1.54 to 1.66 g/cm^3. The composition was dusty and sandy, with slight adhesion provided by molecular adhesion between the grains at the points of contact. Petrochemical analyses of lunar soils showed that they are evidently of volcanic origin and are most similar in terms of mineral content to terrestrial basalt [2, 3].

It is assumed that beneath the surface layer of slightly adhesive granular material at some depth there is a hard stony layer with a specific gravity of 0.8 to 1.2 g/cm^3 or more, and a compression strength from 5 to 100 kg/cm^2.

Selection of an analog of the stony layer does not pose great difficulties, since it is possible to find on Earth rocks of volcanic origin that are similar in their properties to the above-mentioned indices. In particular, it is possible to use successfully as the analog of the stony layer a widespread volcanic stony material from the Armenian SSR, volcanic tuff, slag, and pumice, obtained in large pieces for construction. Table 1 shows the characteristics of four selected samples of these materials from three locations.

It is clear from the data given that the most appropriate of the tested materials with respect to both indices is the light variety of Artik tuff. The mechanized production of tuff in Artik makes it possible and convenient to obtain the material required for experimental work in any quantity. /114

The problem of creating an analog of the upper layer of the lunar soil has proven to be more complicated. It is a simple matter to obtain loose, granular soil with a bulk specific gravity of 0.5 - 1.1 g/cm^3. One can use for this purpose the same volcanic rocks from Armenia. Table 2 shows the values of the bulk specific gravity of

TABLE 1

PHYSICAL AND MECHANICAL PROPERTIES OF SAMPLES OF VOLCANIC ROCKS FROM ARMENIA

Rock	Origin	Specific gravity g/cm^3	Compression strength kgf/cm^2
Volcanic tuff	Artik, No. 1	1.06 (0.93 - 1.28)	65 (41 - 112)
Volcanic slag (in continuous deposit)	Noraduskoye	1.24 (1.05 - 1.60)	150 (70 - 350)
Volcanic tuff	Artik, crater No. 19	1.55 (1.43 - 1.85)	127 (45 - 250)
Pumice	Irindskoye	0.46 (0.40 - 0.51)	21 (10 - 36)

TABLE 2

VOLUMETRIC BULK DENSITY OF GRANULAR MATERIALS FROM VOLCANIC ROCKS OF ARMENIA

Fractions, mm	Volumetric bulk density, kgf/m^3		
	Tuff from Artik deposit	Slag from Karmrashen deposit	Pumice from Irind deposit
10 - 20	526	365	234
5 - 10	559	385	274
2.5 - 5	576	425	311
1.25 - 2.5	577	468	398
0.63 - 1.25	668	480	428
0.31 - 0.63	696	534	497
0.14 - 0.31	726	642	643
<0.14	860	829	678

the granular material of various fractions obtained from these rocks. The one most suited for this purpose is the volcanic slag from the Karmrashen deposit. Its chemical composition is basic (SiO_2 content — 58%), and it is dark grey to black in color. The slag is quite light and does not require additional pulverization, inasmuch as in the natural state it has a small grain size. In addition, the deposit (unlike the Irind deposit of lighter pumice) is located near a railway, which facilitates the transportation of the material. Hence, further experiments in obtaining an analog of the upper layer of lunar soil will be carried out using the volcanic slag from the Karmrashen deposit.

We originally mentioned two ways of obtaining loosely bound materials: in a rigid mineral bond and in a sticky organic bond. In both cases we are not talking about creating the bond of the grains of lunar soil, but merely of simulating it, inasmuch as the adhesion of the lunar soil is evidently explained by the molecular linkage of the grains at the contacts under a deep vacuum. As the mineral bond, we selected molten glass with sodium fluosilicate added. However, the samples of material prepared on the basis of the granular volcanic /115 slag and molten glass turned out to be too hard; the penetrometer could not penetrate them at all.

Then the idea occurred of compacting the volcanic slag by means of vibration. The experiments showed that vibration compacting creates a bond between the rough grains of volcanic slag that simulates the bond between the grains of lunar soil.

To perform the tests, we built a metal form measuring 40 x 40 x 20 cm with a removable bottom. The form was placed on a laboratory vibrating table with the following characteristics: amplitude 0.7 - 0.8 mm, number of oscillations — 2800 - 3000/minute. The form was filled with volcanic slag of diverse granulometric composition, and a 40 kg weight was placed on top, producing a load of 25 g/cm^2 on the sample. The vibration lasted 2 to 30 seconds. After each period of vibration, the height of the compacted layer of volcanic slag and the depth of submersion of the pentrometer were measured. A special guide was used to hold the pentrometer and prevent tilting of the indenter.

The volcanic slag from the Karmrashen deposit was studied in two forms: with natural granulation and with artificial granulation approximating the assumed granulation of the lunar soil (according to the theory of probability of the presence of grains of different sizes if they were formed from the impact of meteorites on the lunar surface).

The granulometric compositions of the slags are shown in Table 3, and the results of the experiments in vibrational compaction — in Table 4.

TABLE 3

GRANULOMETRIC COMPOSITION OF TESTED SAMPLES OF VOLCANIC SLAG FROM KARMRASHEN DEPOSIT

Granulation	Weight content of fractions, %				
	10-20 mm	5-10 mm	2.5-5 mm	0.3-2.5 mm	0-0.3 mm
Natural	27	25	15	20	13
Artificial	17	15	15	30	23

TABLE 4

RESULTS OF EXPERIMENTS IN VIBROCOMPACTION OF VOLCANIC SLAG

Duration of vibration seconds	Volcanic slag			
	Natural granulation		Artificial granulation	
	Volumetric bulk density g/cm³	Penetration of penetrometer mm	Volumetric bulk density g/cm³	Penetration of penetrometer mm
0	0.483	95	0.505	72
2	0.635	27	0.686	23
5	0.661	14	0.722	7
15	0.716	10	0.770	6
30	0.736	5	0.831	3

It is evident from the data in Table 4 that the vibrational compaction of volcanic slag from the Karmrashen deposit for 2 to 5 seconds is completely inadequate to obtain slightly adhesive material that /116
possesses the minimal indices of volumetric bulk density (0.5 - 1.1 g/cm³) specified at the beginning of this paper, as well as the depth of penetration of the calibrating penetrometer (15 - 50 mm). Obtaining denser materials does not entail any difficulty.

On the basis of this work, we can draw the following conclusions and assumptions.

1. The volcanic slag from the Karmrashen deposit can be used as the raw material for obtaining a granular, slightly adhesive layer of lunar soil.

2. The slightly adhesive material must be obtained by vibrocompaction (with weight applied) of volcanic slag from the Karmrashen deposit with a natural granulometric composition without addition of a binder. Vibrocompaction may be carried out in practice by a standard surface vibrator used on concrete projects. The duration of vibration may be 2 to 5 seconds with correction at the site for displacement of the vibrator over the surface of the charge by direct testing of the penetration value.

3. The variety of volcanic tuff from the Artik deposit can be used as the raw material for producing an analog of the lower, hard layer of lunar soil.

4. It is suggested that "50" or "100" brand cement solution be used to ensure monolithicity of the analog of the lower stony layer of lunar soil and its bond with the concrete base according to the hardness of the stone.

5. In order to create a bond between the layers of the lunar soil analog, it is recommended that a thin mix of a solution of the above-mentioned brands with the bulk of the freshly poured slag solution be applied to the stony layer.

The authors wish to take this opportunity to express their appreciation to K. P. Florenskiy who rendered considerable assistance in this work.

References

1. Cherkasov, I. I., A. L. Kemurdzhiyan, L. N. Mikhaylov, V. V. Mikheyev, A. A. Morozov, A. A. Musatov, I. A. Savenko, M. I. Smorodinov and V. V. Shvarev. Determination of the Density and Mechanical Hardness of the Surface Layer of Lunar Soil at the Landing Site of the Luna 13 Automatic Lunar Probe. Kosmicheskiye issledovaniya, Vol. 5, No. 5, 1967.

2. Jaffe, L. D. The Surveyor Lunar Landings. Science, Vol. 164, 1969, pp. 774-788.

3. Preliminary Examination of Lunar Samples from Apollo 11. Science, Vol. 165, 1969, pp. 1211-1227.

N74-19481

U.S. STUDIES IN THE FIELD OF SHAFT DRILLING ON THE LUNAR SURFACE

/117

B. V. Zakhar'yev and V. G. Kardysh

ABSTRACT. American equipment for drilling in the lunar surface is discussed, with emphasis on rotary-percussive methodology and core-sample retrieval techniques.

In the USA, the National Aeronautics and Space Administration (NASA) has developed and is carrying out a broad program of studies aimed at the solution of shaft drilling and collecting soil samples on the lunar surface.

All of the known projects involving drilling equipment are divided among three lunar exploration projects: Surveyor, Apollo, and Post-Apollo. It is planned to drill at various stages shafts that will be 1.5, 3.0, 30, 60 - 90 and 300 - 450 m deep.

More than 12 large US firms such as E. J. Longyear, Joy Mfg., Northrop Corp., Westinghouse Corp., Martin C., and others with NASA contracts have been working since about 1961 on the development of equipment for these purposes.

Drilling shafts in the lunar surface is aimed at collecting rock samples for subsequent study of their mineralogical content, geological features, origin, physical and supporting properties and internal structure, and to determine the possibility of finding water and valuable components in the rocks.

The problem arises of conducting measurements which will provide data on the temperature, thermal conductivity and thermal state of the rocks, their density, hardness and structure, and the velocity of sound in them.

An indirect idea of the hardness of the rocks in the initial stages of drilling will be obtained on the basis of the drilling speed, torque, end thrust, and power consumption.

In the course of the studies in [11], consideration was given to the possibility of using various methods of crushing the rocks, including: rotary, percussive, rotary-percussive, high-frequency vibration, explosions (shaped-charges); heat stream; thermal; electric arc; chemical; abrasive stream.

Many specialists feel that in the future the most effective method of breaking up rock under lunar conditions will be laser and gas plasma. At the present time, however, these methods are far from being technically feasible for drilling.

The complexity of choosing the method of shaft drilling under conditions on the lunar surface is primarily due to the absence of an exact knowledge of the physical and mechanical properties of the rocks, the thickness and sequence of stratification of the individual intercalations. Moreover, other problems are now apparent, such as the impossibility of using known cleaning agents to remove the mud and cool the rock-drilling bit, the existence, in the upper parts of the core, of rocks that differ markedly in hardness and resistance, and the absence of heat exchange. In addition, certain difficulties may arise in conjunction with the phenomena of adhesion and increased friction.

The basic criteria for evaluating a given method of drilling are the following: the power capacity and weight characteristic of the equipment required for its realization, universality of the chosen /118 method for drilling both in hard and weak, soft rock, as well as the variation of the properties of the rock as it is broken up.

At the same time as the method was selected, consideration was given to possible ways of cleaning the drilled-out rock out of the bottom of the shaft, including the following: flushing with liquid, blowing with compressed air or some gas, vacuum suction, or removal of mud with a screw conveyor. The possibility was also studied of drilling in short bursts with removal of the mud by a special mud collector connected to the rock-breaking tool.

As a result of the studies, the shaped-charge, thermal, chemical, heat-stream, electric arc and abrasive methods were eliminated because of the marked distortion of the physical and mechanical properties of the rock when they were used.

The percussive method cannot be used, owing to the high weight characteristics of the equipment and the difficulty of obtaining a core sample, as well as the complexity of cleaning the mud out of the shaft.

The vibration method also does not conform to the set requirements, in view of its unsuitability for passing through hard rock, and where drilling is carried out by the astronaut directly — due to the vibrational stresses imposed on his hands and body.

Hence, as a result of the studies it was established that it is possible to use only two methods of drilling: rotary-percussive using a refractory rock-drilling tool and rotational using hard metal and diamond bits. However, the execution of the rotary method is only possible when significant axial stresses are produced on the drilling instrument to penetrate hard rock. Moreover, drilling in such rock requires the use of diamond bits, and consequently the use of water or gas to clear the shaft of mud and cool the rock-drilling bit.

Attempts at drilling with diamond bits without cooling in most instances have led to breakdown because of graphitization of the diamonds.

The use of water or gas under lunar conditions calls for the development of a closed circulation system, which together with the necessity for considerable axial loads leads to an increase in the total weight of the equipment. Therefore, the use of the rotary method of drilling becomes more realistic only for the later stages of conquest of the Moon, when it will be possible to bring heavy equipment to its surface. Hence, at the present time the most promising method is the one of rotary-percussive breakup of the rock. This method is real · the most advantageous, in view of the fact that it is quite effective when drilling either in comparatively soft or in the hardest rocks. Rotary-percussion drilling is performed with a hard metal rock-drilling tool, which has less of a cooling requirement.

In addition, the combination of rotary and percussive stresses increases the total reserve of useful work of the bit and reduces the probability of jamming of the core sample in core drilling. All of this increases the mechanical drilling speed. The rotary-percussive method is recommended for use in drilling both a continuous shaft for the purpose of obtaining rock mud, and an annular one, for extraction of an intact core sample.

The studies to determine the effectiveness of using one form or another of equipment are performed on stands equipped with various apparatus that allow continuous recording of the mechanical drilling speed, temperature of the heated drill bit, the torque on the motor shaft, and the rpm of the motor.

Along with the studies aimed at the selection of a method of drilling in the USA, work is going forward on a study of the influence of a vacuum on the interaction of several metals and rocks and on the behavior of the finest particles of soil [2]. /119

These studies were related to the solution of problems of interaction of the drill bit and the lateral surface of the drilling gear with the lunar rock and the behavior of mud when transported from the shaft to the surface, which is of great interest in the selection of parameters of drilling equipment — power, torque and drilling procedure.

From the methodological standpoint, the first problem was solved by estimating the resistive forces during the rotation of a metal disk (of aluminum, steel, and stainless steel) on the surface of quartz or basalt. The coefficient of friction (μ) of these materials was determined in air and in a vacuum (10^{-6} to 10^{-7} mm Hg).

An attempt was made to determine the influence of a rise in temperature on μ. However, with a change in temperature from 10 to 150°, no changes were observed in it.

It is suggested that at higher temperatures it is possible to have a significant increase in the coefficient of friction.

Table 1 shows the values of the coefficient of friction on the basis of the results of the studies. It follows from the data presented therein that the mean numerical value of μ in the majority of cases doubled during experiments in a vacuum, in comparison with experiments at atmospheric pressure.

During the removal of particles of drilled rock from the shaft in vacuum, it is possible to have adhesion of it to itself and the drilling tool. The authors of [2] feel that it is primarily electrostatic and chemical forces that act on the surfaces of the particles (less appreciable).

The experiments were conducted mainly in a vacuum on the order of 10^{-9} to 10^{-3} mm Hg and in air.

TABLE 1

COEFFICIENT OF FRICTION IN TESTS UNDER NORMAL CONDITIONS AND IN A VACUUM

Metal	Tested sample			
	Quartz		Basalt	
	Atmosphere, μ	Vacuum, μ	Atmosphere, μ	Vacuum, μ
Aluminum	0.16	0.25	0.21	0.28
Steel	0.19	0.29	0.14	0.28

The behavior of basalt particles measuring less than 44 μm was studied as well as particles of basalt, aluminum, and vitreous spherules measuring 88 to 149 μm.

It was established as a result of the studies in the vacuum that all basalt particles measuring less than 44 μm adhere completely in 4 to 16 hours. The same phenomenon was noted in experiments with aluminum and partly with vitreous spherules (60 - 70% spherules). In tests with large particles of basalt, only 5% adhesive particles was found.

Inasmuch as the adhesion of particles is progressive, the need arises to conduct drilling in a shorter time interval during which it does not develop. In addition, during the drilling of deep shafts, which takes tens of hours, the question of effective cleaning of the shaft to remove mud requires a radical solution to avoid a sharp rise /120 in the power requirement and clamping of the rig.

Some authors [2] feel that on the lunar surface it is possible to have more intensive adhesion of particles. Therefore, it is recommended to use drill bits, containing (in the form of lubricants or erodable additives) substances which can prevent the adhesion of particles of drilled-out rock to the drill bit and each other.

As a result of these studies, several firms have built drilling equipment for the Surveyor program, which, it must be said here, was incomplete with respect to drilling. Data on these devices, published in various sources,[3 — 6], differ somewhat, although on the whole they agree with the parameters in Table 2.

TABLE 2

CHARACTERISTICS OF DRILLING EQUIPMENT

Parameters	Projects			
	Surveyor	Apollo	Post-Apollo	
Type of machine	Automatic	Manual	Operated by astronaut, automated to fullest extent possible	
Drilling method	Rotary-percussive		Rotary	Rotary-percussive
Drilling depth, m	1.5	3.0	30-90	30-90
Shaft diameter, mm	30-40	25-30	30-50	30-50
rpm	500	300	—	200-400
Percussive mechanism				
No. of blows/minute	3000	to 2700	—	1500-2000
Impact energy, kgm	0.5	—	—	0.2-0.5
Axial load, kgf	22.7	11	170-200	—
Type of drive	Electric motor			
Driving power, kW	0.6	—	2.5-3.0	—
Weight of equipment, kg,	13.6	11-12	90	90
Without power supply	—	20	—	—

The device must perform automatic drilling to a depth of 1.5 meters and use the rotary-percussive · thod with a continuous shaft and removal of the soil mud for subsequent analysis on the Moon.

In discussing the characteristics of the machines designed for the Surveyor program, it should be mentioned that, regardless of the large number of blows (3000) produced by the mechanism, the percussive frequency amounts to six per revolution of the drill, which is less than the frequency usually used in rotary-percussive drilling.

The drive power of 600 W ensures about twice the required level, if we keep in mind that the calculated power required to bore the shaft and turn the drill for a given case is roughly 150 - 200 W, and the efficiency of the motor is 0.5 to 0.6.

It was initially assumed that this entire apparatus would weigh about 25 kg, but it was subsequently reduced to 13.6 kg, i.e., to 23 kg per kW of applied power.

The drill for the Surveyor program is mounted on a girder and consists of a movable rotator that includes an electric motor connected directly to a vacuum-compressor impacting device, a power supply system, and devices for removing the mud.

In one version of the device it was suggested [3] that the tool be fed into the shaft by means of two constantly compressed springs, and the drill be removed to the surface by a winch with individual drive fastened to the housing of the spacecraft. /121

In a later version, however [4], the feed and extraction of the tool is accomplished by means of a screw mechanism with a separate electric drive.

The device has a hollow drill tube 1.5 meters long, which allows drilling to the planned depth without extending the tool. The mud is carried upward through openings in the hard metal bit and gathered in a special container mounted above the rock-cutting bit. The distance of one "pass" is 150 mm. The volume of mud collected is 114.7 cm^3. The container, filled with mud, is unloaded into one of six mud collectors mounted on a rotating drum and lowered one by one beneath the drill bit when it is raised out of the shaft. The design of the mud collectors ensures hermetic sealing of the mud.

The construction of the machine was preceded by work on a stand, during which several technological parameters were determined.

It was established that, when using a hard metal tip with a diameter of 25 to 35 mm, it is necessary for effective drilling in concrete and sandstone to have an end thrust of about 11 kgf, and 80 kgf in granite. Drilling was performed without any kind of cleaning agent. As the mud accumulated, the rate of descent decreased, and the energy consumption rose. When drilling in concrete, sandstone and granite, with an annular shaft 25 mm in diameter to produce a core, the rate also dropped sharply after the start of drilling due to the formation of mud and then remained roughly constant. It was found that for each rpm there was an optimal end thrust value which corresponds to the maximum rate of descent and the minimal energy loss. In rotary drilling using a diameter of 25 - 50 mm, it was found that the minimum achievable end thrust is 22 kgf.

Tests of the drill mechanism in a vacuum and under ordinary conditions yielded positive results. The axial load during the tests was 22.7 kgf, which corresponds roughly to 6 to 7 kgf/cm^2, and remained constant. Such a load is 8 to 10 times less than that usually employed in the rotary-percussive method.

When drilling in gabbro and granite (the compressive strength is 2100 - 2800 kgf/cm^2) in a shaft 0.6 m deep 1000 W/hr was expended. The same power is expended in drilling a shaft 1.5 meters deep in sandstone (ultimate compressive strength — 140 - 210 kgf/cm^2).

In order to carry out the drilling in accordance with the Apollo program, several firms [7 - 10] devised different (but, on the whole, quite similar) designs of automatic drilling machinery of the "Motobur" type (see Table 2).

The drilling of two shafts by the crew of the Apollo 15 was accomplished with a drilling machine developed by the firm of Black and Decker under contract to NASA [10]. This drilling machine is an electric hand drill powered by a battery, designed for 40 minutes of continuous operation. The drilling is accomplished in a rotary-percussive manner using a hard metal rock-cutting bit 26.2 mm in diameter to a depth of 2.8 meters. The number of revolutions of the

drill rod is 300 per minute at 2270 impacts per minute. The reactive torque is 2.76 kgf/m. The weight of the entire machine (on Earth) is 11.8 kg. The axial load is produced mainly by the weight of the astronaut. The drill machinery consists of a housing made of magnesium alloy and impregnated with polyethylene resin for hermetic sealing; an impact mechanism; a friction clutch; spindle and drill bit. Inside /122
the housing, filled with nitrogen at a pressure of 1.26 kgf/cm^2, is a DC commutator motor with brushes. The heat that is developed by the operation of the motor is transmitted by the nitrogen to the walls of the housing and radiated into space. The impact mechanism of the cam type develops an impact energy of 0.46 kgf/m. The shaft is cleared of mud by a screw conveyor. The lengthening of the drill string is performed manually. The length of one section is approximately 0.7 meter. The planned drilling speed with this machine is as follows (on the average): 25.4 mm/min in basalt; 127 mm/min in porous basalt; 300 - 700 mm/min in pumice-type rock. The actual drilling speed turned out to be much less.

Inasmuch as the usual methods of cleaning the mud out of the shaft including flushing, blowing and the use of a screw conveyor could be insufficiently effective under high vacuum conditions, one company devised a drill for rotary-percussive drilling without using any kind of cleaning agent at all. The drill consists of an outer tube and an inner rod. The rock is broken up by a refractory cutter welded on the end of the tube. On the surface of the rod is a screw thread with an undulating profile and a sharp asymmetric tip, one side of which is perpendicular to the axis of the string. A similar thread staggered by half a turn is located on the inner surface of the tube. For drilling, a high-frequency longitudinal vibration is applied with simultaneous slow rotation. Under the influence of the vibration, the rod performs longitudinal osciallations. Due to the vibration, and under the influence of the rotation, the mud comes out of the shaft into a space between the outer tube and the rod and moves through helical channels formed by the threads, to discharge windows, whence it is guided into a collecting container. It is possible to have a version in which the rod and external tube with bit form a rigid construction.

With further development of the space program, it is planned to drill to depths of 30 and 60 - 90 meters [8, 11-13]. This work will also be performed by a number of firms and is taking two main directions. The firms of Longyear, Westinghouse, Christiansen and others plan to develop equipment that will perform rotary drilling using diamond bits and a closed cooling system. The firms of Northrop and Bendix are developing equipment for the rotary-percussive method of drilling [11]. In all cases it is planned to drill a shaft 30 - 50 mm in diameter.

The shaft diameter was selected so that its enlargement to 89 mm increases the energy required for drilling a 30 m shaft from 35 to 84 kW/hr. The control of the device must be accomplished by the astronaut with a maximum degree of automation.

In rotary drilling with diamond bits, it is planned to enlarge the tool as the shaft deepens by means of short drill tubes 1.5 meters long that can be hooked together by the astronaut.

Provision is made for the possibility of using samplers on a cable to extract the core samples. In this case, the drilling process will be accomplished as follows: the end will contain a diamond bit with a string 1.5 m, composed of two concentric tubes, the inner one of which serves to receive the core sample.

The bit string is connected to the string of drilling tubes. As the core-holding tube fills with rock, a special catcher will be lowered down the string of drill tubes, pick up the inner tube, and raise it to the surface by means of a winch. Then another inner tube will be lowered into the shaft, and the drilling process will continue. This system does away with the need to pull the whole string of drill tubes out of the shaft to remove a rock sample.

Cooling of the diamond bit is assumed to be performed by means of hydrogen or some other agent that will circulate in a closed system including a compressor. /123

In addition, it is proposed to study the possibility of drilling with diamond bits without using a cleaning agent. The firm of Westinghouse (Aerospace Division) is working on a drilling device to go down 30 meters and has carried out studies in a vacuum chamber at a rarefaction of 10^{-6} - 10^{-7} mm Hg. The drilling was done with a device having a driving power of 370 W for basalt, a string having a helical spring and diamond bit. At a rotational speed for the string of 920 rpm, the mean mechanical drilling speed was 2.5 cm/min, and the durability of the bit was 35 cm. Formation of a carbonaceous film was observed on the facets of the diamonds. When cooling water was introduced, the durability of the drill bit rose to 101 cm. The authors of [14] feel that the use of cubic diamonds oriented in appropriate fashion can increase the durability of drill bits in "dry" drilling to 300 cm or more.

Considerable work has been performed by the firm of Longyear jointly with other organizations [15]. They tested more than 80 specially developed diamond drill bits of 14 types in drilling basalt with a compressive strength of 3000 to 5200 kgf/cm^2 and a Shore hardness of 79 to 94. Tests were conducted over an rpm range from 375 to 1000 and axial loads from 150 to 500 kgf. The results obtained still do not indicate the possibility of drilling with diamond bits without using cleaning agents.

It is suggested that drilling with diamonds to depths of 30 meters requires an axial load of 170 to 200 kgf and a motor power of 2.5 to 3.0 kW. On the basis of existing experience, it must be said that the drive power of 2.5 to 3.0 kW would clearly be inadequate for effective diamond drilling to this depth and would have to be increased in view of the rise in the frictional forces to 5 - 6 kW. In this case it would be practical to drill shafts 30 meters deep in 20 - 40 hours.

For rotary-percussive drilling, it is proposed to use immersible apparatus, since the use of the surface impact activators at depths greater than 20 m sharply reduces the effectiveness of breaking up the rock in view of the significant losses in the drill string. As

N74-19487

a result of an analysis, it has been found that the frequency of the impacts during drilling must be between 90 and 2000/minute and the rotational speed must be 200 to 400 rmp.

One design incorporates a bladed air motor and an annular piston weighing 9 kg, delivering the impact directly to the drill bit. The piston delivers 2000 blows per minute at an impact energy of 225 kgf/cm and a torque of 112 kgf/cm.

The energy required for the equipment to make a 30 meter shaft is 30 to 40 kWh. This value is in some doubt, and evidently must be raised by a factor of 1.5 to 2.

Another design [8] provided for the use of a loaded air hammer that delivers 1600 blows/minute, at 20 revolutions of the string per minute and an axial load of 23 kgf.

The use of air motors that can be lowered into the shaft requires the presence in the drill mechanism of a compressor to supply compressed air to the motor.

In further exploration of the lunar surface, drilling to 300 - 400 m [12, 13] and even to 1 km [16] has been proposed.

References

/124

1. Bruns, M. and L. Gardner. Rotary-Percussive System Favored for Moon Drilling. Technol. Week, Vol. 18, No. 25, 1966.

2. Penn, S. H. An Experimental Investigation Simulating the Behavior of a Rock-Drill on the Lunar Surface. Trans. Soc. Mining Engrs., Vol. 238, No. 1, 1967.

3. Baier, W. H. and J. A. Cambell. Lunar Drilling Study. Rock Mechanics. Proc. Fifth Sympos. Rock Mechanics, May 1962. Pergamon Press, 1963.

4. Thorman, H. C. Review of Techniques for Measuring Rock and Soil Strength Properties at the Surface of the Moon. SAE preprints, No. 632 C, 1963.

5. Evans, C. T. Prospecting the Moon. Flying Rev. Irternat., Vol. 20, No. 2, 1964.

6. Interplanetary Spacecraft "Surveyor" and "Green Cheese" for Studying the Moon. Voprosy raketnoy tekhniki (Problems of Rocket Technology). Collection of translations. No. 9, 1963.

7. NASA Given Lunar Surface Experiment Demonstration. Aviat. Week and Space Technol. Vol. 85, No. 4, 1966.

8. Livin, S. M. Exploring the Lunar Surface. Space Aeronautical, Vol. 47, No. 5, 1967.

9. Lunar Drill. Machine Design, Vol. 38, No. 23, 1966, p. 4.

10. How Lunar Drill Will Work. Space World, Vol. 9, No. NG-9-81, 1970, pp. 12-15.

11. Northrop's Drill. Astronavtika i raketostroyeniye, ekspress-informatsiya, No. 2, 1966.

12. Loo, W. G. Moon Miners will Use Diamond Drills. Industr. Diamond Rev., Vol. 27, N. 314, 1967.

13. Silveri, P. Lunar Exploration. Mining and Minerals Engng., Vol. 3, No. 4, 1967.

14. George, W. W. A Lunar Drill. Res. Developm., Vol. 18, No. 12, 1967.

15. Hampe, W. R., A. B. Simon, W. E. Decker and J. T. Lundy. The Moderate Depth Lunar Drill Programme, Dry Diamond Drilling Success. Indstr. Diamond Rev., Vol. 30, No. 4, 1971, p. 5.

16. Lowman, P. and A. Reattic. Manned Lunar Scientific Operations. Preprint Amer. Astronaut. Soc., No. 18, 1964.

Translated for National Aeronautics and Space Administration under contract No. NASw 2483, by SCITRAN, P.O. Box 5456, Santa Barbara, California, 93108

30° E LAC 61

16° N

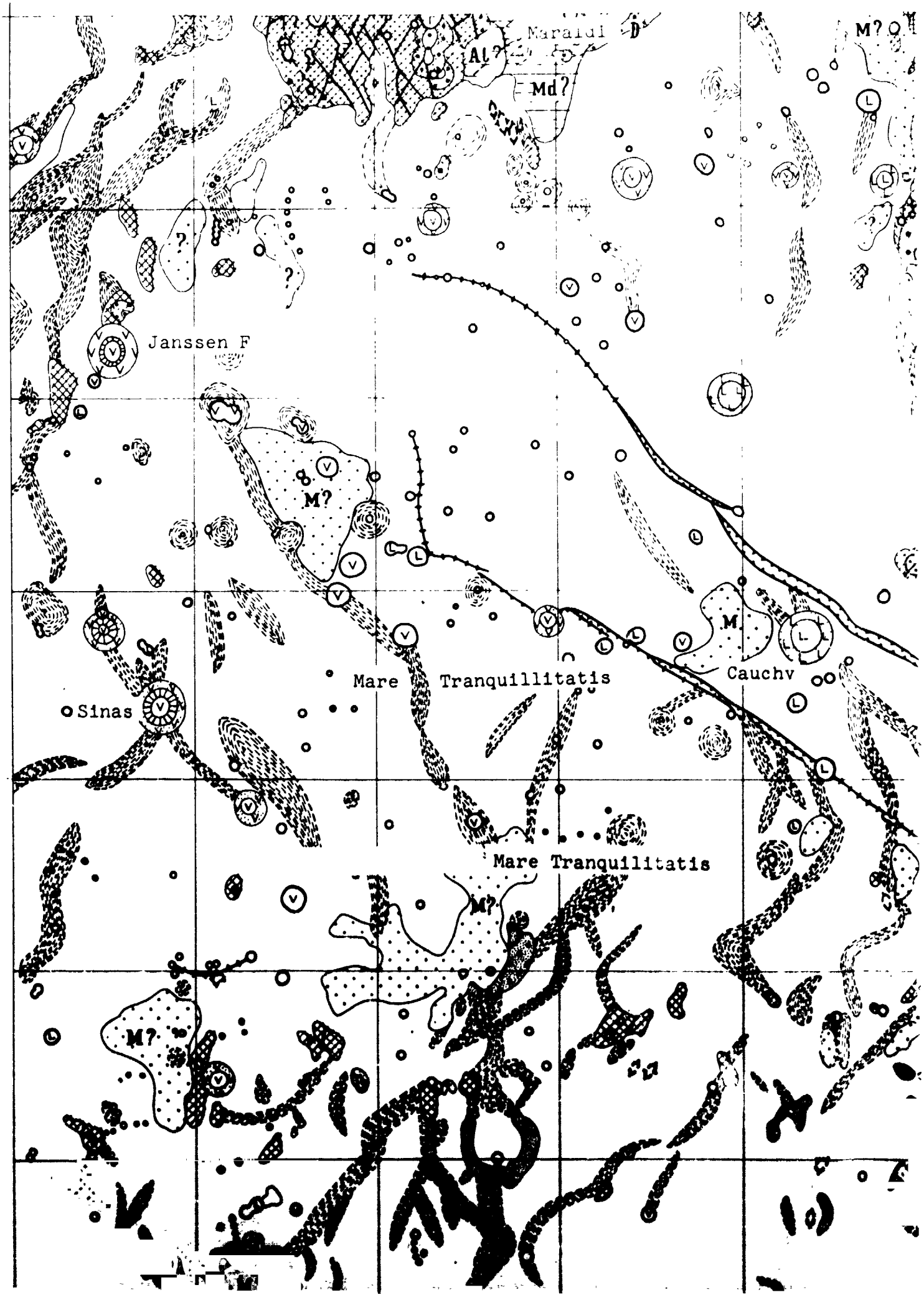

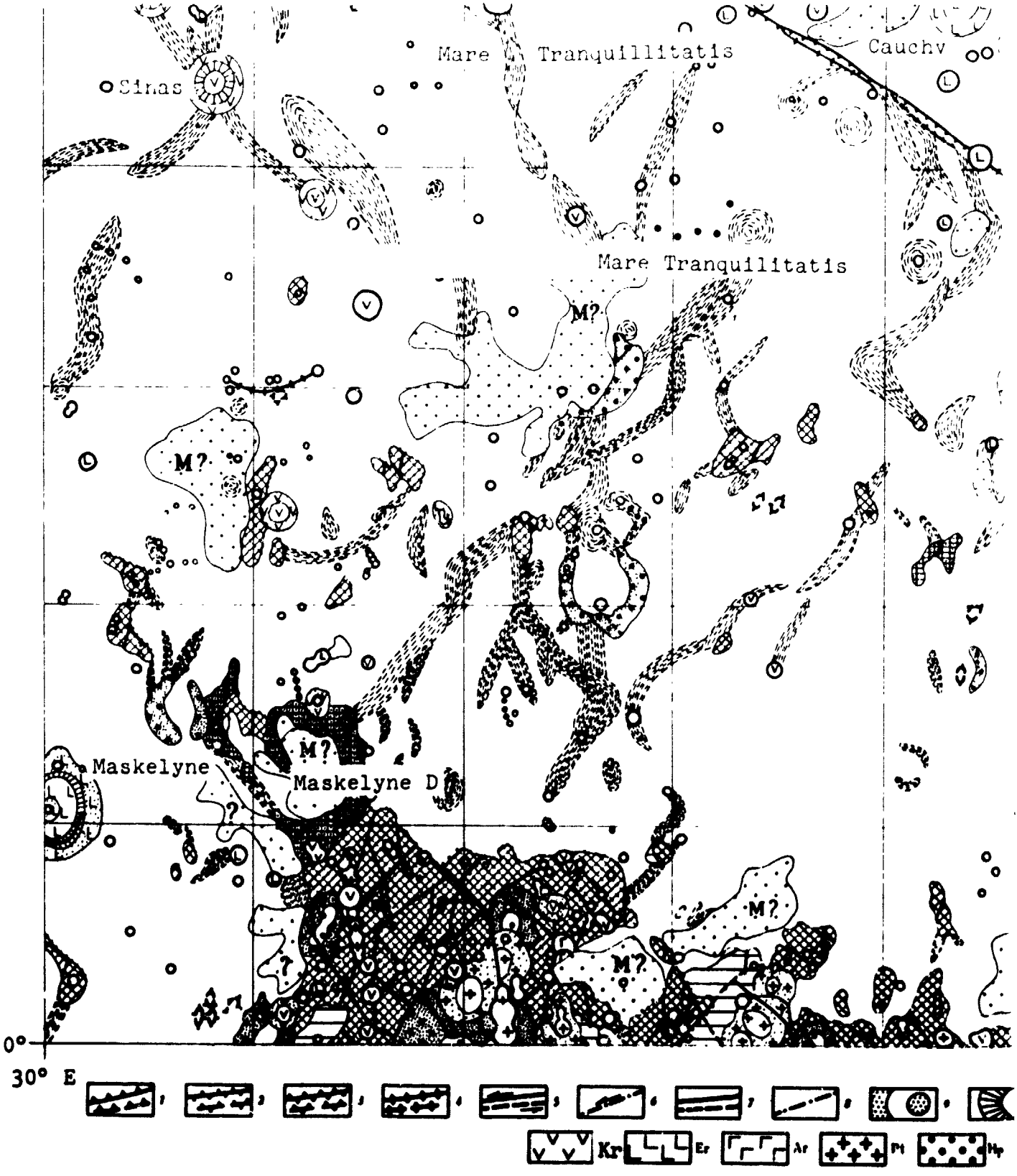

Figure 2. Geological-morphological chart of Sheet LAC-61. Scale ~ 1:1,500,

Structural conditional designations:
1 — pre-Procellarian ejecta (?) slopes, reliable and suggested; 2 — post-
ejecta slopes, relaible and suggested; 3 — pre-Procellarian distrubances o
placement type (?), reliable and suggested; 4 — post-Median disturbances c
placement type (?), reliable and suggested; 5 — pre-Procellarian disturban
displacement type (?), reliable and suggested; 6 — post-Median disturbance
displacement type (?); 7 — pre-Procellarian faults with a known type of di
ment, reliable and suggested; 8 — post-Median faults with unknown type of
placement; 9 — central peak and crater wall (above level of surrounding te

FOLDOUT FRAME 2

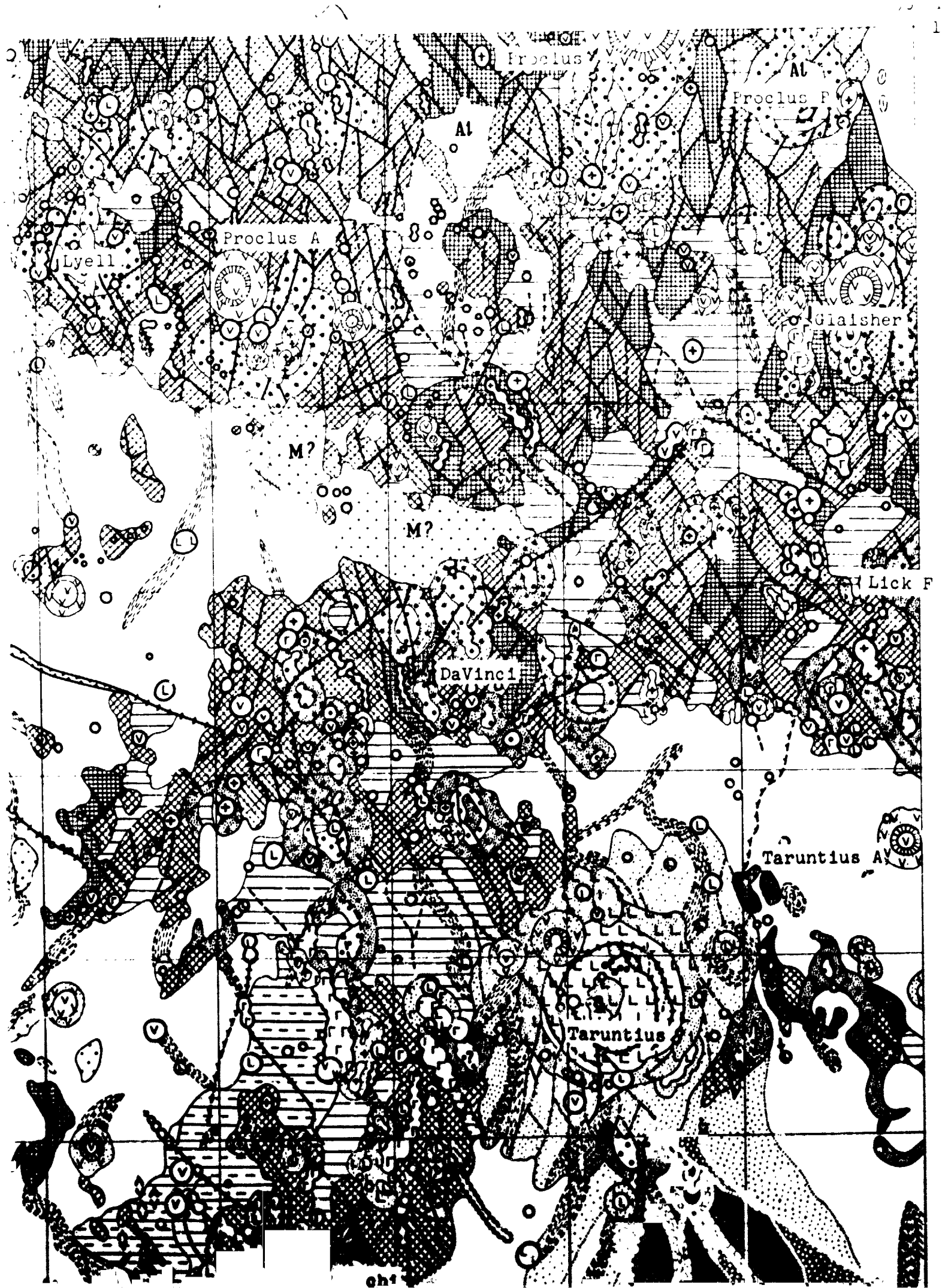
Proclus
Al
Proclus P
Al
Proclus A
Lyell
Glaisher
M?
M?
Lick F
DaVinci
Taruntius A
Taruntius

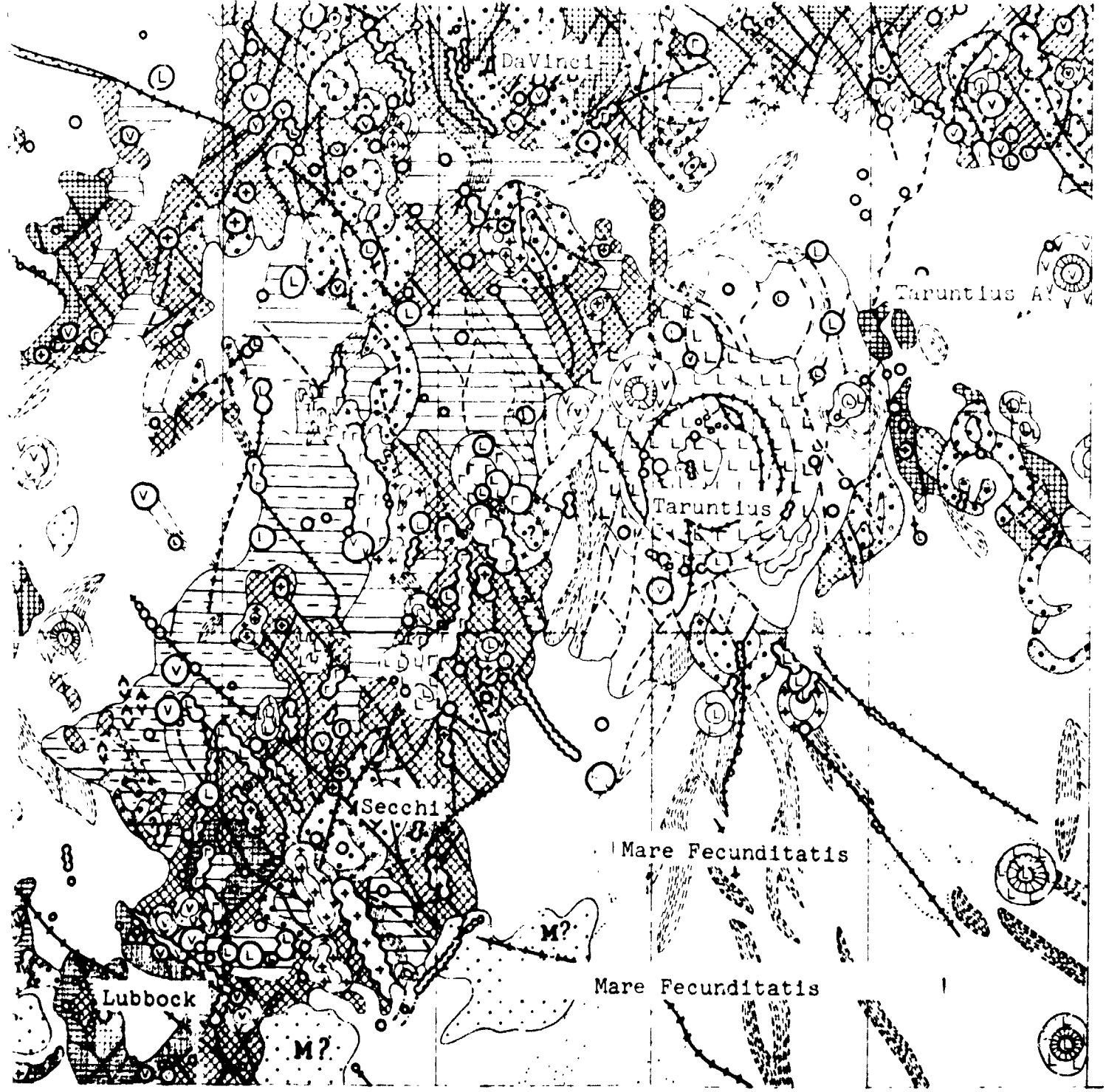

spot entered above age indication; 10 — inner wall of crater wall; 11 — crater floor (unflooded); 12 — terraces of inner slopes; 13 — slopes of outer slopes of crater walls; 14 — craterlets; 15 — chains of disconnected craterlets; 16 — chains of craterlets; 17 — mare walls; 18 — flat broad mare domes; 19 — rays with internally oriented rays; 20 — slightly oriented rays; 21 — small rounded domes.

Conditional stratigraphic designations: Kr — Copernican; Er — Eratosthenian; Ar — archimedean; Pt — Ptolemaic; Hp — Hipparchic; Php — pre-Hipparchic.

Mare Rock Complexes: M — recent; Pr — Procellarian; Md — Median; Al — Altaic; Nb — Nebullarian; Ant — Antique (mixed).

FOLDOUT FRAME 4

FOLDOUT FRAME

LAC 62

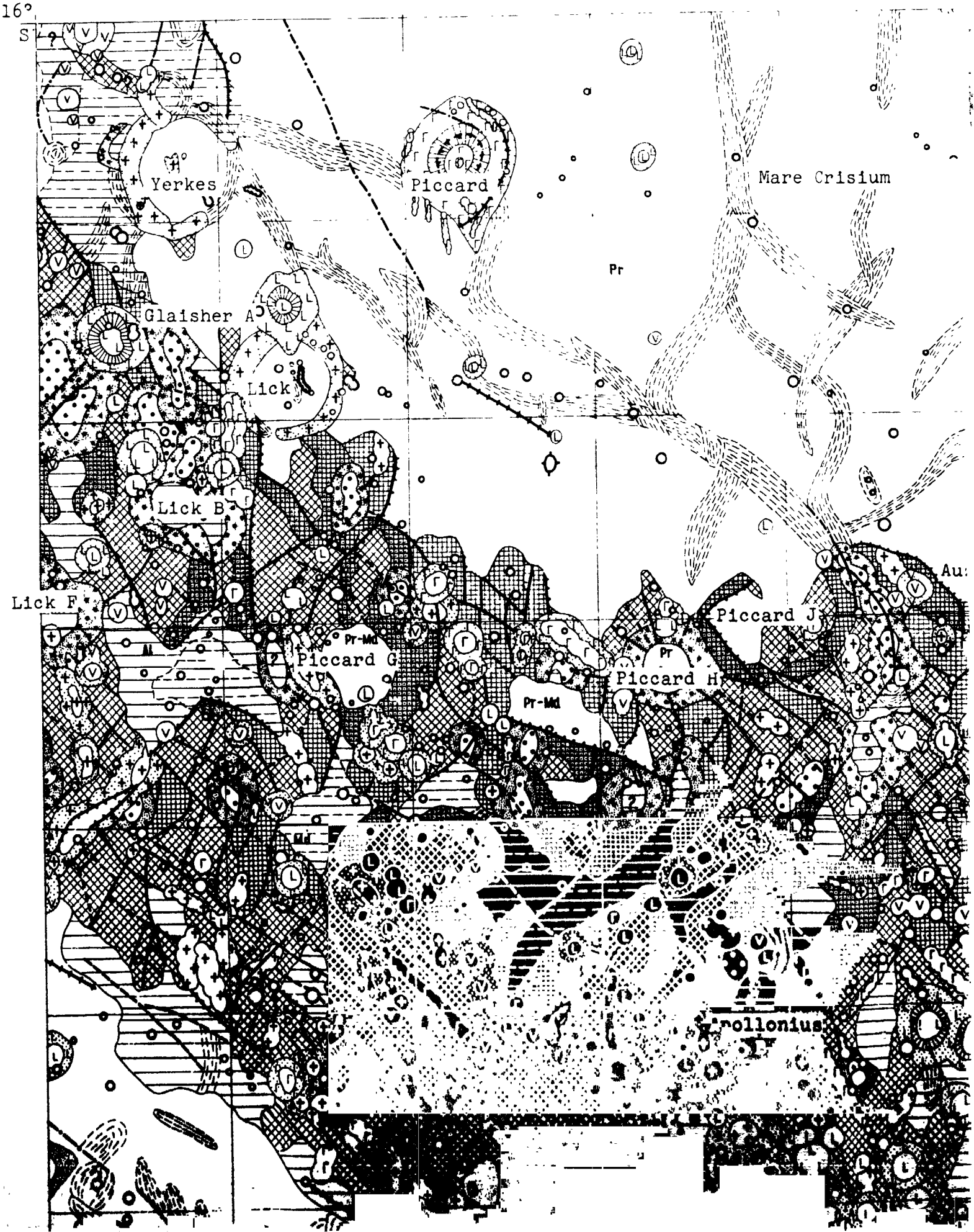

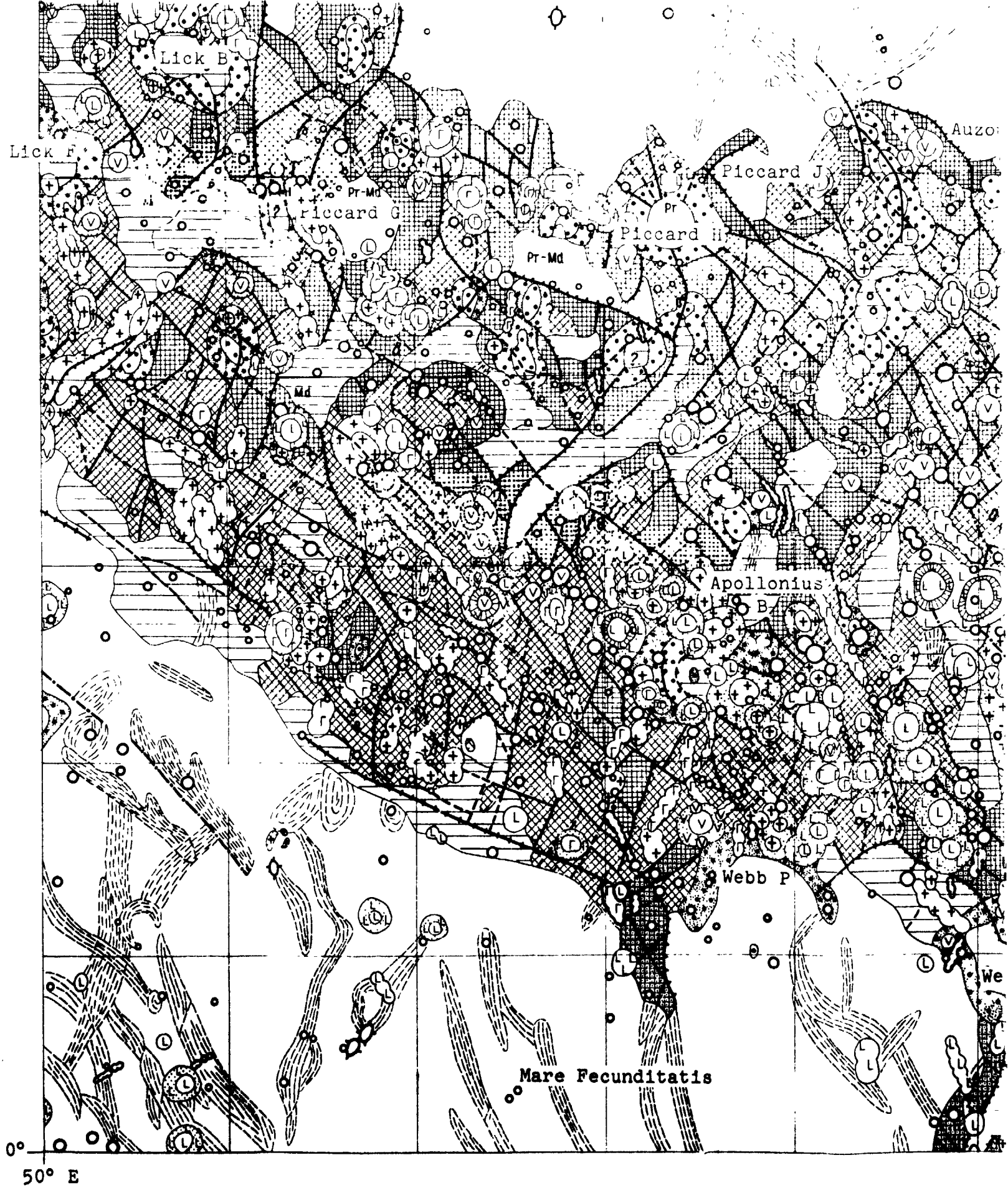

Figure 3. Geological-morphological chart of Sheet LAC-62. Scale ~ 1:1,500,000
Conditional designations are the same as on Figure 2.

FOLDOUT FRAME 2

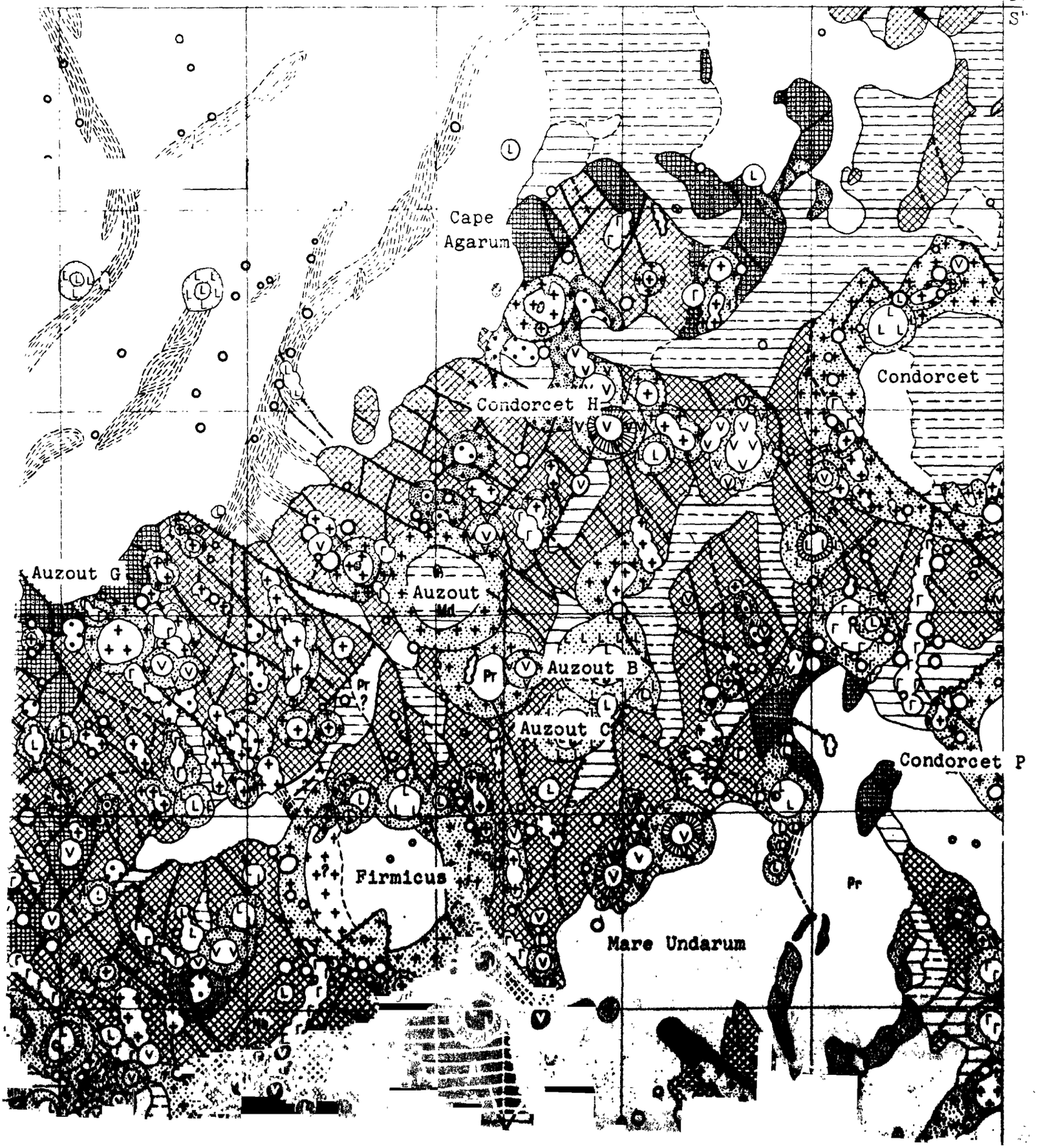
116°
Cape
Agarum
Condorcet
Condorcet H
Auzout G
Auzout
Md
Auzout B
Auzout C
Condorcet P
Firmicus
Mare Undarum
Pr

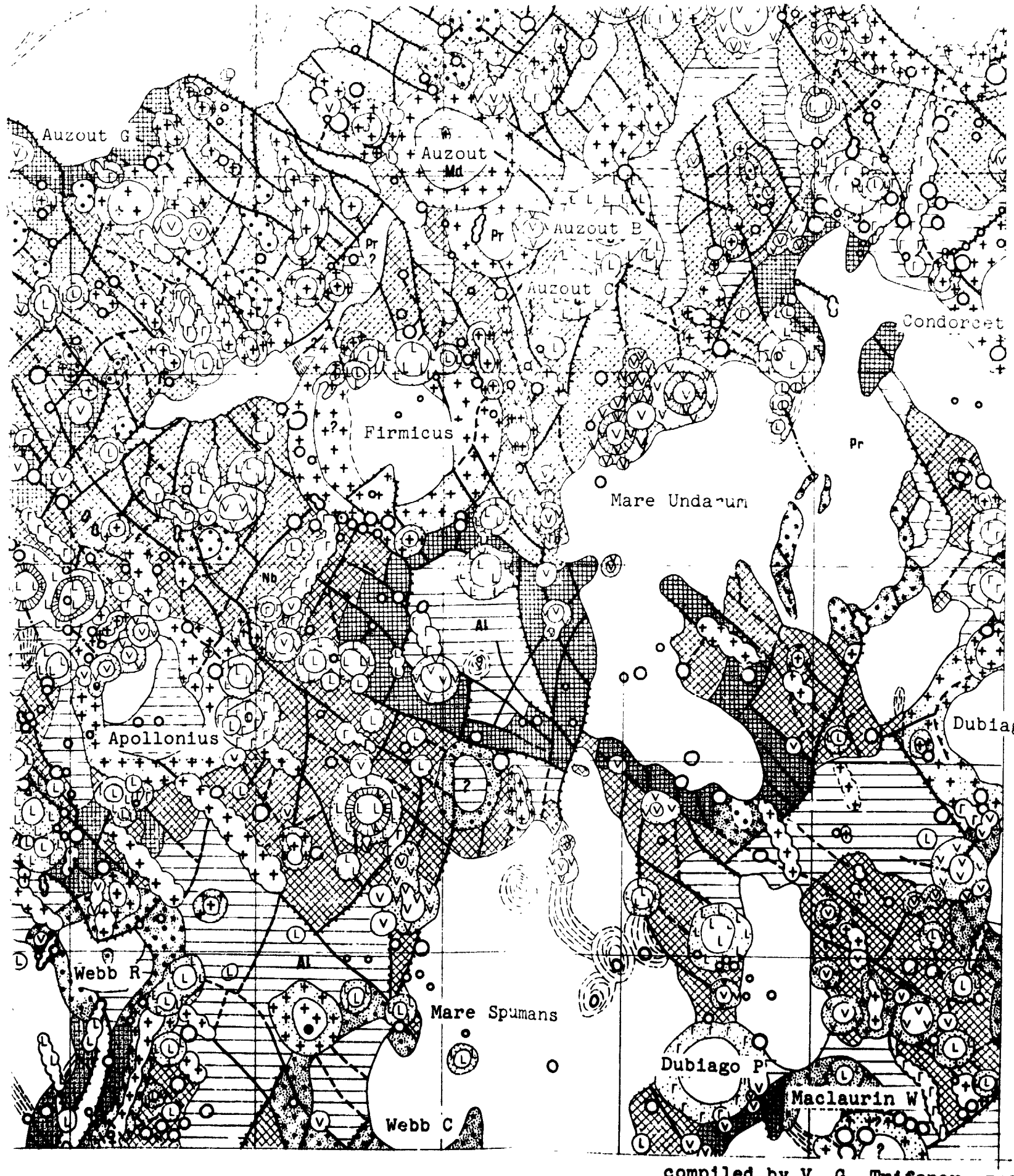

compiled by V. G. Trifonov

FOLDOUT FRAME 4

FOLDOUT FRAME

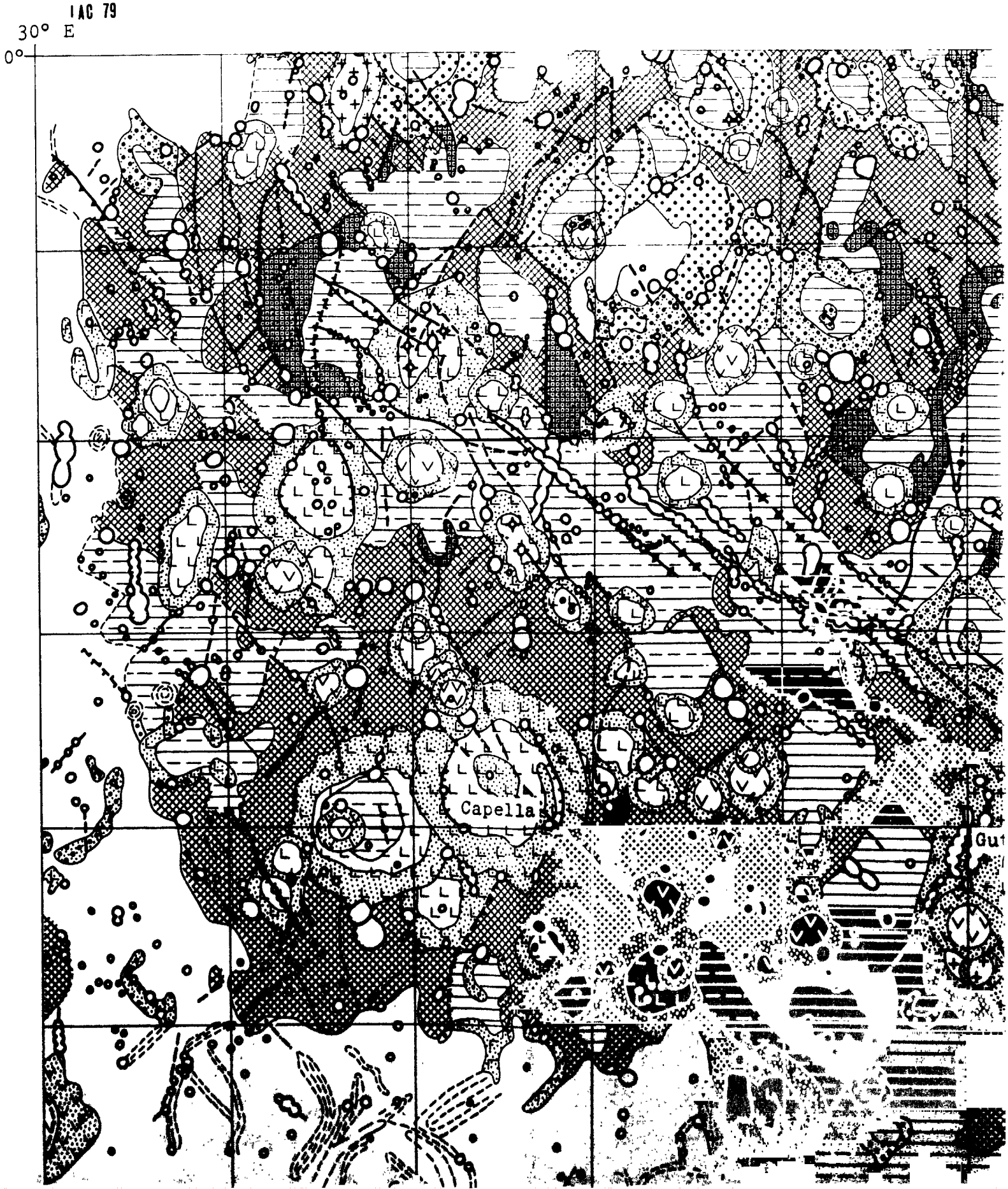

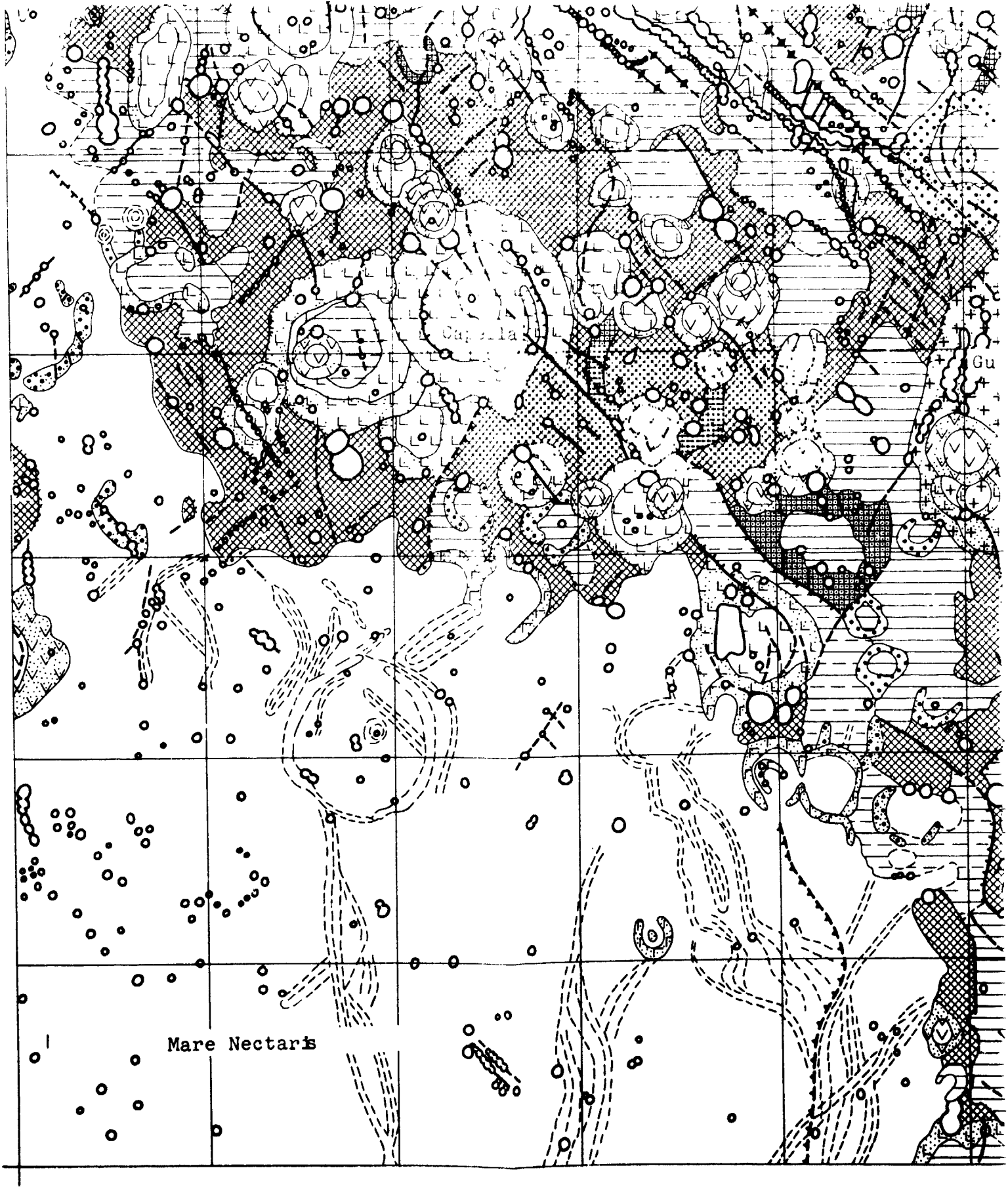

Figure 6. Geological-morphological chart of Sheet LAC-79. Scale ~ 1:1,500,000. Conditional designations are the same as in Figure 2.

FOLDOUT FRAME 3

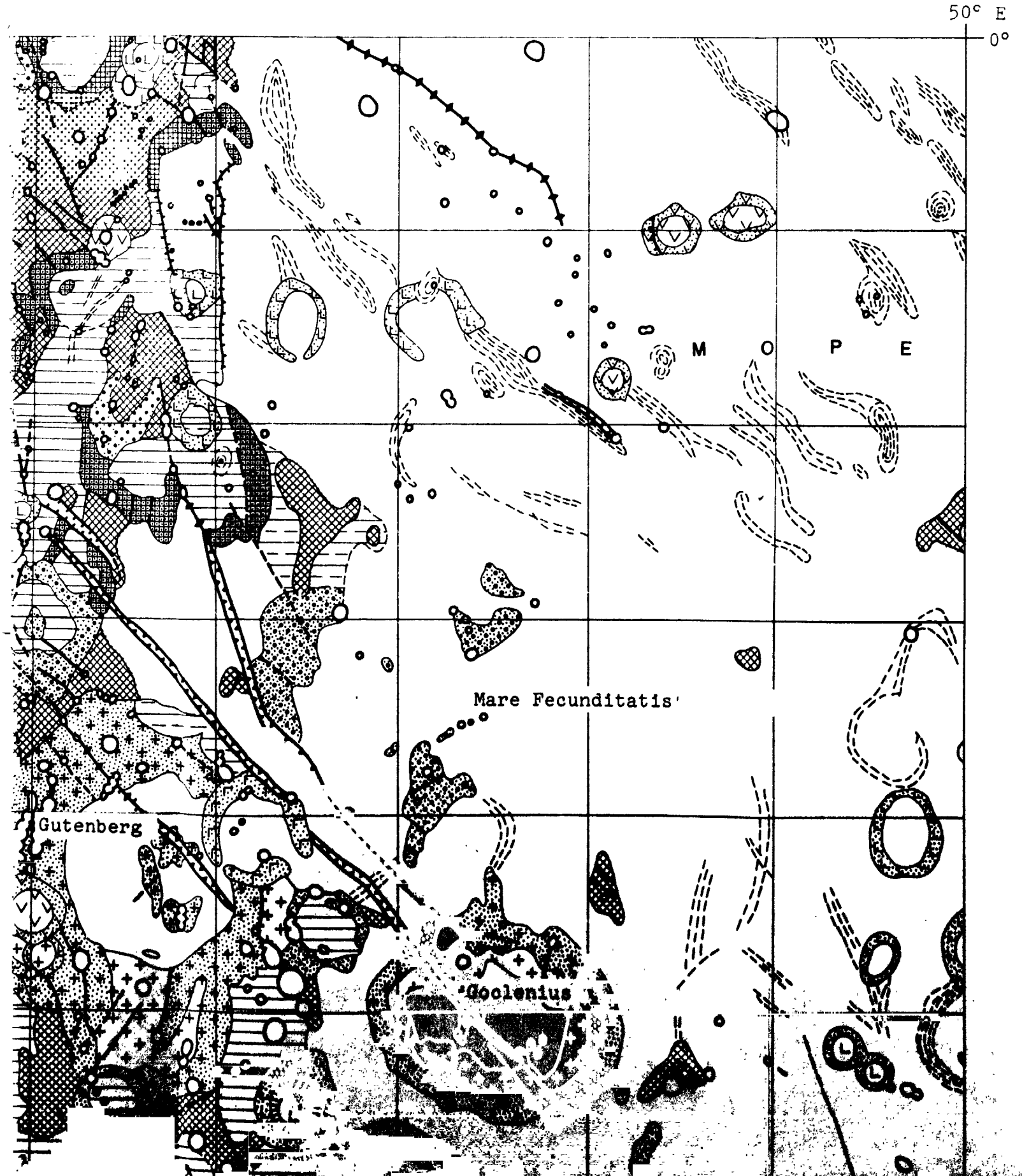

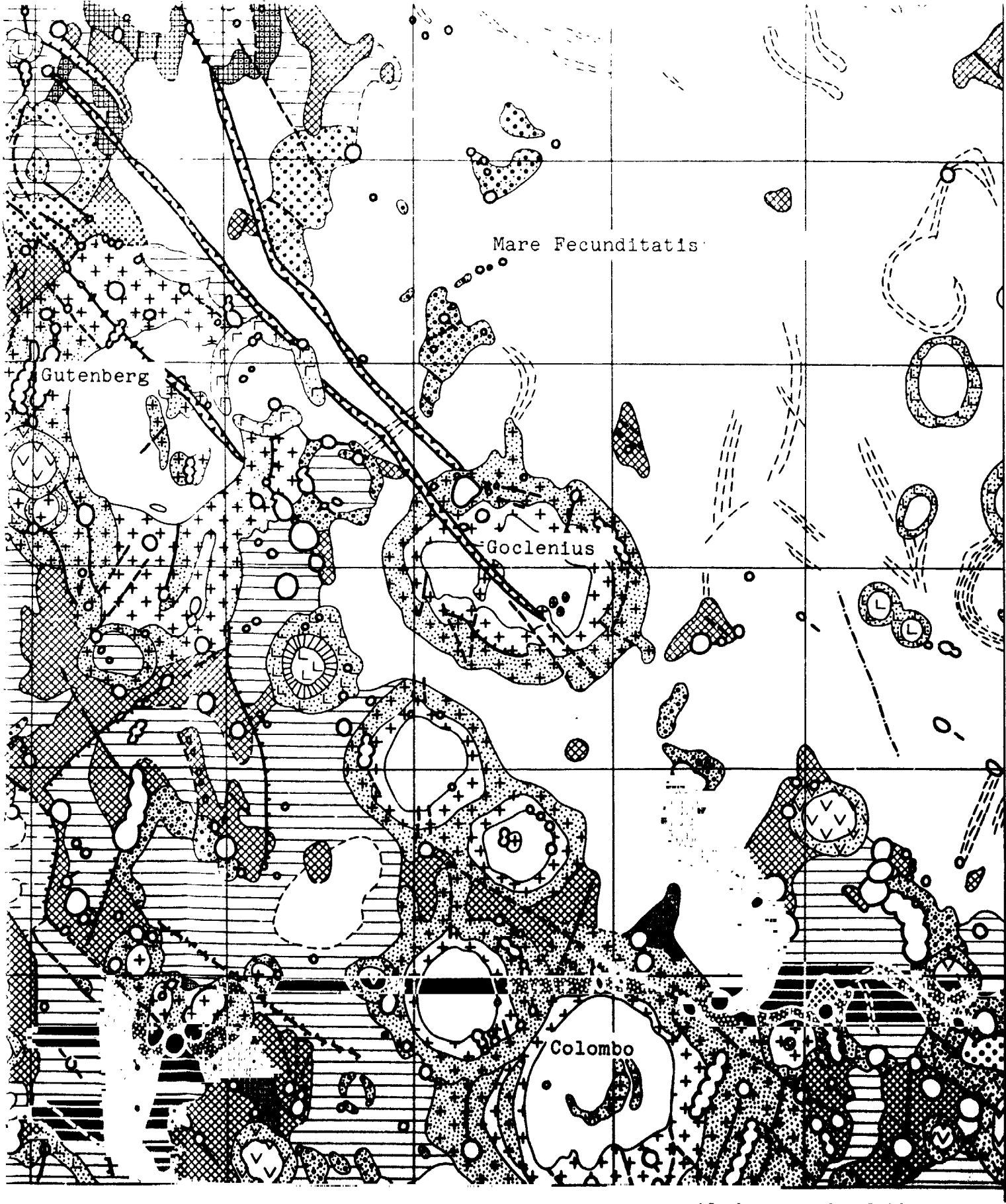

compiled by A. L. Sukhanov

BEST QUALITY FRAME 4

ROLDOUT FRAME

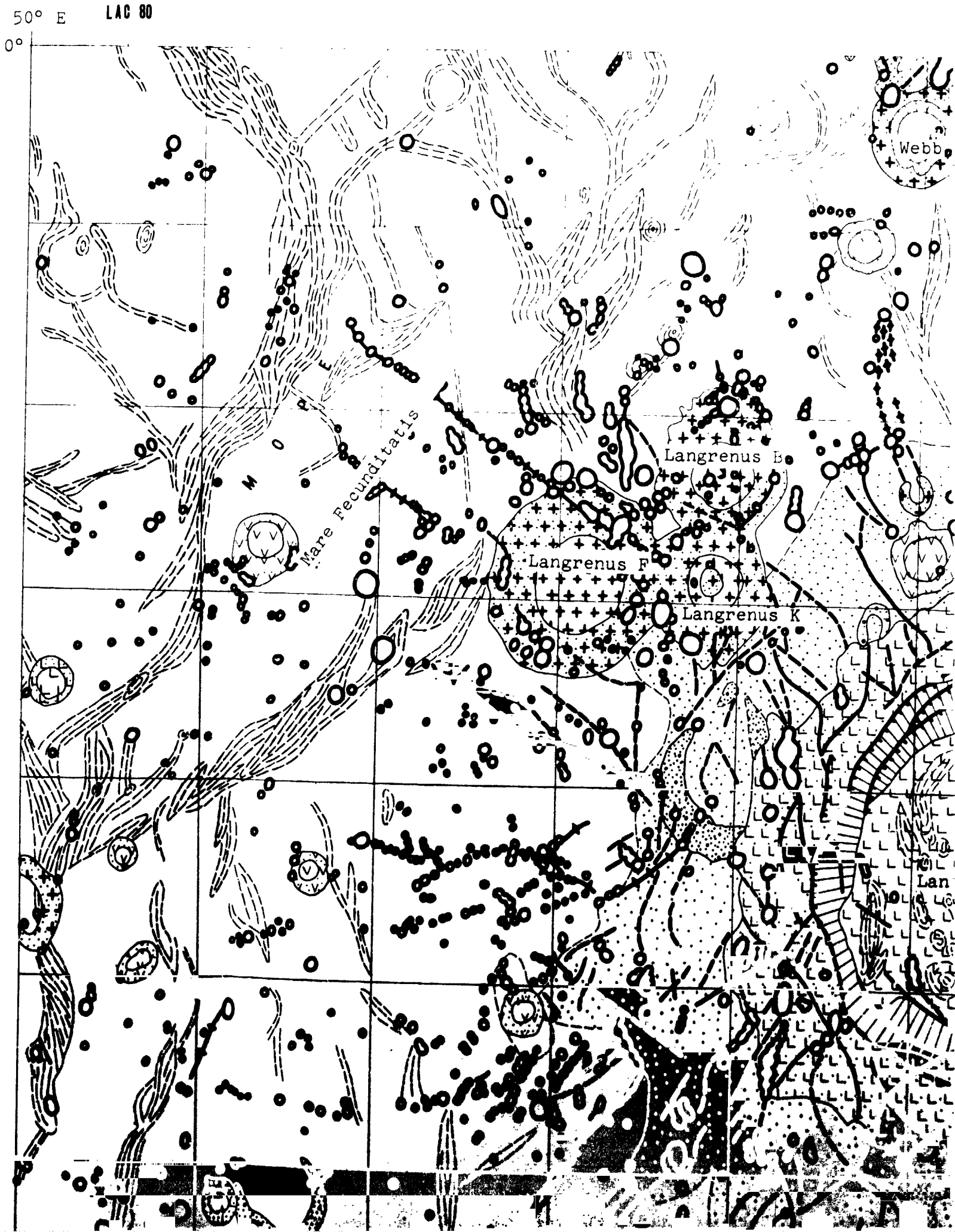

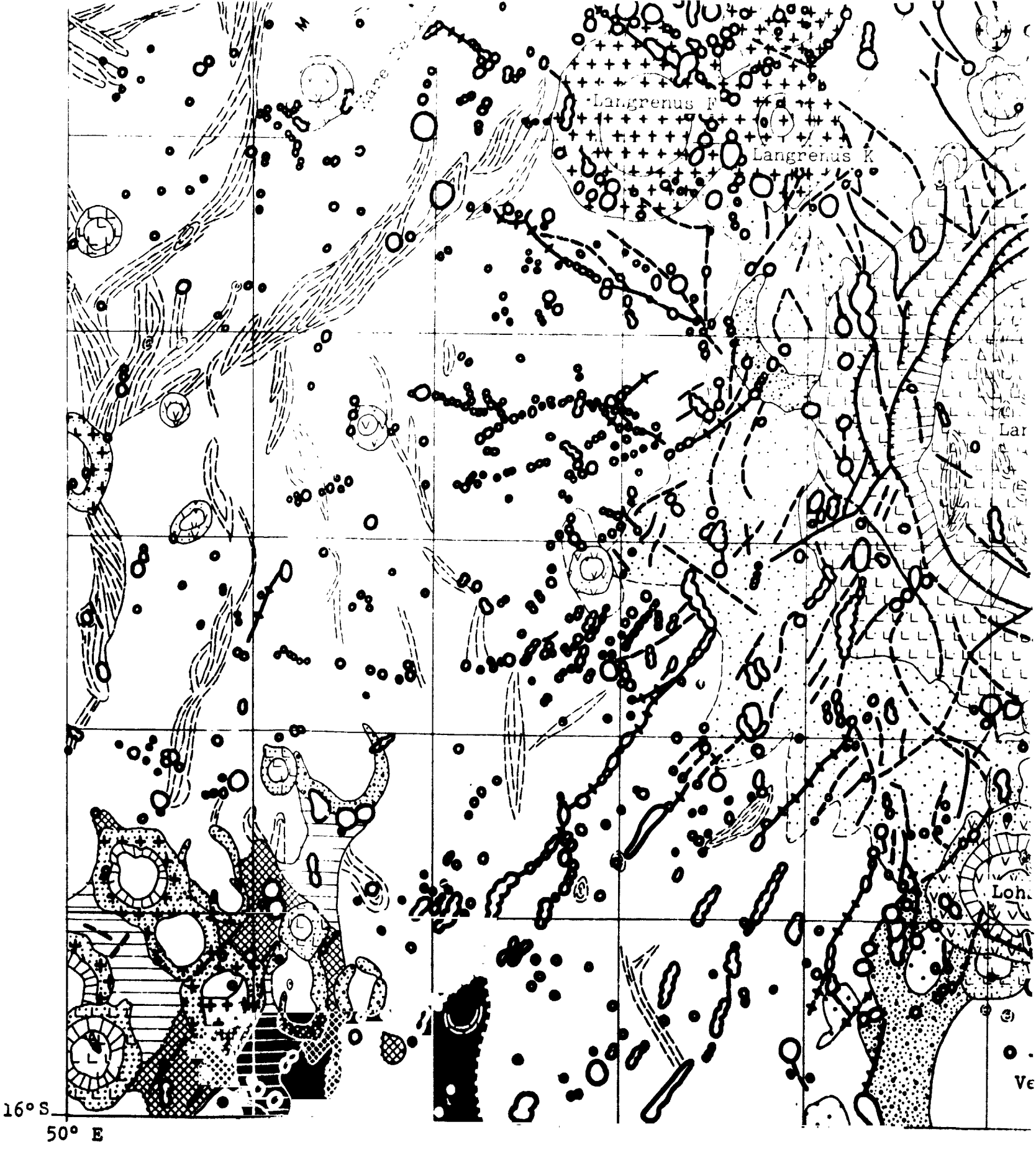

Figure 7. Geological-morphological chart of Sheet LAC-80. Scale ~ 1:1,500,000. Conditional designations are the same as in Figure 2.

FOLDOUT FRAME 2

BOLDOUT FRAME 3

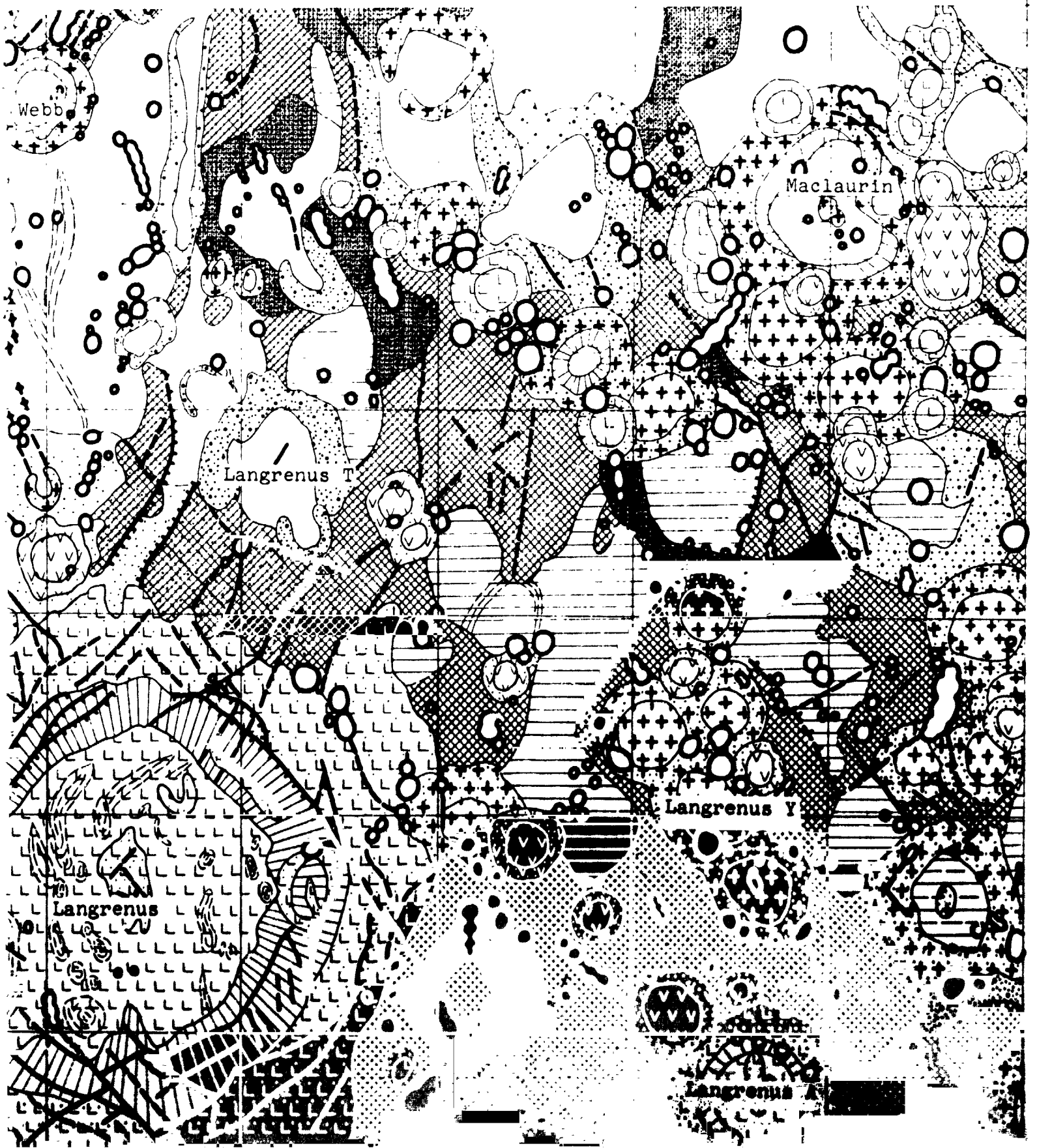

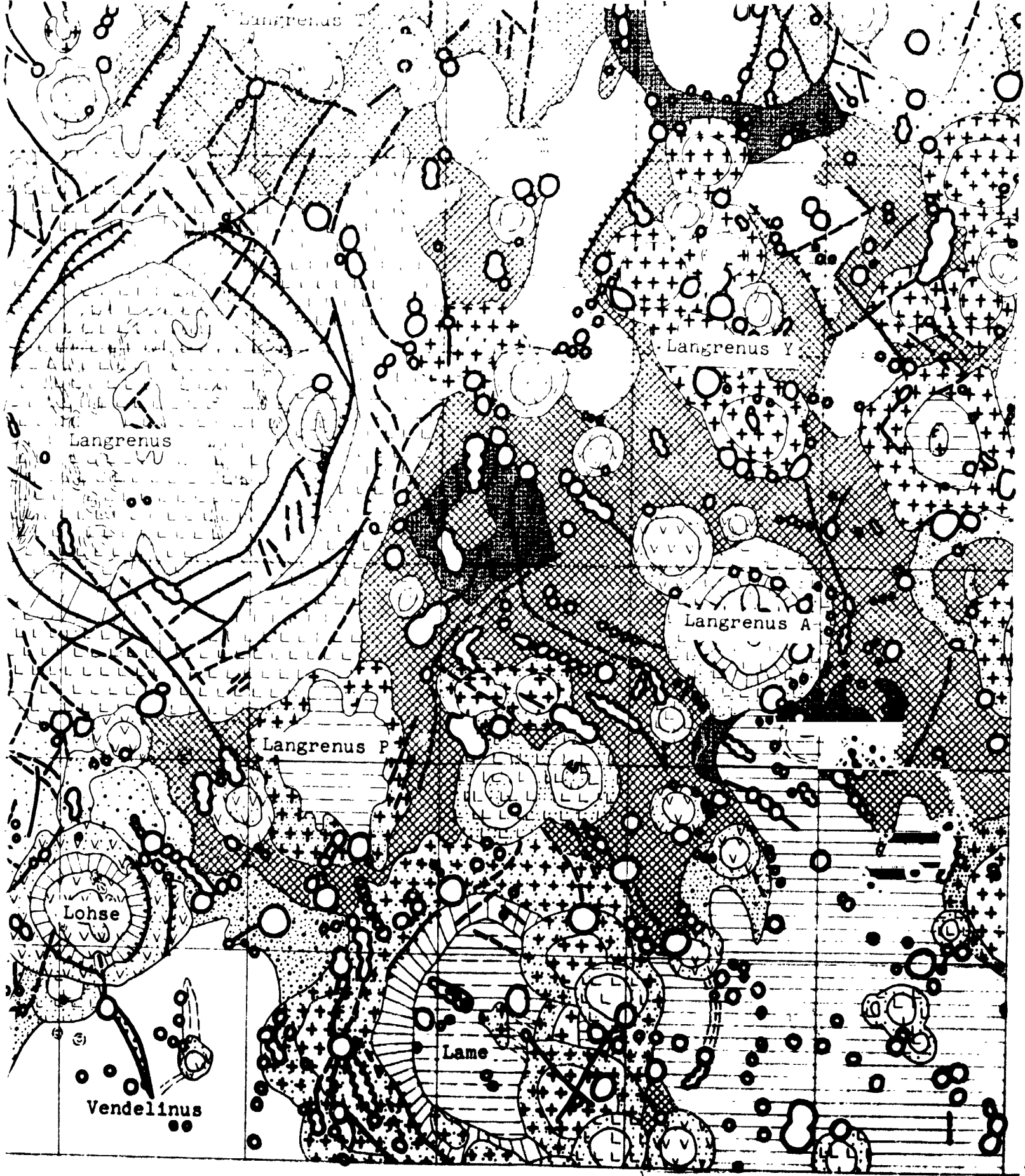

HOLDOUT FRAME

FOLDOUT FRAME

LAC 93

70° E

16° s

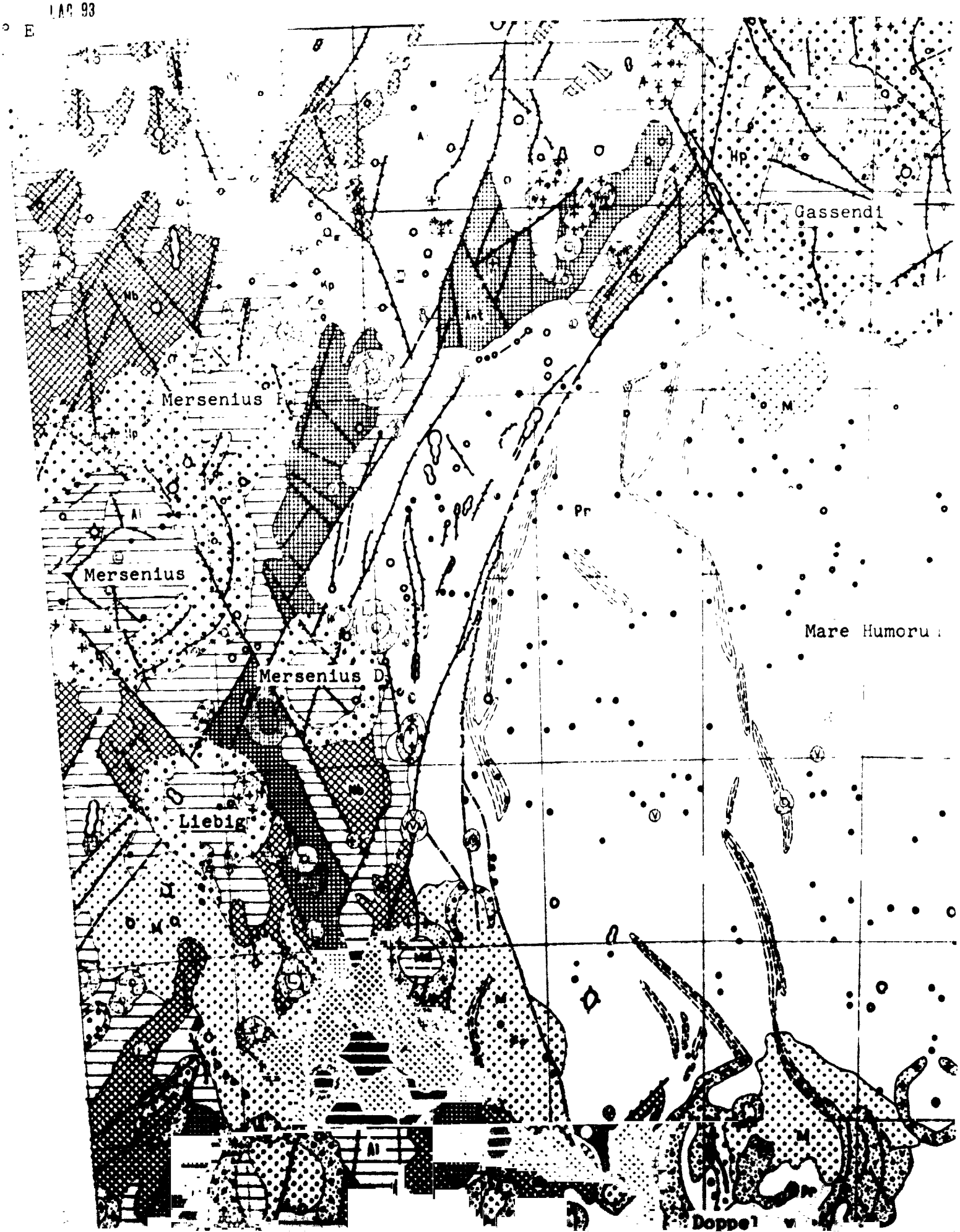

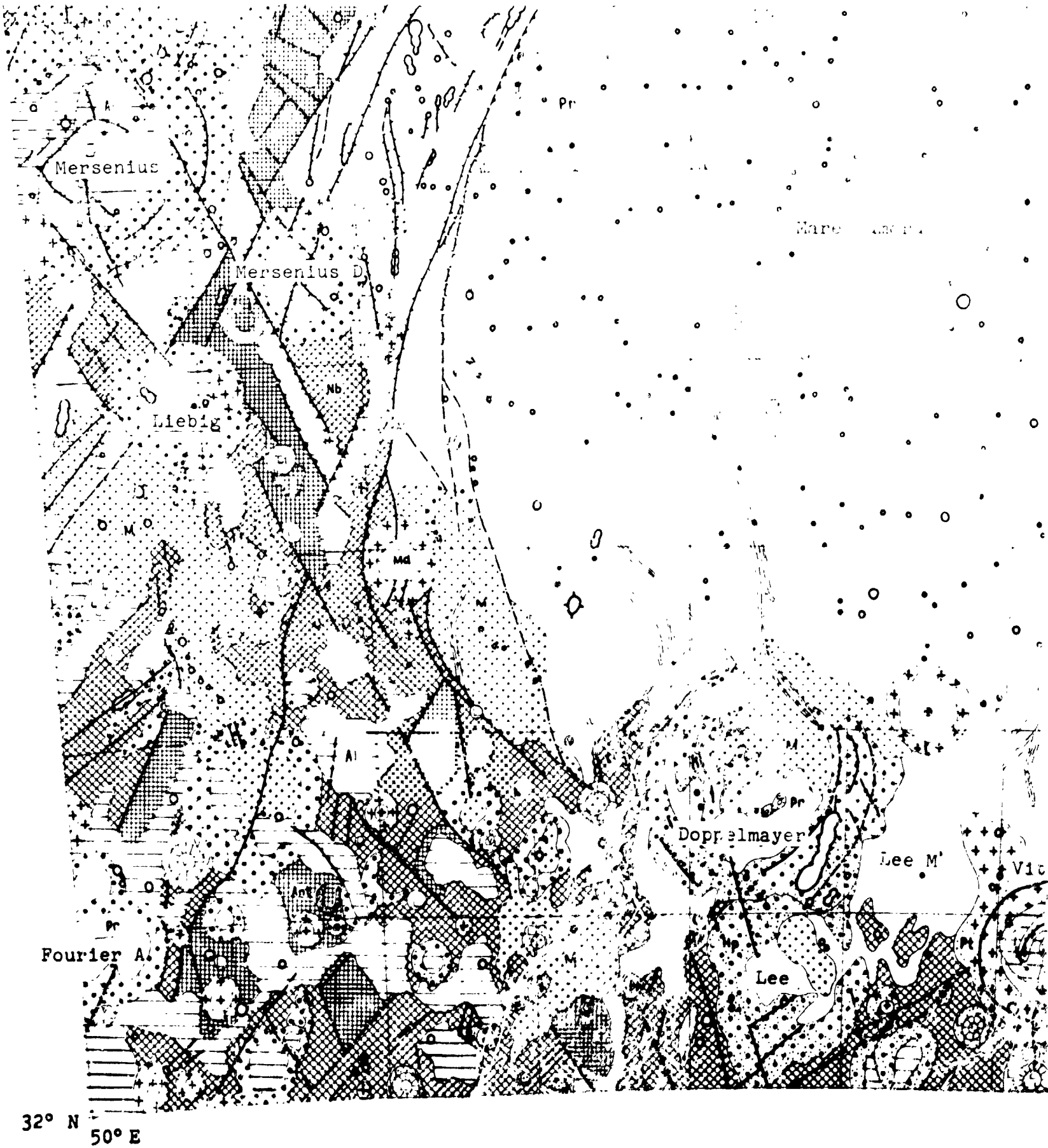

Figure 8. Geological-morphological chart of Sheet LAC-93. Scale ~ 1:1,500,000

FOLDOUT FRAME

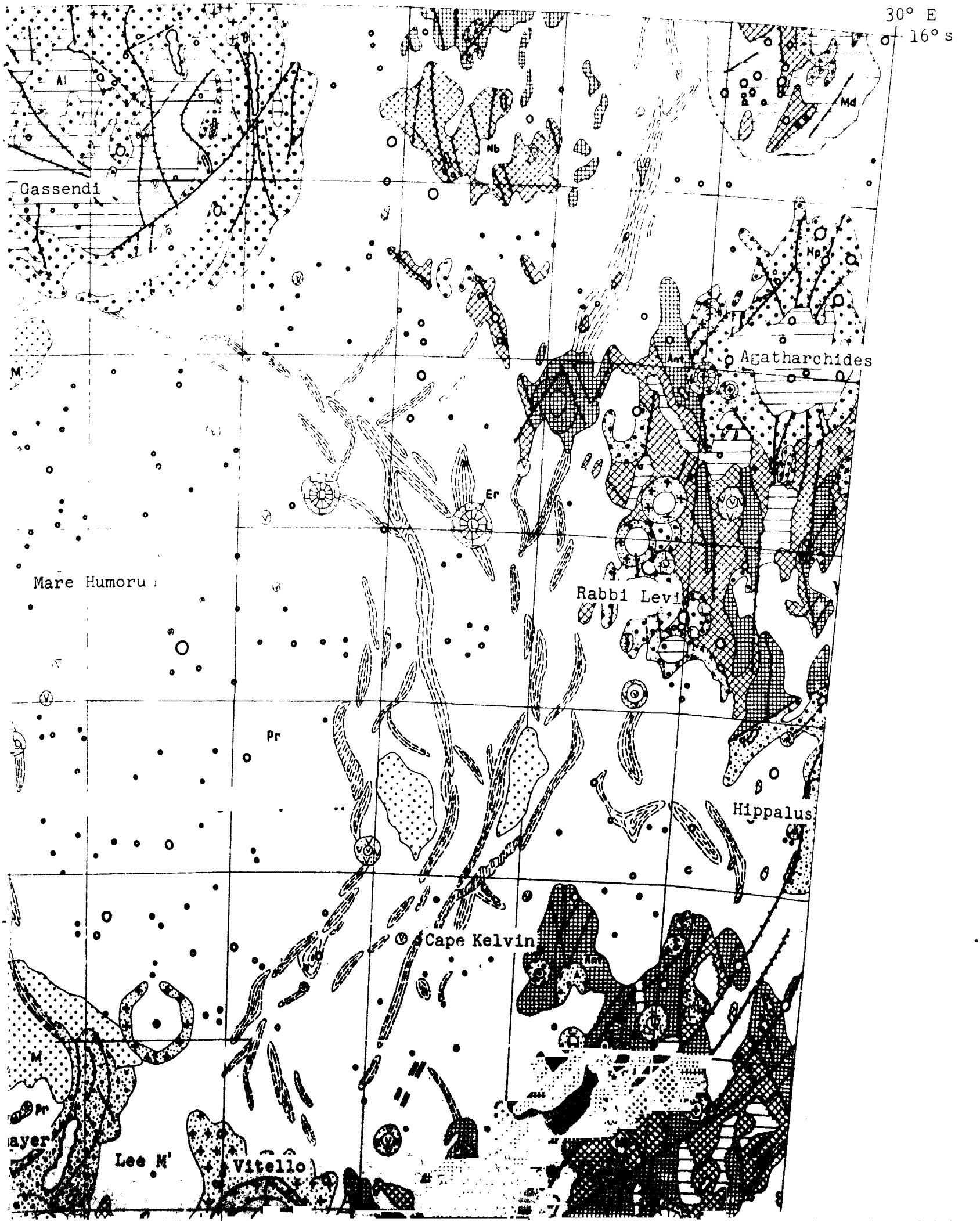
30° E
16° S
Cassendi
Agatharchides
Mare Humoru
Rabbi Levi
Hippalus
Cape Kelvin
Lee M'
Vitello
Nb
Md
Hp
Ant
Er
Pr

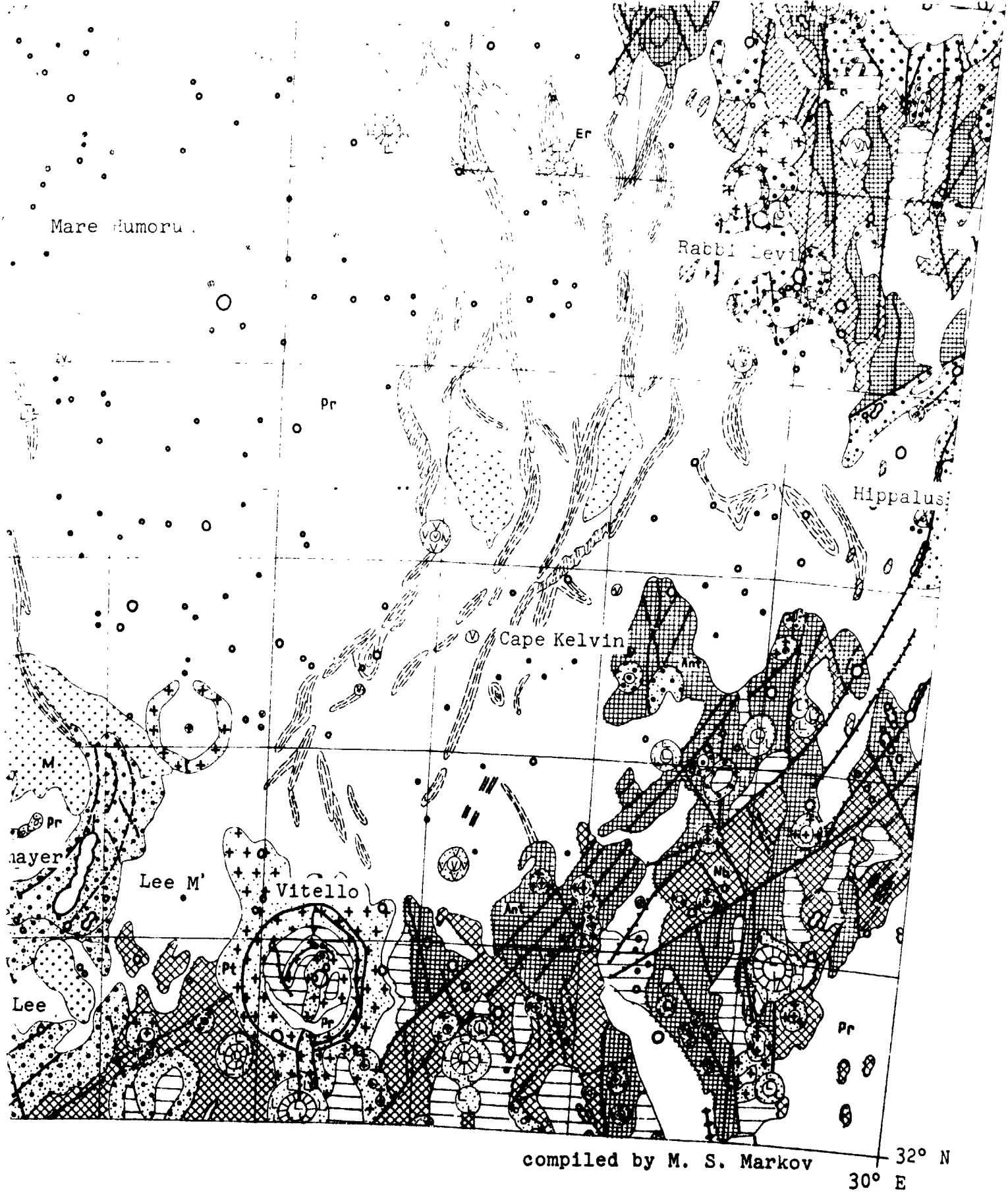

compiled by M. S. Markov

32° N
30° E

Scale ~ 1:1,500,000

FOLDOUT FRAME

FOLDOUT FRAME

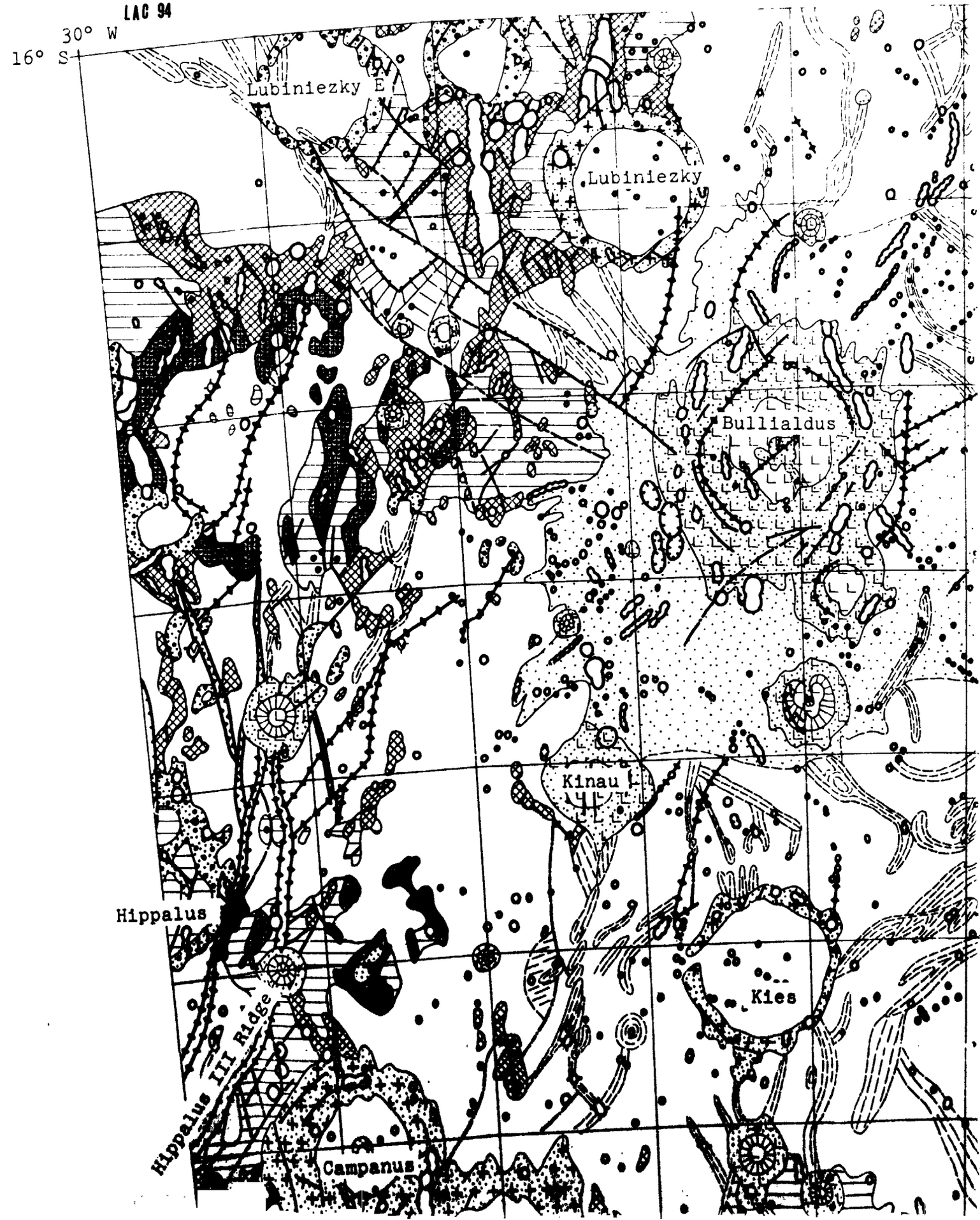

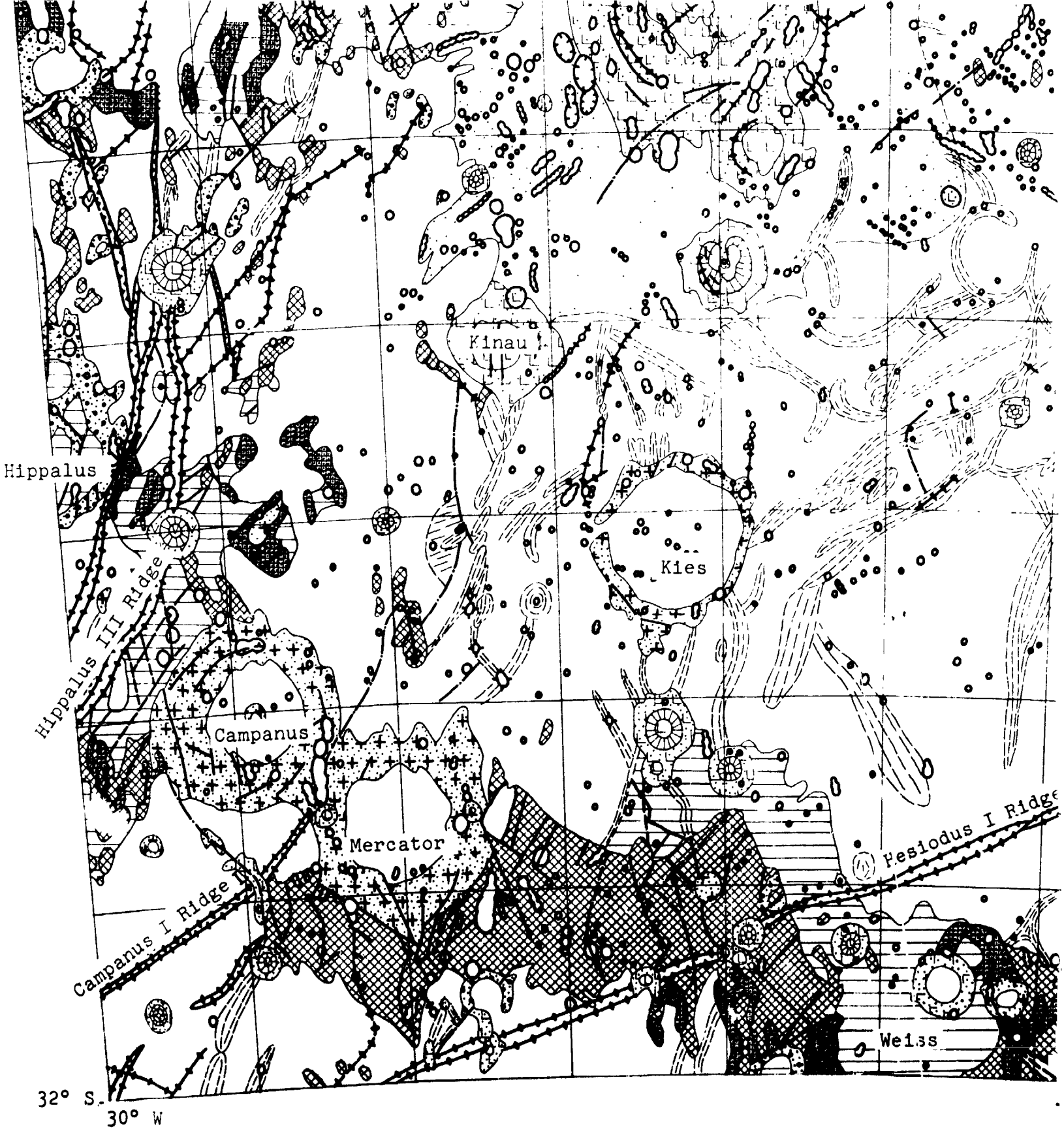

Figure 10. Geological-morphological chart of Sheet LAC-94. Scale ~ 1:1,500,000
Conditional designations are the same as in Figure 2.

FOLDOUT FRAME

FOLDOUT FRAME

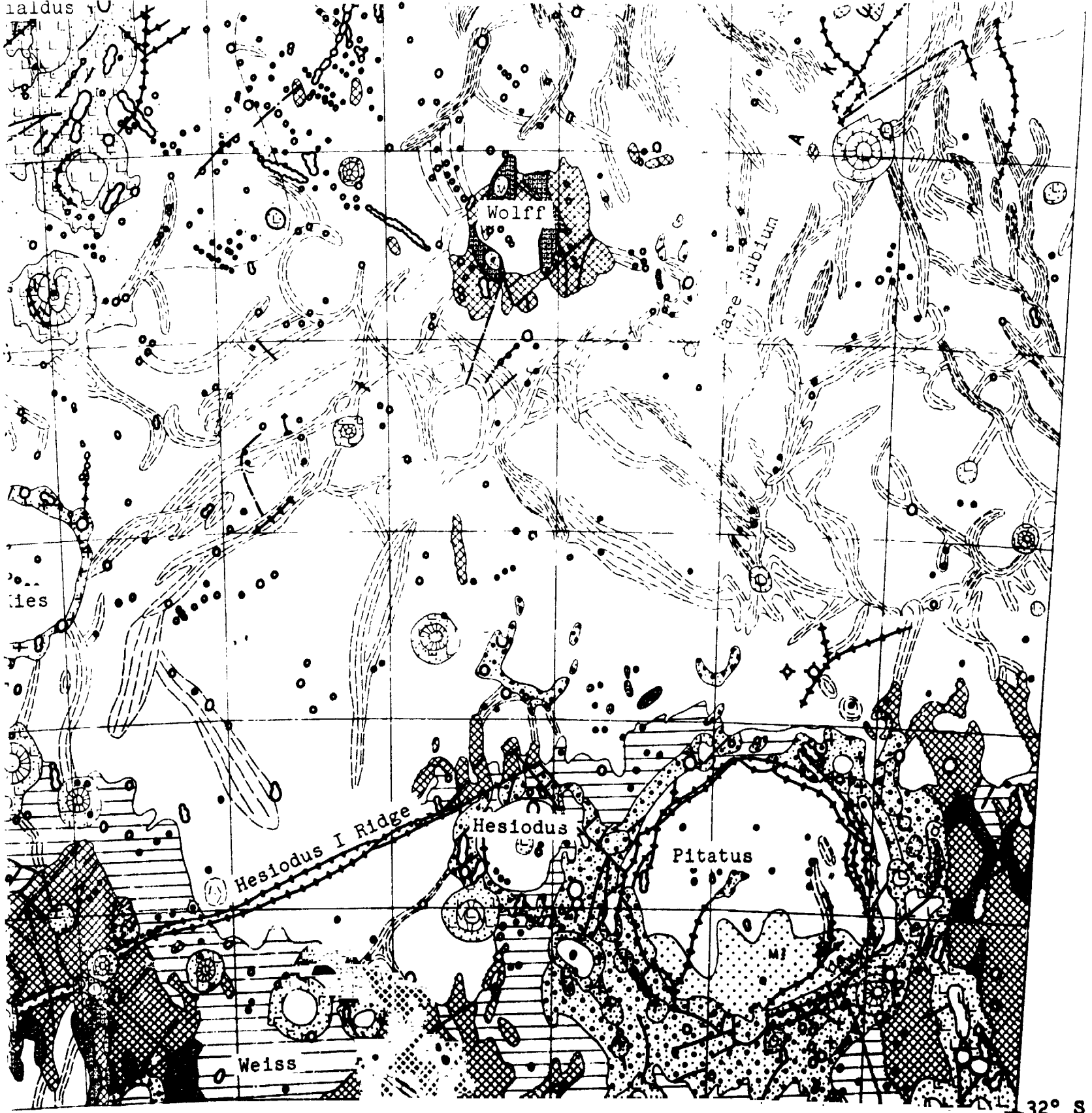

compiled by L. M. Shkerin

Sheet LAC-94. Scale ~ 1:1,500,000

Figure 2.

BOLDOUT FRAME
H

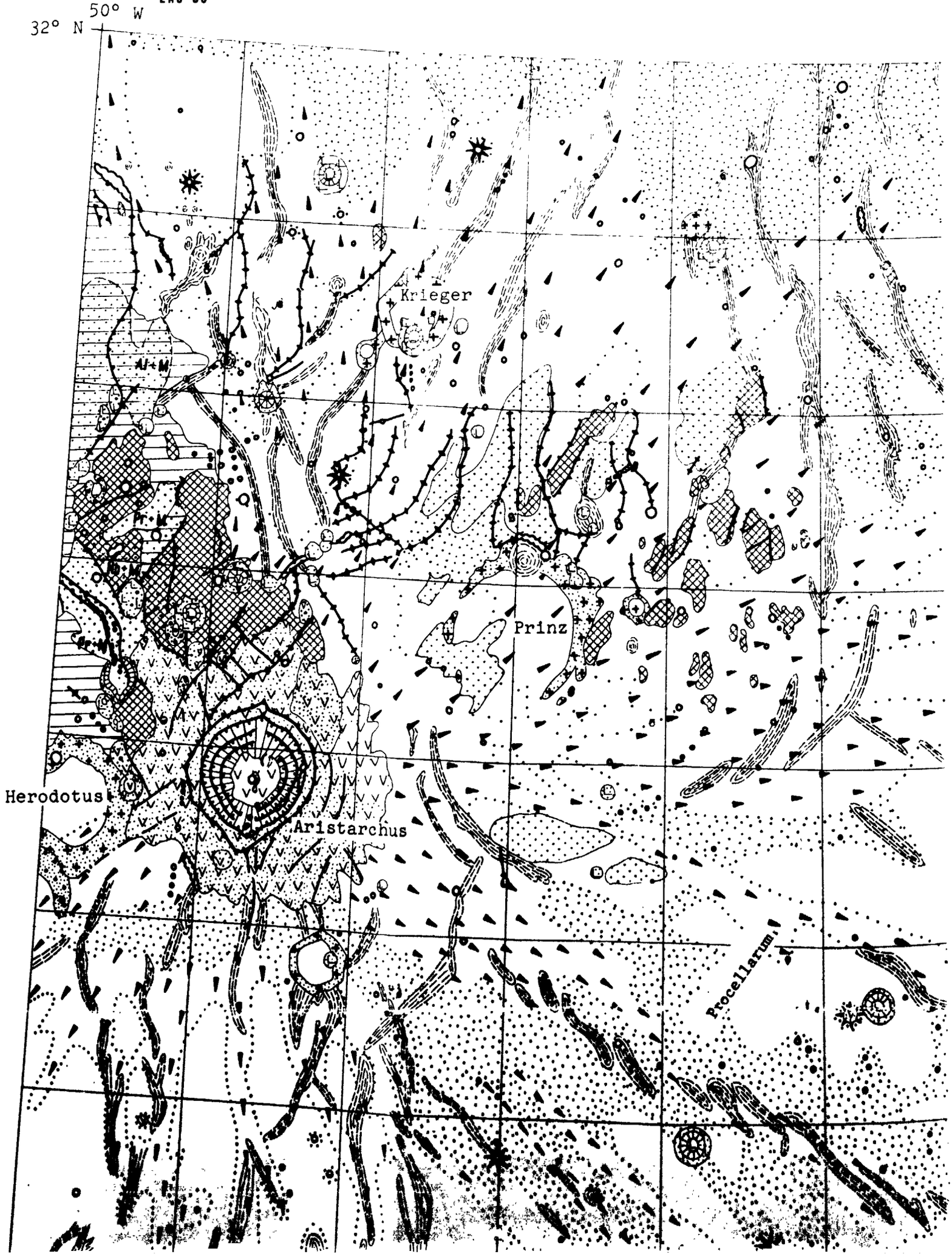
50° W
32° N
Krieger
Prinz
Herodotus
Aristarchus
Procellarum

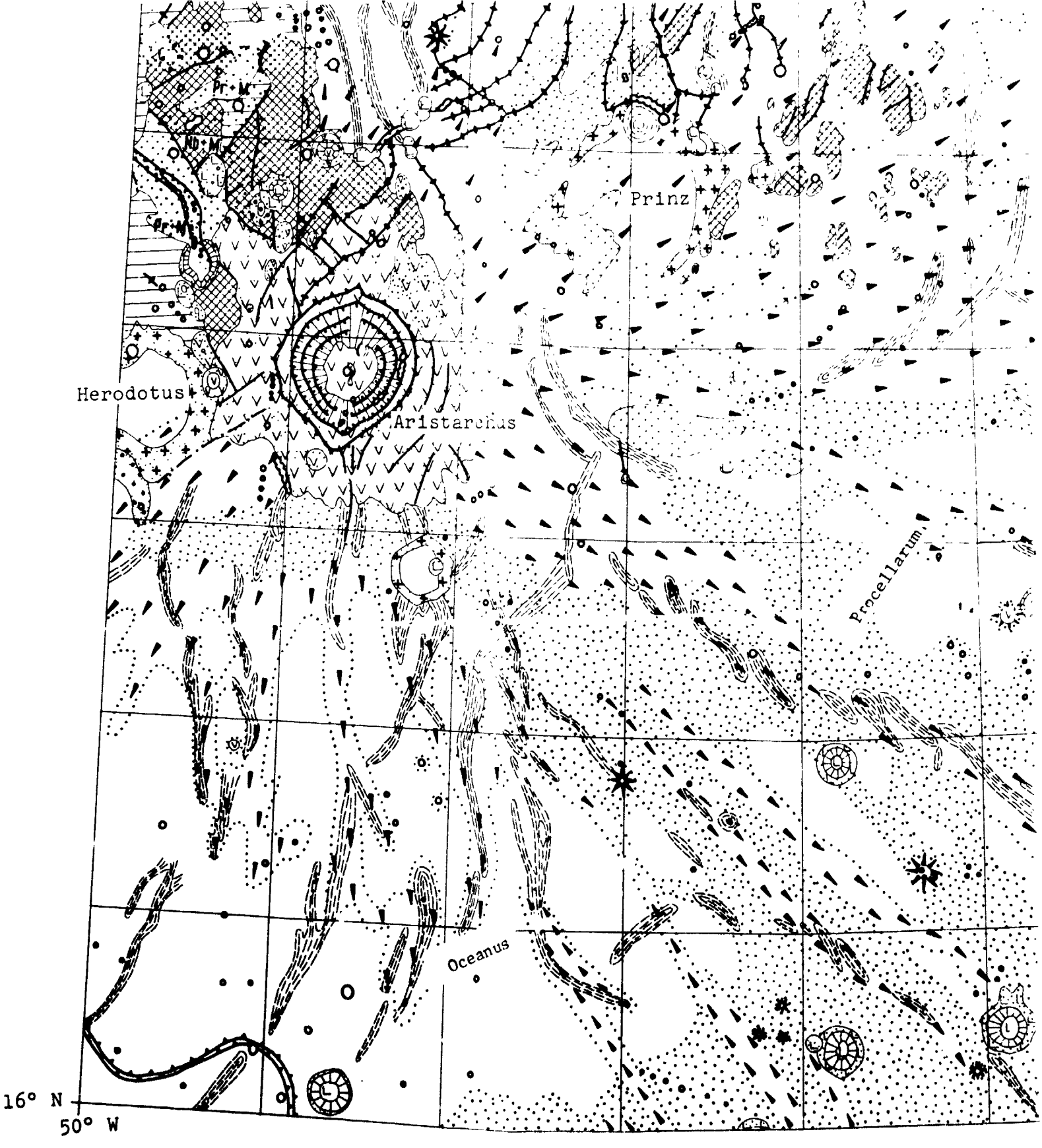

Figure 13. Geological-morphological chart of Sheet LAC-39. Scale ~ 1:1,500,000. Conditional designations are the same as in Figure 2.

HOLDOUT FRAME

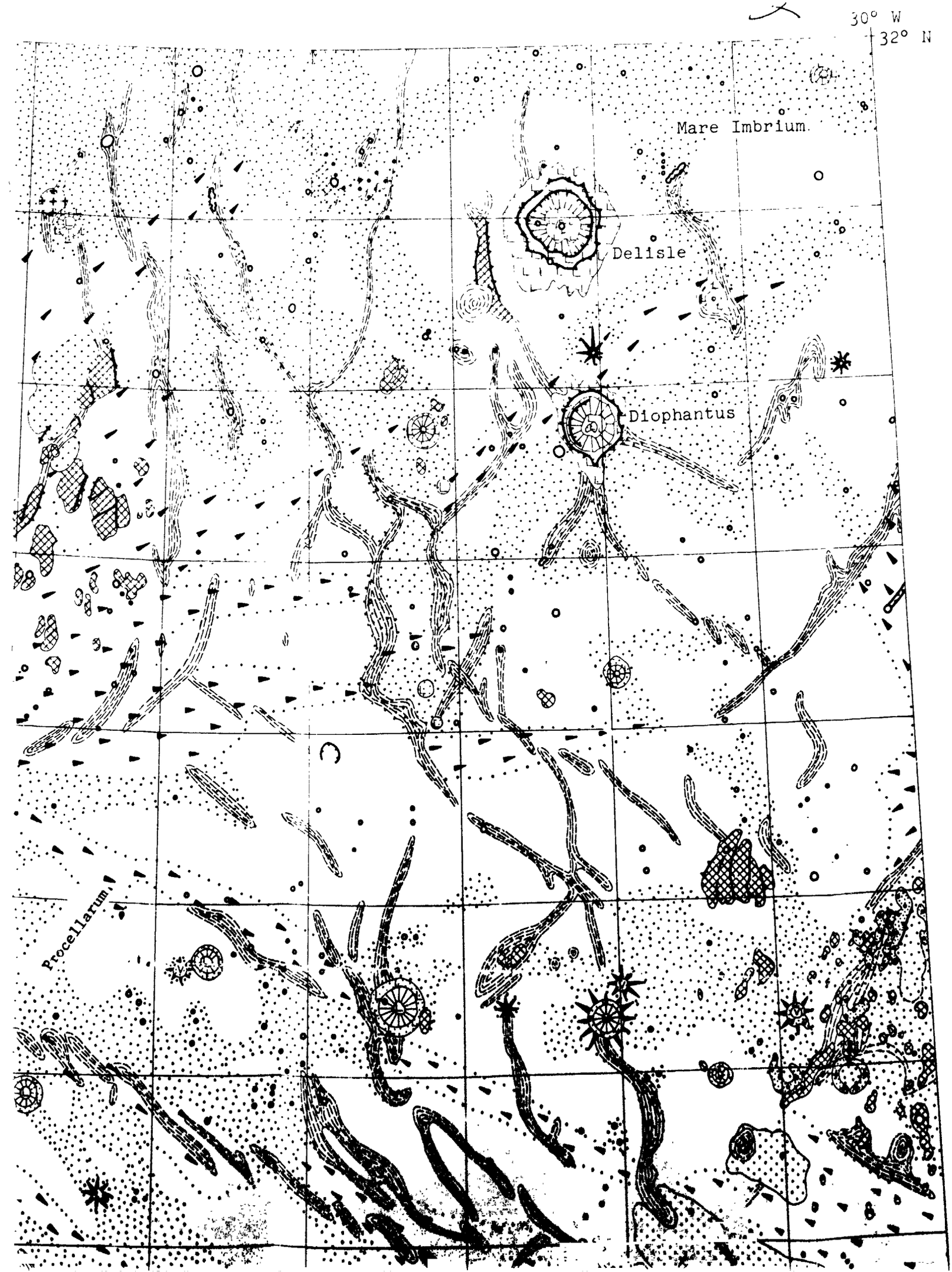
30° W
32° N
Mare Imbrium
Delisle
Diophantus
Procellarum

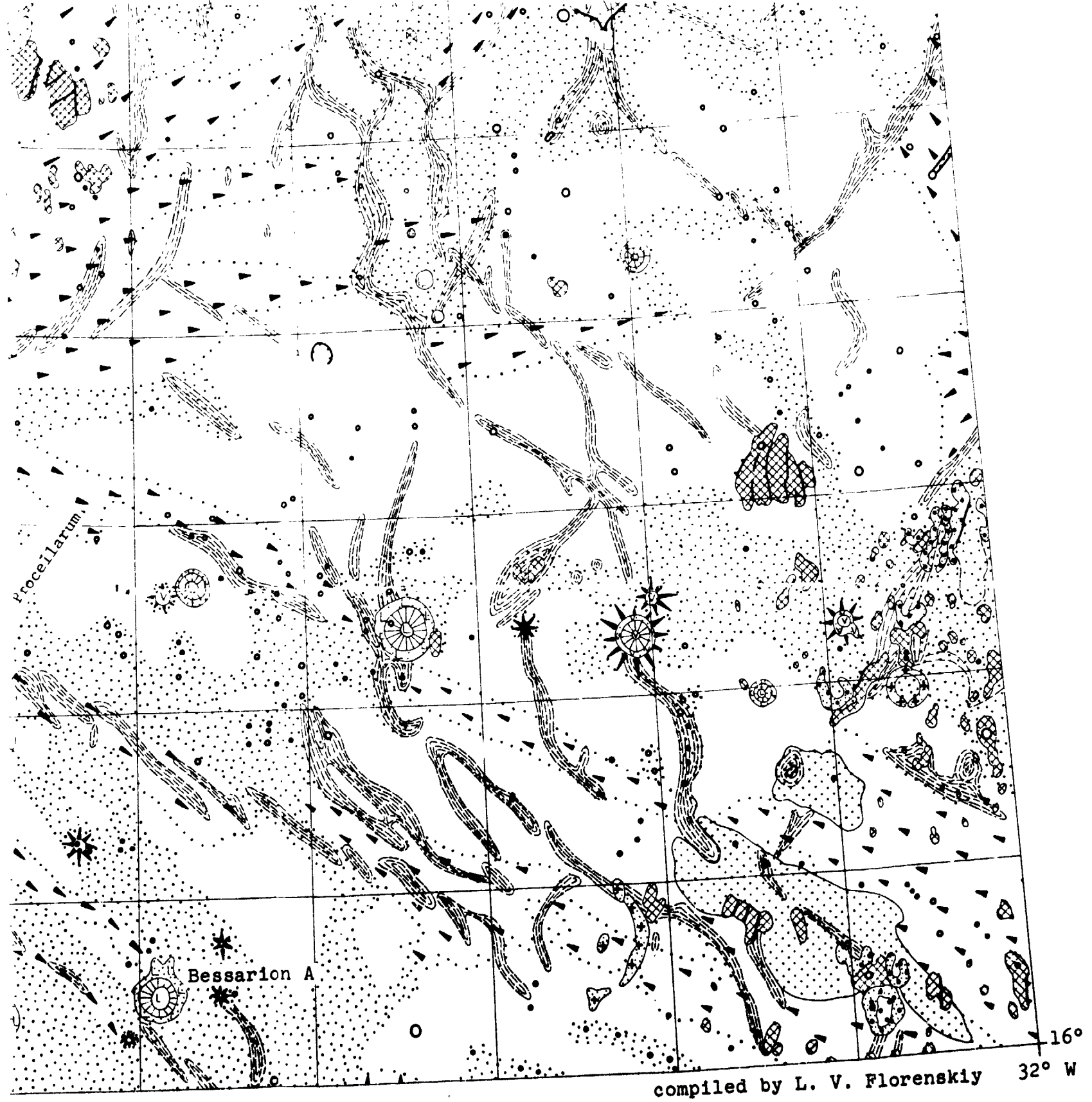

compiled by L. V. Florenskiy

- 1:1,500,000.

[redacted]OUT FRAME

4

FOLDOUT FRAME

LAC 56

70° W

16°N

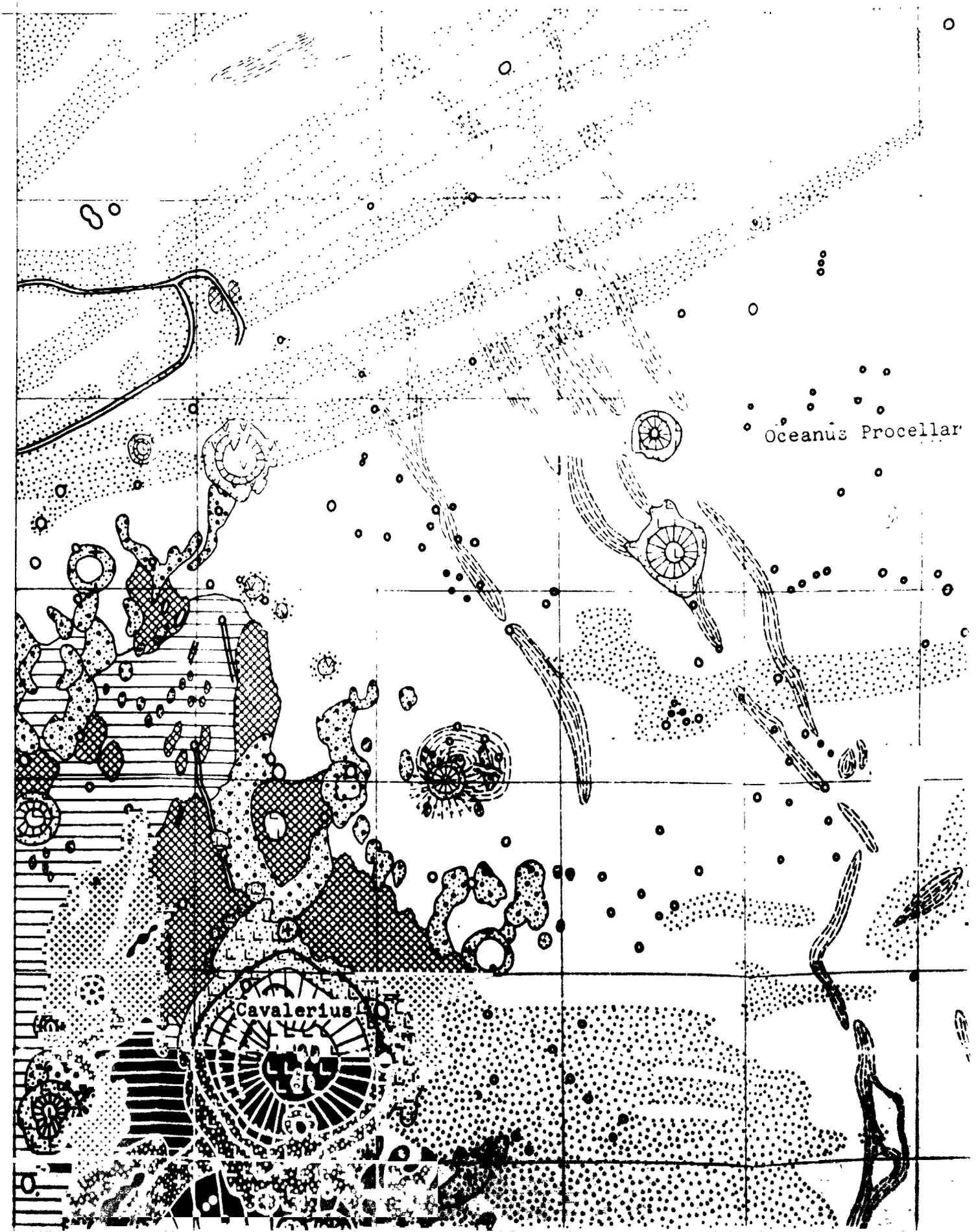

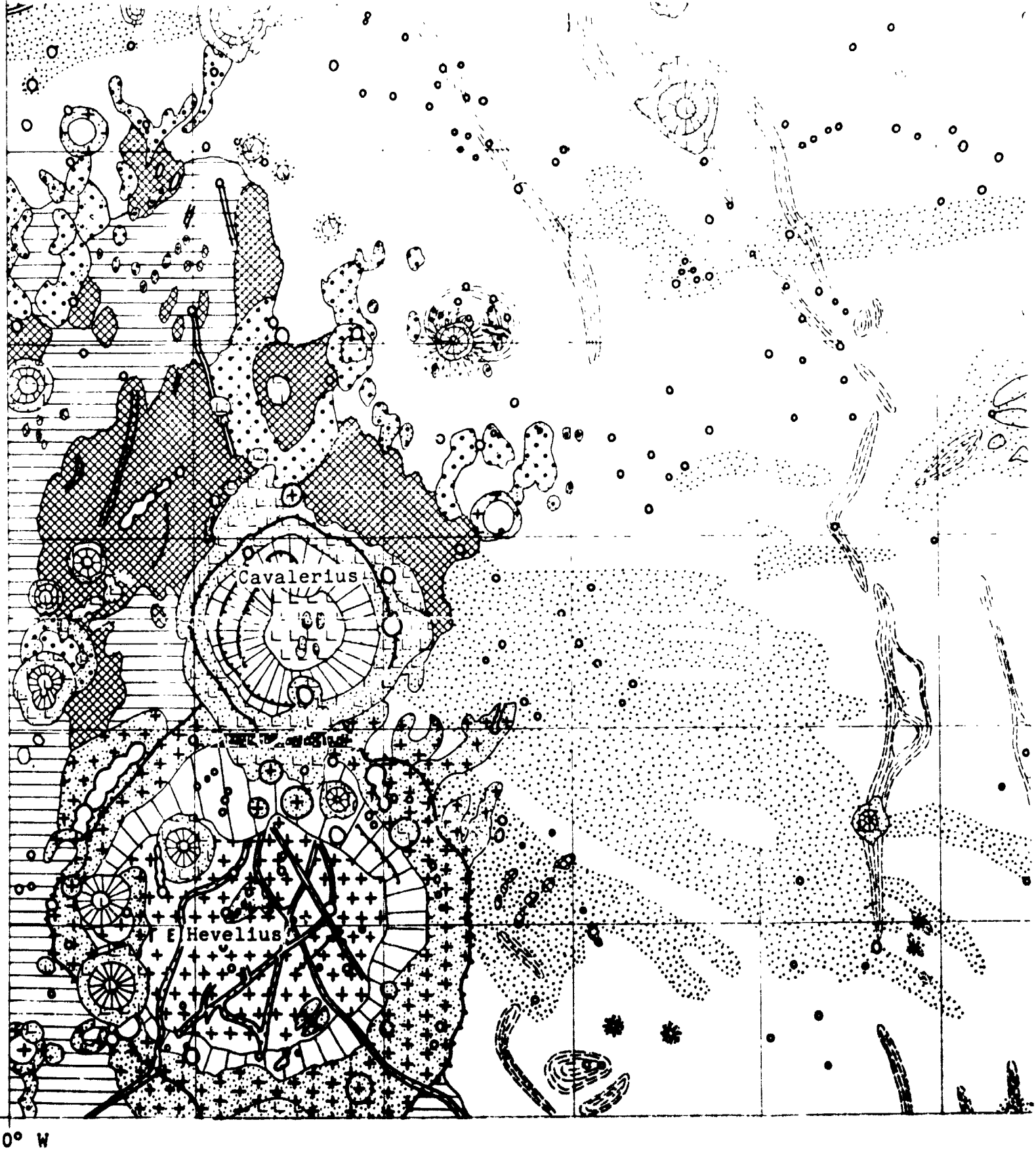

Figure 14. Geological-morphological chart of Sheet LAC-56. Scale ~ 1:1,500,000. Conditional designations are the same as in Figure 2.

FOLDOUT

BLOWOUT FRAME

3

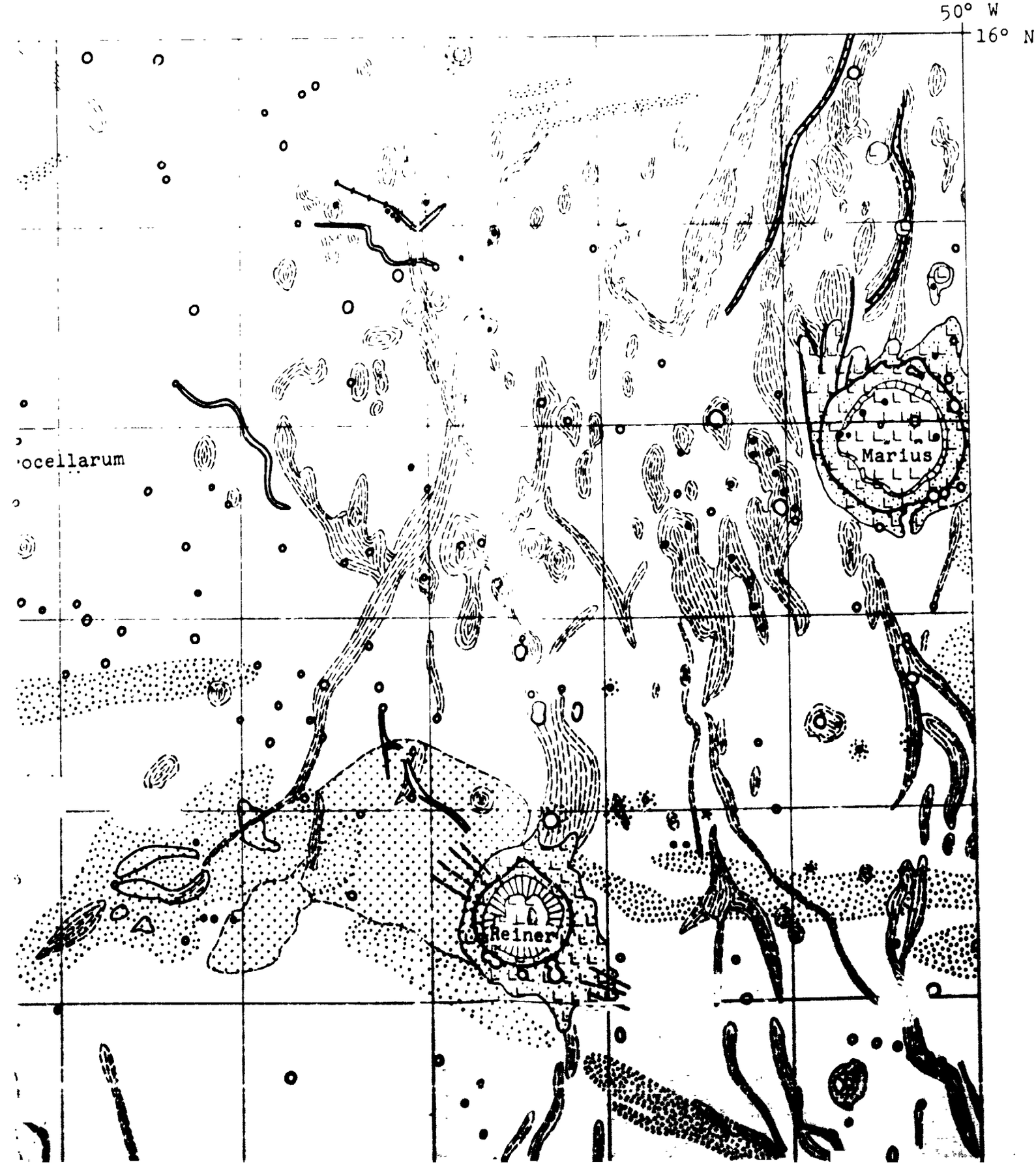

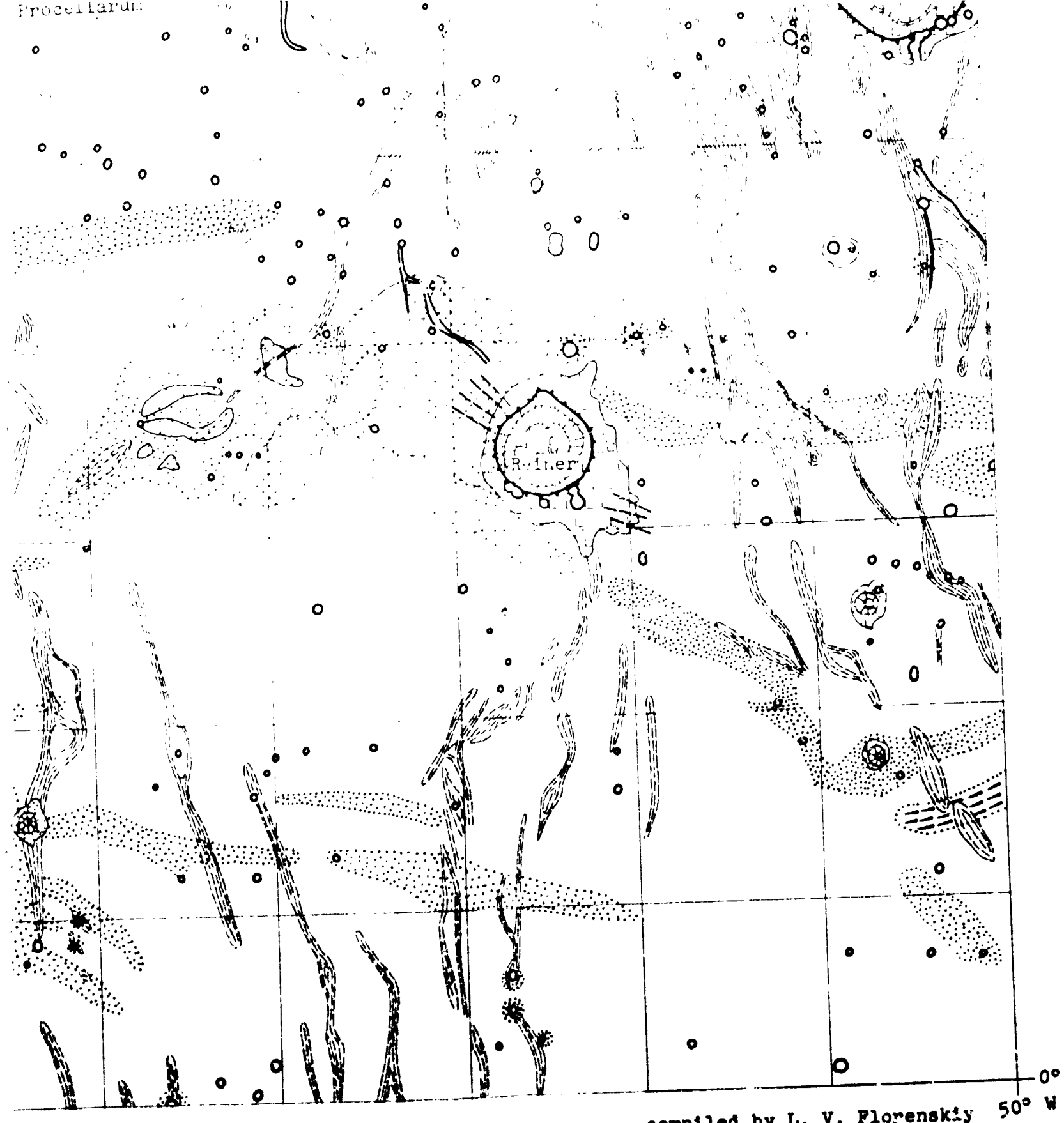

compiled by L. V. Florenskiy

500,000.

[redacted] FRAME
4

FOLDOUT FRAME

LAC 75

50° W

0°

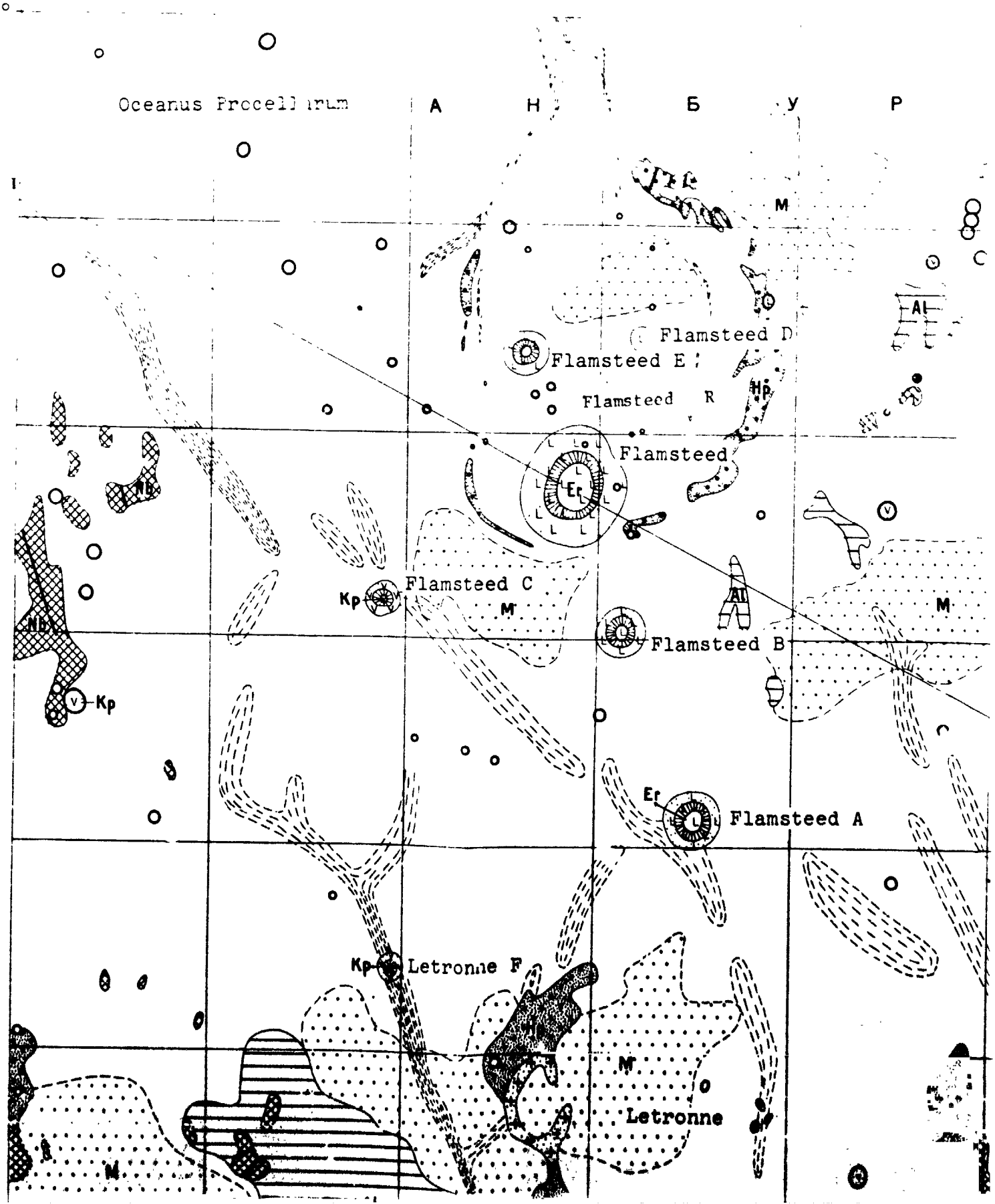

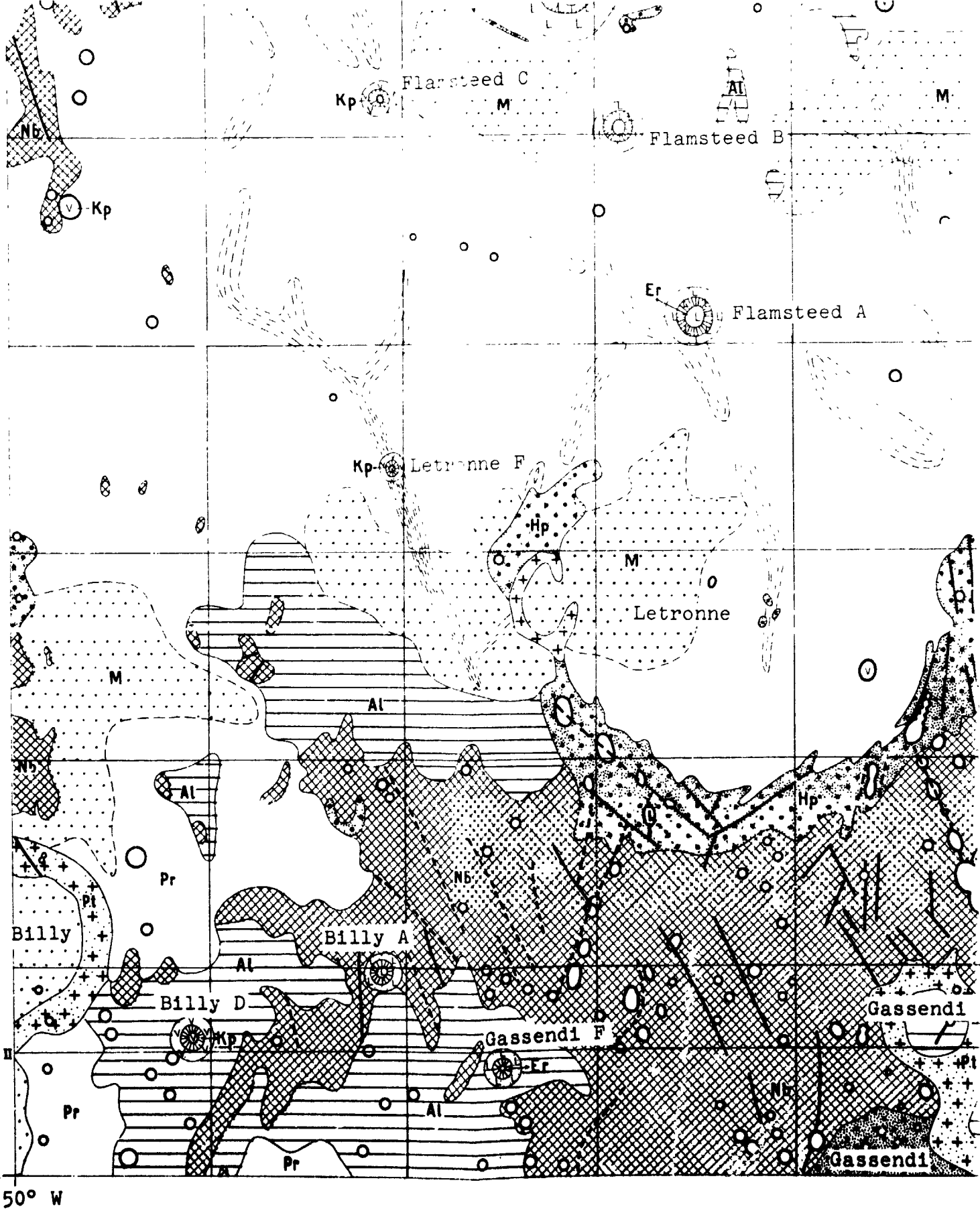

Figure 12. Geological-morphological chart of Sheet LAC-75. Scale ~ 1:1,500,000
Conditional designations are the same as in Figure 2.

HOLDOUT FRAME

POLAROID Film

3

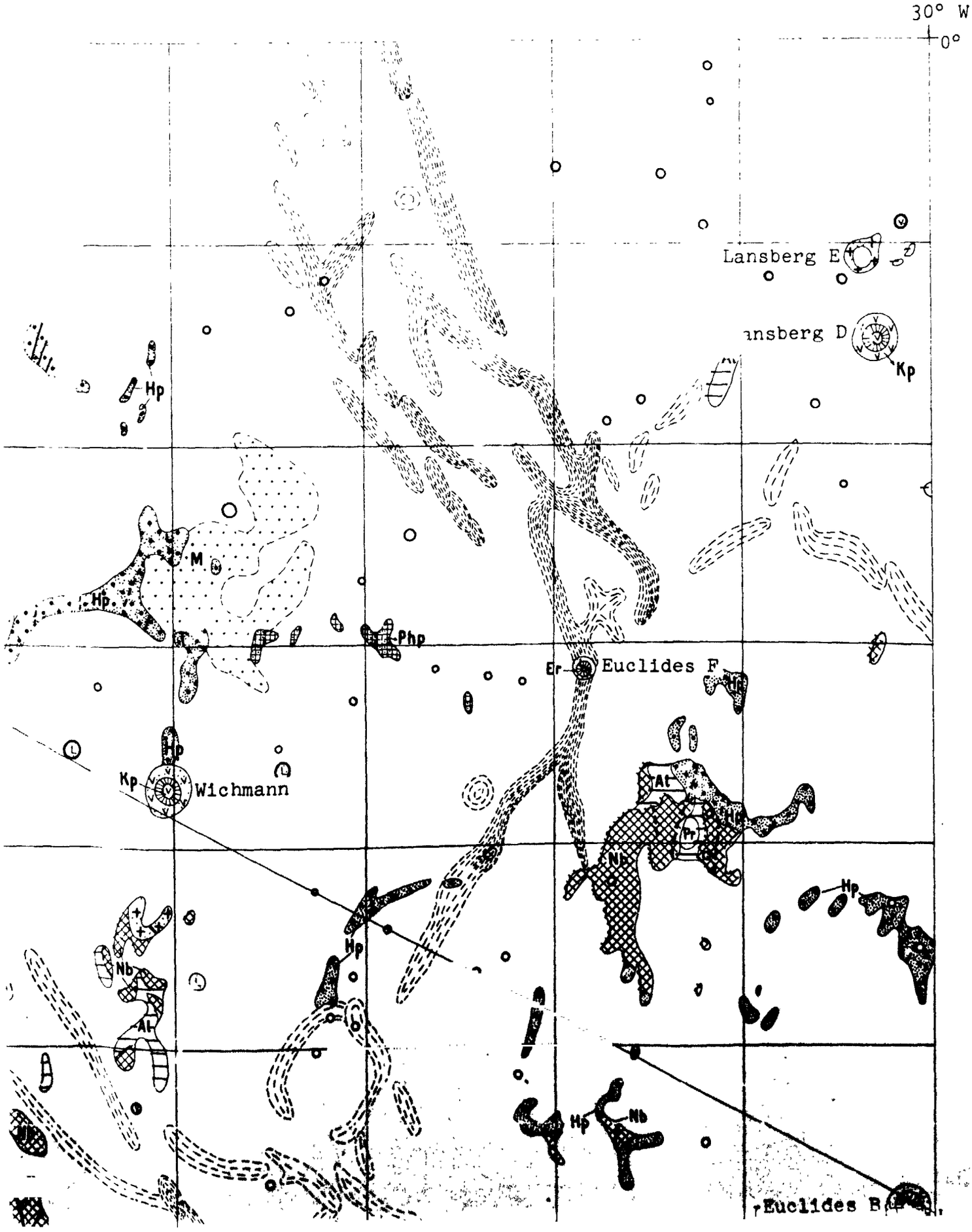

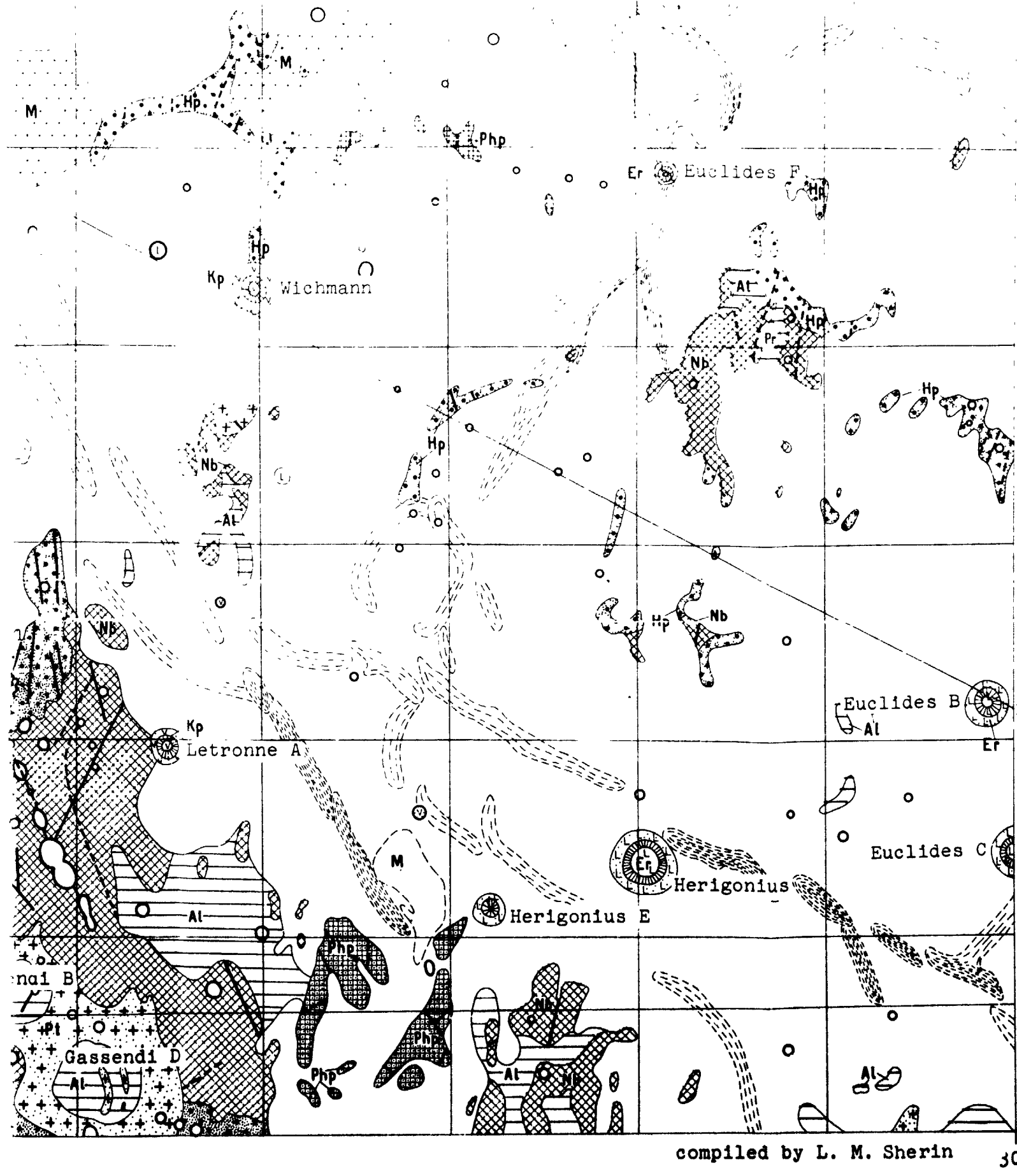

,000.

FOLDOUT FRAME

4

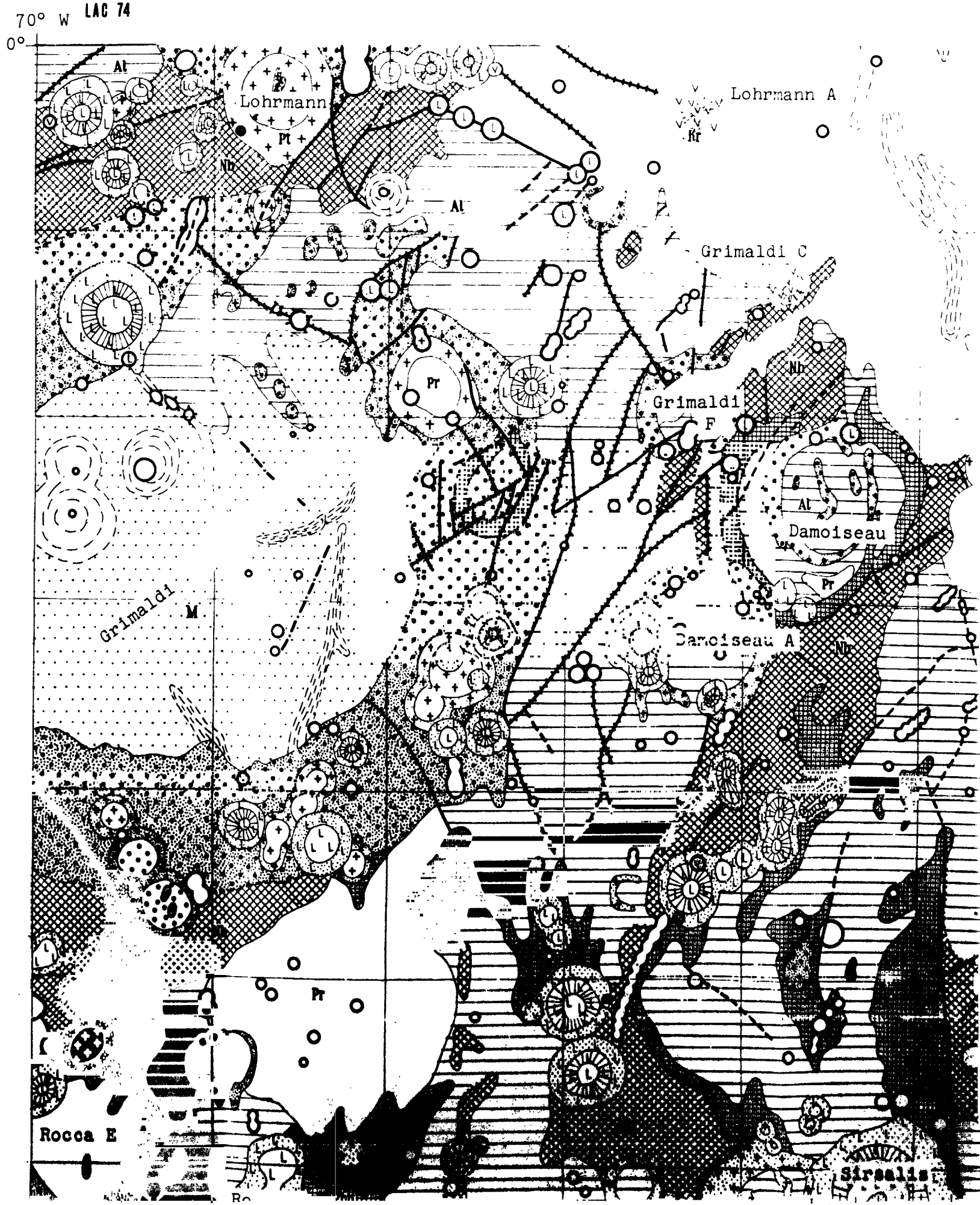
70° W
0°
LAC 74
Lohrmann
Lohrmann A
Grimaldi C
Grimaldi F
Grimaldi M
Damoiseau
Damoiseau A
Rocca E
Sirsalis
Al
Pt
Nb
Pr
Kr

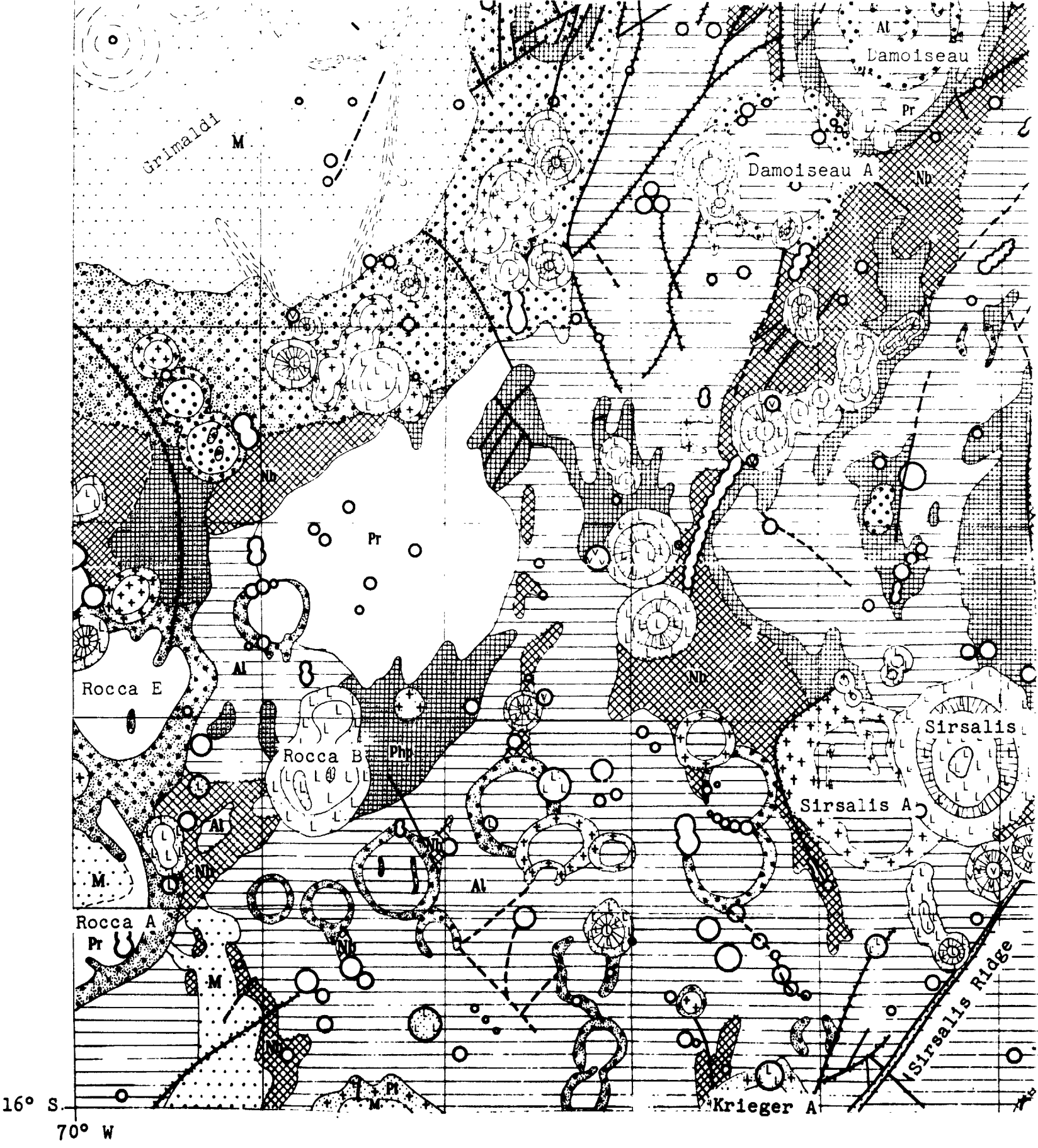

Figure 11. Geological-morphological chart of Sheet LAC-74. Scale ~ 1:1,500,000. Conditional designations are the same as in Figure 2.

FOLDOUT FRAME 2

FOLDOUT FRAME

2

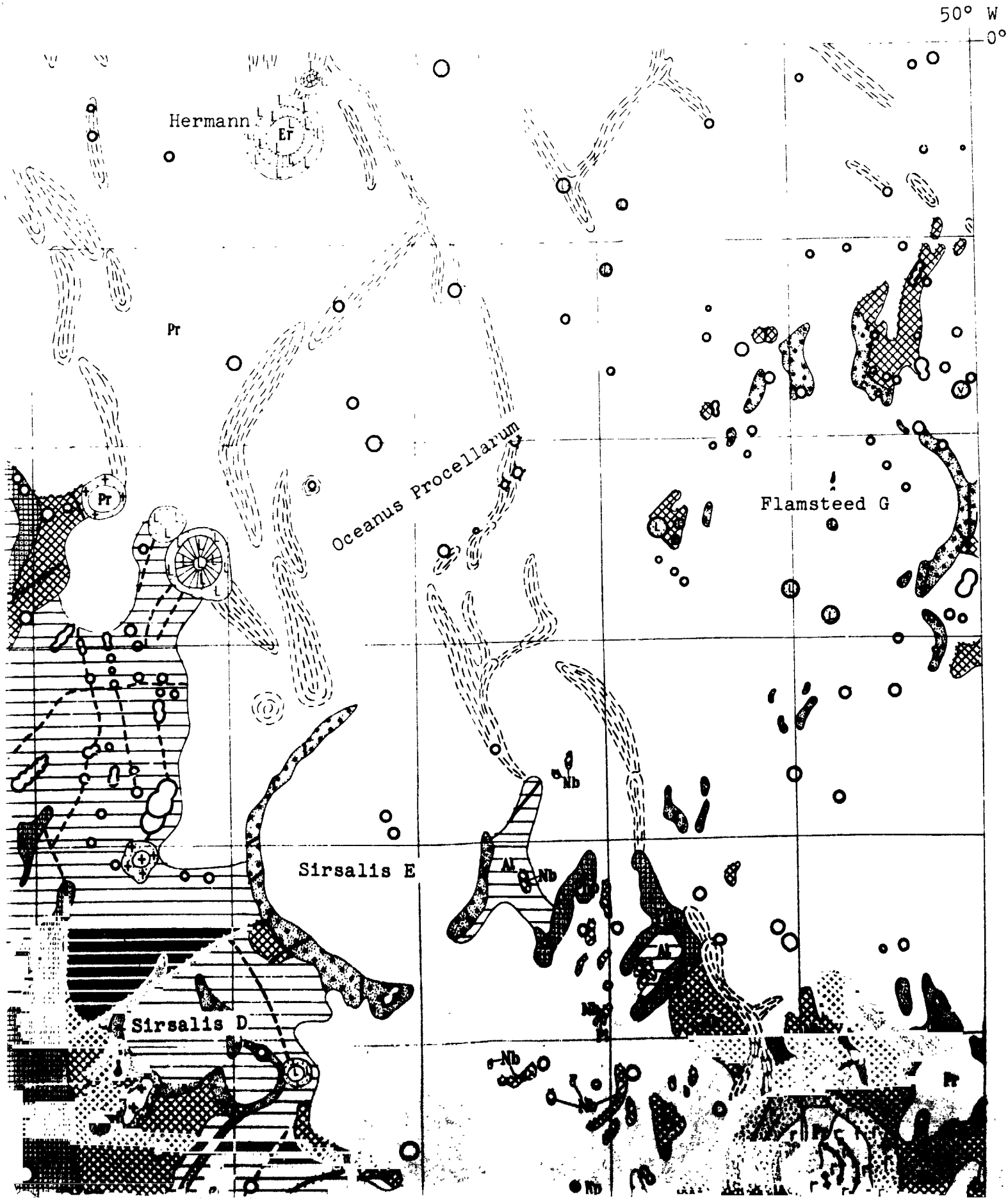

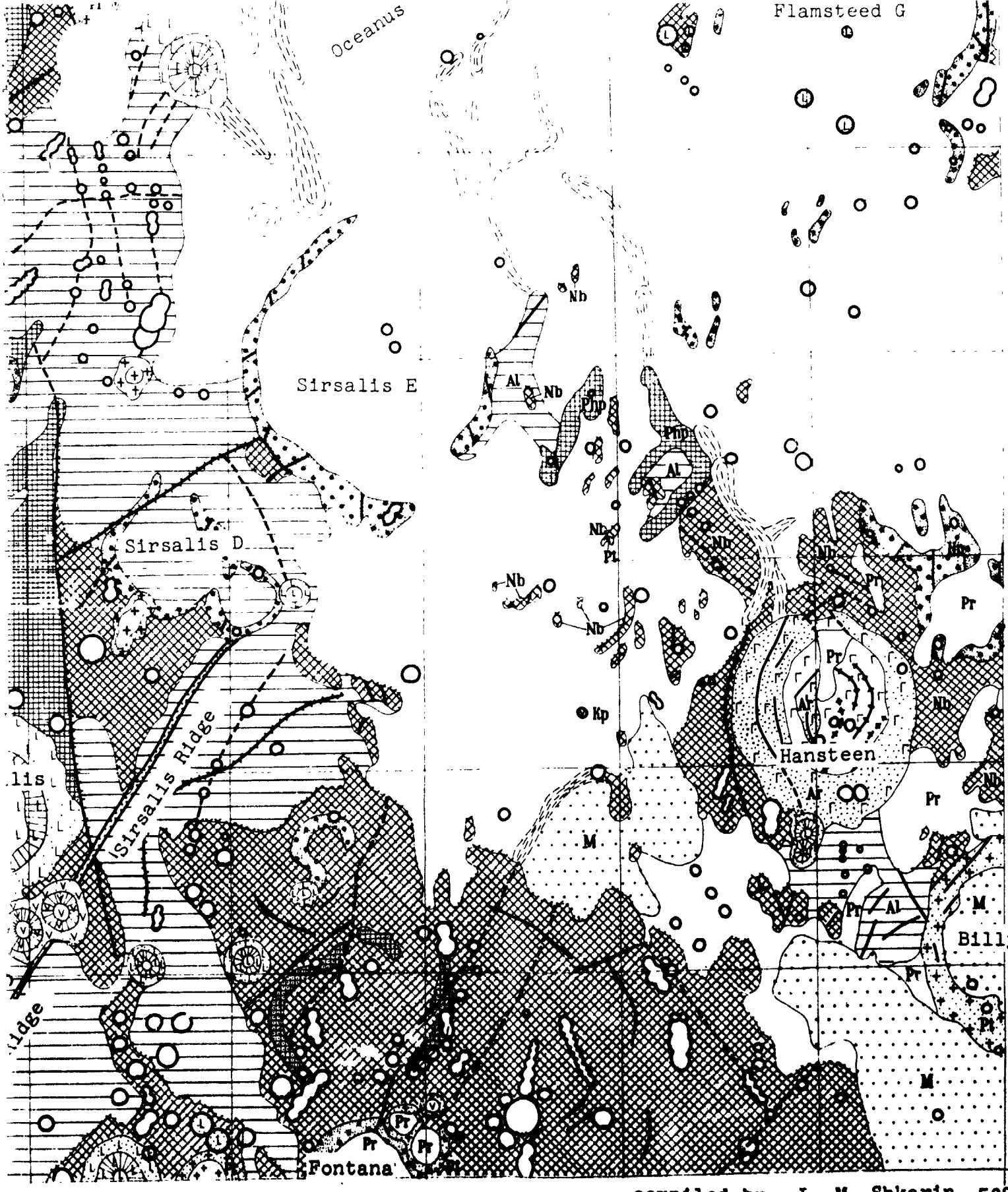

compiled by L. M. Shkerin

FOLDOUT FRAME 5

4

BLACKOUT FRAME

50° W LAC 57

16° N

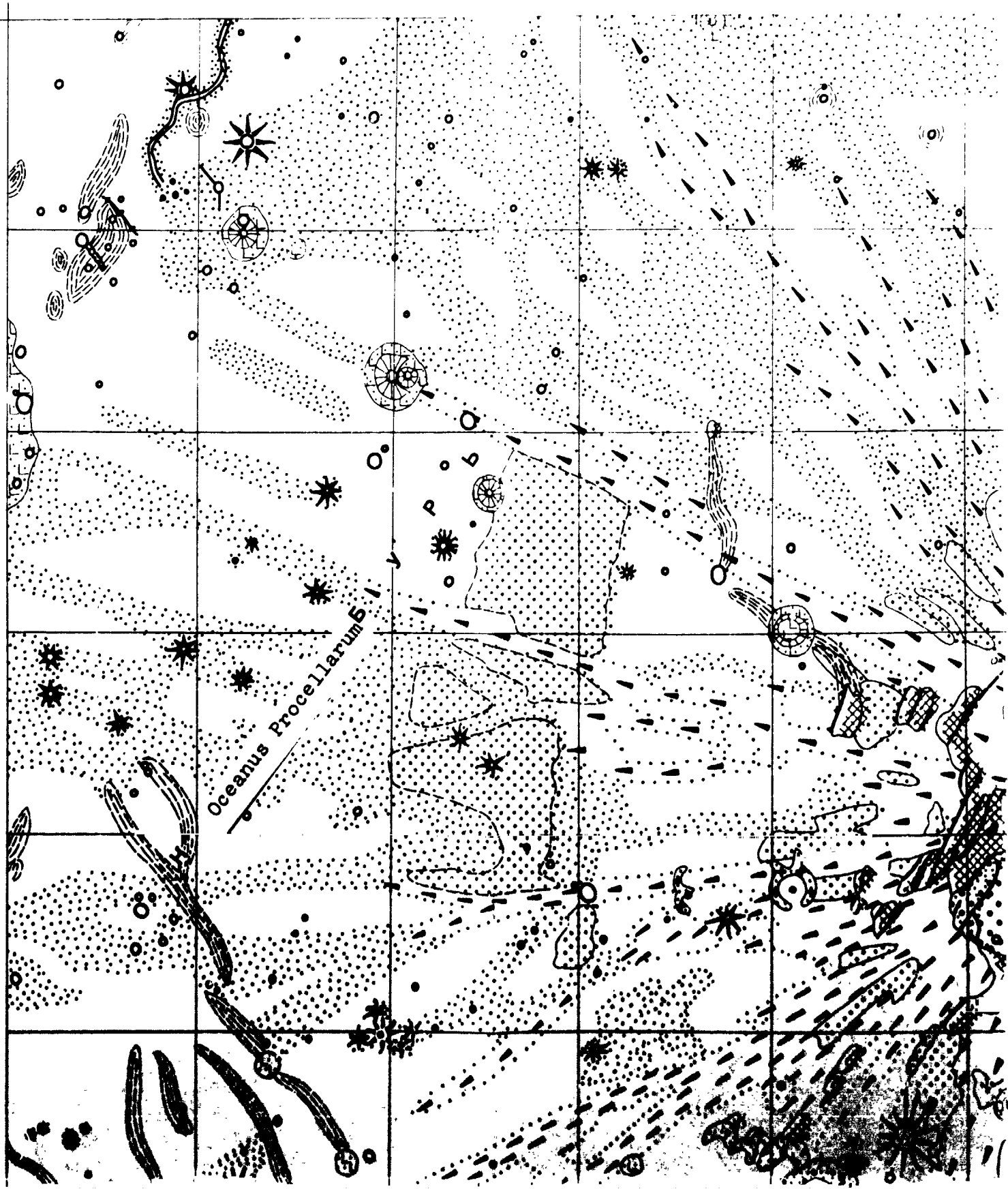

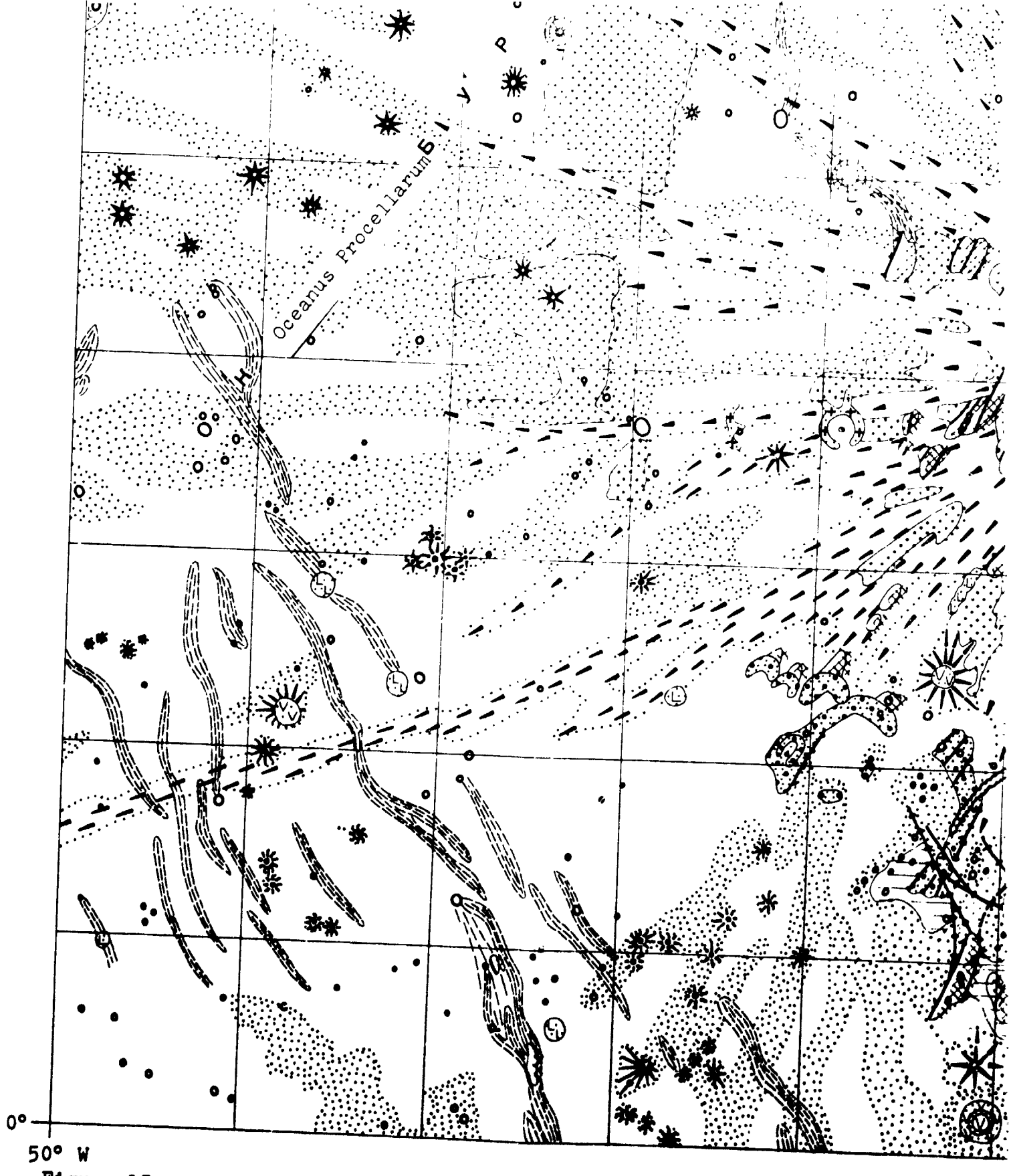

Figure 15. Geological-morphological chart of Sheet LAC-57. Scale ~ 1:1,400,00
Conditional designations are the same as in Figure 2.

BREAKOUT FRAME

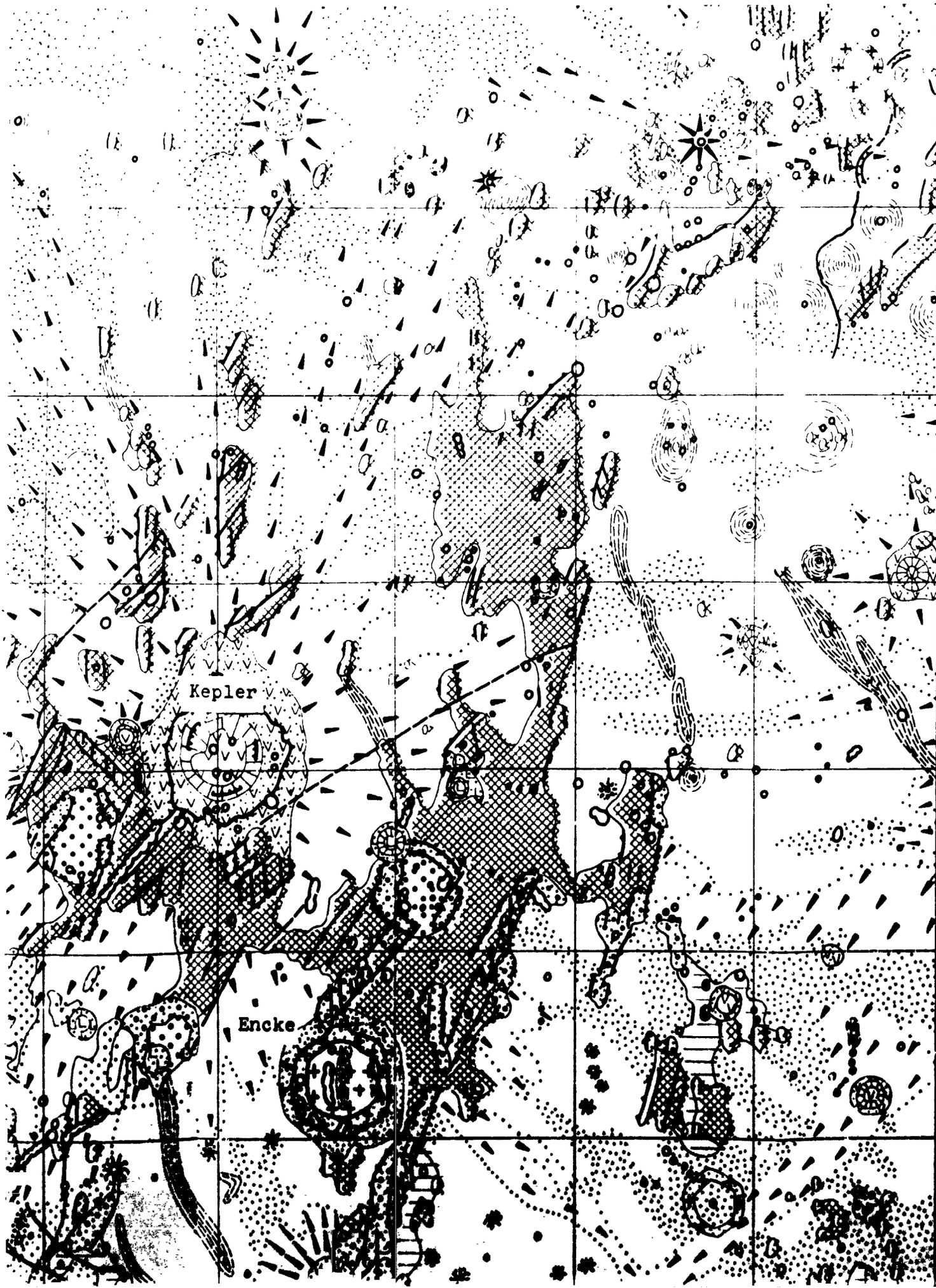
30° W
16° N
Kepler
Encke

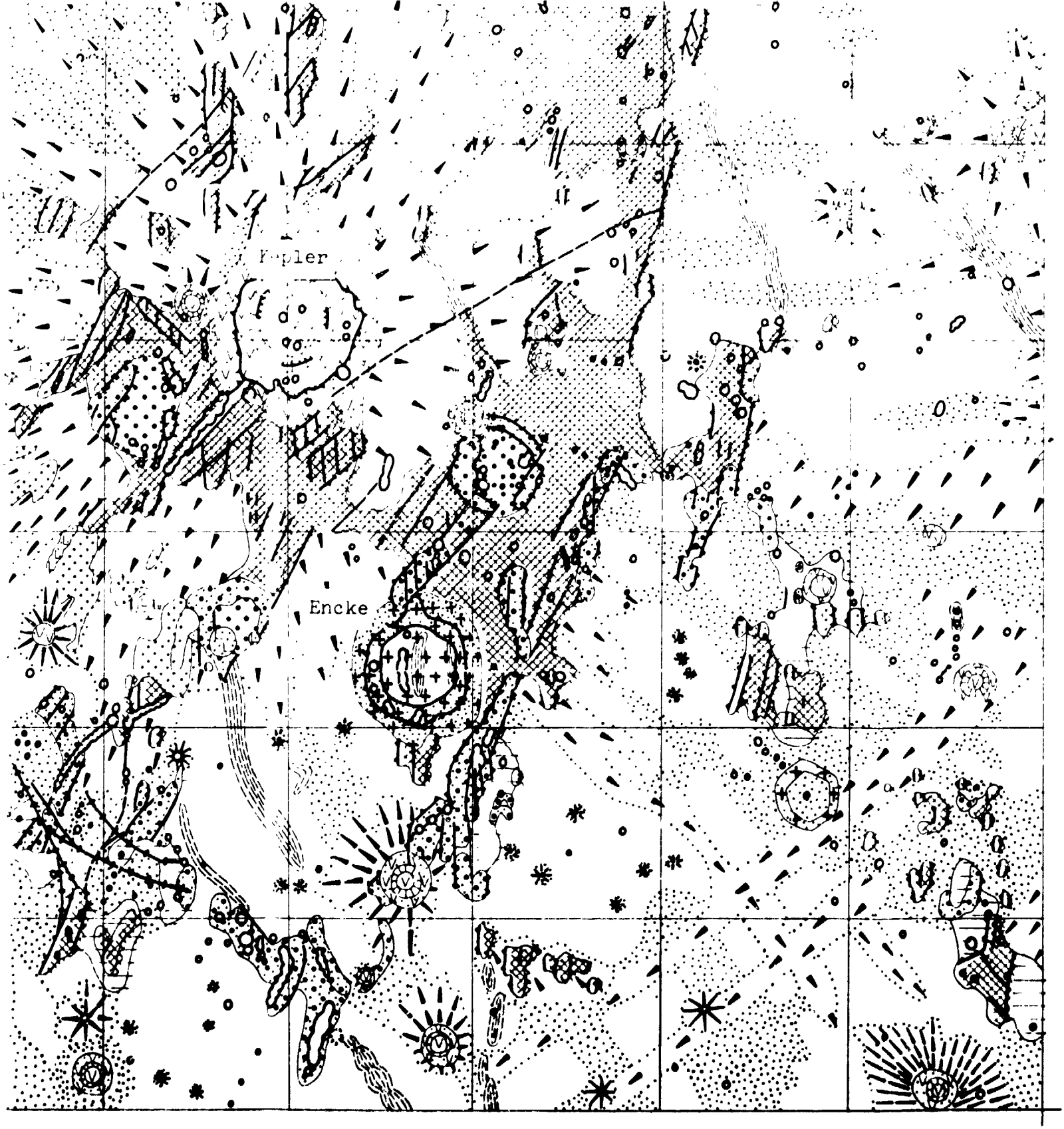

0°

compiled by L. V. Florenskiy 30° W

:1,400,000.

[redacted] FRAME

4

NATIONAL AERONAUTICS AND SPACE ADMINISTRATION
WASHINGTON, D.C. 20546

OFFICIAL BUSINESS
PENALTY FOR PRIVATE USE $300

SPECIAL FOURTH-CLASS RATE
BOOK

POSTAGE AND FEES PAID
NATIONAL AERONAUTICS AND
SPACE ADMINISTRATION
451

POSTMASTER: If Undeliverable (Section 158
Postal Manual) Do Not Return

"The aeronautical and space activities of the United States shall be conducted so as to contribute . . . to the expansion of human knowledge of phenomena in the atmosphere and space. The Administration shall provide for the widest practicable and appropriate dissemination of information concerning its activities and the results thereof."

—NATIONAL AERONAUTICS AND SPACE ACT OF 1958

NASA SCIENTIFIC AND TECHNICAL PUBLICATIONS

TECHNICAL REPORTS: Scientific and technical information considered important, complete, and a lasting contribution to existing knowledge.

TECHNICAL NOTES: Information less broad in scope but nevertheless of importance as a contribution to existing knowledge.

TECHNICAL MEMORANDUMS: Information receiving limited distribution because of preliminary data, security classification, or other reasons. Also includes conference proceedings with either limited or unlimited distribution.

CONTRACTOR REPORTS: Scientific and technical information generated under a NASA contract or grant and considered an important contribution to existing knowledge.

TECHNICAL TRANSLATIONS: Information published in a foreign language considered to merit NASA distribution in English.

SPECIAL PUBLICATIONS: Information derived from or of value to NASA activities. Publications include final reports of major projects, monographs, data compilations, handbooks, sourcebooks, and special bibliographies.

TECHNOLOGY UTILIZATION PUBLICATIONS: Information on technology used by NASA that may be of particular interest in commercial and other non-aerospace applications. Publications include Tech Briefs, Technology Utilization Reports and Technology Surveys.

Details on the availability of these publications may be obtained from:

SCIENTIFIC AND TECHNICAL INFORMATION OFFICE

NATIONAL AERONAUTICS AND SPACE ADMINISTRATION

Washington, D.C. 20546